Imperial College
London

ANISOTROPIC SURFACE PROPERTIES OF CRYSTALLINE PHARMACEUTICAL SOLIDS

By

Jerry Yong Yew Heng

A dissertation submitted to the University of London for the degree of Doctor of Philosophy and the Diploma of Membership of Imperial College London.

Department of Chemical Engineering

Imperial College London

South Kensington Campus

London, U. K.

December 2005

BIBL. LONDON. UNIV

PREFACE

I particularly like to thank Dr. Daryl R. Williams for his supervision, support, encouragement and continued optimism during which this research was undertaken. His advice and guidance at all stages of the research, which included freedom to determine how this project was to take shape, have been immensely invaluable. I will also always remember all this advice.

Many thanks to Dr. Alexander Bismarck for his continuous support, encouragement and faith in the work I undertook. I acknowledge Dr. Frank Thielmann, Dr. Majid Naderi and their team at Surface Measurement Systems, U.K. for their help, in particular with the IGC. The kind assistance of Dr. Adam F. Lee and Dr. Karen Wilson of the Department of Chemistry, University of York, U.K. for XPS analysis is also acknowledged.

The financial support of the Department for Education and Skills (DfES), U.K. in the form of an Overseas Research Scholarship (ORS) award is acknowledged.

Thanks are also recorded to the members of Williams' research group, for the enjoyable working experience and friendship.

Special thanks also go out to my family and loved ones for their continued support, and encouragement to pursue this PhD although it meant being thousands of miles away from home. Finally, I would like to thank Pei Wern Ding for putting up with my constant impatience and moaning when things do not go right, and for her support and encouragements which is beyond comprehension.

DECLARATION

The work described in this thesis was carried out in the Department of Chemical Engineering, Imperial College London, United Kingdom between October 2002 and December 2005. Except where acknowledged, the material is the original work of the author and includes nothing which is the outcome of work in collaboration, and no part of it has been submitted for a degree at any other university.

FOR P & M

ABSTRACT

This thesis presents a detailed study into the surface properties of crystalline pharmaceutical solids, describing the role that surface chemistry plays in determining wetting behaviour. An anisotropic wetting behaviour has been observed experimentally for the first time, made possible by the solution mediated growth of large (>1cm) crystals, permitting direct sessile drop contact angle analysis *on each* individual facet. The relationship between the experimental wettability, surface energetics, surface polarity, XPS surface composition and the known crystallographic structure is investigated, resulting in a coherent understanding of the surface chemistry of various crystalline pharmaceutical solids. The solids investigated included both polymorphs of paracetamol, aspirin, racemic ibuprofen and S-(+)-ibuprofen.

Numerous techniques for characterising the wetting properties of solids are available. Of these techniques; the liquid sessile drop on powder compacts, capillary rise into a powder bed and infinite dilution inverse gas chromatography (IGC) were investigated. Although it is known that organic crystalline materials have highly variable surface properties, conventional techniques tend to yield some type of single valued average property. From this study, it is clear that the measurements of surface energetics on powders, at best, do not reflect the surface heterogeneity present, and are probably simply representative of the most dominant facet.

A direct correlation between the relative surface energy polarity ($\gamma_{SV}^{p}/\gamma_{SV}$), the fraction of exposed polar groups as determined from XPS spectra and the number of non-hydrogen bonded hydroxyl groups per unit area present for each crystal facet, based on the known crystal structures, is described in this thesis. Direct measurements of specific facets enabled the ranking of a hydrophobic/hydrophilic order for the

crystalline facets. A property of particular interest is the weakest attachment energy facet, which is found to be the most hydrophobic facet, for all systems investigated. Upon milling, this facet was found to be preferentially exposed, becoming increasingly dominant with reduction in particle sizes, as detected by IGC techniques.

This original contribution not only highlights the fundamentally anisotropic surface chemistry of crystalline solids, but may also explain a number of the potential problematic issues relating to the processing of powders such as batch to batch variability and poor granulation performance. In addition, this work opens up some exciting possible routes to crystal engineering, especially of crystal habit.

PUBLICATIONS

This thesis has resulted in the following book sections, papers and conference proceedings:

Book Sections

1. Jerry Y. Y. Heng and Daryl R. Williams, "Vapour Sorption for Bulk and Surface Analysis", **2005** *Blackwell Publishing Company,* submitted.
2. Jerry Y. Y. Heng, Duncan F. Pearse, David A. Wilson and Daryl R. Williams, "Characterization of Solid State Materials using Vapor Sorption Methods", **2005** *ASSA Publications*, in Press.

Journal Papers

1. Jerry Y. Y. Heng, Alexander Bismarck, Adam F. Lee, Karen Wilson and Daryl R. Williams, *Anisotropic Wettability of Macroscopic Form I Paracetamol Crystals.* ***Langmuir*** 2006. Accepted.
2. Jerry Y. Y. Heng and Daryl R. Williams, *The anisotropic surface properties of paracetamol polymorphic forms I and II.* ***Journal of the American Chemical Society*** 2005. Submitted.
3. Jerry Y. Y. Heng, Frank Thielmann and Daryl R. Williams, *The effects of milling on the surface properties of form I paracetamol crystals.* ***Pharmaceutical Research***, in preparation.
4. Jerry Y. Y. Heng, Alexander Bismarck and Daryl R. Williams, *Wettability of pharmaceutical crystalline solids: Characterisation techniques.* ***Journal of Pharmaceutical Sciences***, in preparation.
5. Jerry Y. Y. Heng, Alexander Bismarck, Adam F. Lee, Karen Wilson and Daryl R. Williams, *Anisotropic wettability of aspirin single crystals.* ***Langmuir***, in preparation.

Selected Refereed International Conferences

1. Jerry. Y. Y. Heng and Daryl R. Williams, "Specific Facet Surface Chemistry Determination of Paracetamol Single Crystals", 2005 AAPS Annual Meeting and Exposition, Nashville, TN, USA, 6 - 10 November 2005
2. Jerry. Y. Y. Heng, David A. Wilson, Choon M. Yap and Daryl R. Williams, "The Physicochemical and Surface Properties of Solid State Pharmaceutical Solids", 7th World Congress of Chemical Engineering, Glasgow, UK, 10 -14 July 2005
3. Jerry Y. Y. Heng and Daryl R. Williams, "The Surface Properties of Crystalline Pharmaceutical Solids", ACIS 2005 – Australian Colloid and Interface Symposium, Coogee Beach, Sydney, Australia, 13 - 17 February 2005
4. Daryl R. Williams and Jerry Y. Y. Heng, "Surface properties of milled and unmilled form I paracetamol powders", PhandTA 8 – International Conference on Pharmacy and Applied Chemistry, Monte Verita, Switzerland, 26 – 29 September 2004
5. Jerry Y. Y. Heng, Alexander Bismarck and Daryl R. Williams, "Anisotropic Wettability of Macroscopic Form I Paracetamol Crystals", Fourth International Symposium On Contact Angle, Wettability And Adhesion, Philadelphia, PA, USA, 14 – 16 June 2004
6. Jerry Y. Y. Heng, Frank Thielmann and Daryl R. Williams, "Variation in Crystalline Paracetamol Surface Properties Due To Milling", The AAPS Journal, 2004. 6(4):R6143.
7. Jerry Y. Y. Heng and Daryl R. Williams, "Anisotropic Wettability of Paracetamol Crystals", AAPS PharmSci., 2003. 5(4):W4338.

LIST OF FIGURES

Figure 2.1: Reliable and occasional hydrogen bond acceptors and donors [18]. Functionalities are grouped into quadrants with top right (moving anti-clockwise) for reliable donors, reliable acceptors, occasional acceptors and occasional donors respectively. Their individual position is not representative of the potential hydrogen bond strength. 37

Figure 2.2: Interaction between single molecule and a flat surface (a) side view and (b) top view. 39

Figure 2.3: A curved interface across an air bubble – liquid system. 45

Figure 2.4: Classification of adsorption isotherms. 50

Figure 2.5: The contact area predicted by various models against loading force. 55

Figure 2.6: Schematic diagrams indicating the (a) work of cohesion and (b) work of adhesion of materials 60

Figure 2.7: Equilibrium contact angles on (a) clean surface and (b) surface with adsorbed vapour molecules and the balance of forces at the three phase contact points. 62

Figure 2.8: The contact angles for (a) a partial wetting, (b) a non-wetting and (c) a complete wetting case. 63

Figure 2.9: Zisman plot to obtain critical surface energy of Polyethylene (PE) and Polytetrafluoroethylene (PTFE) [6]. 63

Figure 2.10: Comparison between experimental and estimated contact angles based on the UNIFAC approach. 72

Figure 2.11: Schematic diagrams indicating the (a) advancing and (b) receding contact angles 75

Figure 2.12: Determination of the advancing and receding contact angle by tilting plate method. 76

Figure 2.13: Wenzel roughness factor.. 77

Figure 2.14: The effects of roughness on measurable contact angles based on Wenzel's equation. 78

Figure 2.15: Theoretical relationship between θ_W and θ_Y [101]. 80

Figure 2.16: Equilibrium and apparent contact angles according to the Cassie-Baxter relationship for the case of incomplete liquid penetration into grooves... 82

Figure 3.1: The Terrace-Ledge-Kink model of a growing crystal face. 92

Figure 3.2: The Birth and Spread mechanism for crystal growth (a) top view and (b) front view. 93

Figure 3.3: The (a) development of a screw dislocation defect and (b) the growth mechanism 94

Figure 3.4: Growth rates as a function of degree of supersaturation as predicted by the Burton-Cabrera-Frank model. 95

Figure 3.5: Schematic of the principle of powder X-ray diffraction. 97

Figure 3.6: Miller indices of crystalline facets (a) monoclinic and (b) orthorhombic systems. 99

Figure 3.7: Measurement of the dihedral angle between crystalline facets with (a) a protractor and (b) a goniometer..... 101

Figure 4.1: Molecular structure of (a) paracetamol with (1) hydroxyl, (2) amine and (3) carbonyl functional groups, (b) aspirin with the (1) carboxylic, (2) ester groups and (c) ibuprofen with the (1) carboxylic functionality while (*) denotes the chiral centre. 108

Figure 4.2: Single crystals of (a) paracetamol (scale in cm) and (b) aspirin.. 109

Figure 4.3: Procedure for growing macroscopic single crystals..... 110

Figure 4.4: (a) Habit of macroscopic form I paracetamol single crystals grown from (a) methanol saturated solution, (b) acetone saturated solution and (c) the preferred cleavage plane. 112

Figure 4.5: Habit of aspirin crystals grown from (a) acetone solution and (b) methanol solution..... 113

Figure 4.6: Habit of ibuprofen crystals grown from (a) acetone solution and (b) ethanol solution. 113

Figure 4.7: Habit of S-(+)-ibuprofen crystals grown from acetone solution. 114

Figure 4.8: Paracetamol (a) form II single crystals (scale in cm) and (b) its habit.... 115

Figure 4.9: Crystallographic structure of form I paracetamol (a) facet (001) and (b) facet (010). Inset are droplet profiles of water saturated with paracetamol on the crystalline facets showing large variations in droplet profiles..... 117

Figure 4.10: Crystallographic structure of the orthorhombic (form II) paracetamol crystals at (a) facets (010) and (b) facet (001). 118

Figure 4.11: Crystallographic structure of aspirin crystals viewed along (a) b-axis and (b) a-axis..... 119

Figure 4.12: Crystallographic structure of racemic ibuprofen crystals viewed along (a) b-axis and (b) a-axis. 120

Figure 4.13: Crystallographic structure of dexibuprofen crystals viewed along (a) b-axis and (b) a-axis. 121

Figure 5.1: Normalised ideal wetting plot. 129

Figure 5.2: Schematic of equipment for measuring capillary pressure generated by liquid rising through a packed powder bed. 130

Figure 5.3: Forces acting along Wilhelmy plate (a) zero net depth of immersion (b) finite depth of immersion. 132

Figure 5.4: The Dynamic Vapour Sorption equipment used for gravimetric vapour sorption experiments. 136

Figure 5.5: The schematic diagram of the XPS equipment. 140

Figure 5.6: Schematic of the photo-ejection process of the core shell electron by X-rays for XPS analysis. 140

Figure 5.7: Schematic of the cantilever deflection with respect to scanner displacement on approach to and from the solid surface. As the cantilever approaches the solid surface, the cantilever bends upwards due to repulsive forces. The cantilever is bent downwards as the particle is attracted to the surface. As the scanner is moved further away from the surface, the particle is detached from the surface with the force equals to the F_{Adh}. 141

Figure 5.8: Weight gain curves for n-hexane as a function of time measured for paracetamol powders..... 149

Figure 5.9: Weight gain curves for 1-decanol as a function of time measured for paracetamol powders..... 150

Figure 5.10: Normalised wetting rates for paracetamol powder bed..... 151

Figure 5.11: Normalised wetting rates for apolar probe liquids for paracetamol powder bed. 152

Figure 5.12: Normalised wetting rates for liquid capillary rise into ibuprofen powder bed for apolar probe liquids. 152

Figure 5.13: Penetration of water droplet into 20 kN paracetamol compacts at (a) 0 mS, (b) 450 mS, (c) 950 mS, (d) 1450 mS, (e) 1950 mS and (f) 2450 mS. 154

Figure 5.14: Scanning electron micrographs of paracetamol tablet compacted at 20 kN (a) 200 x and (b) 400 x magnification..... 155

Figure 5.15: Scanning electron micrographs of ibuprofen tablet at (a) 10 kN and (b) 20 kN compaction pressure, 200 x magnification..... 155

Figure 5.16: Surface energy of ibuprofen tablets as a function of compaction pressure. 157

Figure 5.17: Free energy of adsorption ($RT \ln V_N$) as a function of dispersive energy of probe vapour, γ_{SV}^d for paracetamol and ibuprofen. 159

Figure 6.1: Droplet profile of water saturated with paracetamol at 20 °C on (a) facet (010) and (b) facet (011). 172

Figure 6.2: θ_a of water and water saturated with paracetamol on specific facets of form I paracetamol crystal, and of water on gold coated surfaces..... 172

Figure 6.3: Aspirin saturated water droplets on (a) facet (001), (b) facet (100) and (c) facet (011). 180

Figure 7.1: Energy levels. 192

Figure 7.2: (a) Ejection of a core shell electron and its resulting relaxation by (b) X-ray fluorescence or (c) an Auger electron. 193

Figure 7.3: C 1s XP spectra for various facets of form I paracetamol crystal..... 199

Figure 7.4: O 1s XP spectra for various facets of form I paracetamol crystal..... 200

Figure 7.5: N 1s XP spectra for various facets of form I paracetamol crystal..... 201

Figure 7.6: Deconvoluted C 1s XP spectra for (001) and (010) facets of form I paracetamol crystal. Note 286.1 eV component required fitting with FWHM = 0.82 eV. 203

Figure 7.7: Deconvoluted O 1s XP spectra for (001) and (010) facets of form I paracetamol crystal.....204

Figure 7.8: Variation in surface composition of polar groups for different facets of form I paracetamol crystal as determined from C 1s and O 1s XP peak-fitting. Surface -OH intensities taken from 534.6 eV component in Figure 7.7.....205

Figure 7.9: C 1s XP spectra of the (001), (100) and (011) facets showing the deconvoluted C environments.....209

Figure 7.10: O 1s XP spectra of the (001), (100) and (011) facets showing the deconvoluted O environments.....210

Figure 8.1: The Inverse Gas Chromatography (IGC) schematic diagram.....215

Figure 8.2: Retention times of probe molecules with increasing injection size for the infinite dilution regime.....216

Figure 8.3: The isotherms and chromatographic peaks for (a) the infinite dilution case where Henry's Law is valid, (b) the Langmuir case and (c) the type II and III adsorption isotherm cases. 216

Figure 8.4: Retention time as a function of increasing chain lengths for a series of n-alkane injections.....218

Figure 8.5: (a) A typical net retention volume plot versus vapour surface property for the determination of solid surface dispersion energy and (b) determination of enthalpy of adsorption. 221

Figure 8.6: Sorption mechanisms of amorphous and crystalline solids. 228

Figure 8.7: Determination of glass transition temperature, T_g for amorphous solids [362].....228

Figure 8.8: Variation in γ_{SV}^{d} for milled and unmilled paracetamol crystals as a function of particle size.....235

Figure 8.9: Acid-base numbers for milled macroscopic paracetamol crystals grown in methanol solution as a function of particle size.....238

Figure 8.10: Acid-base numbers for milled macroscopic paracetamol crystals grown in acetone solution as a function of particle size.....239

Figure 8.11: Acid-base numbers for unmilled fine paracetamol crystals grown from methanol solution.....241

Figure 8.12: Acid-base numbers for unmilled fine paracetamol crystals grown from acetone solution.....241

Figure 8.13: Acid-base numbers for milled and unmilled aspirin crystals.....245

Figure 9.1: Surface polarity of paracetamol crystalline facets determined by XPS and contact angle measurements.....252

Figure 9.2: Comparison between contact angle polarity and predicted free OH surface group concentration for various facets of form I paracetamol.....254

Figure 9.3: Surface polarity of aspirin facets based on surface energies and XPS analysis.....258

LIST OF TABLES

Table 3.1: Crystal Systems 89

Table 4.1: Dihedral Angles for Paracetamol Form I (Monoclinic) Crystals 122

Table 4.2: Dihedral Angles for Paracetamol Form II (Orthorhombic) Crystals..... 122

Table 4.3: Dihedral Angles for Aspirin Crystals 123

Table 4.4: Dihedral Angles for Racemic Ibuprofen Crystals 123

Table 4.5: Dihedral Angles for S-(+)-Ibuprofen Crystals..... 123

Table 4.6: Computed Attachment Energies for Pharmaceutical Crystals 124

Table 5.1: Properties of Contact Angle Liquid Probes Used..... 145

Table 5.2: Capillary Rise Liquid Properties 147

Table 5.3: θ_a (^{o}) on Ibuprofen Tablets..... 156

Table 5.4: Surface Energy Analysis Using the Classical Owens-Wendt Approach for Paracetamol and Ibuprofen Single Crystals 160

Table 6.1: Properties of Liquid Probes Used..... 166

Table 6.2: θ_a (^{o}) Results for Paracetamol Crystals..... 169

Table 6.3: θ_a and θ_r Data for Diiodomethane on Paracetamol Crystals..... 170

Table 6.4: θ_a and R_a Data for Native and Gold Coated Single Crystal Facets of Paracetamol Crystals 171

Table 6.5: θ_a (^{o}) Results for Form I and II Paracetamol Crystals 176

Table 6.6: θ_a (^{o}) Results for Aspirin Crystals..... 180

Table 6.7: θ_a (^{o}) Results for Ibuprofen Crystals..... 185

Table 7.1: C 1s Binding Energies for Methylene and Its Functionalised Derivatives 196

Table 7.2: Atomic Composition of C, N and O on Various Crystalline Paracetamol Facets..... 198

Table 7.3: Surface Composition of Crystal Facets from XPS 211

Table 7.4: Distribution of O 1s Surface Environments from XPS (atom %) 211

Table 8.1: Acid-Base Numbers of Probe Molecules Used in IGC 230

Table 8.2: γ_{SV}^d of Milled Macroscopic Single Crystals Grown from Saturated Paracetamol in Methanol and Acetone Solution..... 232

Table 8.3: γ_{SV}^d of Unmilled Single Crystals Grown from Saturated Paracetamol in Methanol and Acetone Solution..... 233

Table 8.4: Free Energy of Desorption for Paracetamol Crystals Grown From Saturated Methanol Solution. 236

Table 8.5: Free Energy of Desorption for Paracetamol Crystals Grown From Saturated Acetone Solution. 237

Table 8.6: γ_{SV}^{d} of Milled and Unmilled Single Crystals of Aspirin Grown From Acetone Solution 242

Table 8.7: Free Energy of Desorption for Aspirin Fine Crystals Grown From Saturated Acetone Solution and Milled Fractions of Macroscopic Crystals 244

Table 8.8: Acid-Base Numbers for Aspirin Fine Crystals Grown From Saturated Acetone Solution and Milled Fractions of Macroscopic Crystals..... 244

Table 8.9: Free Energy of Desorption for Milled Macroscopic Ibuprofen Crystals Grown From Saturated Methanol Solution 246

Table 8.10: Surface Properties of Milled Ibuprofen 247

Table 9.1: Results of Surface Energy for Paracetamol Using the Classical Owens-Wendt Approach 251

Table 9.2: Results of Surface Energy for Paracetamol by the van Oss et al. Acid-Base Approach 251

Table 9.3: Unit Cell Information for Form I Paracetamol and Predicted Free Hydroxyl Group Surface Concentrations 253

Table 9.4: Results of Surface Energy for Paracetamol by the Della Volpe Acid-Base Approach 255

Table 9.5: Results of Surface Energy for Form II Paracetamol by the Owens-Wendt Approach 257

Table 9.6: Results of Surface Energy for Aspirin by the Owens- Wendt Approach. 257

Table 9.7: Results of Surface Energy for Aspirin by the van Oss et al. Acid-Base Approach 258

Table 9.8: Results of Surface Energy for Aspirin by the Della Volpe Acid-Base Approach 258

Table 9.9: Results of Surface Energy for Racemic Ibuprofen Analysis Using the Classical Owens-Wendt Approach..... 259

Table 9.10: Results of Surface Energy for S-(+)-Ibuprofen Analysis Using the Classical Owens-Wendt Approach..... 260

LIST OF SYMBOLS

A	Area
a	Contact radius of a spherical particle
a	Unit length of crystal at x-axis
A and B	Constants according to BCF model
A_1 and A_2	Properties of system according to Birth and Spread model
a_a	Activity coefficient
A_{ii}	The Hamaker constant for phase *i*
A_{ij}	The Hamaker constant for interface *ij*
a_M	Dimensionless parameters for contact radius
a_m	Surface area of adsorbed molecule
AN	Acceptor numbers
AN^*	Corrected acceptor numbers
a_o	Activity of the dissolved solute in equilibrium with a flat surface
a_{vdW}	van der Waals constant for intermolecular forces
b	Unit length of crystal at y-axis
b_L	Langmuir adsorption constant
b_{vdW}	van der Waals constant for molar volume of gas
b_Z	Slope of the regression line for a Zisman's plot
c	Concentration of the solution
c	Unit length of crystal at z-axis
C_A and C_B	Covalent contribution for component a and b
c_{BET}	BET Constant
c_s	Saturated concentration
d	Length where adhesive stress is constant
d_{hkl}	Interplanar spacing of crystal facet (hkl)
DN	Electron donor numbers

E	Young's modulus
E_A and E_B	Electrostatic contribution for component a and b
E_{BE}	Binding energy of electrons
E_{KE}	Kinetic energy of electrons
F	Applied force
F	Carrier gas exit flow rate
f	Constant converting enthalpy units in terms of surface free energy
F_{Adh}	Adhesion force
f_i	Fraction of component i
F_M	Dimensionless parameters for external force
F_W	Wetting force
G	Gibb's free energy
g	Gravitational force constant
h	Height
h	Plank constant
hv	Energy of the photon
j	James-Martin pressure correction factor
k	Boltzmann constant
K	Reduced Young's modulus
K_A and K_B	Acid and base numbers of the solid phase, respectively
K_b	Bulk partition coefficient
K_C	Capillary constant representing the geometry of the porous network
K_s	Surface partition coefficient
M	Molecular weight
n	Number of molecules
N_A	Avogadro's number
N_{AB}	Number of acid-base pair interactions per unit area
n_B	Integer for Bragg's equation

N_i	Amount of component *i*
n_i	Refractive index
p	Perimeter of the Wilhelmy plate
p	Pressure
p_{eff}	Effective wetting parameter
P_i	Inlet pressure
P_o	Outlet pressure
p_o	Partial pressure
$p_{s,g}$	Adsorbate vapour pressure in the gas phase
r	Radius
R	Universal gas constant
R_a	Roughness
r_{eff}	Effective interstitial pore radius
r_{ii}	The distance between interacting atoms
R_p	Radius of a spherical particle
r_S	Separation distance
r_W	Wenzel's roughness factor
S	Entropy
$S_{i/j}$	Spreading coefficient for liquid *i* over solid *j*
S^s	Surface excess entropy
T	Temperature
t	Time
T_g	Glass transition temperature
t_{max}	The time for peak maximum
t_o	Dead time
t_R	Retention time
U	Potential Energy/Internal Energy
v	Specific molar volume
V	Volume

V_{Ads}	Volume of adsorbed molecules
v_c	Crystal face growth velocity
V_m	Monolayer volume
v_p	Poisson's ratio
V_R^o	Net retention volume
W_A	Work of adhesion
W_A^{AB}	Work of adhesion for the acid-base interactions
W_C	Cohesive work
W_S	Mass of sample
W_{SL}	Solid-liquid work of adhesion
W_{SP}	Spectrometer work function
x	Relative pressure (p/p_o)
z_o	Equilibrium separation distance between the bodies in contact
Γ	Surface excess (surface concentration) at the interface
γ_C	Critical surface energy
γ_i^d	Dispersive component surface energy of *i*th component
γ_{ij}	Interfacial tension between phase i and j
γ_{LV}^-	Liquid basic component surface energy
γ_{LV}	Liquid surface tension
γ_{LV}^+	Liquid acid component surface energy
γ_{LV}^d	Liquid dispersive component surface energy
γ_{LV}^{LW}	Lifshitz-van der Waals contribution to liquid surface energy
γ_{LV}^p	Liquid polar component surface energy
γ_r	Residual activity coefficients
γ_{SL}	Solid-liquid interactions
γ_{SV}^-	Solid basic component surface energy
γ_{SV}	Solid surface energy
γ_{SV}^+	Solid acid component surface energy
γ_{SV}^d	Solid dispersive component surface energy

γ_{sv}^{dp}	Dipole-dipole bondings contribution to solid surface energy
γ_{sv}^{h}	Hydrogen-bonding contribution to solid surface energy
γ_{sv}^{i}	Induction bondings contribution to solid surface energy
γ_{sv}^{LW}	Lifshitz-van der Waals contribution to solid surface energy
γ_{sv}^{m}	Metallic bondings contribution to solid surface energy
γ_{sv}^{o}	Solid (clean) surface energy
γ_{sv}^{p}	Solid polar component surface energy
$\Delta \rho$	Density difference between the solid plate and the liquid
ΔF	Free energy of adhesion
ΔF^{coh}	Free energy of cohesion
ΔG^{AB}	Acid-base adsorption energy contribution
ΔG_A^{o}	Free energy change
ΔG_i	Gibbs free energy of immersion
ΔH^{AB}	Enthalpy of adsorption for the acid-base interactions
ΔH_{Ads}	Heat of adsorption
ΔH_A^{o}	Enthalpy change
ΔH_i	Enthalpy of immersion
ΔS_A^{o}	Entropy change
β	Neumann equation of state constant
σ	Specific surface area
Γ	Surface excess
η	Viscosity
ρ_d	Dihedral angles
(hkl)	Miller index for crystalline facets
ρ_L	Density of the adsorbate
ϕ_{SL}	Interaction parameter
ρ	Density
ρ^{α}	Density of liquid phase

ρ^{β}	Density of gas phase
δ_M	Dimensionless parameters for elastic compression
ε_0	Dielectric permittivity in vacuum
ε_i	Dielectric constant
ε_{SL}	Potential energy parameters
θ	Contact angle
Θ	Total amount adsorbed
θ_a	Advancing contact angle
θ_{Ads}	Amount adsorbed
θ_B	Bragg's diffraction angle
θ_e	Equilibrium contact angle
θ_r	Receding contact angle
θ_W	Wenzel's apparent contact angles
θ_Y	Young's contact angles
λ	Dimensionless parameter to describe the amount of adhesion
λ_X	Wavelength of the X-ray source
μ	Chemical potentials
μ	Dipole moment
μ_i	Chemical potential of each component *i*
μ_T	Tabor's parameter
π_e	Equilibrium Spreading pressure
σ	Degree of supersaturation
α	Polarisability

CONTENTS

PREFACE 2

DECLARATION 3

ABSTRACT 5

PUBLICATIONS 7

LIST OF FIGURES 9

LIST OF TABLES 13

LIST OF SYMBOLS 15

CONTENTS 21

CHAPTER 1 INTRODUCTION 27

1.1 Background 27

1.2 Objectives 31

1.3 Thesis Outline 32

CHAPTER 2 INTERMOLECULAR FORCES & WETTING THEORIES 33

2.1 Introduction 33

2.2 Intermolecular Forces 33
2.2.1 van der Waals Forces 34
2.2.2 Hydrogen Bonding 36

2.3 Thermodynamics of Intermolecular Forces 38
2.3.1 Dispersion Forces between Macroscopic Bodies 38
2.3.2 Lifshitz Approach 42

2.4 Thermodynamics of Interfaces 43
2.4.1 Liquid-Vapour Interfaces 43
2.4.1.1 Surface Tension and Surface Energy 43
2.4.1.2 Laplace Equation 45
2.4.1.3 Kelvin Equation 46
2.4.2 Solid-Gas Interface/Adsorption 48
2.4.3 Solid-Liquid Interactions 52

2.5 Thermodynamics of Particle-Particle Interactions 52
2.5.1 Hertz Model 52
2.5.2 Johnson-Kendall-Roberts (JKR) Model 53
2.5.3 Derjaguin-Muller-Toporov (DMT) Model 54
2.5.4 Tabor Parameter 56
2.5.5 Maugis Theory 56

2.6 Thermodynamics of Wetting 58

2.7 The Young Equation 61

2.8 Zisman's Approach 62

2.9 Surface Energy Component Approaches 64
2.9.1 Fowkes' Approach 64
2.9.2 Owens-Wendt Approach 65
2.9.3 Acid-Base Approaches 67

2.10 UNIFAC Approach 71

2.11 Equation of State Models 73

2.12 General Problems with Wetting Theories 74
2.12.1 Contact Angle Hysteresis 76
2.12.2 Wenzel and Cassie-Baxter Equations 77
2.12.3 Use of Hysteresis for Surface Energy Evaluation 84
2.12.4 The Equilibrium Spreading Pressure 85

CHAPTER 3 PROPERTIES OF PHARMACEUTICAL SOLIDS 88

3.1 Introduction 88

3.2 Crystal Growth 90
3.2.1 Solvent Mediated Growth 90
3.2.2 Crystal Growth Mechanisms 91
3.2.2.1 Surface Nucleation 92
3.2.2.2 Screw Dislocation 93
3.2.2.3 Continuous Growth 95
3.2.3 Crystalline Habits 95

3.3 Determination of Crystal Properties 96
3.3.1 Miller Indices 98
3.3.2 Dihedral Angles 99

3.4 The Crystalline State 101
3.4.1 Polymorphs and Enantiomorphs 101
3.4.2 Hydrates and Solvates 102
3.4.3 Amorphous 104

CHAPTER 4 PREPARATION OF CRYSTALLINE SOLIDS AND EXPERIMENTAL METHODOLOGY 107

4.1 Introduction 107

4.2 Materials 107

4.3 Crystal Growth 109
4.3.1 Growth of Thermodynamically Stable Macroscopic Crystals 109
4.3.2 Growth of Thermodynamically Metastable Macroscopic Crystals 114
4.3.3 Cambridge Crystallographic Data Services 115
4.3.4 Facet Identification 122
4.3.5 Attachment Energies 123

4.4 Conclusions 124

CHAPTER 5 EXPERIMENTAL DETERMINATION OF CRYSTALLINE SOLID SURFACE CHEMISTRY 125

5.1 Introduction 125

5.2 Sessile Drop 126

5.3 Capillary Rise 128

5.4 Wilhelmy Plate 131

5.5 Inverse Gas Chromatography 133

5.6 Gravimetric Vapour Sorption 135

5.7 Contact Angles from the Enthalpy of Immersion 137

5.8 X-ray Photoelectron Spectroscopy 138

5.9 Atomic Force Microscope 141

5.10 Experimental Comparison of Characterisation Techniques 144

5.11 Experimental Section 145
5.11.1 Materials 145
5.11.2 Powder Compact Preparation 146
5.11.3 Capillary Rise Measurements 146
5.11.4 Sessile Drop Measurements 148
5.11.5 Inverse Gas Chromatography 148

5.12 Results and Discussion 149
5.12.1 Capillary Rise 149
5.12.2 Sessile Drops on Powder Compacts 153
5.12.3 Vapour Probe Characterisation - IGC 158
5.12.4 Sessile Drop on Single Crystals 160

5.13 Discussion **160**

5.14 Conclusions **162**

CHAPTER 6 CONTACT ANGLES AND SURFACE ENERGETICS OF MACROSCOPIC CRYSTALLINE PHARMACEUTICAL SOLIDS **163**

6.1 Overview **163**

6.2 Introduction **163**
6.2.1 Anisotropic Wettability 165

6.3 Experimental Section **166**

6.4 Results and Discussion **167**
6.4.1 Paracetamol Form I 167
6.4.1.1 Form I Identification *168*
6.4.1.2 Contact Angles for Monoclinic Paracetamol *169*
6.4.2 Paracetamol Form II 175
6.4.2.1 Paracetamol Polymorphs *175*
6.4.2.2 Crystal Habits *175*
6.4.2.3 Contact Angles for Orthorhombic Paracetamol *176*
6.4.3 Aspirin Single Crystals 179
6.4.3.1 Contact Angles for Aspirin *180*
6.4.4 Ibuprofen Crystals 184
6.4.4.1 Contact Angles for Racemic Ibuprofen Crystals *185*
6.4.4.2 Contact Angles for S-(+)-Ibuprofen Crystals *186*

6.5 Conclusions **188**

CHAPTER 7 QUANTIFICATION OF SURFACE CHEMISTRY **191**

7.1 Introduction **191**
7.1.1 Theory 191
7.1.2 The XPS System 194
7.1.3 Photoelectron Emission 195
7.1.4 Application of XPS 196

7.2 Experimental Section **197**
7.2.1 XPS on Single Crystals 197

7.3 Results and Discussion **198**
7.3.1 XPS Analysis on Paracetamol 198
7.3.2 XPS Analysis on Aspirin 207

7.4 Conclusions **212**

CHAPTER 8 SURFACE PROPERTIES OF MILLED AND UNMILLED PHARMACEUTICAL SOLIDS **213**

8.1 Introduction **213**

8.2 Background **213**

8.3 Inverse Gas Chromatography **214**

8.4 Theoretical Aspects of IGC **215**
8.4.1 Infinite and Finite Dilution 215
8.4.2 Determination of Retention Time 217
8.4.3 Determination of Retention Volumes 219
8.4.4 Determination of Thermodynamic Properties 219
8.4.5 Determination of Surface Energy 221

8.5 Experimental Conditions **222**

8.6 Determination of Properties of Crystalline Solids **224**
8.6.1 Crystalline Forms 224
8.6.2 Crystalline Habits 225
8.6.3 Amorphous and Glass Transition 225

8.7 Materials and Methods **230**
8.7.1 Materials 230
8.7.2 Preparation of Fine Crystalline Particulates 231

8.8 Results and Discussion **232**
8.8.1 Dispersive Surface Energy of Milled Paracetamol Crystals 232
8.8.2 Dispersive Surface Energy of Unmilled Paracetamol Crystals 234
8.8.3 Acid-Base Properties of Paracetamol Crystals 235
8.8.4 Dispersive Surface Energy of Aspirin Crystals 242
8.8.5 Acid-Base Properties of Aspirin Crystals 243
8.8.6 Ibuprofen Crystals 246

8.9 Conclusions **248**

CHAPTER 9 DISCUSSION **250**

9.1 Surface Energy Evaluation **250**
9.1.1 Paracetamol Form I and Form II 250
9.1.2 Aspirin 257
9.1.3 Ibuprofen and S-(+)-Ibuprofen 259

9.2 Crystal Habit **262**
9.2.1 Influence of Solvent on Crystal Habit of Aspirin 262
9.2.2 Influence of Solvent on Crystal Habit of Ibuprofen 264

9.3 Conclusions **265**

CHAPTER 10 CONCLUSIONS 266

10.1 Introduction 266

10.2 Overall Summary 266

10.3 Future Work 271

10.4 Final Remarks 272

REFERENCES 273

CHAPTER 1 INTRODUCTION

1.1 Background

On the 20th December 1804, Dr. Thomas Young delivered a lecture entitled "Essay on the Cohesion of Fluids" at the Royal Society of London, which was subsequently published in 1805. His essay, surprisingly, does not contain a single mathematical equation or symbol but marked a starting point in the quest to understand the wetting behaviour of liquids on solid surfaces. Quoting from Young [1]:

"But it is necessary to premise one observation, which appears to be new, and which is equally consistent with theory and with experiment; that is, that for each combination of a solid and a fluid, there is an appropriate angle of contact between the surface of the fluid, exposed to the air, and to the solid."

It is from this statement that the now famous 200 year old Young equation is formed and is given below:

$$\gamma_{SV} = \gamma_{SL} + \gamma_{LV} \cdot \cos\theta \tag{1.1}$$

where γ_{SV}, γ_{SL} and γ_{LV} are the solid-vapour, solid-liquid and liquid-vapour interfacial energies, respectively and θ is the contact angle.

It was not until the work of Duprè who in 1869 introduced the concept of the work of adhesion [2], that the more elegant Young-Duprè relationship was established

as shown in Equation 1.2. The work of adhesion, W_A, is defined as the difference in interfacial energy between adhering and individual separated phases.

$$W_A = \gamma_{LV} \cdot (1 + \cos\theta) \tag{1.2}$$

The Young-Duprè relationship enabled the possibility of determining the solid surface energy from the measurement of liquid contact angles. The use of contact angles in the determination of solid surface energies is complicated by several uncertainties; the validity of the Young-Duprè equation for chemically and/or physically heterogeneous solids, the applicability or suitability of the available experimental techniques for determining the liquid contact angle on a solid, and the intrinsic limitations imposed by the various empirical models used to calculate the surface energy. These issues have been studied for years by many research groups, but have not resulted in a thorough understanding of wetting phenomenon and surface energy determinations.

Contact angles can be obtained via various experimental techniques. For liquid sessile drop measurements, solids are typically prepared by casting the material onto a film or are compacted to form a tablet. Alternatively, particulate solids may be packed into a column, and the rate of liquid rise into the column is measured. This wicking rate may be related to the contact angle via the Washburn equation [3]. The sedimentation volume of particles in a liquid, or the determination of the liquid wetting force for particles adhered to a Wilhelmy plate are also established methods. The adsorption behaviour of vapour on solids can also reveal useful information on the physico-chemical properties of these solids. Mechanical techniques such as zero creep, cleavage and bending plate experiments, as well as calorimetric techniques,

such as the measurement of the heat of immersion, can also reveal surface thermodynamic properties [4].

The applicability and suitability of these techniques are often material dependent. For instance, the conceptually simple mechanical cleavage method suffers severe drawbacks due to plastic deformations in the crack zone which will cause the measured work to be significantly larger than the solid surface energy due to this bulk energy dissipation. The strategy developed here in this thesis aims to evaluate the applicability and suitability of some of these techniques for the evaluation of the surface energy for crystalline pharmaceutical solids. Various measurements with liquid probes for contact angle determination and adsorption of vapour probes are undertaken on both particulate and single crystal samples and are reported in detail in this thesis.

Nicolas Steno, a 17th century Danish physician was probably the first person to study crystalline solids. Crystalline solids are made up by molecules arranged systematically in an ordered manner, which is categorised by its crystal lattice and space group. Such solids assume a characteristic natural shape with well defined facets described as the crystal habit. Each facet is a specific plane which intercepts the axes of the crystal lattice in a particular orientation. An Englishman, Robert Hooke was the first to note that each crystalline solid will preferentially cleave along one specific plane. Frenchman Hauy, in 1784, realised that the angles between crystalline facets for crystals of different sizes, for the same crystalline form, are constant, thus proposing the Law of Interfacial Angles. Although these angles are always constant, the size of each facet may not be and is dependant on their growth conditions. The resulting habit is also of considerable importance for pharmaceutical solids.

As each crystal facet is of a precise orientation, one may well expect that the surface chemistry of different facets to be dissimilar, as each of these planes intersect the lattice uniquely. Though it may appear a rather simple premise that these crystalline facets may possess different surface chemistry, no detailed study on this subject has been reported for crystalline pharmaceutical solids. Furthermore, one could envisage that the cleavage planes observed by Hooke, may possess different surface chemistries. At this point, though it may be sensible to suggest that crystal growth can be explained by surface thermodynamics, one would be imprudent to discount the importance of kinetic effects.

In the seminal work of Zisman and co-workers [5, 6] they observed that the cosine of the contact angles of a homologous series of liquids was linear with respect to the liquid surface tension. This implies that a higher surface tension liquid will exhibit greater contact angles and such that a critical point exists for which the liquid just wets a solid ($\theta \rightarrow 0^{\circ}$). At this critical point, the liquid and solid possess the same surface energy, γ_C. Following on from Zisman's work, two alternate and somewhat opposing surface energy ideas were developed; a surface component approach pioneered by Fowkes [7, 8] and an equation of state model proposed by Neumann [9, 10]. The former assumes that surface energy of both the liquid and solid are made up of various independent components, and that the surface chemistry influences the wetting behaviour. However, the Neumann approach states that for any given set of solids with a surface energy, γ_{SV}, and for a liquid with surface tension, γ_{LV}, there is only one unique contact angle, θ. The applicability of these models to describe the wetting behaviour of crystalline pharmaceutical solids was also investigated and discussed in this thesis.

From the discovery and synthesis of commercial aspirin over a century ago, the pharmaceutical industry has certainly come a long way. Over the past 30 years, with increasing awareness and demands for a healthier and better lifestyle, this industry is, and continues to be amongst of the fastest growing technology sectors. With nearly a quarter of the world's top medicines discovered and developed in Britain, the pharmaceutical industry is certainly of great significance; providing a trade surplus of £2.6 billion in 2002 (£10.03 billion export, £7.45 billion import and is consistently in the top three industrial sectors) and over 300,000 people work directly and indirectly in this industry. With over 80% of drugs administered in the solid form (e.g. tablets, capsules and aerosols), manufacturing continues to be problematic due to the poor knowledge of the properties, such as surface properties, of these complex organic solid materials.

1.2 Objectives

The general objective of this research is to broaden and deepen our understanding of the wetting and surface chemical behaviour of complex organic crystalline solids. The specific aims of this thesis are:

- To establish the validity and suitability of experimental methods for determination of surface properties of pharmaceutical solids,
- To measure the wetting behaviour of crystalline solids, including polymorphs and racemic compounds,
- To review current models for determining the solid surface energy,
- To determine the effects of manufacturing operations, such as milling, on the surface properties of pharmaceutical solids.

1.3 Thesis Outline

This thesis is structured as follows. Chapter 1 describes the background of the current research work, motivation and objectives. Theoretical principles of intermolecular and surface forces, including wetting theories are described in Chapter 2 with an introduction of properties of pharmaceutical solids reported in Chapter 3. Chapter 4 is dedicated to the general methodology of macroscopic single crystal growth, and their crystalline habit identification. The solids prepared include both polymorphs of paracetamol, aspirin, racemic ibuprofen and S-(+)-ibuprofen. Other crystallisation techniques, sample preparation and their subsequent characterisation are detailed in the relevant chapters. Chapter 5 focuses on the techniques for surface characterisation. The experimental evaluation of traditional wetting techniques, and comparisons with our novel method, are discussed in this chapter. In Chapter 6, the contact angles of various probe liquids as measured by the sessile drop for the crystalline systems investigated are presented. Chapter 7 describes the surface chemistry as determined by X-ray photoelectron spectroscopy (XPS). An introduction to Inverse Gas Chromatography, coupled with a literature review of the technique with specific application to pharmaceutical powders, is presented in Chapter 8. This is followed by the evaluation of crystallisation condition and process induced modification effects such as milling on solid surface energy. Further discussion on the computed surface energetic and crystalline habits is given in Chapter 9. Chapter 10 contains the conclusions and suggestions for further work.

This thesis will not only highlight the fundamentally anisotropic surface chemistry of crystalline solids, but also emphasize its potential significance in powder processing operations.

CHAPTER 2 INTERMOLECULAR FORCES & WETTING THEORIES

2.1 Introduction

Intermolecular forces refer to the forces which exist between individual molecules. These are different from the intramolecular forces which hold individual atoms within a molecule. Intermolecular forces exist in all states of matter, but their orders of magnitude can vary enormously. They are responsible for phenomena as diverse as the liquefaction of nitrogen to the solidification of carbon dioxide.

2.2 Intermolecular Forces

The behaviour of gases was observed and described by Englishman Robert Boyle (1627-1691) who proposed the relationship between volume and pressure, while Frenchman Jacques Charles (1746-1823) proposed the proportionality of volume to temperature. This gave rise to a simple relationship for gases known as the perfect gas law described by $pV = nRT$. Unfortunately, this relationship does not apply for real gases due to the presence of intermolecular forces and the finite size of gas molecules which were neglected by the perfect gas law. Dutchman Johannes Dideric van der Waals (1837-1923), proposed a relationship which took into account both the molecular volume and intermolecular forces between molecules in gases, which resulted in him being awarded the 1910 Nobel Prize for Physics. The van der Waals equation is shown as:

$$\left(p + \frac{a_{vdW}}{v^2}\right)(v - b_{vdW}) = RT \tag{2.1}$$

where p is the pressure, T the temperature, ν the specific molar volume of the molecules and R the universal gas constant. The constants a_{vdW} and b_{vdW} are the van der Waals constants which take into account the attractive intermolecular forces and molecular volume respectively.

Although the van der Waals forces are generally smaller than Coulombic or hydrogen bonding interactions, they are of considerable importance due to their presence in all materials.

2.2.1 van der Waals Forces

van der Waals forces refer to all intermolecular interactions that arise due to temporary fluctuating dipoles (London dispersion forces), dipole-dipole interactions (Keesom forces) and dipole-induced dipoles forces (Debye forces). A special type of dipole-dipole interaction is the hydrogen bonding and will be elaborated in the next section, though it is not considered to be a type of van der Waals force. Israelachvili has discussed all these intermolecular forces in detail [11], and they are summarised here in this thesis below.

The electrons within an atom or molecule orbit around the nucleus chaotically causing random fluctuations in the electron cloud density. Instantaneously, such fluctuations result in the formation of instantaneous dipoles. These temporary dipoles, which can also reverse in direction which will induce dipoles in neighbouring atoms, and these induced dipole - induced dipole interactions are termed the London dispersion forces. Such temporary fluctuations are present in all molecules, including the most symmetrical ones. The magnitude of the London dispersion forces generally increases with increasing number of electrons.

London in 1930 proposed that the potential energy due to these interactions between a pair of neutral molecules can be written as:

$$U(r) = \frac{-3\alpha^2 h\upsilon}{4(4\pi\varepsilon_0)^2 r_s^{\,6}} \tag{2.2}$$

where α is the polarisability, ε_0 is the dielectric permittivity in vacuum (8.854 x 10^{-12} $C^2\ J^{-1}\ m^{-1}$), *h* the Plank constant of 6.626 x 10^{-34} J s, υ the frequency of fluctuation and r_S the separation distance. London dispersion forces are inversely proportional to the sixth power of their interatomic distances.

Now, let us consider a molecule such as HCl, where the chlorine atom is much more electronegative than the hydrogen. The HCl molecule will have a permanent dipole resulting in a negatively charged chlorine side and a positively charged hydrogen side. The permanent dipole, in addition to the London dispersion forces already present, will cause the HCl molecules to exhibit a stronger interaction with each other, resulting in higher boiling points.

For two molecules with permanent dipoles, Keesom suggested that their potential energy can be written as:

$$U(r) = \frac{-\mu_1^2 \mu_2^2}{3(4\pi\varepsilon_0)^2 kTr_s^{\,6}} \tag{2.3}$$

where μ is the dipole moment (C m) with the subscript denoting species 1 and 2, k is the Boltzmann constant of 1.381 x 10^{-23} J K^{-1} and T the absolute temperature in Kelvin. The Keesom potential energy between dipole-dipole molecules is inversely proportional to the sixth order of their interatomic distances.

Additionally, in the case of polar molecules where intermolecular forces arise due to induced dipole - dipole interactions, Debye proposed that their potential energy be related by:

$$U(r) = \frac{-\alpha\mu^2}{(4\pi\varepsilon_0)^2 r_s^{\,6}} \tag{2.4}$$

The Debye potential energy is also inversely proportional to the sixth order of their interatomic distances.

2.2.2 Hydrogen Bonding

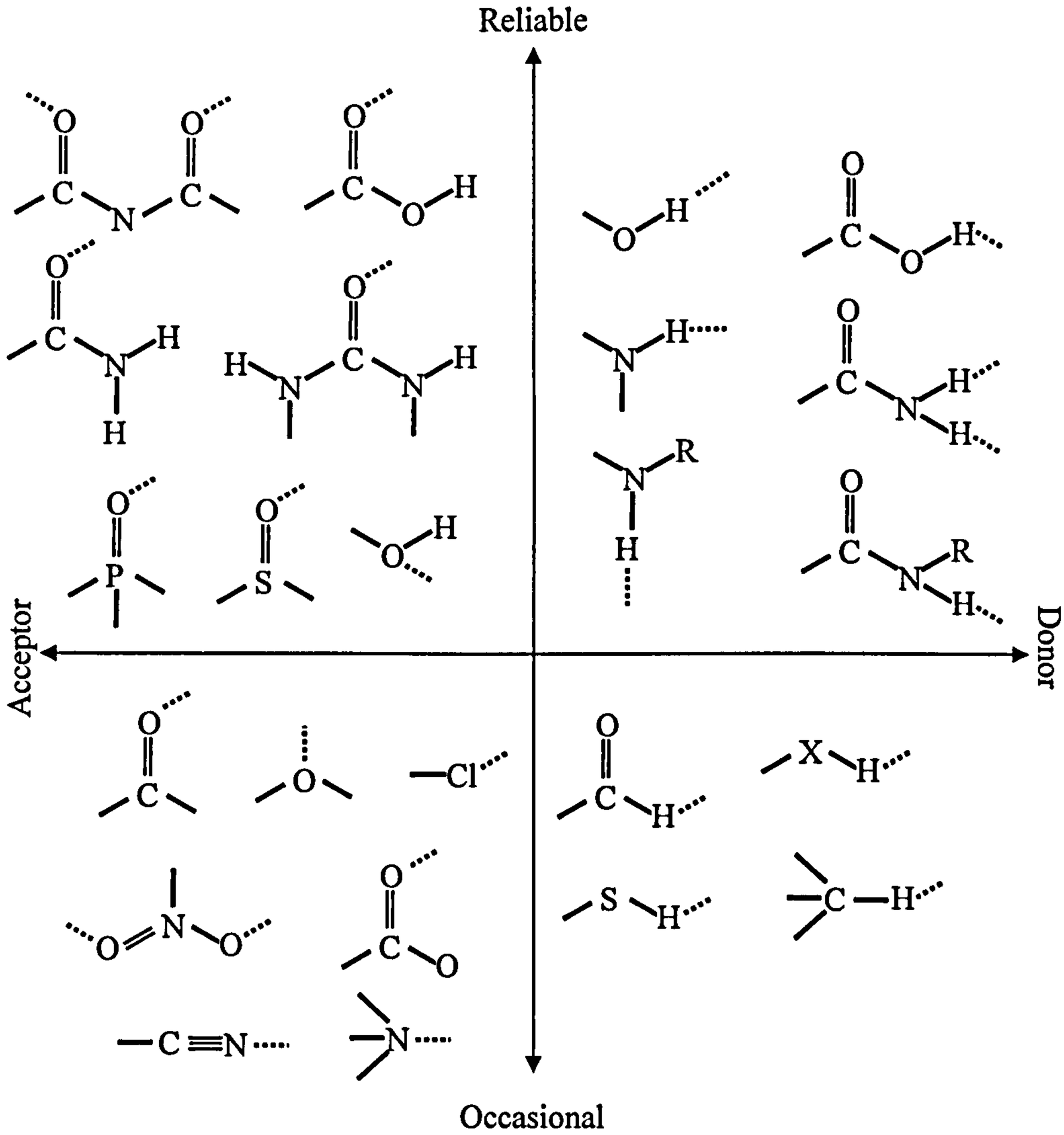
Hydrogen bonds can be regarded as a specific type of dipole-dipole interaction. They occur via the interaction of an electron poor hydrogen atom, which is typically attached to an electron rich atom with lone pair electrons, such as oxygen, fluorine or nitrogen. Hydrogen bonds are much stronger than ordinary dipole-dipole interactions and are very directional by nature, and operate over much shorter distances. They are also known as specific forces or short range interactions in which a partial chemical bond is formed via the donation of electron density from electron pair donor, to the acceptor. Electron redistribution is an essential feature of these bonds.

Although hydrogen bonds can be the most important intermolecular forces, they are still relatively poorly understood and our understanding is rudimentary at present. Recently, Pak et al. investigated the nature of hydrogen bonds for a range of systems, illustrating the great range in hydrogen bonding characteristics [12]. For the organic materials investigated in this thesis, hydrogen bonds could form between carbonyl, hydroxyl, amide, amine or ester groups. These groups are classified as reliable and occasionally donors or acceptors as shown in Figure 2.1 [13]. The hydrogen bond is also present in crystalline structures and is thought to have a critical effect on the alignment or arrangement of molecules in the crystal lattice [14, 15]. A comprehensive review on the theory of hydrogen bonds is given by Kollman and Allen [16], and on hydrogen bonds in the solid-state by Steiner [17].

In the case of neutral organic solids it is currently safe to assume that van der Waals and hydrogen bonds are the two most important for types of intermolecular forces. Those forces which could arise from the likes of electrostatic or columbic

interactions will not be discussed, though these interactions will be very important in the case of salt complexes, commonly encountered in industrially manufactured pharmaceutical products.

Figure 2.1: Reliable and occasional hydrogen bond acceptors and donors [18]. Functionalities are grouped into quadrants with top right (moving anti-clockwise) for reliable donors, reliable acceptors, occasional acceptors and occasional donors respectively. Their individual position is not representative of the potential hydrogen bond strength.



2.3 Thermodynamics of Intermolecular Forces

London dispersion forces are present in all molecules and are of greater significance and prevalence than the Keesom and Debye interactions. The following derivations for interactions between macroscopic bodies will only consider the dispersion forces.

2.3.1 Dispersion Forces between Macroscopic Bodies

Let us consider a single molecule interacting with a flat solid surface (Figure 2.2). If we assume the total interaction to be the summation of all its intermolecular interaction with all the molecules at the flat surface, and assuming simple additivity, the potential energy, U can be written as:

$$dU = \frac{-3\alpha^2 h\nu}{4(4\pi\varepsilon_0)^2 r_s^{\,6}} dn \tag{2.5}$$

where n is the number of molecules given by:

$$dn = 2\pi\rho da \cdot dx \tag{2.6}$$

where ρ is the density of molecules on the surface.

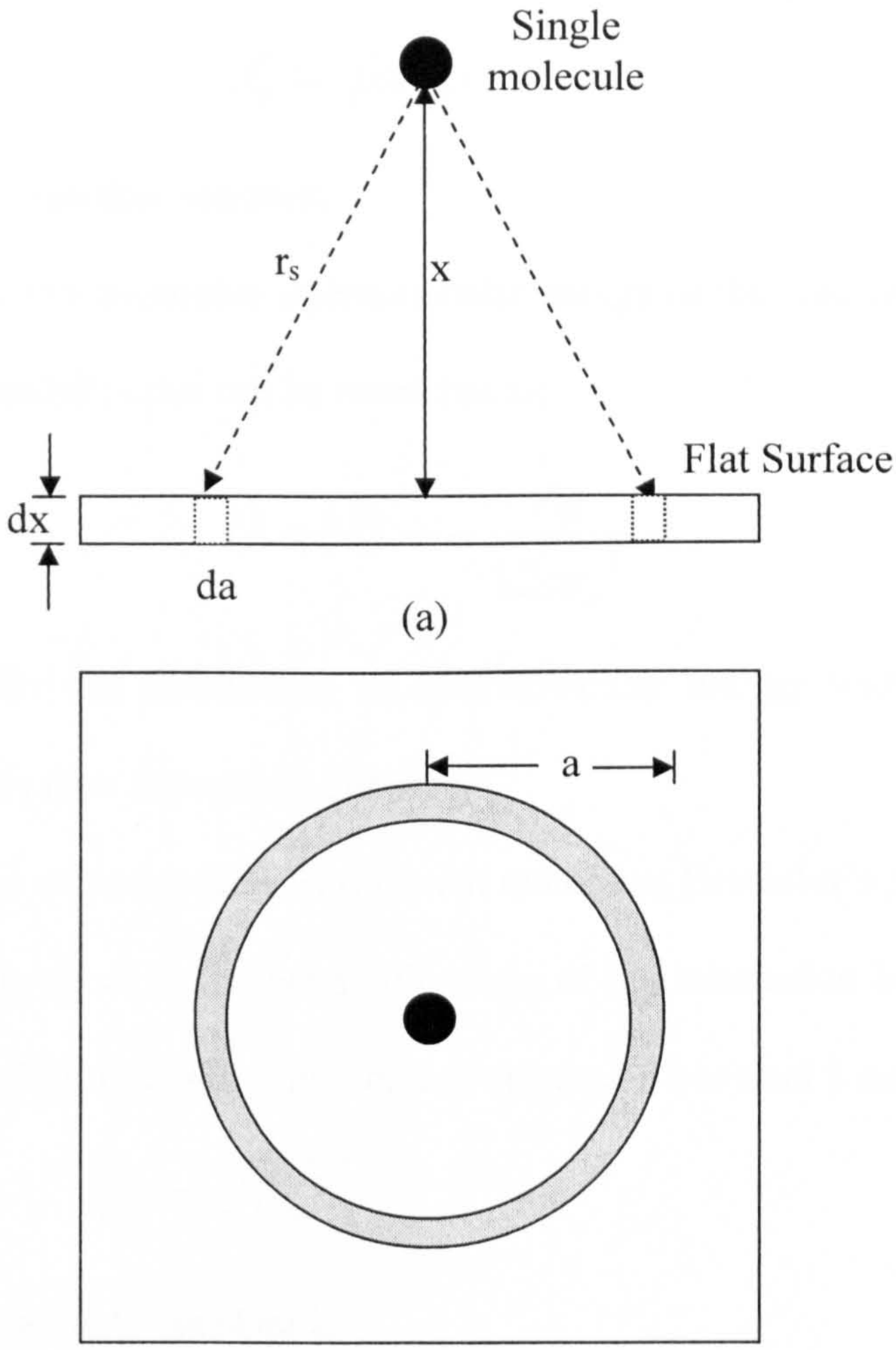
By integrating Equation 2.5 for da from 0 to ∞ and for dx from H to ∞, one will obtain the following:

$$U = \int_H^\infty \int_0^\infty \frac{-3\alpha^2 h\nu}{4(4\pi\varepsilon_0)^2 (x^2 + a^2)^3} \cdot 2\pi\rho \cdot da \cdot dx \tag{2.7}$$

$$U = \frac{-\beta\pi\rho}{6H^3} \tag{2.8}$$

where β is a constant of $\frac{-3\alpha^2 h\nu}{4(4\pi\varepsilon_0)^2}$.

Figure 2.2: Interaction between single molecule and a flat surface (a) side view and (b) top view.



In the case of two parallel surfaces, the number of molecules now present has increased and can be given by dn = ρ dh, which will result in the following:

$$U = \frac{-\beta\pi\rho^2}{12H^2} \tag{2.9}$$

Derivations for the potential energy between various geometries can be found elsewhere [11, 19].

Hamaker conducted pair-wise summation of the dispersion energies and proposed that the interaction between two macroscopic bodies at short distances can be given by:

$$A_{ii} = \beta\pi^2\rho^2 \tag{2.10}$$

where A_{ii} is the Hamaker constant.

As such, the dispersive intermolecular energy or the free energy of interaction between two parallel plates can be rewritten as:

$$U = \Delta G = -\frac{A_{ii}}{12\pi r_s^{\,2}} \tag{2.11}$$

which allows for the calculation of intermolecular energy with known Hamaker constants and r is their separation distances.

In the case of two bodies of different materials, Berthelot's principle states that the interaction is equal to the geometric mean of the interaction between each of the same materials [20]. Likewise, the London dispersion constant β can be written as:

$$\beta_{ij} = \sqrt{\beta_{ii}\beta_{jj}} \tag{2.12}$$

And the Hamaker constant is:

$$A_{ij} = \sqrt{A_{ii}A_{jj}} \tag{2.13}$$

Fowkes [21] proposed that the dispersive surface energy, $\gamma_i^{\,d}$ can be written as:

$$\gamma_i^d = -\frac{\pi\rho^2\alpha^2}{8r_s^2}\frac{h\nu}{(4\pi\varepsilon_0)^2} \tag{2.14}$$

The Hamaker constant can now be written in terms of dispersive surface energies as given by:

$$A_{ii} = 6\pi r_{ii}^2\gamma_i^d \tag{2.15}$$

where r_{ii} is the distance between interacting atoms. The value of πr_{ii}^2 is found to be approximately constant for most material (but seriously underestimated for highly polar hydrogen bonded liquids) and as such allows for the direct calculation of the Hamaker constants from values of γ_i^d and vice versa [22].

For two identical bodies interacting via a third medium phase, the Hamaker combining rule can be written as:

$$A_{131} \approx A_{11} + A_{33} - 2A_{13} \tag{2.16}$$

$$A_{131} \approx \left(\sqrt{A_{11}} - \sqrt{A_{33}}\right)^2 \tag{2.17}$$

where A_{11} and A_{33} are the Hamaker constants of the solid and the medium respectively in vacuo.

In the case where the two bodies are different, interacting in a medium, the Hamaker combining rule can be written as:

$$A_{132} \approx A_{12} + A_{33} - A_{13} - A_{23} \tag{2.18}$$

$$A_{132} \approx \left(\sqrt{A_{11}} - \sqrt{A_{33}}\right)\left(\sqrt{A_{22}} - \sqrt{A_{33}}\right) \tag{2.19}$$

Good, Girifalco and Fowkes proposed that if only dispersive forces are present, the interaction forces between two condensed phases can be written as:

$$\gamma_{12}^d = \left(\sqrt{\gamma_1^d} - \sqrt{\gamma_2^d}\right)^2 \tag{2.20}$$

$$\gamma_{12}^d = \gamma_1^d + \gamma_2^d - 2\sqrt{\gamma_1^d \gamma_2^d} \tag{2.21}$$

The work of adhesion defined by Duprè is given by:

$$W_A = \gamma_1 + \gamma_2 - \gamma_{12} \tag{2.22}$$

Substituting Duprè's relation to Good, Girifalco and Fowkes' combining rule, the dispersive work of adhesion can be written as:

$$W_A = 2\sqrt{\gamma_1^d \gamma_2^d} \tag{2.23}$$

The above equation, with Young's contact angle equation, is routinely used for characterisation of solid surface energy and is elaborated in detail in Section 2.6.

2.3.2 Lifshitz Approach

Lifshitz avoided the problems associated to additivity proposed by the earlier approaches of Hamaker. By ignoring the atomic structure and treating the forces macroscopically between large bodies as continuous media, the Lifshitz theory is derived from dielectric constants and refractive indices [11]. The derivations involved with the formulation of the Lifshitz model are very complicated, requiring a thorough understanding of quantum field theory. The Hamaker constants evaluated by the Lifshitz model are given by Equations 2.24 and 2.25 for like and unlike bodies interacting in a medium, respectively and are shown as follows:

$$A_{131} = \frac{3}{4}kT\left(\frac{\varepsilon_1 - \varepsilon_3}{\varepsilon_1 + \varepsilon_3}\right)^2 + \frac{3h\nu}{16\sqrt{2}}\left[\frac{\left(n_1^2 + n_3^2\right)^2}{\left(n_1^2 - n_3^2\right)^{\frac{3}{2}}}\right] \tag{2.24}$$

$$A_{132} = \frac{3}{4}kT\left(\frac{\varepsilon_1 - \varepsilon_3}{\varepsilon_1 + \varepsilon_3}\right)\left(\frac{\varepsilon_2 - \varepsilon_3}{\varepsilon_2 + \varepsilon_3}\right) + \frac{3h\nu}{8\sqrt{2}}\frac{\left(n_1^2 - n_3^2\right)\left(n_2^2 - n_3^2\right)}{\left(n_1^2 + n_3^2\right)^{\frac{1}{2}}\left(n_2^2 + n_3^2\right)^{\frac{1}{2}}\left\{\left(n_1^2 + n_3^2\right)^{\frac{1}{2}} + \left(n_2^2 + n_3^2\right)^{\frac{1}{2}}\right\}} \tag{2.25}$$

where n_i and ε_i are the refractive index and dielectric constant respectively for phase i.

The main limitation to the Lifshitz approach is that the theory based on the continuum theory is only true when the interacting surfaces are further apart than molecular dimensions. The practical use of this theory is dependent on the availability of the dielectric constant for the materials of interest.

2.4 Thermodynamics of Interfaces

2.4.1 Liquid-Vapour Interfaces

2.4.1.1 Surface Tension and Surface Energy

Within the bulk of a material each molecule is attracted symmetrically in all directions. However, for a molecule at the surface there is a net attractive force towards the interior of the fluid. This force imbalance causes the molecules at the surface to be attracted towards the bulk. The contractile force is also known as the surface tension, which for a liquid tends to minimise the surface area to volume ratio. This phenomenon results in liquid droplets adopting a spherical shape as the internal pressure of the droplet is in equilibrium with the surface tension.

The term surface tension and surface energy are often assumed identical, but this analysis has been disputed [23]. In this thesis, we shall express the surface tension, γ_L as the force which is in equilibrium with the pressure difference for a curved interface while the surface energy, γ_S is the free energy of a solid surface, calculated from the contact angle between a liquid droplet and a solid surface [23].

Surface tension and surface free energy are often defined as the reversible work, W required to create a new surface area, A as shown in Equation 2.26.

$$\gamma \cdot dA = \Delta W \tag{2.26}$$

Equation 2.26 can be substituted into the first law of thermodynamics where the work term is for both a pressure-volume and the associated chemical work. For a reversible process, the second law describes that dQ = T dS, resulting in:

$$dU = dQ + dW \tag{2.27}$$

$$dU = TdS + \gamma dA - pdV \tag{2.28}$$

where γdA is associated with the work to create new surface areas and pdV the work done by the system due to the increase in volume and hence the negative convention for work done by the system.

Recalling Gibbs energy, Equation 2.28 can be rewritten as:

$$dG = dH - d(TS) \tag{2.29}$$

$$dG = dU + d(pV) - d(TS) \tag{2.30}$$

$$dG = TdS + \gamma dA - pdV + pdV + Vdp - TdS - SdT \tag{2.31}$$

For a system at constant temperature, pressure and volume, Equation 2.31 is reduced to:

$$dG = \gamma dA \tag{2.32}$$

$$\gamma = \left(\frac{\partial G}{\partial A}\right)_{T,p,V} \tag{2.33}$$

This shows that the change in Gibbs free energy due to a change in surface area and is related directly to the non pressure-volume work term. It also goes on to show that the surface tension can now be described solely as a thermodynamic state function which is totally independent of the path taken.

Since the surface tension is identical to the excess Gibbs free energy, the change in surface excess entropy, S^s can also be evaluated as shown by:

$$-S^s = \left(\frac{dG^s}{dT}\right)_p = \left(\frac{d\gamma}{dT}\right)_p \tag{2.34}$$

The free energy at the surface results in attractive forces between materials. For two separate and different bodies, the work associated with holding them together at an interface is termed the adhesive work, W_A while the work associated to holding together molecules within the same body is called the cohesive work, W_C.

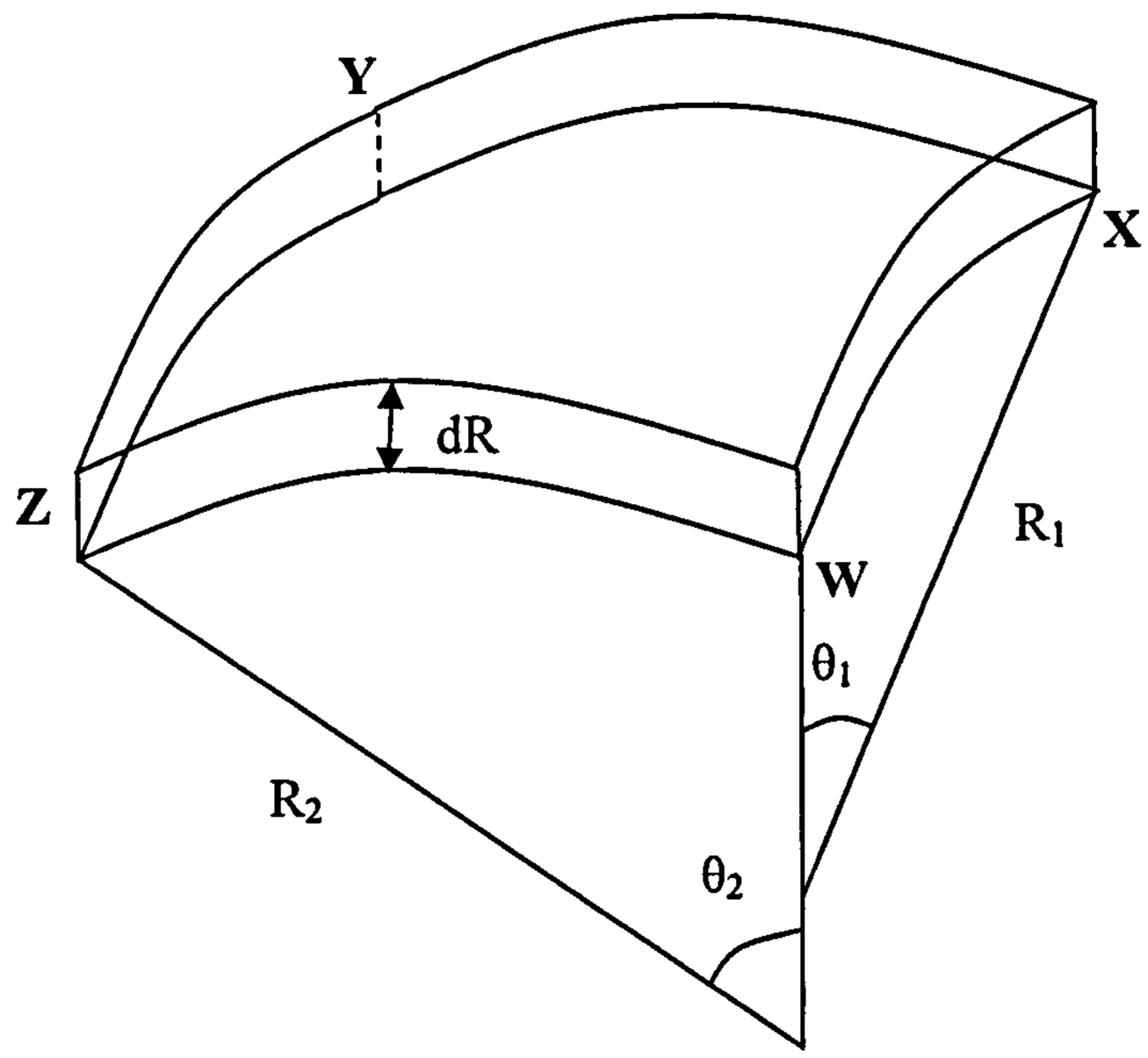
2.4.1.2 Laplace Equation

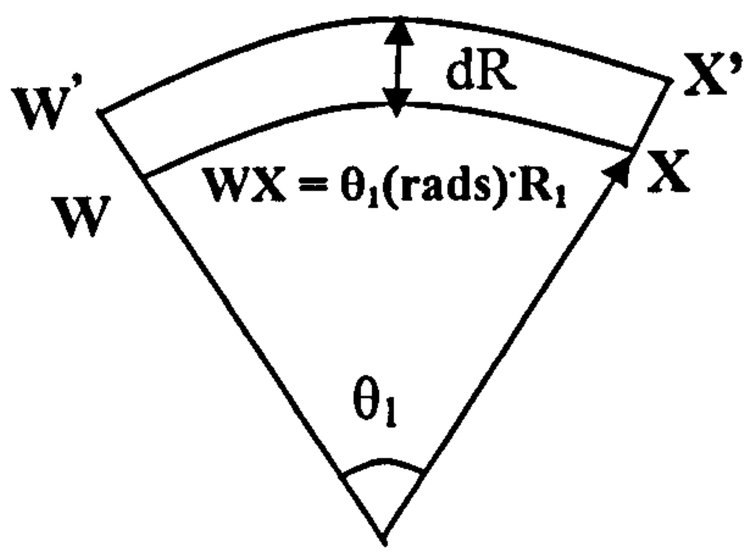
For a bubble of air with a curved interface within a liquid phase, the pressure difference across this interface can be described by the Laplace equation. A non-symmetric curved interface can be defined by two radii (R_1 and R_2) of curvatures as shown in Figure 2.3. If the bubble is increased in size, then the associated increase in surface area is given by:

$$dA = \frac{WX}{R_1}\left(R_1 + dR\right)\cdot\frac{WZ}{R_2}\left(R_2 + dR\right) - WX \cdot WZ \tag{2.35}$$

$$dA = WX \cdot WZ \cdot dR \cdot \left(\frac{1}{R_1} + \frac{1}{R_2}\right) \tag{2.36}$$

Figure 2.3: A curved interface across an air bubble – liquid system.





$$W'X' = \theta_1(rads)\cdot\left(R_1 + dR\right)$$

$$W'X' = \frac{WX}{R_1}\cdot\left(R_1 + dR\right)$$

The increase in surface energy is γdA while the work done by the bubble is shown in Equation 2.37. Because the surface tension is balanced by the internal pressure, their relation is shown as Equation 2.38, which is the Laplace equation.

$$\Delta p \cdot WX \cdot WZ \cdot dR = \gamma \cdot dA \tag{2.37}$$

$$\Delta p = \gamma \cdot \left(\frac{1}{R_1} + \frac{1}{R_2} \right) \tag{2.38}$$

Since the radius of a bubble is always positive, the pressure difference $\Delta p = p_1 - p_2$ is also positive indicating that the pressure on the concave side is always greater. In a simpler case, we shall consider the case of a spherical bubble. The spherical bubble will have an equal radius of R with the increase of surface area $dA = 8\pi Rdr$ while the increase in surface energy is γdA. The Laplace equation for a spherical bubble can be written as:

$$\Delta p \cdot 4\pi R^2 \cdot dR = \gamma \cdot dA \tag{2.39}$$

$$\Delta p \cdot 4\pi R^2 \cdot dR = \gamma \cdot 8\pi R \cdot dR \tag{2.40}$$

$$\Delta p = \frac{2\gamma}{R} \tag{2.41}$$

This result is exactly the same if one replaces $R_1 = R_2 = R$ in Equation 2.38. The Laplace equation can be used to describe liquid capillary rise phenomena.

2.4.1.3 Kelvin Equation

The Laplace equation describes the pressure difference between two regions of a liquid-vapour interface of radius R. The actual pressure above a spherical drop can be described by the Kelvin equation. There are various ways to derive the Kelvin equation, one of which is based on the equality of chemical potentials for equilibrium systems as shown below.

For a system in equilibrium, the chemical potentials, μ within (α) or outside (β) a droplet of radius R or infinite radius (R = ∞), in the case of a flat plane surface, can be written as:

$$\mu_r^{\alpha} = \mu_r^{\beta} \quad and \quad \mu_{\infty}^{\alpha} = \mu_{\infty}^{\beta} \tag{2.42}$$

Hence:

$$\mu_r^{\alpha} - \mu_r^{\beta} = \mu_{\infty}^{\alpha} - \mu_{\infty}^{\beta} \tag{2.43}$$

$$d\mu^{\alpha} = d\mu^{\beta} \tag{2.44}$$

However, $dp=\rho d\mu + sdT$ which can be reduced to $d\mu = dp/\rho$ for a constant temperature system. Replacing this relationship into Equation 2.44 will result in:

$$\int_{p_{\infty}^{\alpha}}^{p_r^{\alpha}} \frac{dp}{\rho^{\alpha}} = \int_{p_{\infty}^{\beta}}^{p_r^{\beta}} \frac{dp}{\rho^{\beta}} \tag{2.45}$$

Assuming that the liquid phase is non-compressible, the term ρ^{α} is then a constant and can be taken out of the integrals. The ρ^{β} term can be approximated if the gas phase is assumed to be ideal by the perfect gas relationship. The pressures p^{α}_{∞} and p^{β}_{∞} are assumed to be equal to the vapour pressure, p_v and $p^{\alpha}_r - p^{\beta}_r$ is given by the Laplace equation. The combination of all these relationships results in the following:

$$\frac{1}{\rho_L} \cdot \int_{p_v}^{\frac{2\gamma}{r}+p} dp = \int_{p_v}^{p} \frac{RT}{pM} dp \tag{2.46}$$

$$\frac{1}{\rho_L} \cdot \left[\frac{2\gamma}{r} + p - p_v\right] = \frac{RT}{M} \ln\left(\frac{p}{p_v}\right) \tag{2.47}$$

where R in Equation 2.47 relates to the universal gas constant (8.314 J mol^{-1} K^{-1}) while M is the molecular weight and T the absolute temperatures in Kelvin.

In the case where $2\gamma/r$ is much larger than $(p-p_v)$, one can neglect the latter term which reduces Equation 2.47 to the following, which is the Kelvin equation.

$$\ln\left(\frac{p}{p_v}\right)=\frac{M}{RT\rho_L}\cdot\left(\frac{2\gamma}{r}\right) \tag{2.48}$$

The Kelvin equation can also be applied to the case of a solid, where the solid's solubility in liquid is determined by its activity. The term p/p_v is replaced by this activity term, a_a/a_a^o where a_a^o is the activity of the dissolved solute in equilibrium with a flat surface. A conceptually simpler derivation was provided by Galvin, based on hydrodynamics as opposed to the thermodynamics approach given above [24].

2.4.2 Solid-Gas Interface/Adsorption

In this section, the adsorption of vapour and gas phase molecules onto a solid surface is reviewed. The adsorption of solute molecules from solution is however not considered here.

The phenomenon of gaseous molecules attaching themselves onto a solid surface can occur via two general mechanisms; physisorption and chemisorption [25]. Of course, fundamentally this distinction is arbitrary, and cases exist which are difficult to classify as being simply physisorption or chemisorption. The latter involves the formation of chemical bonds of which the enthalpy involved is comparable to the heat of reaction. In physisorption, the energy involved is similar to those required for liquefaction and is completely reversible for a non-porous solid. A third mechanism for gas-solid interactions can also occur whereby the vapour molecules are "dissolved" into the interior of the solid, and the phenomenon is referred to as absorption. The term sorption is usually used to describe a process in which both adsorption and absorption occurs. The solid is termed the adsorbent whilst the vapour molecules are the adsorbate. It is also often difficult to distinguish adsorption at the surface from adsorption within pores of solid. Two important

theories (Langmuir and Brunaeur, Emmett and Teller, BET) for the evaluation of the adsorption phenomena consider this issue and they will be described briefly.

During a physisorption process, no chemical bonds need be broken and it is a spontaneous process typically due to van der Waals forces (since the interaction between two bodies possesses a negative Gibbs free energy). As such, the process of adsorption is an exothermic process which is less favourable at higher temperatures. At constant temperatures, the amount of vapour molecules able to adsorb will be dependant on its vapour pressure. Adsorption behaviour is typically evaluated by experimentally measuring the amount of adsorbate adsorbed as a function of the vapour pressure, resulting in an adsorption isotherm.

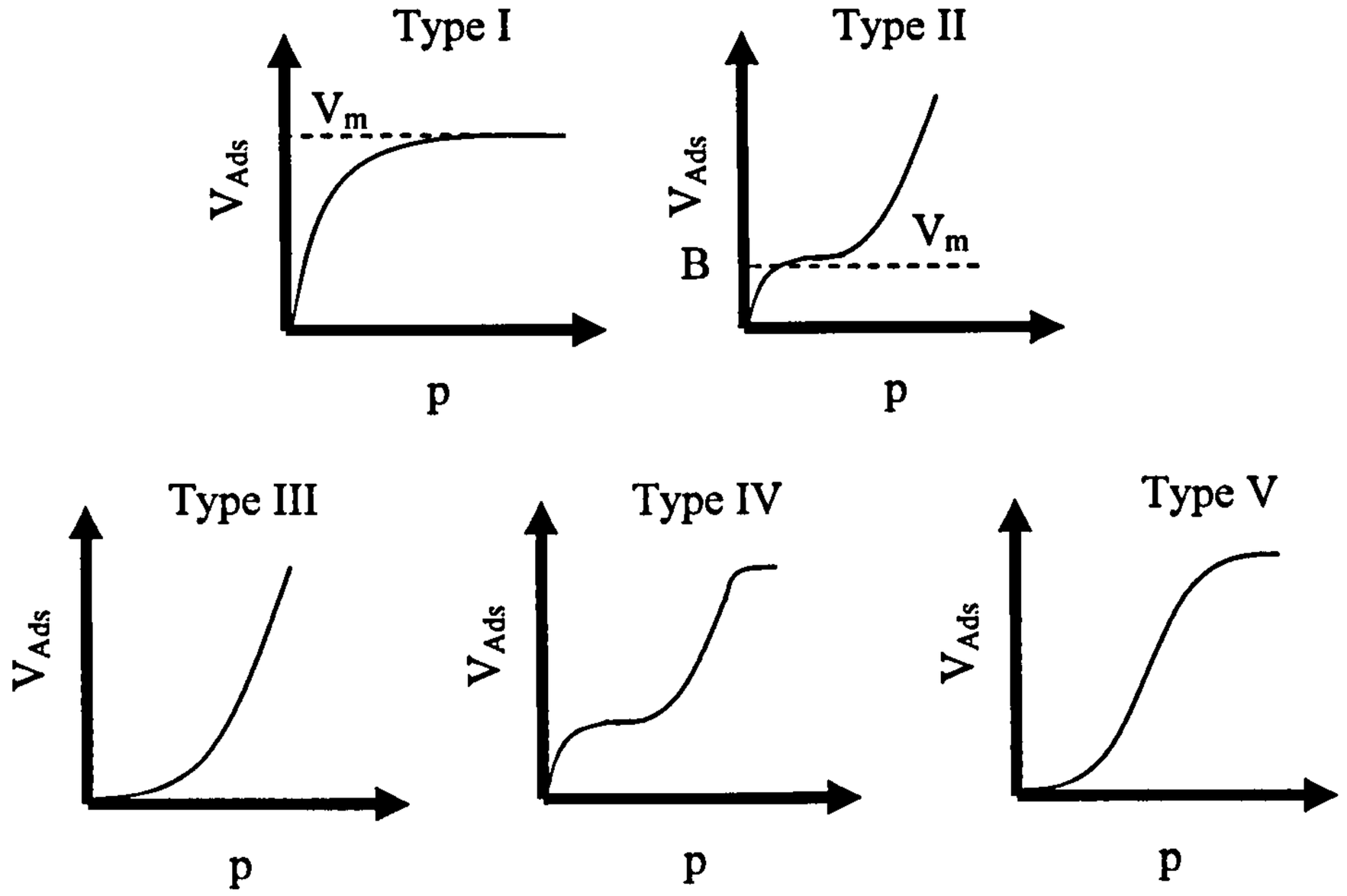
There are five main types of adsorption isotherms (Figure 2.4), the differences arise due to variations in the thermodynamics and the adsorption mechanisms involved. The plateau exhibited for type I adsorption represents the formation of an adsorbate monolayer, and is described by Langmuir's isotherm. The rapid rise in amount adsorbed for the initial increase of pressure is indicative that the adsorption process is more likely a chemisorption rather than a physisorption event, as the former phenomenon normally does not go beyond the formation of a monolayer. This adsorption type has been described by Langmuir [26, 27]. The surface coverage can be predicted assuming that heat of adsorption is independent of surface coverage, using Langmuir's equation (2.49):

$$\theta_{Ads} = \frac{b_L p}{1 + b_L p} \tag{2.49}$$

where θ_{Ads} is the amount adsorbed, p is the pressure and b_L the equilibrium constant. Equation 2.49 can be derived from both thermodynamic and kinetic theories.

BIBL. LONDON. UNIV

Figure 2.4: Classification of adsorption isotherms.



Type II adsorption isotherms are representative of a multilayer physical adsorption process. At point B (Figure 2.4), the formation of a monolayer of adsorbate is complete, which is followed by multilayer adsorption with increasing vapour pressure. The asymptote represents the point where liquefaction occurs. Type II is typically associated with physisorption. This type of adsorption isotherm has been described by BET [28] and is given by:

$$\frac{x}{V_{Ads}(1-x)} = \frac{1}{V_m c_{BET}} + \frac{x \cdot (c_{BET} - 1)}{V_m c_{BET}} \tag{2.50}$$

where V_{Ads} is the volume of adsorbed molecules with V_m the monolayer volume, x is the relative pressure (p/p_o). The term c_{BET} arises from the algebraic rearrangement of the series approximation for the determination of subsequent i^{th} layer adsorption volumes. By plotting x/V(1-x) versus x, the value of V_m can be determined from the addition of the slope and intercept without the need to evaluate c_{BET} *a priori*. This equation forms the basis of the standard BET method for surface area analysis.

Type III isotherms are typical where the forces between adsorbent and adsorbate are weak. The amount of adsorbate adsorbed starts to increase only at higher pressures and after the initial adsorption, which provides more favourable sites for adsorption. Type III is characteristic for adsorption of moisture on a hydrophobic surface where surface clustering will occur. Type IV meanwhile is reflective of capillary condensation of the adsorbates in pores. Types II and IV are closely related as are types III and V. Often, it may be difficult to distinguish or assign an experimental adsorption isotherm to a sole isotherm type, as they may well be a combination of two or more types.

The thermodynamics for adsorption was given by Gibbs in the form of an equation of state for 2-dimensional matter. Bare solid surfaces are recognised to possess higher surface energy compared to one with vapour adsorbed. The adsorption of molecules onto a surface is known to result in a 2-dimensional pressure termed the spreading pressure, π_e which can be evaluated via ellipsometry or a gravimetric vapour sorption technique as described in Section 5.6.

The energies involved in the adsorption of vapour could be written as:

$$\ln\left(\frac{p_2}{p_1}\right) = -\frac{\Delta H_{Ads}}{R} \cdot \left(\frac{1}{T_2} + \frac{1}{T_1}\right) \tag{2.51}$$

where ΔH_{Ads} is the heat involved in the adsorption process. The derivation of Equation 2.51 is essentially the same as that proposed by Clausius-Clapeyron for determination of vapour pressures.

Two types of heterogeneity; a physical and a chemical can be observed for adsorption phenomena. For heterogeneous systems, various models have been developed for the evaluation of pore size and energy distributions. The evaluation of pore distribution for mesopores are given by the Barrett, Joyner and Halenda model

(BJH) [29] and for micropores, by the Dubinin-Radushkevich model. The evaluation of energetic heterogeneities from a single adsorption isotherm was recently given by Liu et al. [30]. The phenomena of adsorption have been reviewed extensively and can be found in the following literature [31-33] and for binary mixtures by Talu [34].

2.4.3 Solid-Liquid Interactions

In this thesis, the discussion of solid-liquid interactions will focus on the phenomena of wetting and spreading. The wetting behaviour of materials is governed by the solid surface energies. A range of techniques for evaluation of solid surface energy are investigated and are presented in Chapter 5. The thermodynamics involved in wetting and the evaluation of solid surface energy from contact angle measurements, including certain associated complications and problems are presented in Section 2.6.

2.5 Thermodynamics of Particle-Particle Interactions

2.5.1 Hertz Model

The first analysis of contact mechanics was initiated by German Heinrich Hertz who investigated the contact between two smooth elastic bodies [35]. This model neglects both adhesion and surface forces, and considers a smooth elastic sphere in contact with a rigid flat surface. Hertz demonstrated that the contact radius, a of a spherical particle with radius, R_p subjected to a force, F where its adhesion force is zero can be described by:

$$a^3 = \frac{R_p}{K} F \tag{2.52}$$

and the reduced Young's Modulus, K is given by:

$$\frac{1}{K} = \frac{3}{4}\left(\frac{1-v_p{}^2}{E} + \frac{1-v_{pi}^2}{E_i}\right) \tag{2.53}$$

where ν_p is the Poisson's ratio and E the Young's modulus of the flat surface. The subscript *i* denotes the properties for the two contacting bodies.

This model assumes linear elasticity of the bodies and normal loading conditions. The contacts between the surfaces are frictionless resulting in the transfer of only normal stresses. In the case of high loadings or low surface forces, the Hertz theory may be applicable. At high loads, the additional adhesive contact forces, which are typically small, may be negligible. As loading is decreased, these adhesive forces may become more prominent. Experiments at low loads for smooth rubber spheres and glass spheres have confirmed that surface attraction was strong in the case of clean and dry surfaces [36]. The effect of surface attraction forces are taken into account by subsequent models discussed below.

2.5.2 Johnson-Kendall-Roberts (JKR) Model

In the case where the surface forces are considerable, the contact radius at equilibrium is expected to be larger than the contact radius predicted by the Hertz model. The contact radius, *a* is estimated as follows:

$$a = \left[\frac{R_p}{K} \left(F_{Adh} + 3\pi R W_{Adh} + \sqrt{6\pi R F_{Adh} W_{Adh} + (3\pi R W_{Adh})^2} \right) \right]^{\frac{1}{3}} \quad (2.54)$$

where F_{Adh} is the adhesion force, W_{Adh} the work of adhesion and R the particle radius.

The apparent load can be calculated based on the Hertz theory by substituting the contact radius with this corresponding contact radius. Johnson et al. consider the case where the attractive forces are short range and occur within the contact area neglecting long range forces outsides this area [36].

The additional attraction is thought to result in the formation of a neck region due to compression within, and tension at the annulus of the contact area. As such,

during unloading, the tip and surface are linked by this neck region. When the applied load is reversed, the contact radius will decrease. At the point of unloading, this neck will rupture abruptly. Johnson et al. proposed that this point is equal to the pull off force, F_{Adh} which can be directly related to the work of adhesion, W_{Adh} between the tip and surface and is given by [36]:

$$F_{Adh} = \frac{3}{2}\pi R_p W_{Adh} \tag{2.55}$$

When separation occurs, the contact radius, a_s will have decreased to $a_s = 0.63a_o$. The JKR model however predicts that the stress at the edge of the contact areas to be infinite due to the assumption that surface force acts over an infinitesimally small area, which is of course physically unrealistic. In reality, this stress is liberated when the surface at the edge is separated slightly. The JKR model however, is found to be suitable for systems where the work of adhesion is large.

2.5.3 Derjaguin-Muller-Toporov (DMT) Model

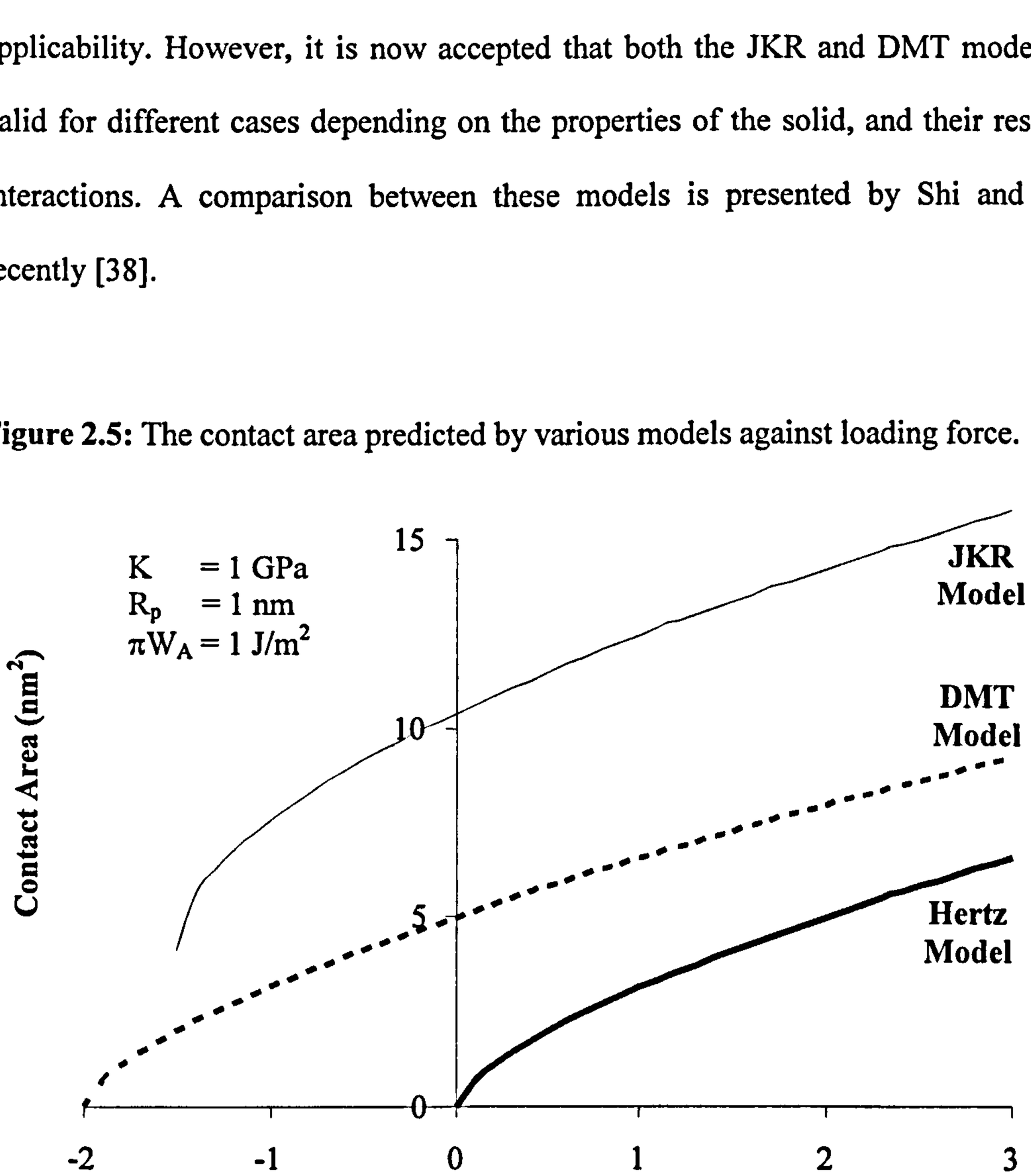
In addition to incorporating the surface attraction forces, the Derjaguin-Muller-Toporov model also includes the molecular attraction energy at the annular region. The DMT model predicts that the separation of two bodies will occur only as the contact area reduces to zero, and as such the contact radius and adhesion force are written respectively as [37]:

$$a = \left[\frac{R_p}{K}\left(F_{Adh} + 2\pi R W_{Adh}\right)\right]^{\frac{1}{3}} \tag{2.56}$$

$$F_{Adh} = 2\pi R W_{Adh} \tag{2.57}$$

This model was derived based on the assumption that the surface forces act outside the contact region, contrary to the JKR model assumption. The DMT model is found to be suitable for materials of lower surface energy, which includes non-deforming contacts. As shown in Figure 2.5, the contact areas for a system is dependent on the models employed. The JKR and DMT models may appear to be in opposition, which resulted initially in many workers discussing their suitability and applicability. However, it is now accepted that both the JKR and DMT models are valid for different cases depending on the properties of the solid, and their resulting interactions. A comparison between these models is presented by Shi and Zhao recently [38].

Figure 2.5: The contact area predicted by various models against loading force.



2.5.4 Tabor Parameter

The particle-particle interaction models derived are based on the nature of the surface forces; being negligible, to act inside the contact radius or to act outside the contact radius. These models are acknowledged to be applicable dependant on the system being studied. Tabor [19] proposed an approach for selection of the appropriate model. In the absence of any loading, the elastic deformation is caused by adhesion.

Tabor's parameter is presented as the ratio between the deformations to the spatial range of adhesion forces resulting in a dimensionless parameter. The Tabor's parameter, μ_T is shown as:

$$\mu_T = \left(\frac{16 R_p W_{Adh}^2}{9 K^2 z_o^3} \right)^{\frac{1}{3}} \tag{2.58}$$

where z_o is the equilibrium separation distance between the bodies in contact. For values of $\mu_T > 5$, the JKR model is applicable whereas the DMT model when $\mu_T < 0.1$.

The work of Tabor was subsequently confirmed numerically by Muller et al. [39] and reviewed by others [40, 41]. Maugis later showed that it was possible to represent both the JKR and DMT models, and this is described in the following section.

2.5.5 Maugis Theory

Maugis [40] proposed a model which was found to be the general case for describing contact mechanics, with the JKR and DMT models as limiting cases. A dimensionless parameter, λ is proposed which describes the amount of adhesion and is shown as:

$$\lambda = \frac{2.06}{z_o} \sqrt[3]{\frac{R_p W_{Adh}^2}{\pi K^2}} \tag{2.59}$$

where the DMT theory is applicable as λ approaches 0 whilst the JKR theory is applicable when λ approaches ∞.

The Maugis model is derived for the contacts of an elastic asperity based on linear elastic fracture mechanics. This model assumes that the attractive forces act via an annulus of the contact area, with the ratio of the annular width, c to the contact radius, R given by m. Several dimensionless parameters are introduced for contact radius, a_M external force, F_M and elastic compression, δ_M shown as:

$$a_M = a\left(\frac{K}{\pi R_p^2 W_{Adh}}\right)^{\frac{1}{3}} \tag{2.60}$$

$$F_M = \frac{F}{\pi R_p W_{Adh}} \tag{2.61}$$

$$\delta_M = \delta\left(\frac{K^2}{\pi^2 R_p W_{Adh}^2}\right)^{\frac{1}{3}} \tag{2.62}$$

This results in the relationship for dimensionless contact radius and ratio of annular width to the contact radius, m given by:

$$\frac{\lambda a_M^2}{2}\left[\sqrt{m^2-1}+\left(m^2-2\right)\tan^{-1}\sqrt{m^2-1}\right] + \frac{4\lambda^2 a_M}{3}\left[\sqrt{m^2-1}\cdot\tan^{-1}\sqrt{m^2-1}-m+1\right]=1 \tag{2.63}$$

By assuming that the adhesive stress outside the contact area follows a simple step distribution, the adhesive stress is constant over a length of d where d = c-a. The integration of the adhesive stresses over the outside of the contact area yields the adhesion forces given by:

$$F_{Adh} = 1.03\frac{\pi W_{Adh}}{z_o}\left(c^2-a^2\right) \tag{2.64}$$

For high values of λ, both the inside and outside adhesive stresses need be taken into account in the integration. The adhesion forces for such conditions are given by:

$$F_{Adh} = 1.03 \frac{W_{Adh} \cdot a^2}{z_o} \left(m^2 \tan^{-1} \sqrt{m^2 - 1} + \sqrt{m^2 + 1} \right) \qquad (2.65)$$

At present, the Maugis theory is widely accepted as the most comprehensive model, suitable for systems of both high and low energy materials. Schwarz [42] recently proposed a new model to incorporate both long range and short range interactions for inside and outside the contact areas, for a sphere on a flat surface.

2.6 Thermodynamics of Wetting

The most fundamental description of an interface is the thermodynamic free energy per unit area, γ_{ij}. In accordance with the first laws of thermodynamics, the internal energy of a closed system is given by:

$$dU = TdS - pdV + \sum_{i=1}^{C} \mu_i dN_i + \gamma_{ij} dA \qquad (2.66)$$

where U is the internal energy, S the entropy, p and T the state conditions of pressure and temperature, μ_i the chemical potential of each component, N_i the amount of component *i*, A the area of the interface and γ_{ij} the interfacial free energy.

The interfacial free energy, γ_{ij} can be defined as the increase in the internal energy of the entire system per unit increase in interface area at constant entropy and volume of the system under closed conditions, and is shown in Equation 2.67.

$$\gamma_{ij} = \left[\frac{\partial U}{\partial A}\right]_{S,V,N_i} \tag{2.67}$$

As such, the following can be obtained:

$$\left[\frac{\partial G}{\partial A}\right]_{T,P,N_i} = \frac{\partial}{\partial A}\left[(U + PV)\right]_{T,P,N_i} - \frac{\partial}{\partial A}(TS)_{T,P,N_i} \tag{2.68}$$

whereby the interfacial free energy in terms of the Gibbs free energy is shown as Equation 2.69:

$$\gamma_{ij} = \left[\frac{\partial G}{\partial A}\right]_{T,P,N_i} \tag{2.69}$$

The spreading of a liquid over a solid substrate is determined by their interfacial free energies. For a liquid to spread over a solid substrate, new interfaces will be created by replacing another surface. At the interface, every new liquid surface area, A_i will result in the diminishing of the solid surface area, A_j. This process will also cause the creation of the interface surface area, A_{ij}. Spontaneous liquid spreading over a solid substrate, $S_{i/j}$ is given by the solution to the exact differential Equation 2.70. A positive value of $S_{i/j}$ would indicate a spontaneous spreading of liquid *i* over solid *j*.

$$\partial G = \left(\frac{\partial G}{\partial A_i}\right)_{T,P} dA_i + \left(\frac{\partial G}{\partial A_{ij}}\right)_{T,P} dA_{ij} + \left(\frac{\partial G}{\partial A_j}\right)_{T,P} dA_j \tag{2.70}$$

$$-\left(\frac{\partial G}{\partial A_i}\right)_{T,P} = S_{i/j} = \gamma_j - \gamma_i - \gamma_{ij} \tag{2.71}$$

The $S_{i/j}$ can be related to the work of cohesion, W_C and work of adhesion, W_A as shown in Equation 2.72. The work of cohesion is defined as the reversible work required to separate two like bodies, whereas, the work of adhesion is defined as the reversible work to separate two un-like bodies (Figure 2.6).

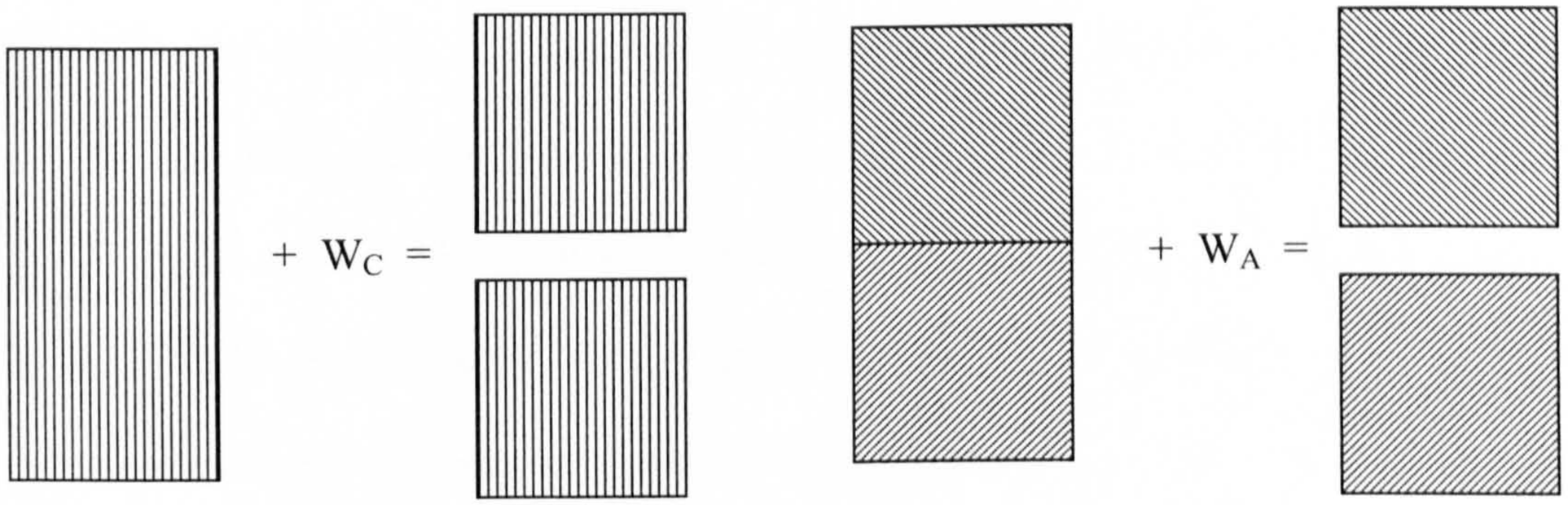
$$W_C = 2\gamma_i \tag{2.72}$$

$$S_{i/j} = W_A - W_C \tag{2.73}$$

The work of adhesion, as defined by Dupre is:

$$W_A = \gamma_i + \gamma_j - \gamma_{ij} \tag{2.74}$$

Figure 2.6: Schematic diagrams indicating the (a) work of cohesion and (b) work of adhesion of materials.



In most cases, liquid droplets do not continuously spread across the entire surface of a solid substrate. The liquid droplet may eventually reach an equilibrium thermodynamic state whereby a contact angle, θ can be defined. The work of cohesion is the direct measurement of work required to create new surfaces, but direct mechanical measurements of this property have been tedious, and results may differ by orders of magnitude due to bulk energy dissipation processes. As a result, the

determination of solid surface free energy and the work of adhesion are often achieved by liquid wetting characteristics via contact angle measurements by use of suitable combining rules [43, 44]. The contact angle and its interpretation will be described in further detail in the following sections while solid surface free energy characterisation techniques will be described in Chapter 5.

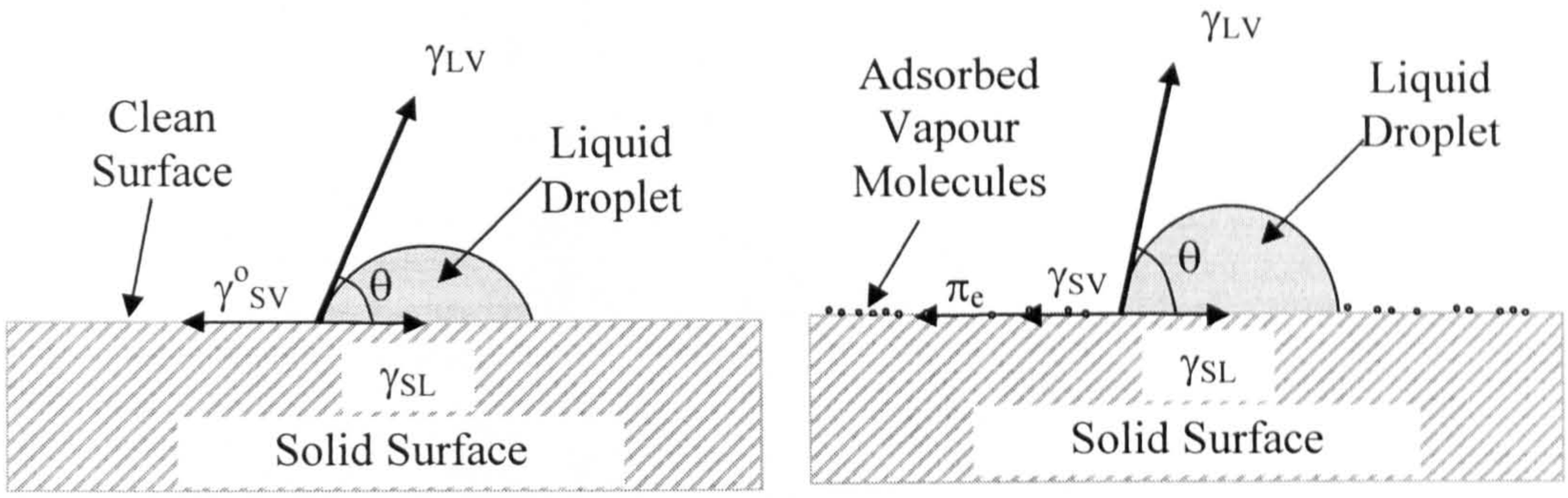
2.7 The Young Equation

Liquid droplets on ideally smooth, flat, isotropic, rigid and non-deformable surfaces in thermodynamic equilibrium with its own vapour will form a sessile drop and possesses a unique profile (Figure 2.7). This droplet profile was first observed and a detailed description was put forward by Thomas Young in 1805 [1]. At the solid-liquid-vapour interface, the angle formed by the tangent of the liquid-vapour interface and the solid substrate is defined as the contact angle, θ_e. By balancing the forces at the three phase point, along the horizontal axis, the surface energy of the solid can be obtained. The contact angle is the manifestation of the solid surface energy, and is often the preferred method of choice for its determination. The Young equation is written as:

$$\gamma^{\circ}_{SV} = \gamma_{SL} + \gamma_{LV} \cdot \cos\theta_e \tag{2.75}$$

where γ°_{SV}, γ_{SL} and γ_{LV} are the solid-vapour, solid-liquid and liquid-vapour interfacial energies, respectively. The superscript nought represents a bare clean surface, free of any adsorbed molecules. In the case of solid surfaces with adsorbed vapour molecules, the spreading pressure, π_e may be appreciable and this will be discussed in further detail in Section 2.12.4.

Figure 2.7: Equilibrium contact angles on (a) clean surface and (b) surface with adsorbed vapour molecules and the balance of forces at the three phase contact points.



2.8 Zisman's Approach

Partial wetting ($\theta > 0^o$) and non-wetting ($\theta > 90^o$) occurs when a liquid with a higher surface tension interacts with a solid of lower surface energy, and wetting ($\theta = 0^o$) occurs for the reverse case (Figure 2.8). It can be expected that contact angles, θ be greater for liquids of higher surface tension, and vice versa. The hypothetical scenario when a liquid just about wets the solid ($\theta \rightarrow 0^o$) was introduced by Zisman as the concept of the critical surface energy, γ_C [5, 6]. At this critical point, the solid surface energy is thought to be equivalent to the surface tension of liquid. Contact angle of near 0° may be difficult to measure, consequently the γ_C is typically extrapolated from a plot of cos θ versus γ_{LV} to cos $\theta = 1$ ($\theta = 0^o$).

The surface energies of polyethylene (PE) and polytetraflouroethylene (PTFE) were characterised by measuring the contact angles of a homologous series liquids on these two low surface energy solids [45, 46]. A smooth trend in the cosine of the contact angle versus liquid surface tension was observed. This relationship can be described by Equation 2.76 and a Zisman plot [6] is shown in Figure 2.9:

$$\cos\theta = 1 - b_Z\left(\gamma_{LV} - \gamma_{SV}\right) \tag{2.76}$$

where b_Z is the slope of the regression line.

Figure 2.8: The contact angles for (a) a partial wetting, (b) a non-wetting and (c) a complete wetting case.

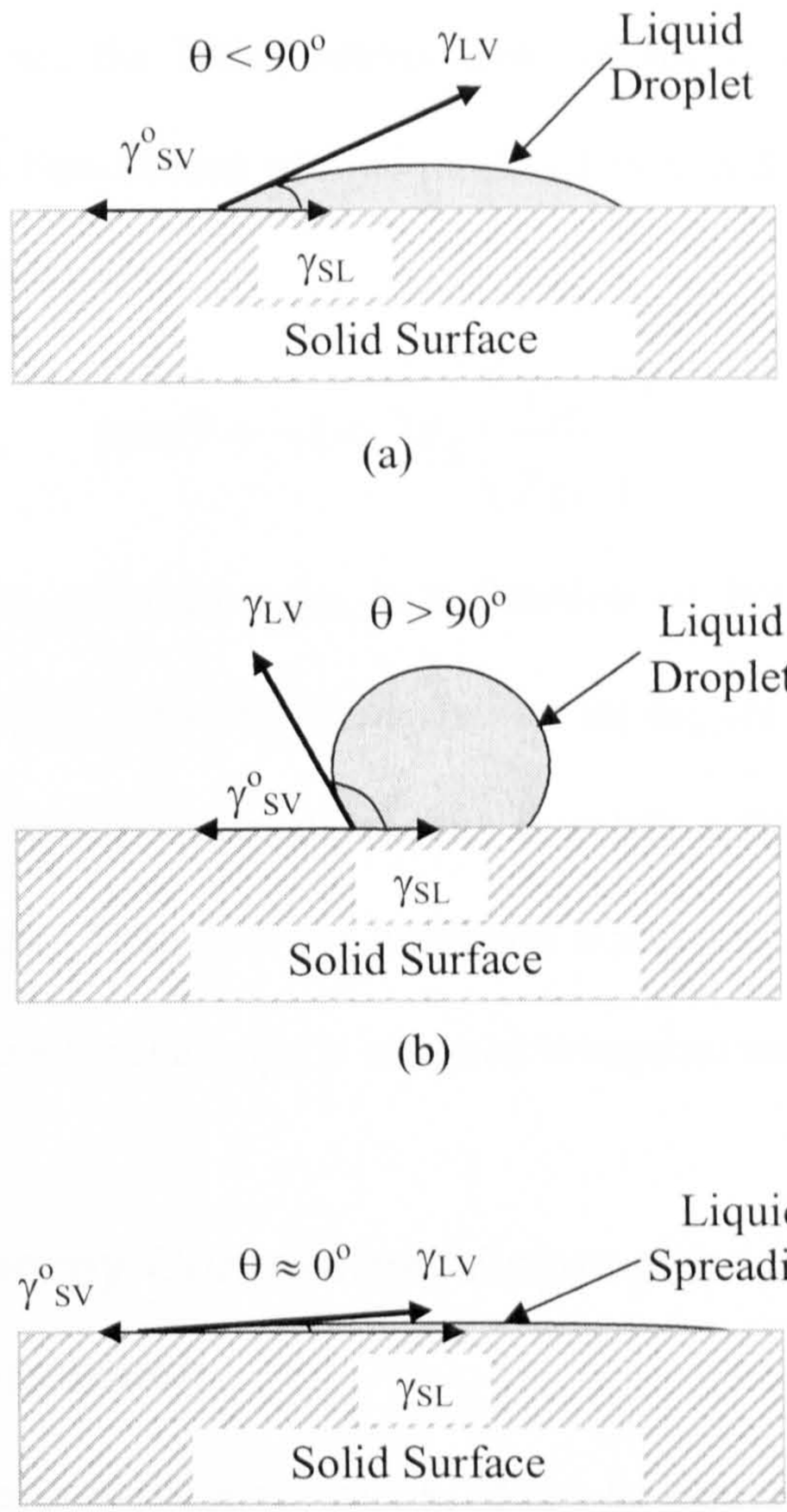
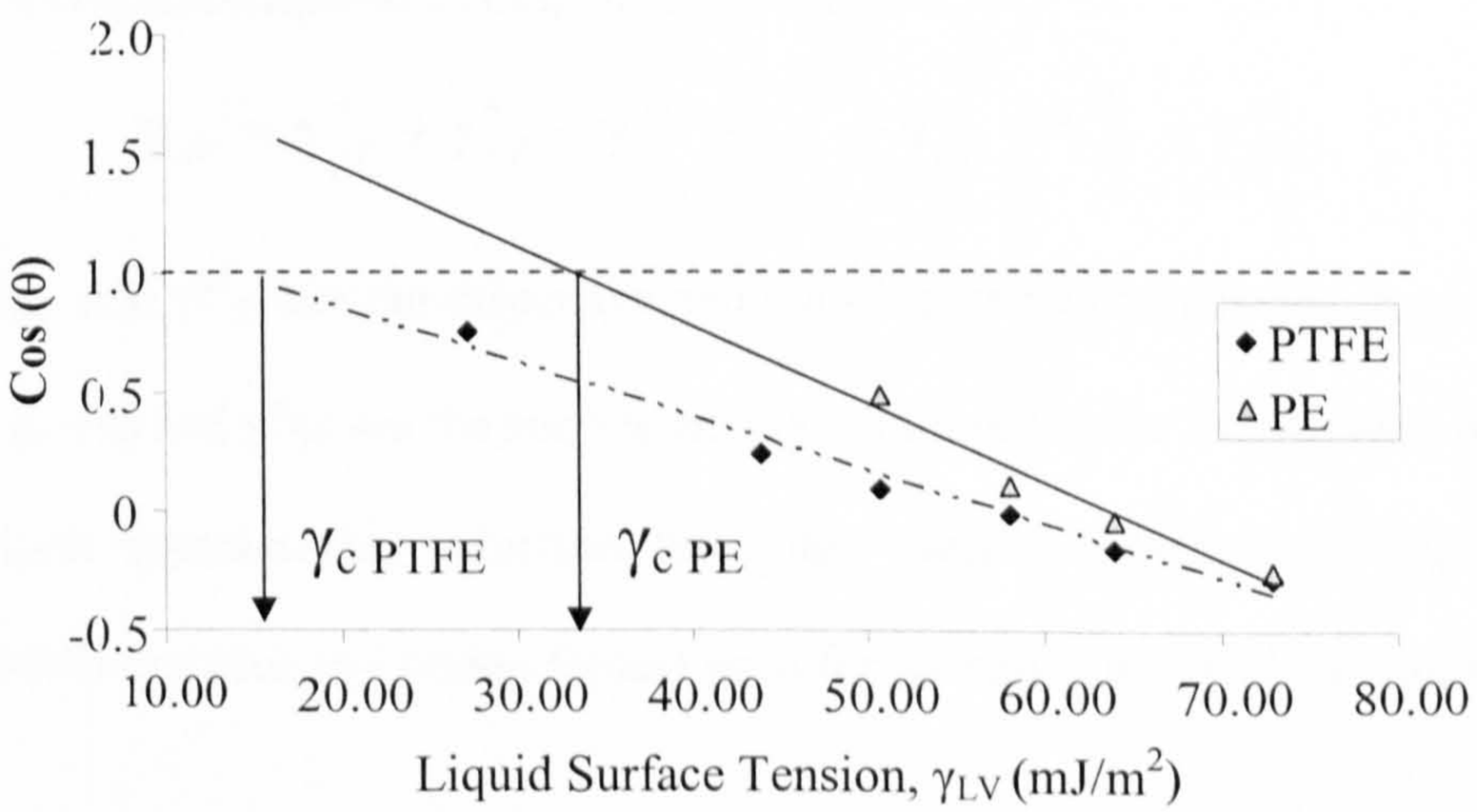


Figure 2.9: Zisman plot to obtain critical surface energy of Polyethylene (PE) and Polytetrafluoroethylene (PTFE).



The surface energy of PTFE shown here is lower than other reported literature values. It has been suggested that if γ_{LV} for the test liquid being used is considerably larger (>25%) than γ_C, the linear extrapolation of the Zisman plot may lead to inaccuracies, and the Fox-Zisman method modified by Good and Girifalco (Equation 2.77) [47] may be more useful.

$$\cos\theta = -1 + 2\phi_{SL}\left(\frac{\gamma_{SV}}{\gamma_{LV}}\right)^{\overline{2}} \tag{2.77}$$

where the interaction parameter, ϕ_{SL} is a function of both the solid and liquid molecular properties [48]. Theoretical calculations for ϕ_{SL} are given by Good. In cases where the dipole moments are small, the ϕ_{SL} is solely a function of the ionisation energies of each phase. Therefore, for non-polar liquids on non-polar solids, where only London forces predominate, ϕ_{SL} is assumed to approximate unity.

2.9 Surface Energy Component Approaches

2.9.1 Fowkes' Approach

Fowkes proposed that surface energy of a solid can be expressed as a summation of a number of independent surface energy components, each arising for specific type of intermolecular forces [8, 21]. The surface energies are normally grouped into the dispersive and non-dispersive components as follows:

$$\gamma_{SV} = \gamma_{SV}^{d} + \gamma_{SV}^{h} + \gamma_{SV}^{dp} + \gamma_{SV}^{i} + \gamma_{SV}^{m} = \gamma_{SV}^{d} + \gamma_{SV}^{nd} \tag{2.78}$$

where γ^{d}_{sv} and γ^{nd}_{sv} are the dispersive and non-dispersive components, respectively. γ^{h}_{sv}, γ^{dp}_{sv}, γ^{i}_{sv} and γ^{m}_{sv} are the surface energy components due to hydrogen bonding, dipole-dipole interactions, induction force and metallic interactions respectively. Dispersive forces (due to London forces) exist for all molecules whilst non-dispersive

forces occur only between molecules with permanent dipole moments. Fowkes also assumed that for interfacial interactions, thermodynamic terms such as the work of adhesion, $\mathbf{W_A}$ could likewise be approximated as a simple sum of the independent terms, each relating to a specific type of intermolecular interactions:

$$\mathbf{W}_A = \mathbf{W}_A^d + \mathbf{W}_A^h + \mathbf{W}_A^{dp} + \mathbf{W}_A^i + \mathbf{W}_A^m = \mathbf{W}_A^d + \mathbf{W}_A^{nd} \tag{2.79}$$

A range of semi-empirical approaches were subsequently developed by Fowkes and other workers [49, 50] which allows the various components of $\mathbf{W_A}$, dispersive or acid-base interactions for example, to be calculated.

The non-bonding interactions between molecules are made up by the London, Debye and Keesom forces. Fowkes estimated the interaction between purely dispersive molecules to be a geometric mean based on Berthelot's principle. By using a purely dispersive liquid ($\gamma^{nd}_{LV} = 0$), the interfacial interactions can be described as:

$$\gamma_{SL} = \gamma_{SV} + \gamma_{LV} - 2\sqrt{\gamma_{SV}^d \gamma_{LV}^d} \tag{2.80}$$

Combining Equation 2.80 with the Young's equation yields:

$$\cos\theta = 2\sqrt{\gamma_{SV}^d} \cdot \frac{1}{\sqrt{\gamma_{LV}^d}} - 1 \tag{2.81}$$

By plotting cos θ versus $1/(\gamma^d_{LV})^{1/2}$ with an intercept of -1, the dispersive energy for a solid is obtained from the slope of the line.

2.9.2 Owens-Wendt Approach

Owens and Wendt [49] extended Fowkes' equation by grouping the non-bonding London, Debye and Keesom interactions into a similar term which they called dispersive (also recognised as the Lifshitz-van der Waals interactions) while the

remaining terms were grouped as the polar contributions. This approach was also adopted by several other workers.

This Owens-Wendt relationship is also known as the extended Fowkes' equation and is shown as:

$$\gamma_{SL} = \gamma_{SV} + \gamma_{LV} - 2\sqrt{\gamma_{SV}^{d}\gamma_{LV}^{d}} - 2\sqrt{\gamma_{SV}^{p}\gamma_{LV}^{p}} \qquad (2.82)$$

Combining Equation 2.82 with the Young's equation yields:

$$\frac{(1+\cos\theta)\cdot\gamma_{LV}}{2\sqrt{\gamma_{LV}^{d}}} = \sqrt{\gamma_{SV}^{p}}\cdot\sqrt{\frac{\gamma_{LV}^{p}}{\gamma_{LV}^{d}}} + \sqrt{\gamma_{SV}^{d}} \qquad (2.83)$$

By plotting $\frac{(1+\cos\theta)\cdot\gamma_{LV}}{2\sqrt{\gamma_{LV}^{d}}}$ versus $\sqrt{\frac{\gamma_{LV}^{p}}{\gamma_{LV}^{d}}}$, the solid dispersive energy is obtained from the intercept while the polar component from the slope of the linear regression.

It was proposed by Wu that a harmonic mean relationship for the interfacial tension could describe low surface energy surfaces more accurately, based primarily on the mathematical fits [51]:

$$\gamma_{SL} = \gamma_{SV} + \gamma_{LV} - 4\left(\frac{\gamma_{SV}^{d}\gamma_{LV}^{d}}{\gamma_{SV}^{d}+\gamma_{LV}^{d}} + \frac{\gamma_{SV}^{p}\gamma_{LV}^{p}}{\gamma_{SV}^{p}+\gamma_{LV}^{p}}\right) \qquad (2.84)$$

Combining Equation 2.84 with the Young's equation yields:

$$\gamma_{LV}(1+\cos\theta) = 4\left(\frac{\gamma_{SV}^{d}\gamma_{LV}^{d}}{\gamma_{SV}^{d}+\gamma_{LV}^{d}} + \frac{\gamma_{SV}^{p}\gamma_{LV}^{p}}{\gamma_{SV}^{p}+\gamma_{LV}^{p}}\right) \qquad (2.85)$$

Arithmetic, quadratic and anharmonic means were also proposed by others but did not gain popularity [52]. The Debye forces arising from dipole-induced dipole interactions normally accounts for only a few percent of the van der Waals forces

while Keesom forces from dipole-dipole interactions may be comparable in magnitude to the London forces. While Debye interactions within a bulk phase may cancel out, γ^i can be significant between two phases. The grouping of van der Waals interactions may also be incorrect as a polar molecule may induce a molecule of the other phase at the interface [52]. Since dipoles of one phase can only interact with dipoles of the other phase at the interface, and likewise for induced dipoles, the combination of these forces into one term is theoretically unsound. Furthermore, the polar components interactions were modelled as geometric means, including for hydrogen bonds, is theoretically unjustified.

2.9.3 Acid-Base Approaches

While molecules containing ester, ether and aromatic functions do not themselves possess significant hydrogen bonds, these materials may exhibit a significant W_A^H [53]. van Oss et al. proposed an acid-base approach by the combination of London, Debye and Keesom interactions into the apolar Lifshitz-van der Waals component, γ^{LW} and an acid-base component, γ^{AB} [50, 54, 55]. However, the short-range interactions were divided into acid, γ^+ and base, γ^- parameters. They assumed that the acid-base interactions between phases were dissimilar, where the acid part of one phase interacts with the basic part of the other [56, 57]. The total surface energy is given by:

$$\gamma_i = \gamma_i^{LW} + 2\sqrt{\gamma_i^+ \gamma_i^-} \tag{2.86}$$

where *i* denotes solid or liquid phase, and γ_i^+ the electron acceptor (Lewis acid) and γ_i^- the electron donor (Lewis base) components.

The interfacial interactions can be shown as:

$$\gamma_{SL} = \gamma_{SV} + \gamma_{LV} - 2\sqrt{\gamma_{SV}^{LW}\gamma_{LV}^{LW}} - 2\sqrt{\gamma_{SV}^{+}\gamma_{LV}^{-}} - 2\sqrt{\gamma_{SV}^{-}\gamma_{LV}^{+}} \qquad (2.87)$$

Combining Equation 2.87 with the Young's equation yields:

$$\gamma_{LV}(1+\cos\theta) = 2\sqrt{\gamma_{SV}^{LW}\gamma_{LV}^{LW}} + 2\sqrt{\gamma_{SV}^{+}\gamma_{LV}^{-}} + 2\sqrt{\gamma_{SV}^{-}\gamma_{LV}^{+}} \qquad (2.88)$$

Three liquids with known surface tension components, of which at least two are polar (with γ^+ and γ^-), are needed to calculate the surface energy components of solid. Whilst this approach yields the most information of a surface, liquid properties of different scales proposed by van Oss et al. ($\gamma_{H2O}^{+}:\gamma_{H2O}^{-} = 1$) and Della Volpe and Siboni ($\gamma_{H2O}^{+}:\gamma_{H2O}^{-} = 6.5$) [58] yield results differing in magnitude, whilst the order or acidity/basicity is often unchanged [59].

The van Oss et al. scale utilised water as reference with γ^+: γ^- ratio equal to unity. Evaluation of surface energies with the van Oss scale often predicts an excess basic property. Della Volpe [58] proposed a different ratio suggesting that water was not amphoteric but acidic. The acid-base approach of van Oss et al. assumes that W_A^{AB} is always greater than zero while the Chang-Chen model allows for both attractive and repulsive interactions [60].

The status of polar or acid-base interactions is at present rather simplistic, and assumes that the free energy of interaction can be approximated by the geometric mean rule. Fowkes' however argued such an approximation, while it may be valid to describe the London dispersion interactions, is fundamentally erroneous for acid-base interactions. Fowkes and Mostafa [53] proposed that the acid-base work of adhesion be written as:

$$W_{Adh}^{AB} = -f \cdot N_{AB} \cdot \Delta H^{AB} \qquad (2.89)$$

where ΔH^{AB} is the enthalpy of adsorption for the acid-base interactions, N_{AB} the number of acid-base pair interactions per unit area and f is a constant which converts the enthalpy units in terms of surface free energy. The f constant can be evaluated by Equation 2.90 but for simplicity, is typically assumed to be equal to unity.

$$f = \left[1 - \frac{\partial \ln W_{Adh}^{AB}}{\partial \ln T}\right]^{-1} \tag{2.90}$$

Acid base interactions can be described by either the Bronsted theory where an acid is a proton donor and base a proton acceptor, or a Lewis theory where an acid is an electron acceptor and base an electron donor. The Lewis approach is preferred for the description of acid-base components in wetting.

The determination of ΔH^{AB} has been proposed by both Drago [61] and Gutmann [62] to evaluate the acid-base properties of solids. Drago introduced his model based on Pearson's Hard and Soft Acids and Bases (HSAB) Principle and Mulliken's theory [63]. Robert Mulliken studied the electrostatic and covalent contribution to charge transfer based on the valence bond model for ground state energy. His work won him the 1966 Nobel Prize for Chemistry.

Drago proposed a model to describe the acid-base hardness of solid substances, which is related to the polarisability as follows:

$$-\Delta H^{AB} = E_A E_B + C_A C_B \tag{2.91}$$

where E_A and E_B describes the electrostatic contribution and C_A and C_B describes the covalent contribution to the acid-base interactions. The ratio of E/C is a measure of hardness, with materials of low polarisability categorised as hard, and high polarisability as soft. Iodine was taken as reference material with assigned values of

$E_A = 1$ (kcal/mol)$^{1/2}$ and $C_A = 1$ (kcal/mol)$^{1/2}$. This concept however fails for strongly interacting materials, either dominantly hard or soft. Drago and co-workers later expanded their list for E and C values, and also took into account the possibility of steric effects [64, 65].

To accommodate the interactions of bipolar compounds, Gutmann introduced the electron donor numbers (DN) and acceptor numbers (AN) concept. The Gutmann model is given by:

$$-\Delta H^{AB} = K_A DN + K_B AN \tag{2.92}$$

where K_A and K_B are the acid and base numbers of the solid phase, respectively.

The donor number (DN) was evaluated in terms of the exothermic heat of mixing for antimony pentachloride ($SbCl_5$) in a dilute solution (10^{-3} M) of dichloroethane. The van der Waals interactions are mostly confined to the solvent, and as such the measured heat of mixing will not reflect any of contribution from the dispersion interactions component. The acceptor number (AN) meanwhile is determined from the ^{31}P-NMR shift induced by triethylphosphine oxide $(C_2H_5)_3PO$. AN has arbitrary units, with zero assigned for the shift produced by hexane and a value of 100 for $SbCl_5$. These values however, were found to be influenced by the dispersive forces contributions, and were later corrected by Riddle and Fowkes [66]. The determination of AN was later defined as the heat of mixing for a probe of interest in a base Et_3PO. The corrected values of the acceptor number, AN^* is found to be given by:

$$AN^* = 0.288(AN - AN^d) \tag{2.93}$$

Gutmann's approach allows for the determination of bipolar interactions, and has been employed with much success. The Gutmann approach is also used to

evaluate acid-base contributions of particulate samples as determined by the IGC approach (Chapter 8). The acid-base properties for solid materials can be determined by several techniques such as colloid titration, calorimetry and inverse gas chromatography (IGC), and is reviewed elsewhere [67]. The IGC approach is detailed in Chapter 8.

2.10 UNIFAC Approach

Fredenslund et al. proposed a UNIFAC (UNIQUAC Functional-group Activity Coefficients) model, to predict the activity coefficients for non-electrolyte liquid mixtures based on the quasi chemical theory of liquid mixtures (UNIQUAC) [68]. The UNIFAC model is a group contribution method which represents the activity coefficients as a result of both combinatorial components and residual contributions. The combinatorial component is due to the difference in size and shape between the mixtures, which can be obtained from van der Waals parameters. While the residual contribution evolves from heat effects and is determined experimentally. Banerjee and Etzler modified the UNIFAC approach for the estimation of contact angles by calculating the residual component of the activity coefficient from interaction parameters proposed by Hansen et al. [69], while the combinatorial components were thought to be non-essential.

Banerjee and Etzler proposed a semi-empirical relation for the estimation of contact angles of liquids based on the residual activity coefficients and solid surface energy [70]. This relationship was computed from published data for relatively hydrophobic materials; polyethylene, poly (ethylene terephthalate), poly (tetrafluoroethylene), paraffin, polystyrene and poly (methyl methacrylate) films

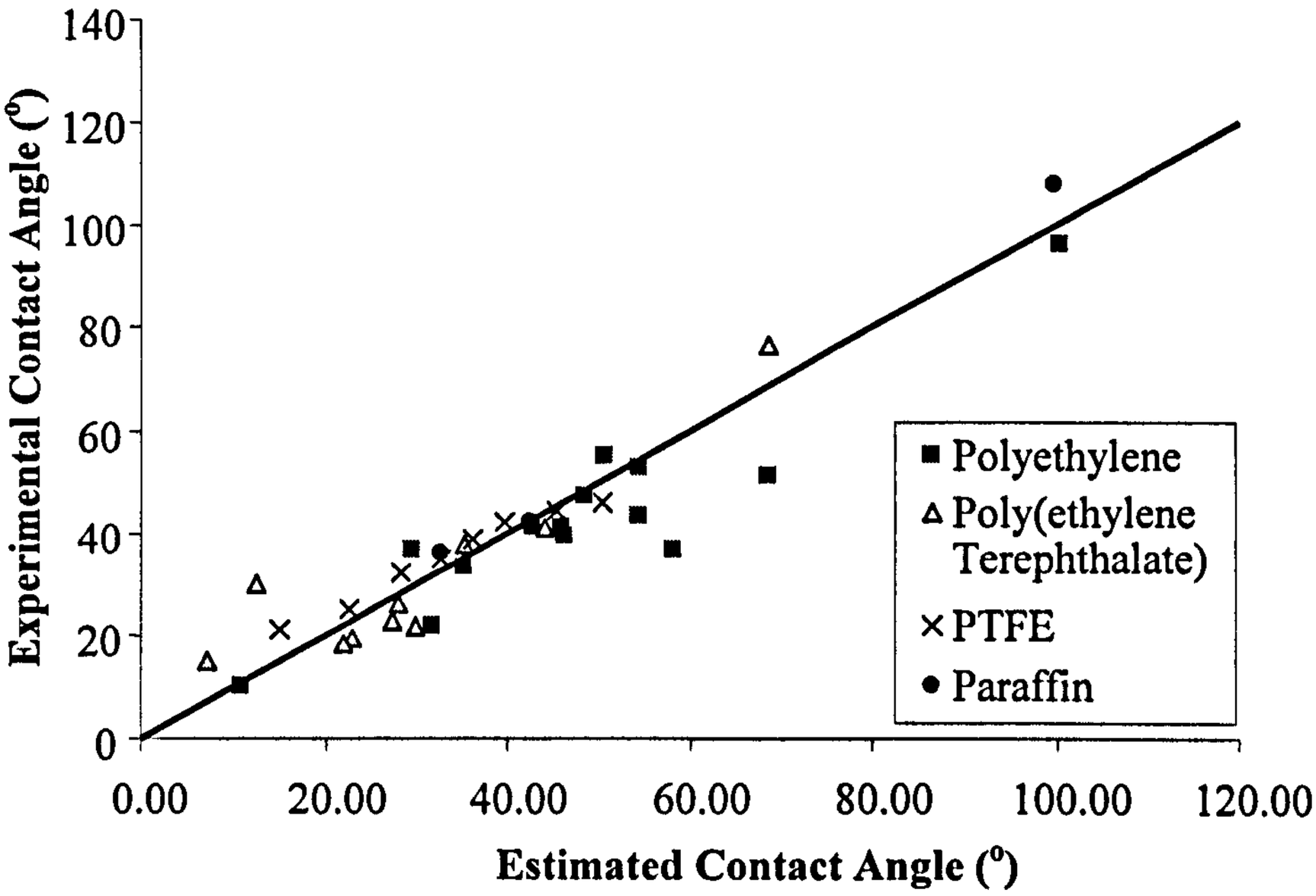
while the probe liquids covered both purely dispersive and polar liquids. Regression of the data (n = 54) with a regression coefficient of 0.95 resulted in:

$$\cos\theta = 1.42 - 0.102 \ln \gamma_r - 0.0115 \gamma_{LV} \qquad (2.94)$$

where γ_r is the residual activity coefficients.

The estimated contact angle values obtained from Equation 2.94, were within 7 ° and are in good agreement with the experimental values, as shown in Figure 2.10.

Figure 2.10: Comparison between experimental and estimated contact angles based on the UNIFAC approach.



2.11 Equation of State Models

In contrast to the components approach, Neumann et al. [9, 71] proposed an equation of state approach. The equation of state approaches stipulates that interaction between two phases is governed solely by liquid and solid surface energies, and that the measurable contact angle is only a function of these two variables. As such, surface energies are not made up of different components and contact angle measurements do not reflect local surface chemical information. This approach was modelled purely from a thermodynamic perspective.

Antonow's rule relates solid-liquid interaction to liquid surface tension and solid surface energy [72], without derivation by:

$$\gamma_{SL} = \left|\gamma_{LV} - \gamma_{SV}\right| \tag{2.95}$$

Combining Equation 2.95 with the Young's equation yields:

$$\cos\theta = -1 + 2 \cdot \frac{\gamma_{SV}}{\gamma_{LV}} \tag{2.96}$$

Berthelot's rule has a theoretical base, derived from the molecular interactions of like molecule pairs. The basis of the Berthelot rule is the geometric mean combining rule of the potential energy parameters of like-pair interactions, giving the unlike-pair interactions ($\varepsilon_{SL} = \sqrt{\varepsilon_{SS}\varepsilon_{LL}}$). This can also be expressed thermodynamically as work of adhesion for a solid-liquid pair. This leads to the interfacial tension:

$$\gamma_{SL} = \gamma_{SV} + \gamma_{LV} - 2\sqrt{\gamma_{SV}\gamma_{LV}} = \left(\sqrt{\gamma_{LV}} - \sqrt{\gamma_{SV}}\right)^2 \tag{2.97}$$

Combining Equation 2.97 with the Young's equation yields:

$$\cos\theta = -1 + 2 \cdot \sqrt{\frac{\gamma_{SV}}{\gamma_{LV}}} \tag{2.98}$$

Li et al. proposed a modification to the geometric mean rule, to take into account the over-predictions of unlike-pair interactions, by introducing an empirical parameter [71]. This parameter should be a decreasing function to equal unity when potential energy parameters of like-wise pairs are equal. The interfacial tension is therefore described as:

$$\gamma_{SL} = \gamma_{SV} + \gamma_{LV} - 2\sqrt{\frac{\gamma_{SV}}{\gamma_{LV}}} \cdot e^{-\beta(\gamma_{LV}-\gamma_{SV})^2} \tag{2.99}$$

where β is an empirical constant with an average value of 1.057×10^{-4} $(m^2\ mJ^{-1})^2$. Combining Equation 2.99 with the Young's equation yields:

$$\cos\theta = -1 + 2\sqrt{\frac{\gamma_{SV}}{\gamma_{LV}}} \cdot e^{-\beta(\gamma_{LV}-\gamma_{SV})^2} \tag{2.100}$$

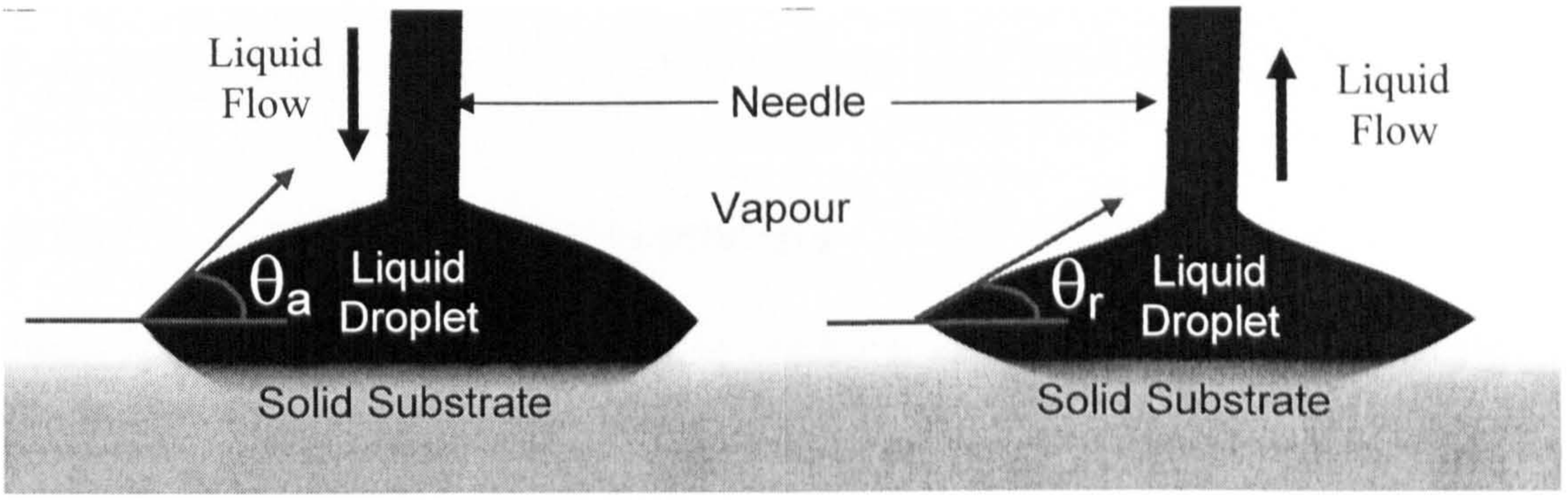
The equation of state approach enables calculation of the surface energy of a solid by measuring the contact angle of a single liquid, with a known surface tension, on a solid surface [72]. Applicability of the equation of state approach or the components approach remain debatable and without conclusion [73-75] with a recent report discussing its invalidity for determination of interfacial energies [74, 76].

2.12 General Problems with Wetting Theories

The Young contact angle, θ defines the profile of a droplet of liquid on an ideal solid surface which is in thermodynamic equilibrium at its three phase contact point. For any one system, thermodynamics requires a minimisation of energy for stable or equilibrium conditions, as in the case of wetting. The classification of an ideal condition is one where the surface is molecularly smooth and homogenous while the

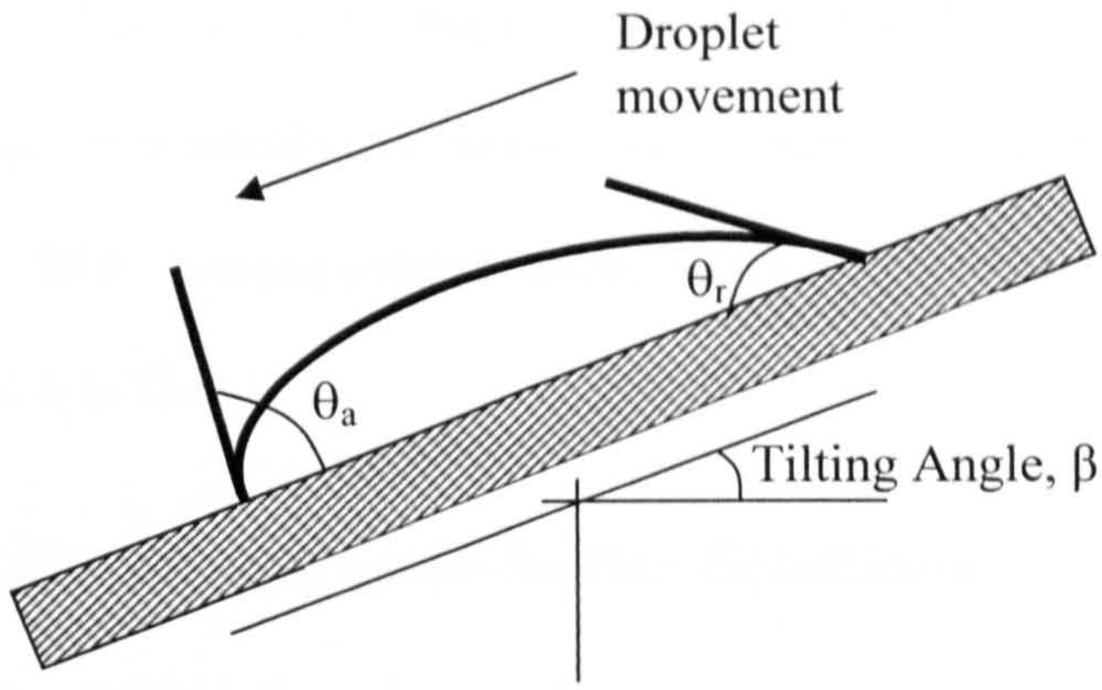
liquid is non-reactive to the solid surface. However, in the case of real solid surfaces, which are often far from the idealised case, experimental observations have revealed that various stable regimes exist resulting in a maximum and a minimum contact angle corresponding to the advancing, θ_a and receding, θ_r contact angles respectively (Figure 2.11).

Figure 2.11: Schematic diagrams indicating the (a) advancing and (b) receding contact angles.



θ_a and θ_r respectively can be evaluated by adding and retracting liquid to/from a liquid drop causing the contact line to advance and recede. Alternatively, if the substrate surface is tilted until the drop starts to slide across the surface, forming a tear shaped drop as shown in Figure 2.12, then θ_a and θ_r will be observed directly from the profile, although this generally accepted viewpoint has been theoretically disputed recently [77]. The difference between θ_a and θ_r is termed the contact angle hysteresis. In the case where hysteresis is zero, the drop should slide down the inclined surface with θ_a equal to θ_r for $\beta > 0^{\circ}$. The hysteresis phenomenon has been the focus of numerous research groups in order to understand its nature and origin, and therefore any resulting implication to the evaluation of solid surface energy from contact angle determinations.

Figure 2.12: Determination of the advancing and receding contact angle by tilting plate method.



2.12.1 Contact Angle Hysteresis

Hysteresis illustrates a non ideal wetting condition which may be a thermodynamic effect due to roughness or chemical heterogeneity which is time independent, as opposed to a kinetic effect such as swelling of solid and penetration of liquid into bulk. In this section, we shall review the effects of roughness and chemical heterogeneity on both the θ_a and θ_r.

The relationship of θ_a and θ_r to θ_Y is not straightforward, and a number of interpretations have been proposed, such as the use of an arithmetic mean of θ_a and θ_r. It is common practice that θ_a, which is observed to be the most reproducible contact angle, is approximated to θ_Y for the purpose of surface characterisation [56]. This methodology is supported by Li and Neumann who observed that the θ_a approaches the minimum free energy state, and hence the equilibrium Young state, for model patterned heterogeneous surfaces [78]. Therefore, θ_a is commonly used in the surface energetic determination of solid surfaces as in this study.

The hysteresis however may reveal additional information regarding the surface. The effects of surface roughness on contact angles were first described by

Wenzel [79] whilst the effects of heterogeneities and porosity were addressed by Cassie [80, 81]. The contact angle hysteresis has been investigated both experimentally and theoretically by many, surprisingly with limited conclusions to date [82-87]. A fully comprehensive understanding of contact angle hysteresis remains elusive to this day.

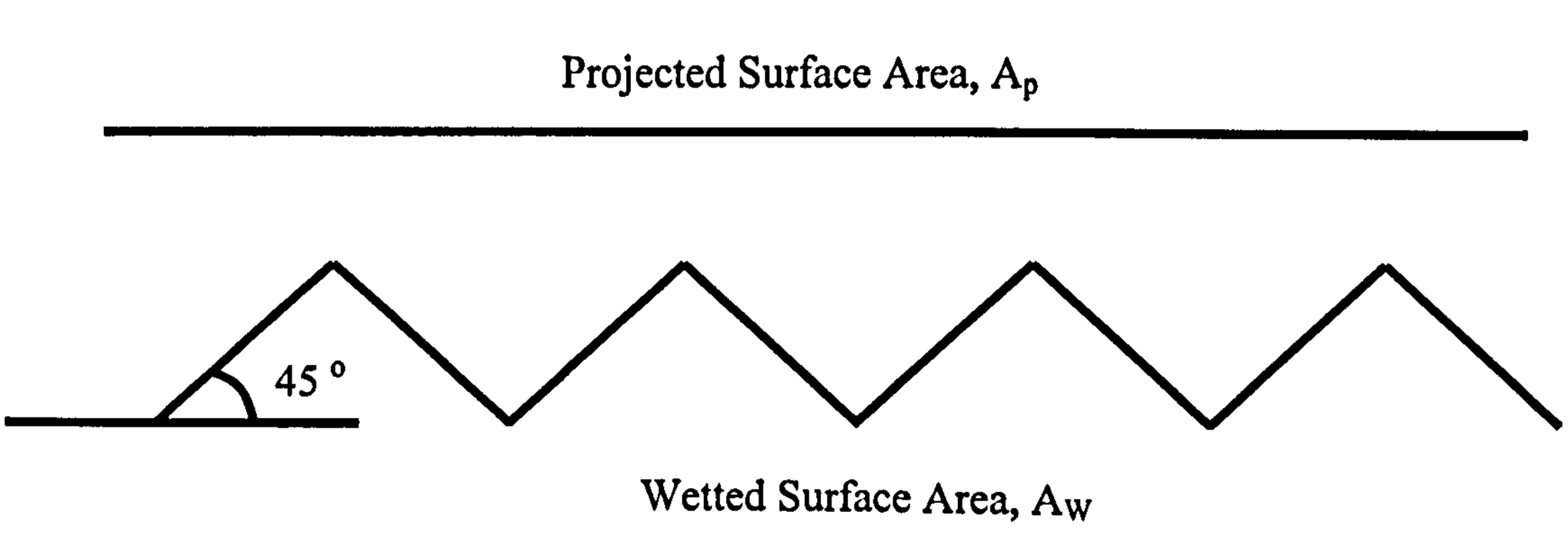
2.12.2 Wenzel and Cassie-Baxter Equations

The analysis of the effects of surface roughness on contact angles by Wenzel simply takes into account the additional area to be wetted by the probe liquid on a rough surface compared to a smooth surface. Wenzel proposed a roughness factor r which is defined as the ratio of the total surface area to be wetted due to roughness, to the projected surface area (Figure 2.13). The roughness factor will be equal to $\sqrt{2}$ for the case of this corrugated surface with an angle of 45 °. It is obvious that the roughness factor is always greater than 1 with $r_W = 1$ for an ideal smooth flat surface. Wenzel proposed a model to include this roughness effect on the equilibrium contact angle as shown:

$$r_W \cdot \cos\theta_Y = \cos\theta_W \tag{2.101}$$

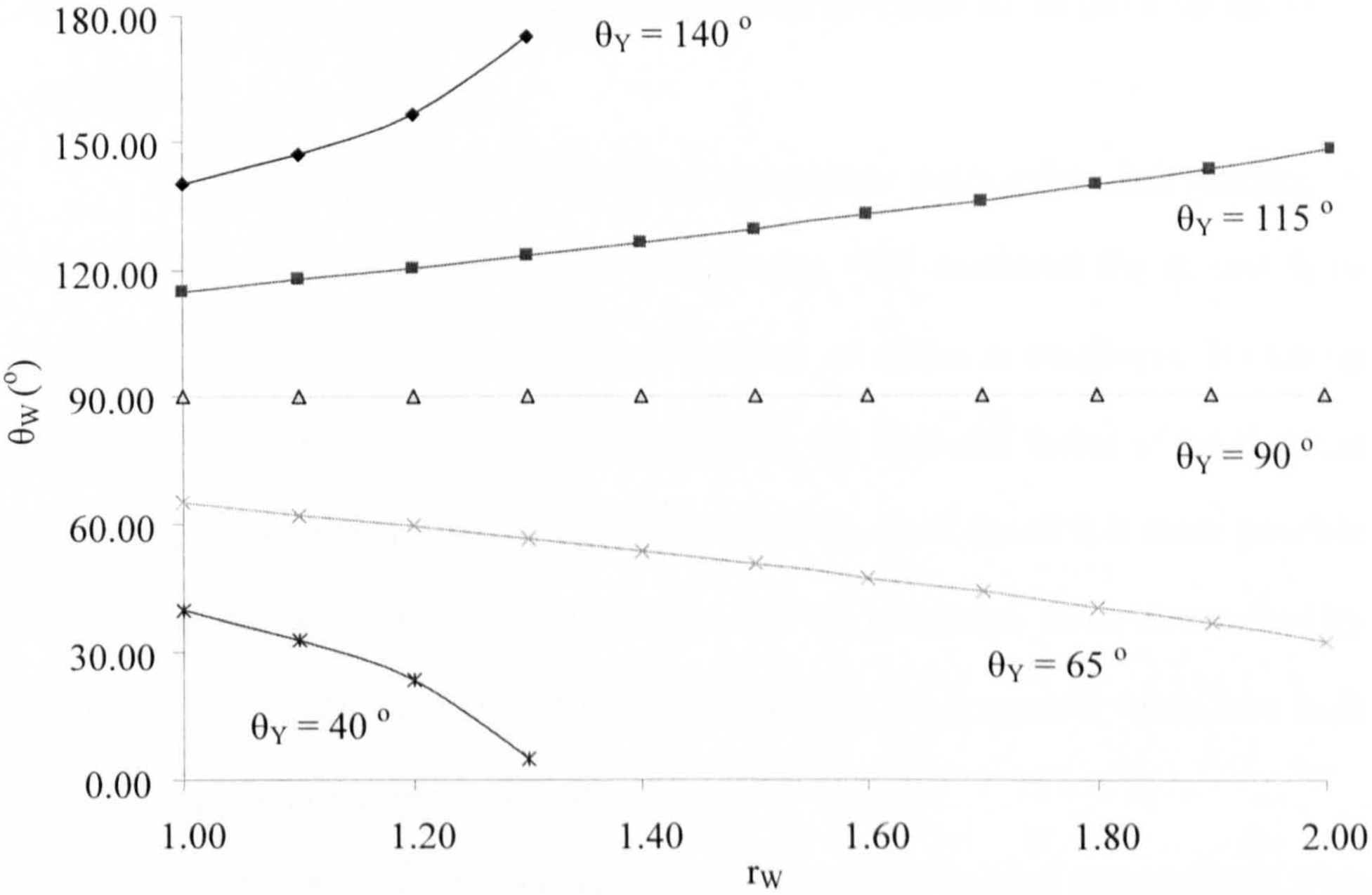
where θ_Y is the Young equilibrium contact angle and θ_W is the measurable Wenzel contact angle due to the surface roughness.

Figure 2.13: Wenzel roughness factor.



Equation 2.101 shows that for $\theta > 90^{o}$ roughness causes an increase in the measurable contact angle while for $\theta < 90^{o}$ the opposite case holds (Figure 2.14). The Wenzel equation predicts that surface roughness will emphasize the intrinsic hydrophobicity or hydrophilicity of a surface. A thermodynamic derivation confirming the validity of the Wenzel equation was performed amongst others by Good [88] and Shuttleworth and Bailey [89]. For liquid droplets on rough surfaces, the Wenzel regime is applicable only if the droplet diameter is sufficiently larger than the roughness dimensions [90] and if the droplet completely penetrates the grooves [91, 92]. In the case where the liquid droplet sits on the asperities, a composite case may apply as described by the Cassie-Baxter equations [81].

Figure 2.14: The effects of roughness on measurable contact angles based on Wenzel's equation.



Bikerman measured the contact angles of water on a series of stainless-steel plates of different degrees of roughness, measured with a tracer instrument. The roughness, R_a varied by over a factor of 100 and he found no definite effect of roughness on θ as proposed by Wenzel [93]. This potential contradiction was defended by Wenzel himself, emphasizing that the roughness factor, as expressed in the equation is strictly speaking a precisely defined ratio of true surface area to projected area and not one of average height [94]. Barthell and Shepard [95-97] investigated the effects of surface roughness on both the θ_a and θ_r for various systems including water, ethylene glycol, glycerol in air on paraffin films. It was found that the θ_a increased with increasing roughness while the θ_r slightly decreased resulting in an increase in hysteresis. They proposed that this variation is due to the mechanism of the advancing liquid being controlled by the movement over pyramid faces resulting in the increase in θ_a. The observed hysteresis was attributed to the physical nature of the surfaces.

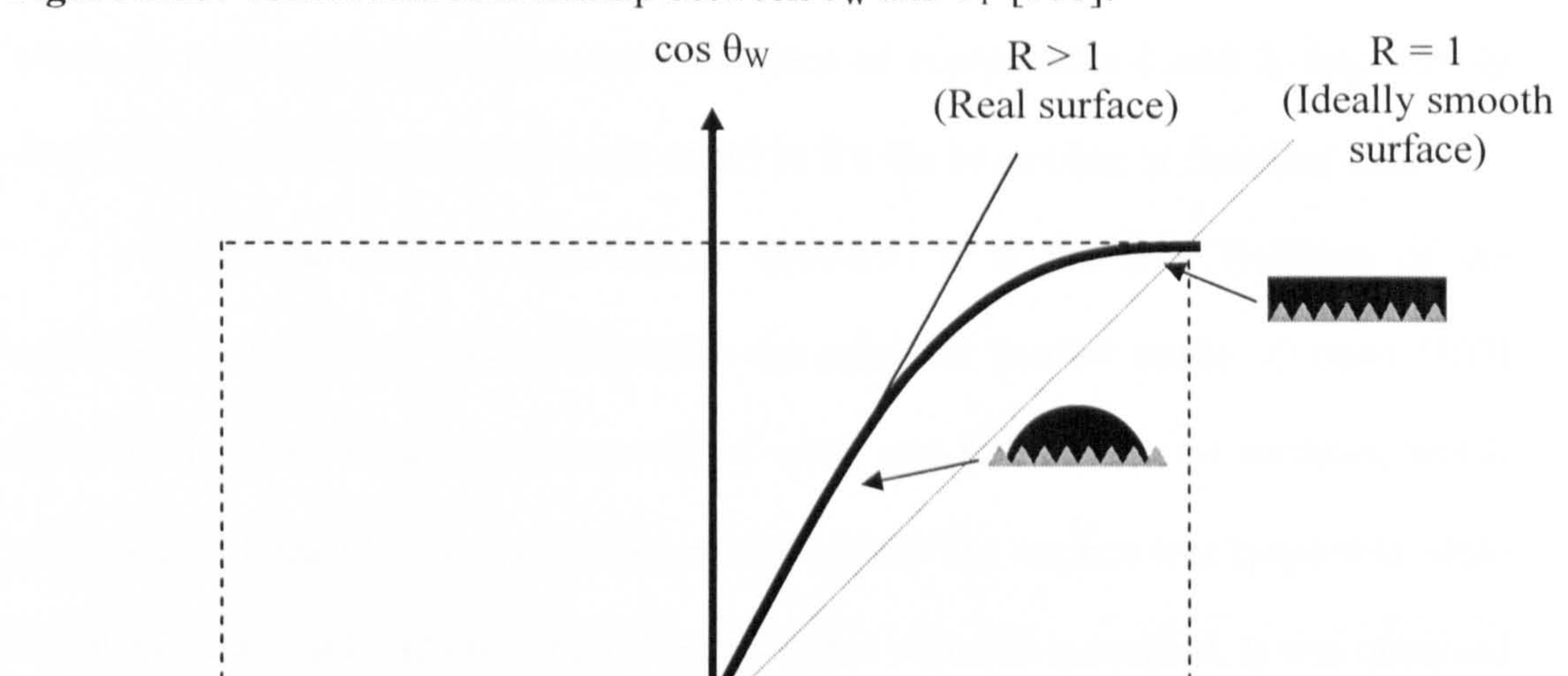
Deviating from the ideal conditions, metastable states exist often resulting in non distinguishable θ_W. Kamusewitz and Possart [98] measured the θ_a and θ_r of ethylene glycol drops on polypropylene surfaces of different roughness. By taking into account frictional forces, and assuming that the frictional forces of wetting and de-wetting are identical [99], the prediction of the θ_W from θ_a and θ_r is made possible by a simple average. They went on to show that the roughness factor determined by Scanning Force Miscroscopy (SFM) is comparable to the computed value from both θ_a and θ_r and hence θ_Y can be determined.

The Wenzel equation relates θ_W to θ_Y in a linear fashion (Figure 2.15). This linear dependency starts to deviate for the extreme values of θ, that for the fully wetting and the superhydrophobic events. This deviation is thought to be due to

displacement of some liquid molecules of the liquid layer nearest to the surface [100]. For fractal surfaces, it was demonstrated that their dimensions can induce a superhydrophobic/hydrophilic behaviour [101, 102] as predicted theoretically by the Cassie-Baxter relationship. In the case of superhydrophobicity, liquid droplets bead up resulting in air-pockets forming in the grooves.

Often, it is difficult to distinguish whether a stationary liquid droplet on a solid surface behaves according to the Wenzel or Cassie-Baxter regime. A mathematical-thermodynamic analysis is discussed by Marmur [92] to distinguish and determine the transition between homogenous to heterogeneous wetting regimes. A critical pressure for transition of wetting regimes was reported by Carbone and Mangialardi [103]. In the quest for designing superhydrophobic surfaces, Extrand proposed a contact line density approach for prediction of drop suspension or collapse [104, 105].

Figure 2.15: Theoretical relationship between θ_W and θ_Y [101].



Extrand investigated the effects of roughness on both θ_a and θ_r for polyethylene (PE) and polyamide (PA) films of various amide concentrations [106]. These surfaces had roughness, R_a, ranging from 23-130 nm. It appeared that θ_a on PA films were higher on rougher surfaces although the contact angles were $< 90^\circ$. Both θ_a and θ_r were found to decrease, resulting in an increase of hysteresis on smoother films. This was concluded to have resulted from the increase in amide fractions, and that the influence of roughness at such scale was probably insignificant. The first model to relate θ_a and θ_r on heterogeneous surfaces was proposed by Cassie and Baxter [80, 81].

The Cassie-Baxter equation describes the apparent contact angle as a function of the surface area fractions of each component. For a two component surface where the liquid fully wets the entire surface, the Cassie-Baxter equation is written as [80]:

$$\cos\theta_i = \alpha_1 \cos\theta_{i1} + \alpha_2 \cos\theta_{i2} \tag{2.102}$$

where α_1 and α_2 are the surface area fractions of components 1 and 2, respectively while *i* denotes that the contact angle could be for the advancing or receding case.

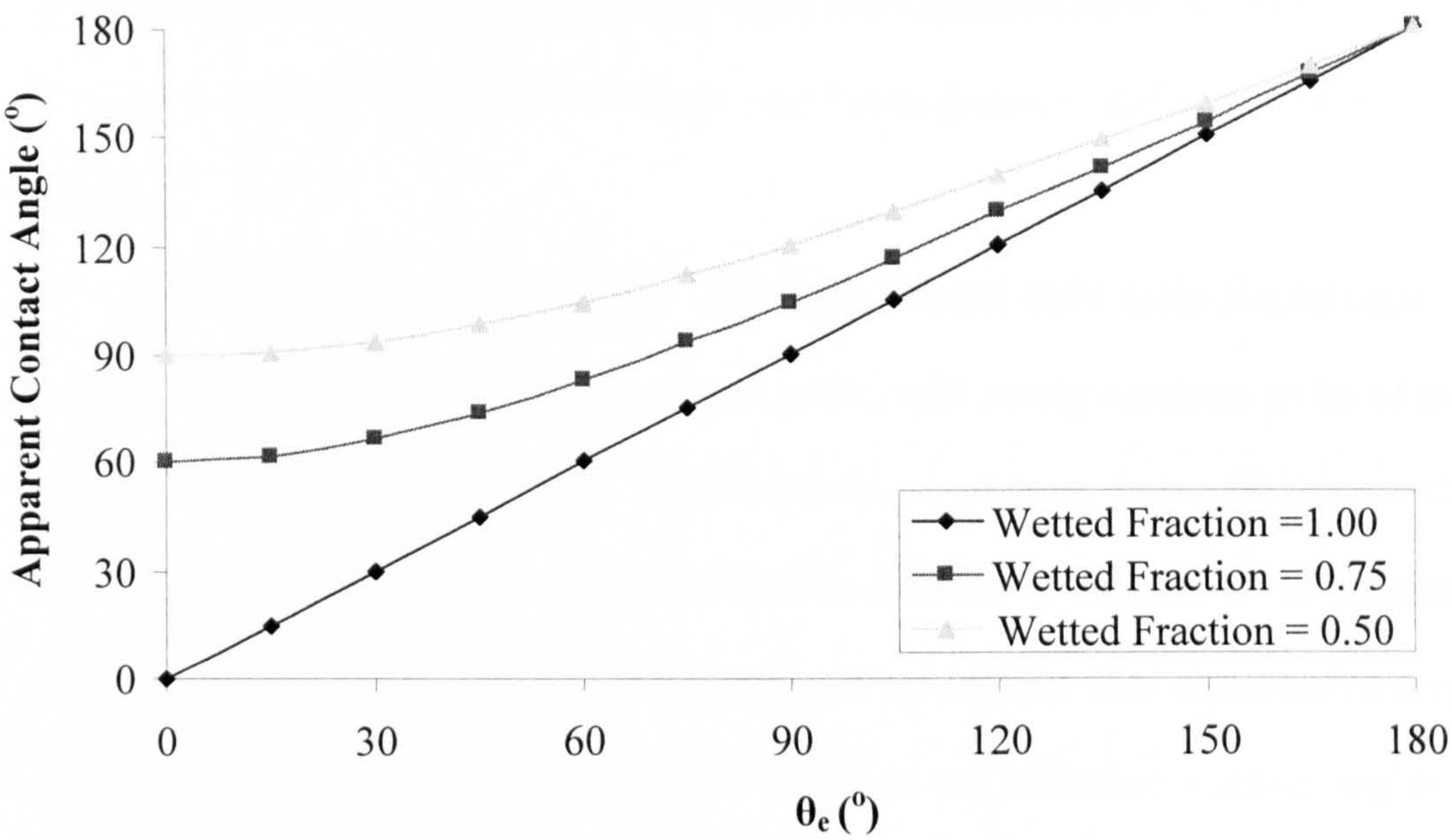
According to the Cassie-Baxter equation, it is the area fractions of the individual components which determine the apparent contact angle. Extrand [107] performed contact angle measurements of water and hexadecane on surfaces, which possessed a single chemically heterogeneous island. The surface was lyophobic while the island was non-lyophobic and the reverse case was also examined. It was observed that for droplets placed within the island diameter, the contact angles were representative of the homogeneous island and were only reflective of contact angles of the other surface once the diameter was greater than that of the island. This finding implies that heterogeneity which is contained within the wetted area does not

influence the apparent contact angle, and that the interaction at the three phase contact line of the drop is plausibly the more important factor.

In the case where liquid does not fully penetrate or wet the grooves, resulting in pockets of air, the contact angle of the liquid droplet is assumed to be 180 ^{o} (cos 180 ^{o} = -1). As such, Equation 2.102 can be rewritten as follow (Figure 2.16):

$$\cos\theta_i = \alpha_1 \cos\theta_{i1} - \alpha_2 \tag{2.103}$$

Figure 2.16: Equilibrium and apparent contact angles according to the Cassie-Baxter relationship for the case of incomplete liquid penetration into grooves.



This implies that in the case of liquid droplets sitting on grooves with trapped air pockets, the apparent contact angle can increase dramatically especially as the fraction of wetting areas decreases. Such behaviour has been employed by many in the design of superhydrophobic surfaces, for applications such as self-cleaning surfaces and microfluidics. This area has been aided by recent advancements in fabrication of microstructures and precise surface patterning.

Regular microstructures and nanostructures pores/columns of various geometrical dimensions, shapes and height have been fabricated, and the wettability of various droplet sizes has recently been investigated [108-111]. While most studies reveal that hydrophobicity can be enhanced greatly by the use of microstructures suggesting an increase in roughness, Extrand suggested that asperity height may be less important than the asperity shape [104]. Line-patterned surfaces resulted in anisotropic wetting behaviour of drop movement parallel and perpendicular to the surface patterns [112]. It has been suggested that such behaviour is due to line-tension effects [113]. Studies on patterned surfaces are typically aimed at the fabrication of superhydrophobic surfaces, which may result in an imprecise conclusion regarding the wetting behaviour of liquids on rough and heterogeneous surfaces of low contact angles.

The validity and applicability of both the Wenzel and Cassie-Baxter equations, and the transition from one regime to the other, will surely continue to be of major interest for some time to come. Unfortunately, at present, it is still not precisely known at what length-scale would one need to consider roughness as an influencing factor especially when coupled with heterogeneity effects. The commonly accepted view is that roughness (R_a) below 100 nm does not influence contact angles and hysteresis [114]. Current research has also focused on the evaluation of contact angles on rough solid surfaces, by supplying energy in the form of vibration to overcome the energy barriers [115, 116]. Recently, a study based on 2D thermodynamic modelling on rough heterogeneous surface introduced a surface feature factor, ω to define the category to which the surface belongs [117]. The prediction of θ_a and θ_r were found to be dependant on this parameter ω. The proposed model is still at its initial stages of development but appears rather promising.

2.12.3 Use of Hysteresis for Surface Energy Evaluation

Contact angle hysteresis is evident in cases where heterogeneity, physical or chemical, is present as discussed in the previous section. However, even on carefully prepared films where physical roughness or chemical heterogeneity should not be present, the θ_a and θ_r are still not exactly the same. It has also been suggested that the hysteresis may be reproducible, and hence may actually represent the surface chemistry of the solid. Chibowski used this viewpoint to propose a method of evaluating the solid surface energy from θ_a and θ_r data. In the model, it is assumed that the receding angle represents the surface energy of a film left behind from the advancing drop. Detailed development of this model is found elsewhere [118]. The equation proposed is as follows:

$$\gamma_{SV} = \gamma_{LV} \cdot (\cos\theta_r - \cos\theta_a) \frac{(1+\cos\theta_a)^2}{(1+\cos\theta_r)^2 - (1+\cos\theta_a)^2} \qquad (2.104)$$

This analysis implies that the solid surface energy can be determined from the measurements of θ_a and θ_r of a single liquid, including for the case of a stable liquid film ($\theta_r = 0^o$). However, in the case where hysteresis is zero, the proposed model will fail. Although such systems are almost never encountered, a recent paper suggests that there may be no hysteresis on ultrasmooth self-assembled monolayers of alkanethiolates [119].

The average surface energies obtained from the θ_a and θ_r of various probe liquids on glass, PMMA, steel and cadmium were found to be in good agreement with literature values obtained from acid-base theories [120]. The γ_{SV} values obtained were dependent on the test liquid used and may represent certain specific solid-liquid interactions, but no direct information on the solid surface properties is available. More recently, Chibowski proposed an extension to the earlier model by investigating

the contribution of the dispersion component. It was reported that γ_{SV}^{d} as well as γ_{SV} for silyl layers were dependent on the probe liquid used to a certain extent [121]. The evaluation of γ_{SV} from the θ_a and θ_r of probe liquids is useful, but at present, the models may need further refinement and have yet to widely accepted.

2.12.4 The Equilibrium Spreading Pressure

The classic description of a contact angle is for a liquid in thermodynamic equilibrium with its own saturated vapour phase. This vapour phase may adsorb on the solid surface and as a result reduces the solid surface energy. The reduction in solid surface energy due to the adsorption of this vapour phase is known as the equilibrium spreading pressure, π_e. Adding this term into Young's equation leads to:

$$\gamma_{SV} + \pi_e = \gamma_{SL} + \gamma_{LV} \cdot (1 + \cos\theta_e) \tag{2.105}$$

The distinction between the γ_{SV}^{o} and γ_{SV} was first reported by Bangham and Razouk [122] and efforts to measure the value of π_e have been attempted by many workers. For a gas-solid system, the Gibb's adsorption equation can be written as:

$$-d\gamma = RT \cdot \Gamma \cdot d\ln p \tag{2.106}$$

where Γ is the surface excess (surface concentration) at the interface due to amount of adsorbate adsorbed as a function of increments of vapour pressure, p. Thus, the spreading pressure can be obtained by integrating the above equation.

$$-\int_{\gamma_{sv}^{o}}^{\gamma_{sv}} d\gamma = RT \cdot \int_{0}^{p} \Gamma \cdot d\ln p \tag{2.107}$$

$$\pi_e = RT \cdot \int_{0}^{p} \Gamma \cdot d\ln p \tag{2.108}$$

Adamson and co-workers [123, 124], in their pioneering work employed the sensitivity of the ellipsometry technique for measurements of vapour film thickness to calculate the π_e. They reported that even for θ_a of water of 90 ^{o} on smooth carbon films, polyethylene and on stearic acid-coated copper, the adsorbed film thicknesses were substantial. It was also noted that large contact angles do not necessarily imply low π_e. The π_e of n-propanol and water on a range of polymers (PTFE, PS, PMMA and PC) and glass were also found to be significant, although they were similar for both liquids [125].

In a more elegant approach, Fowkes et al. [126] measured the contact angles of diiodomethane and water, both in air and in the presence of an adsorbing vapour, on low energy polyethylene and PTFE polymers. This data was compared to the predicted π_e obtained from equation 2.109, assuming that the interaction between solid and liquid is purely dispersive.

$$\pi_e = 2\sqrt{\gamma_S^d \gamma_L^d} - 2\gamma_L \tag{2.109}$$

They concluded that in the case of these low energy solids, high surface tension liquids such diiodomethane and water do not adsorb or spread appreciably [126]. van Oss et al. also came to similar conclusions by observing a non-wetting case for high γ_L on low energy solids in wicking experiments [127].

The measurement of π_e is not easy and for obvious reasons, has often been neglected in the evaluation of solid surface energy when the contact angle is greater than 10°. Like many issues relating to contact angle measurements, the π_e remains an unresolved issue, and is the on-going focus of various research groups. The accepted view by physical chemist for many decades, is that the π_e of a vapour is positive. In 2000, Schrader claimed that the π_e does not necessarily reduce a solid's surface

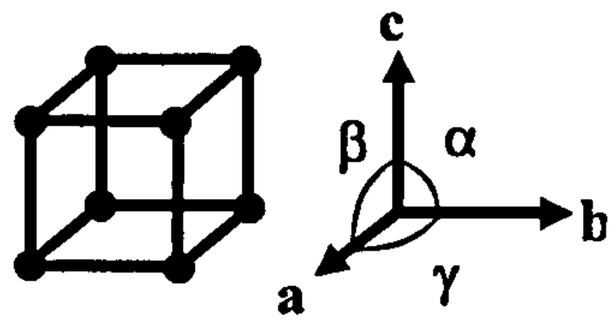
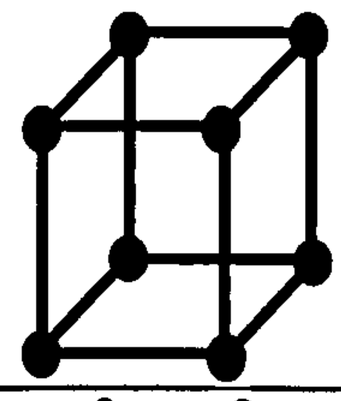
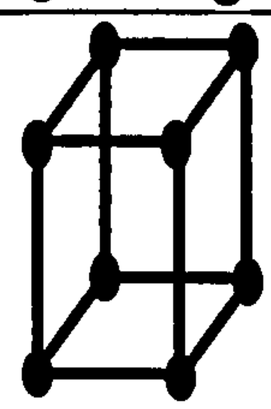
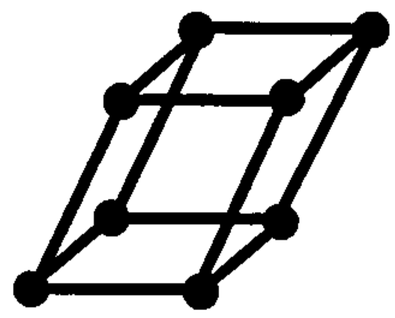
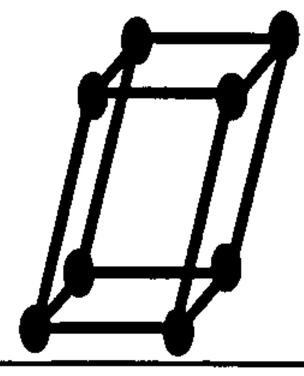
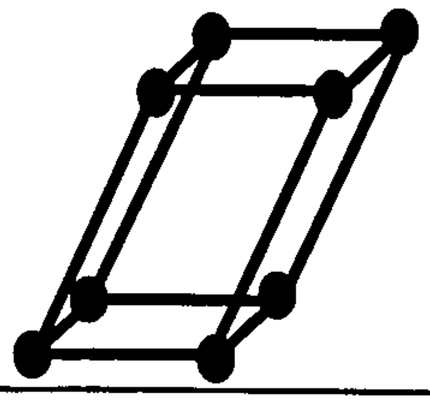
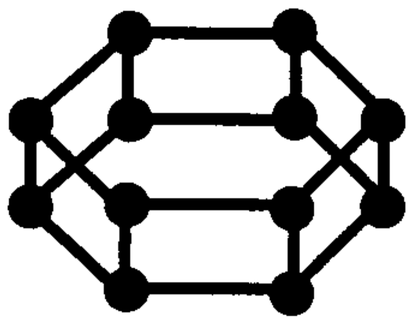
energy, as in the case of water vapour adsorption on PTFE [128]. In cases where the π_e is appreciable, be it positive or negative, it will have serious implications to our current understanding of the wetting phenomena.

CHAPTER 3 PROPERTIES OF PHARMACEUTICAL SOLIDS

3.1 Introduction

Crystalline solids possess rigid structures which are held together in long-range order, with each atom or molecule occupying a specific position in an organised and repetitive lattice structure. Their solid state behaviour is significantly determined by the types of forces which hold the molecules together. In this thesis, the ionic and metallic forces are not discussed as organic pharmaceutical solids are held in place predominantly by van der Waals forces and hydrogen bonding. Molecular crystalline solids are made up of unit cells which describe the spacing and angles between each molecule and are classified into one of the seven crystal systems (Table 3.1) [129]. On the other hand, the amorphous state possesses no long range order, and the solid exhibits a liquid-like structure. More than 90% of all drugs are administered in the solid form with a majority in the crystalline form [130].

Table 3.1: Crystal Systems

System	Unit Cell Dimensions	Schematic
Cubic	$a = b = c$ $\alpha = \beta = \gamma = 90^\circ$	
Tetragonal	$a = b \neq c$ $\alpha = \beta = \gamma = 90^\circ$	
Orthorhombic	$a \neq b \neq c$ $\alpha = \beta = \gamma = 90^\circ$	
Rhombohedral	$a = b = c$ $\alpha = \beta = 90^\circ, \gamma \neq 90^\circ$	
Monoclinic	$a \neq b \neq c$ $\alpha = \gamma = 90^\circ, \beta \neq 90^\circ$	
Triclinic	$a \neq b \neq c$ $\alpha = \beta, \gamma \neq 90^\circ$	
Hexagonal	$a = b \neq c$ $\alpha = \beta = 90^\circ, \gamma = 120^\circ$	

3.2 Crystal Growth

3.2.1 Solvent Mediated Growth

A solution is formed when solids (solutes) dissolve into a liquid (solvent). This process continues until no more solute can dissolve, and the solution is said to achieve a saturated state. The amount of solid which can be dissolved by a solvent is dependant on the temperature and also on type of solvent. Typically, a polar solid will be dissolved by a polar liquid and vice versa. By increasing the temperature of a saturated state, additional solid can then be dissolved as solubility increases with increasing temperature, until a new saturated point is reached. Upon cooling, one would expect that the dissolved solid would immediately precipitate but this expectation is not always the case. The solute may remain dissolved and the solution is termed to be supersaturated. A supersaturated solution is typically defined by:

$$\sigma = \ln\left(\frac{c}{c_s}\right) \tag{3.1}$$

where c is the concentration of the solution while c_s is the saturated concentration and σ is the degree of supersaturation.

In a supersaturated state, the solution is thermodynamically unstable. It has to overcome an energy barrier prior to nucleation and crystallisation, which is the reverse of dissolution. Without nucleation, crystallisation will not happen and the solution will remain in a metastable state. Three types of nucleation are known to exist; homogenous, heterogeneous and secondary nucleation. Crystallisation is described in detail by Mullins [129], and is summarised here.

Homogenous nucleation occurs as a result of solutes within a bulk solution overcoming the activation energy barrier, but generally occurs infrequently. The most common mechanism is a heterogeneous nucleation process due to presence of

impurities which act as nucleation sites. If a seed crystal is added to the metastable solution, the solute will precipitate or crystallise on this seed and the solution will achieve a stable state with the resulting growth in the crystal seed. Such secondary nucleation is also controlled by several other mechanisms such as agitations as well as concentration and temperature gradients.

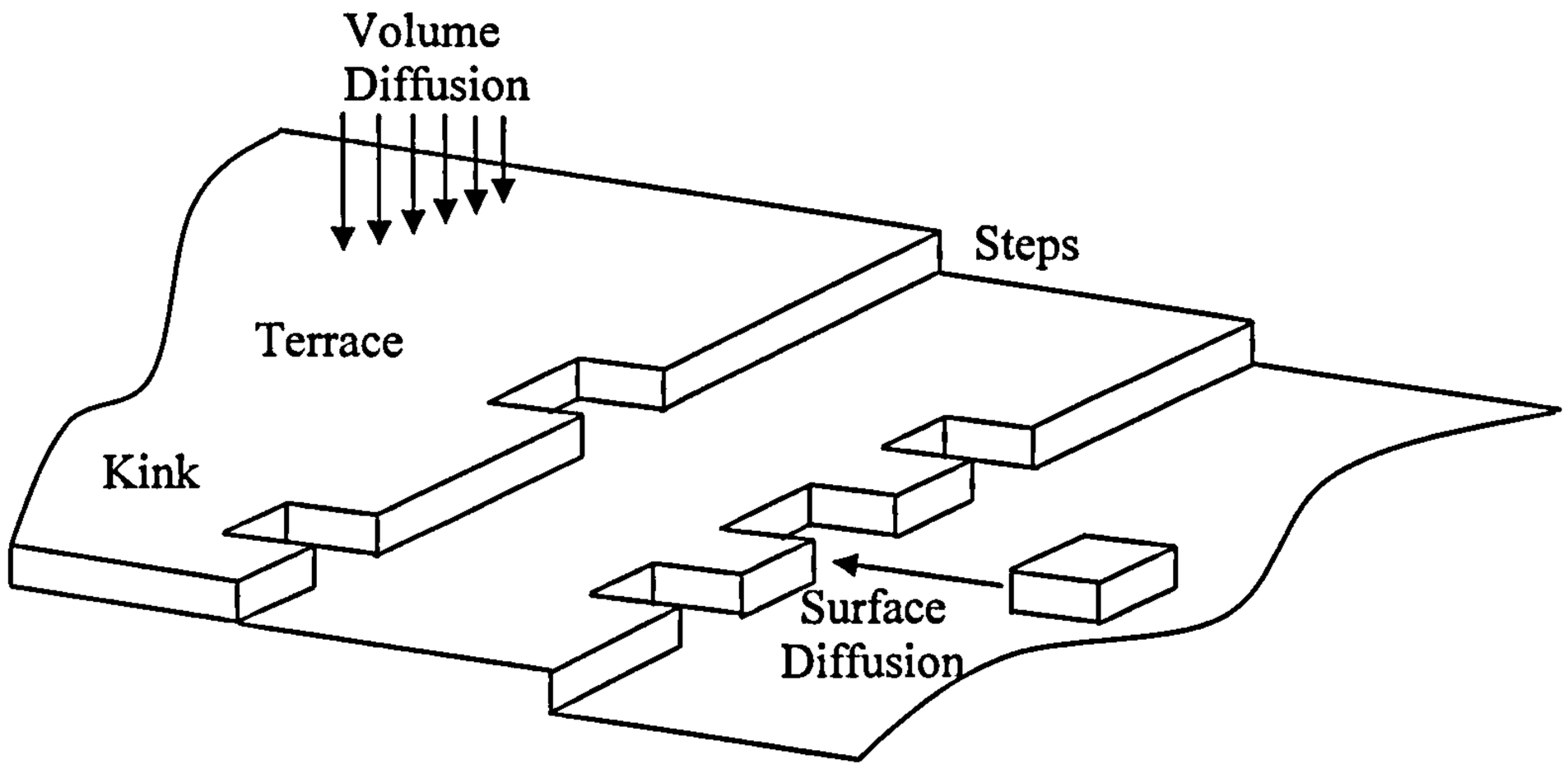
3.2.2 Crystal Growth Mechanisms

Once nuclei are formed, any subsequent successful inclusion of molecules will result in the growth of crystals, including macroscopic ones, over a prolonged period of time. The inclusion of molecules onto the crystal surface is dependant on the availability of sites to accommodate the molecules, with a kink site being the most energetically favourable.

The most commonly used model to describe crystal growth is known as the Terrace-Ledge-Kink (TLK) model as shown in Figure 3.1 [131]. A molecule must firstly diffuse from the bulk to the surface, which is envisaged to be made up of layers or steps of monoatomic height. At the surface, this molecule can either attach itself directly onto the crystal lattice if it arrives at a kink, or could undergo surface diffusion to a kink, or otherwise desorb back to the bulk solution. Each layer may contain several kinks, which molecules could attach to resulting in the advancement of the terrace. A kink is the energetically favourable site as an incorporated molecule is attached to molecules from all three dimensions. As the terraces advance, a new surface layer is formed with fresh steps created by surface nucleation. Crystal growth is thought to be faster on rough surfaces as many kink sites are thought to be present.

Crystal growth can occur via several mechanisms; continuous growth, surface nucleation and spiral growth. Crystals can also be imperfect suffering from point defects, line defects and surface defects.

Figure 3.1: The Terrace-Ledge-Kink model of a growing crystal face.



3.2.2.1 Surface Nucleation

In the event a molecule does not arrive at a kink site, it will either desorb back into the solution or undergo surface diffusion with the possibility of meeting another molecule and then forming surface nuclei. At high degrees of supersaturation, the possibility of surface nucleation is greater than desorption, resulting in a higher density of kink sites. These surface nuclei are often referred to as two dimensional islands, resulting from a two dimensional nucleation. The formation of such surface nuclei can proceed until a whole surface is fully formed, also known as the Birth and Spread mechanism as shown in Figure 3.2 [132, 133].

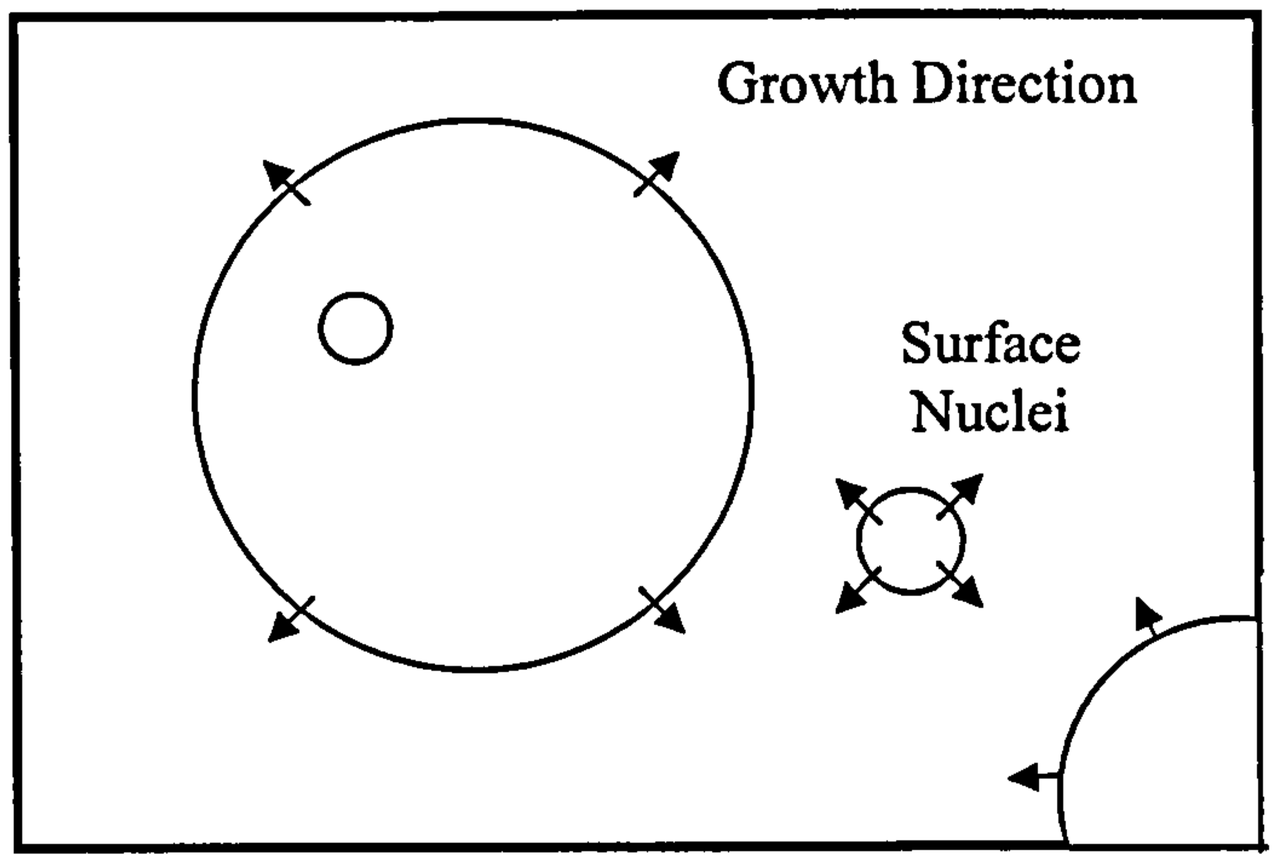
As the probability of surface nucleation increases with degree of supersaturation, the growth rates will also follow suit. The Birth and Spread model relates crystal face growth velocity, v_C to degree of supersaturation and is given by:

$$v_C = A_1\left(\frac{c - c_S}{c_S}\right)^{\frac{5}{6}} \exp\left(\frac{-A_2 c_S}{c - c_S}\right) \tag{3.2}$$

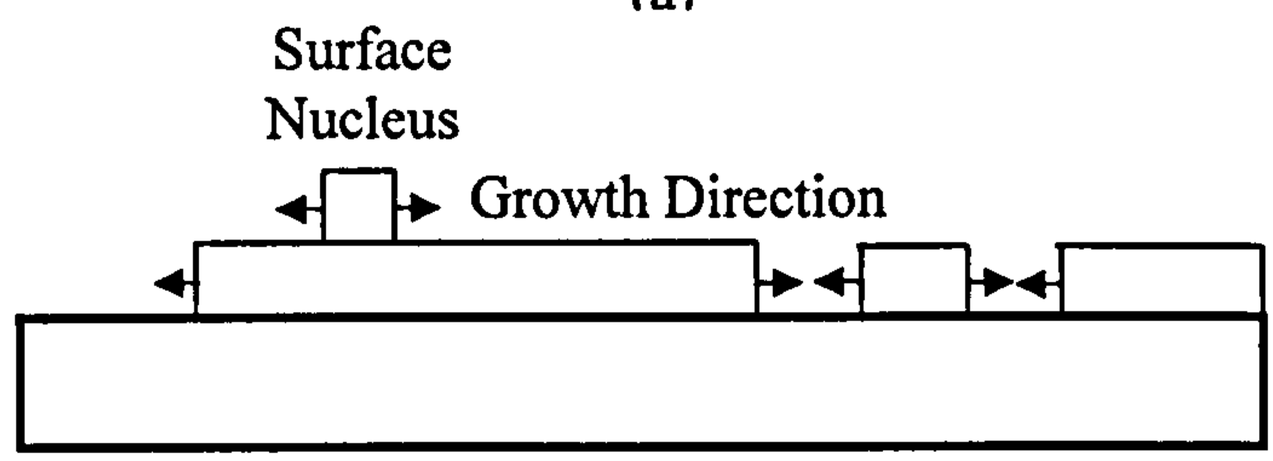
where A_1 and A_2 are properties of the system. In the case of a high concentration, the exponential term approaches unity which indicates that surface nucleation is not the

limiting step to crystal growth. For lower concentration values, the activation energy becomes dominant.

Figure 3.2: The Birth and Spread mechanism for crystal growth (a) top view and (b) front view.



(a)



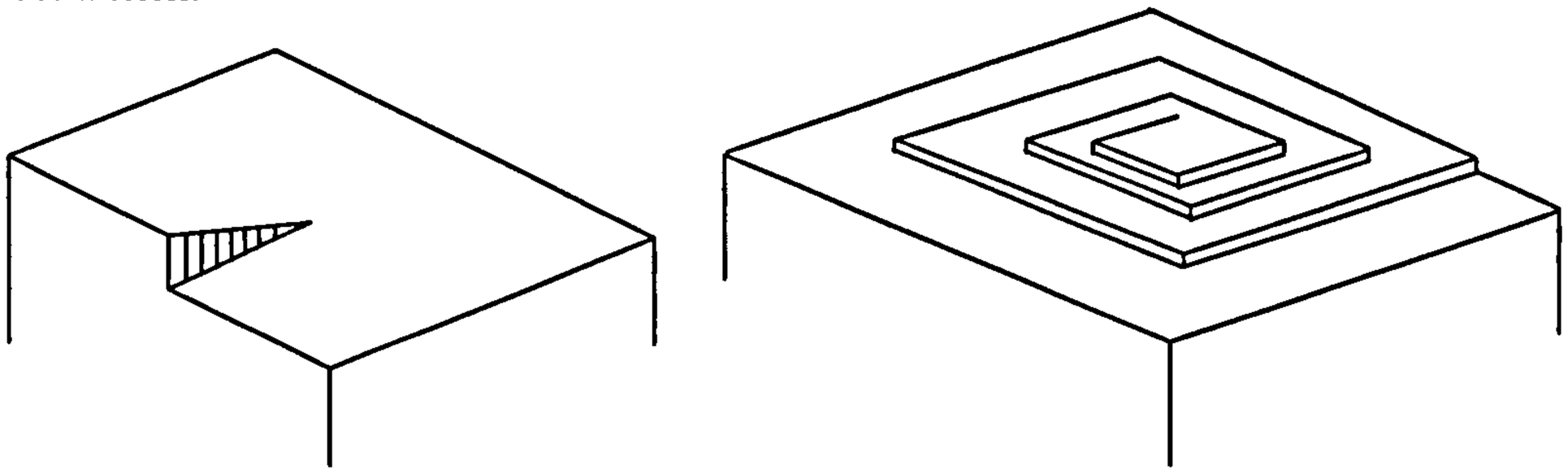
(b)

As crystal growth proceeds, the degree of supersaturation will eventually decrease to a level when it can no longer support the formation of surface nuclei. Since crystal growth is usually imperfect, a screw dislocation defect will eventually dominate the growth mechanism.

3.2.2.2 Screw Dislocation

A screw dislocation defect occurs when a region of the crystal surface is elevated by a unit or more, relative to the other regions. In the presence of such defect, a completely smooth surface is almost never present, and this defect will allow molecules to attach onto it allowing continued crystal growth even at reduced degrees of supersaturation. More importantly, the defect is not eradicated with growth (Figure 3.3).

Figure 3.3: The (a) development of a screw dislocation defect and (b) the growth mechanism.



(a) (b)

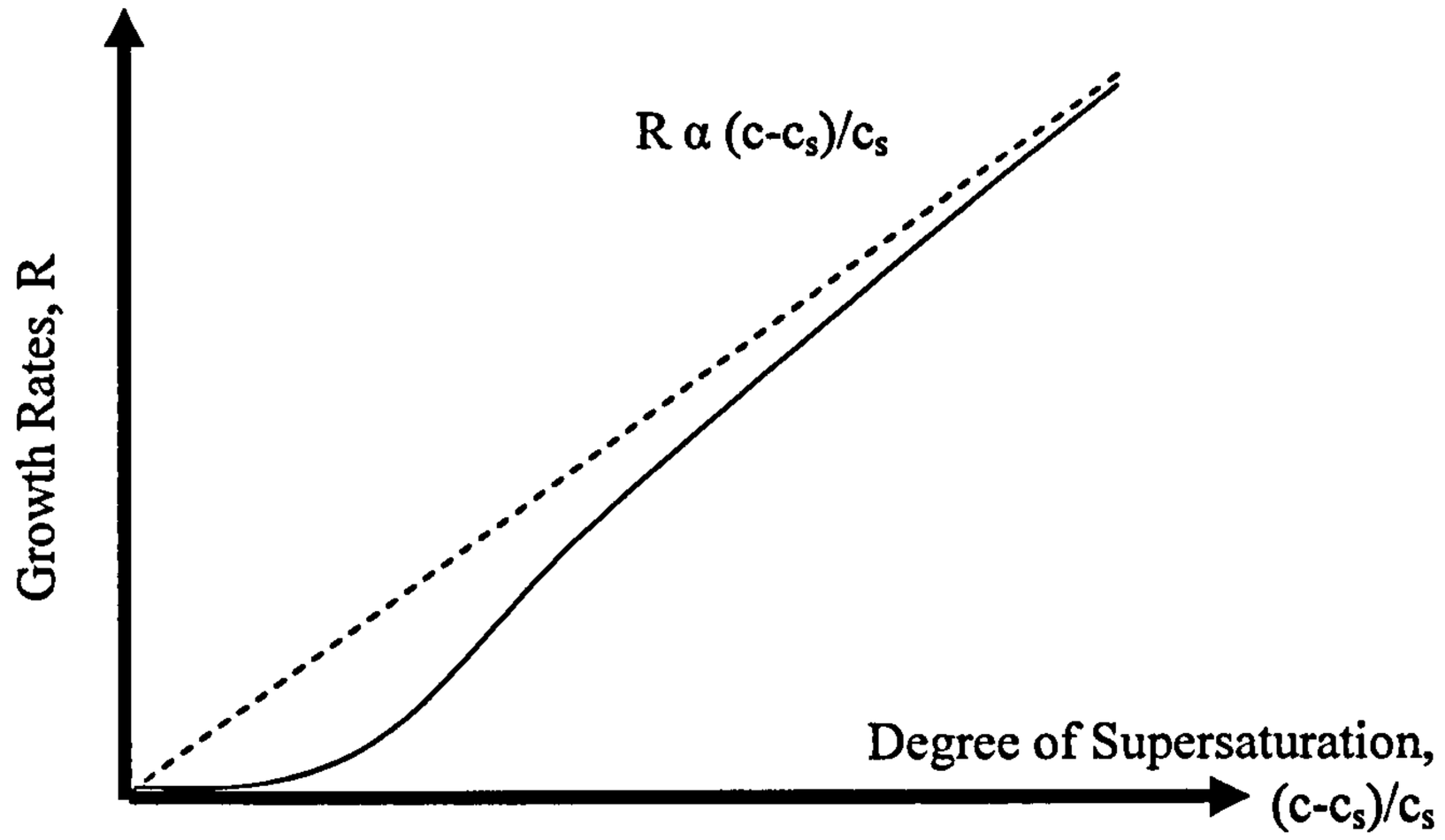
Such growth rates are described by the Burton-Cabrera-Frank (BCF) model [134]. The BCF model is used to describe the growth rate where surface nucleation is not sufficient for continued growth, such as at low degrees of supersaturation. The model is based on the addition of molecules to the endless series of steps, which are separated at equal distance due to surface dislocation. It relates the kinetic theory of growth and the predicted kink population from Boltzmann statistics, and assumes that surface diffusion is an essential step. The crystal growth rate according to the BCF model can be written as:

$$Rate = A\left(\frac{c-c_s}{c_s}\right)^2 \tanh\left(\frac{Bc_s}{c-c_s}\right) \tag{3.3}$$

where A and B are temperature dependent constants and include parameters influenced by crystal step spacings.

At low degrees of supersaturation, the growth rate is proportional to $[(c\text{-}c_s)/c_s]^2$ while at higher degrees of supersaturation, it is proportional to $(c\text{-}c_s)/c_s$. As supersaturation increases, the growth rate curve is expected to change from a parabolic to a linear shape (Figure 3.4). The BCF model was derived for crystal growth from the vapour phase and although it should be applicable for solvent mediated growth, the latter system has added complications which arise from the complex nature of the transport phenomena in solution.

Figure 3.4: Growth rates as a function of degree of supersaturation as predicted by the Burton-Cabrera-Frank model.



3.2.2.3 Continuous Growth

The continuous growth mode refers literally to one which occurs without interruption. This mode is due to the presence of multiple or infinite number of kinks or sites for the incorporation of molecules onto the crystal face. Energy requirements for such formation are also thought to be low and the resulting crystal faces are typically rough. Such mechanisms are predominant in crystallisation from melt or vapour phase deposition.

3.2.3 Crystalline Habits

As described in the previous sections, the growth rates of crystalline facets may depend on the degree of supersaturation within the crystallisation solvent. The relative growth rates of each individual facet will determine the final crystal habit, with the slowest growing face being most dominant in the final form. Crystal shapes have puzzled scientists for centuries, and many have tried to explain the resulting crystal habits unsuccessfully. The traditional approach considers the intrinsic properties of

the crystals such as its interplanar spacing and attachment energies, without taking into account the importance of external influences.

Crystallisation of aspirin from different solvents has been reported to result in a range of crystal habits. Needles were produced from hexane due to optimum growth rate of facet (100) while plate shaped crystals were obtained for growth from ethanol solution due to optimum growth of facet (001) [135]. These observations will be discussed further in Chapter 9 where the habit of aspirin is rationalised based on the wetting studies and crystallographic information. However, it is difficult to predict the presence or disappearance of certain facets purely based on the surface chemistry and growth rates. As a note of caution, the potentially important role of surface chemistry in contributing to crystal habit determination is debatable, as crystal growth is known also to be influenced by various kinetic factors [129].

3.3 Determination of Crystal Properties

Diffraction of a wave occurs if the wave interacts with a regular structure whose atomic spacing is similar to its wavelengths. The wavelengths of X-rays are typically in the order of a few angstroms, which is similar to the spacing within crystalline solids. As such, an incident X-ray beam will be diffracted by crystalline solids of a regular repeating structure. The ability to determine crystalline structures is of immense importance and no technique has yet to surpass the importance of X-ray diffraction for crystal structure determination. Such has been exemplified by the award of Nobel prizes to Max van Laue for the discovery of diffractions of X-rays by crystals in 1914 and followed on the very next year to a father and son team (William Henry Bragg and William Lawrence Bragg), for the use of X-rays for analysis of crystallographic structures. The first analysis on organic structures was obtained by

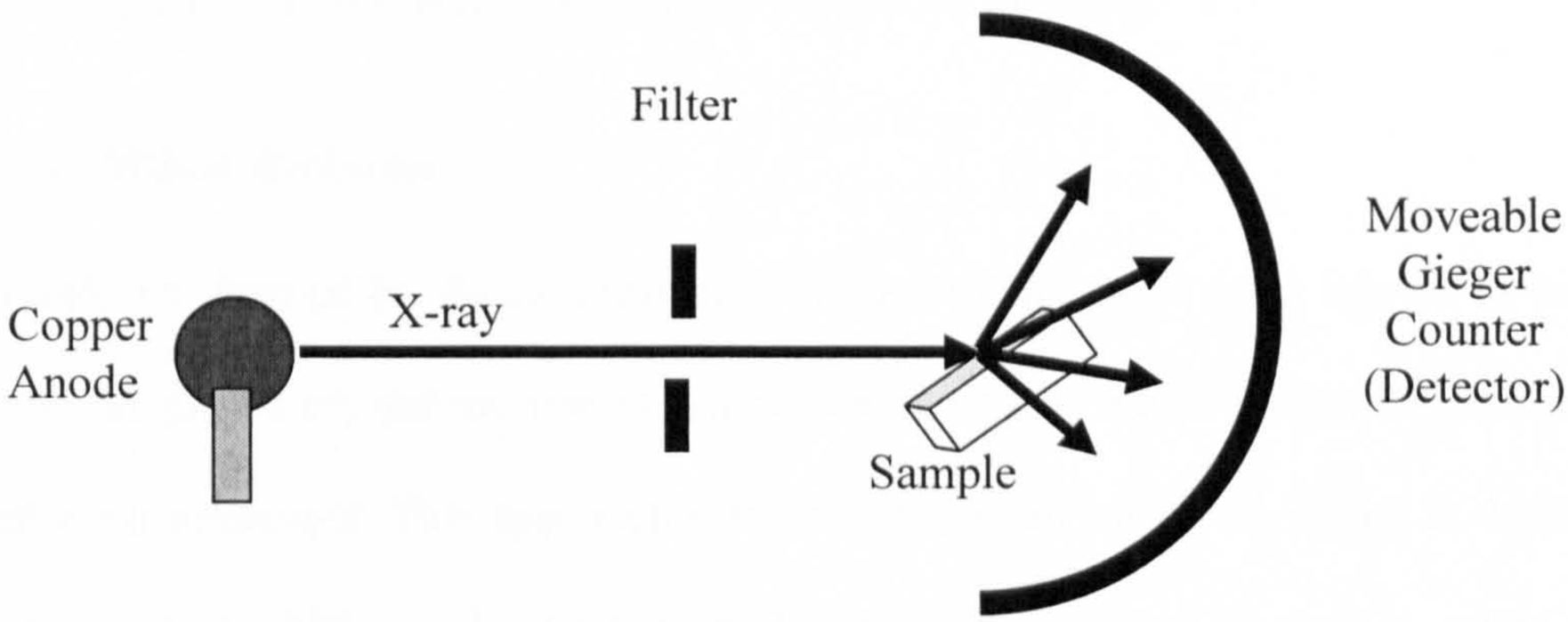
Perutz and Kendrew, who went on to win the chemistry Nobel Prize in 1962. X-rays are capable of identifying the compound and from the diffraction pattern, reveals bond lengths and angles of a crystal structure [136].

The principle behind the X-ray diffraction (XRD) technique is rather simple (Figure 3.5). A copper X-ray source is typically used, where electrons are supplied from a tungsten filament and are accelerated to the copper target by a 40 kV potential difference. A slit allows only a portion of collimated copper X-ray with a wavelength of 1.54 Å to reach the sample. The X-rays diffracted by the sample are detected by a scintillation counter which measures the diffracted beam intensity, and the detector is moved through a range of angles. The characteristics of the crystal can then be determined by Bragg's Law:

$$n_B \lambda_X = d_{hkl} \cdot \sin 2\theta_B \tag{3.4}$$

where n_B is an integer, λ_X the wavelength of the X-ray source, d_{hkl} the interplanar spacing of the crystal and θ_B the diffraction angle (not the Young's contact angle).

Figure 3.5: Schematic of the principle of powder X-ray diffraction.



XRD for the determination of pharmaceutical solids crystallinity is routinely performed, including for the characterisation of polymorphs [18]. It is also useful for the study of the amorphous phase, as this phase does not diffract X-rays due to their

irregular internal structures. The quantification of relative amounts of anhydrous and dihydrates [137] of carbamazepine and α- and β-carbamazepine [138] in a mixture, was also obtained from powder XRD. XRD has also been applied to study the crystallisation behaviour and the transformation of the α-, β- and anhydrous form of lactose in situ [139]. The introduction of synchrotron X-rays has improved the quality of the diffraction patterns obtained [140], which enables the detection of crystallinity of as low as 0.2 % [141].

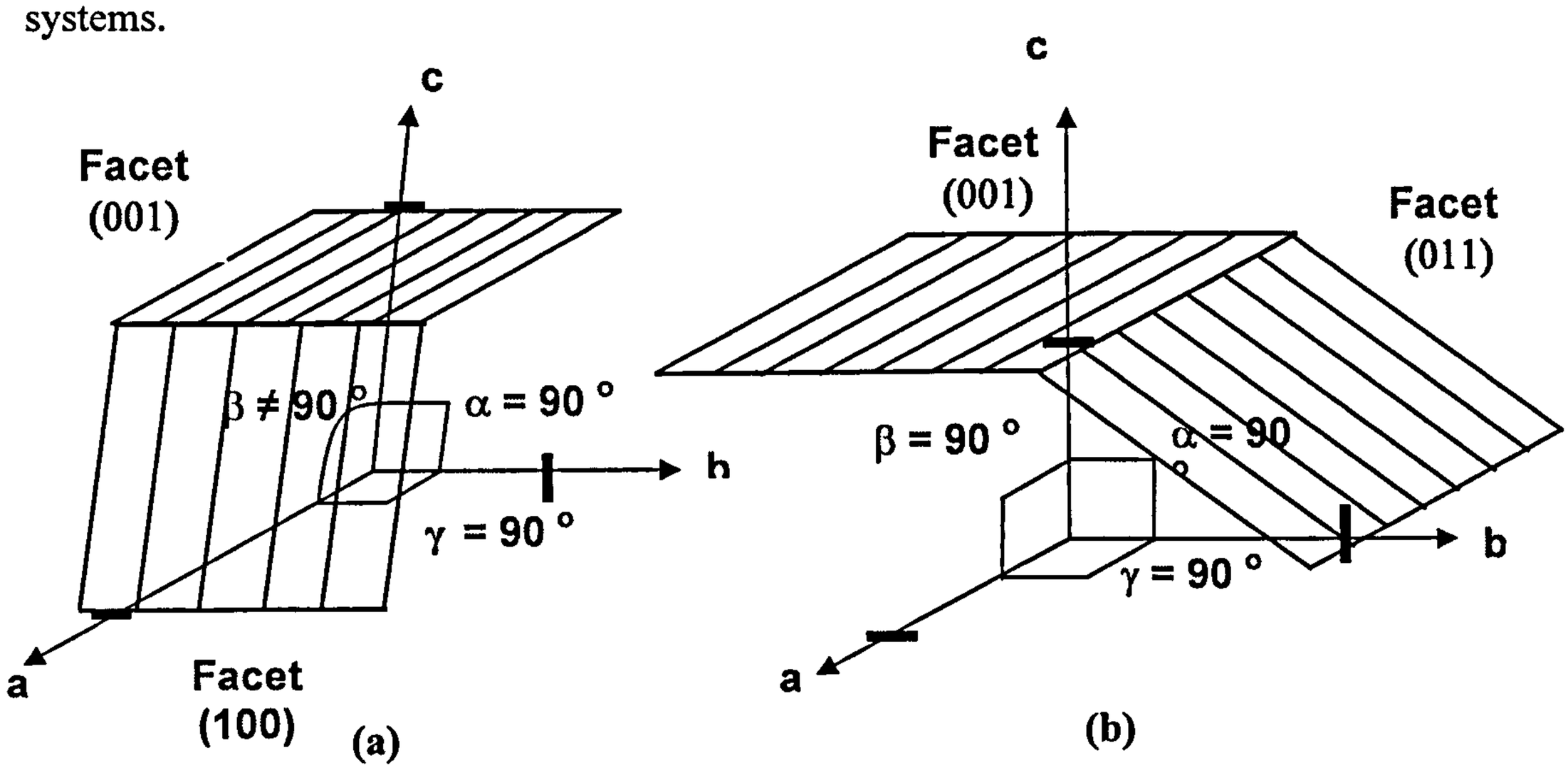
The determination of crystalline solid properties often entails the use of numerous techniques. A single XRD test may only reveal the internal crystal dimensions and is usually complemented with thermal analysis, microscopy, spectroscopy including sorption studies for a more comprehensive determination of their physico-chemical properties. It will be beyond the scope of this thesis to provide a comprehensive examination of all the techniques available. The reader is directed to available literature which reviews these techniques, with particular applications to pharmaceutical solids [142-151], including computational techniques [152]. However, selected techniques will be highlighted throughout the thesis, with a focus given to those which relate to the surface properties of solids.

3.3.1 Miller Indices

Crystals are formed by facets forming a characteristic shape (also known as habit). These facets are crystalline planes which are described and numbered according to their axial intercepts. This approach was first suggested by W. H. Miller in 1839 and is known as the Miller indices where each facet is denoted by its corresponding (hkl) indices. The integers h, k and l are the reciprocal of the unit length of the a-, b- and c-axis, respectively to the plane axis intercept (Figure 3.6), in whole numbers. In the case where the plane is parallel to the axis and thus does not intercept the axis, it is

denoted as a 0. The dihedral angle, ρ_d is the angle between two crystalline facets and is distinctive for the facets and its crystal system. In the hexagonal and rhombohedral crystal systems, a fourth index is used and is known as the Viller index. While the use of [hkl], <hkl> and {hkl} denotes the direction in real space, a family of directions and a family of planes respectively, the use of (hkl) in this thesis indicates the specific crystalline faces which forms the crystal habit.

Figure 3.6: Miller indices of crystalline facets (a) monoclinic and (b) orthorhombic systems.



3.3.2 Dihedral Angles

Hauy, in 1784 proposed his laws of constant interfacial angles. He found out that the angles between two crystalline faces were always constant regardless of their size, except in a polymorphic case. The interplanar spacing and the dihedral angles, ρ_d, can be calculated as follows [153].

For an orthorhombic system, the interplanar spacing is calculated by Equation 3.5 and the dihedral angles by Equation 3.6:

$$\frac{1}{d_{hkl}^2} = \frac{h^2}{a^2} + \frac{k^2}{b^2} + \frac{l^2}{c^2} \tag{3.5}$$

$$\cos\rho_d = \frac{\frac{h_1h_2}{a^2}+\frac{k_1k_2}{b^2}+\frac{l_1l_2}{c^2}}{\sqrt{\left(\frac{h_1^2}{a^2}+\frac{k_1^2}{b^2}+\frac{l_1^2}{c^2}\right)\left(\frac{h_2^2}{a^2}+\frac{k_2^2}{b^2}+\frac{l_2^2}{c^2}\right)}} \tag{3.6}$$

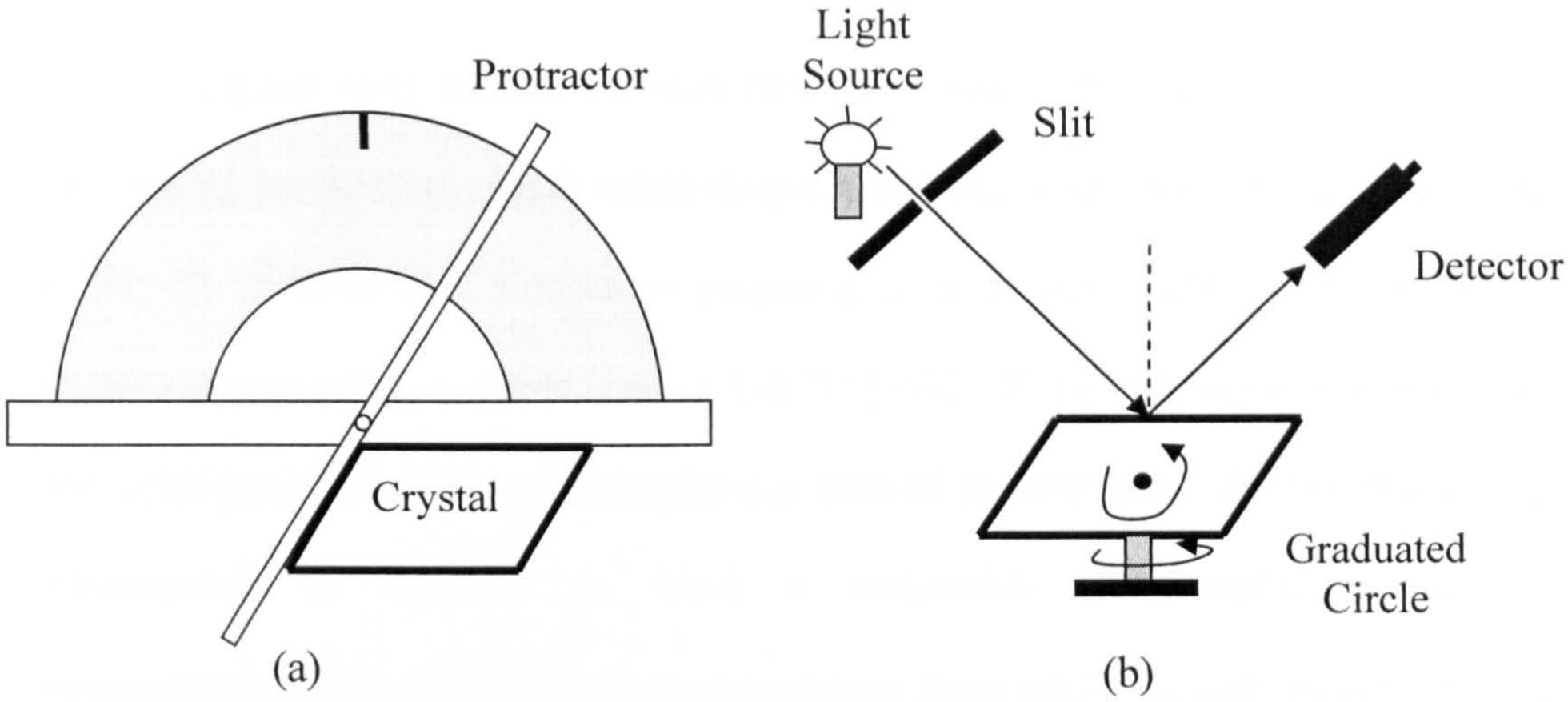
For a monoclinic system:

$$\frac{1}{d_{hkl}^2}=\frac{1}{\sin^2\beta}\left(\frac{h^2}{a^2}+\frac{k^2\sin^2\beta}{b^2}+\frac{l^2}{c^2}-\frac{2hl\cos\beta}{ac}\right) \tag{3.7}$$

$$\cos\rho_d=\frac{d_1d_2}{\sin^2\beta}\left(\frac{h_1h_2}{a^2}+\frac{k_1k_2\sin^2\beta}{b^2}+\frac{l_1l_2}{c^2}-\frac{(l_1h_2-l_2h_1)\cos\beta}{ac}\right) \tag{3.8}$$

The dihedral angles of centimeter sized crystals can also be directly measured, with a protractor, but with limited resolution (Figure 3.7). An optical goniometer offers more precise and accurate measurements. A light source emerges from a slit and is reflected at the crystal surface, and the reflection is detected by a microscope or telescope. The crystal is held on a goniometer head, which is made up of two graduated circles so that all crystalline facets can be positioned such that their facet reflects the light source to the detector. The crystal is then rotated until a point when the light source is reflected by the adjacent facet and is detected, and the angle or rotation is recorded. This angle corresponds to the dihedral angle. An experienced crystallographer may be able to deduce or identify the miller indices of a crystalline solid based on the dihedral angles.

Figure 3.7: Measurement of the dihedral angle between crystalline facets with (a) a protractor and (b) a goniometer.



3.4 The Crystalline State

Crystalline solids can exists in a variety of states; crystalline, polymorphs, hydrates, solvates, and these can interconvert during pharmaceutical processing or storage. It is the ability to quantify, control and predict these transformations that is of major interest to both academia and industry. The various types of crystalline solids will be explained in the following sections.

3.4.1 Polymorphs and Enantiomorphs

Crystallisation conditions such as degree of supersaturation, solvent and temperature may influence the resulting crystal structure. Molecules which are chemically identical can be packed in different crystal lattices, with differering spacing, angles or even the crystal system, and such systems are known as a polymorphs. Polymorphism is common in virtually all classes of pharmaceutical solids, but especially for barbiturates, sulphonamides and steroids [18].

Polymorphism results in the material having different physicochemical [154] and thermodynamic properties [155] such as the melting temperature, densities,

refractive indices, spectra properties [156], crystal habits, processibility [157] and solubilities including bioavailabilities.

Crystals may exhibit enantiotropic behaviour, where the order of stability depends on temperature. Such enantiotropic behaviour is exhibited by caffeine, which is known to form two anhydrous polymorphs, a β form stable at 25 °C with a transition in stability to the α form at 141 °C [158]. If the stability of polymorphs is not interchangeable, the polymorphs are termed monotropic. In this work, only paracetamol is reported to have a metastable polymorphic form. The thermodynamically stable form is the monoclinic form while the orthorhombic form is metastable at room temperature. There are experimental results suggesting a possible transition temperature for paracetamol ranging from -40 °C to -120 °C [159], but this temperature remains in disputable.

Mirror images of molecules which do not superimpose or have planes or centres of symmetry are termed as enantiomers. Such molecules are capable of rotating the plane of light to the left or right, depending on the enantiomorphic form, denoted by the R and S convention. Crystallisation of enantiomers can lead to one of the following, the optically active R or S crystals or in the case of a correct proportion, a racemic compound. Racemism can also be due to a mechanical mixture of two enantiomers of equal proportion, and is termed as conglomerates. In this thesis, the surface properties of an ibuprofen racemic compound and the S-(+)-ibuprofen are also studied and compared, and are reported in Chapter 6.

3.4.2 Hydrates and Solvates

The nature of a water molecule, being small and capable of multiple hydrogen bonding, makes is very suitable to be incorporated into a crystalline structure. Water molecules can either be adsorbed to the surface or they can be situated within the

crystalline lattice. The amount of water within the crystal lattice can either be stoichiometric or non-stoichiometric. Stoichiometric hydrates will typically exhibit different X-ray patterns as in the case of α-lactose monohydrate [139]. Non-stoichiometric hydrates exist due to water molecules forming hydrogen bonded networks, probably tetrahedrally coordinated. Such networks are normally not part of the crystal lattice. They are found to exist within large void spacings within the crystal lattice, commonly known as channel hydrates.

The inclusion of water molecules in a crystal structure disrupts the intermolecular forces, and hence crystal enthalpy and entropy which in turn affects the material's thermodynamic stability. Hydrates for example, are stable within specific conditions of relative humidity and temperature, and the hydration/dehydration transition conditions are often investigated via a controlled sorption/desorption studies, where the mass uptake of a sample is recorded as a function of % relative humidity [160]. Such studies have proven to provide direct information on the hydration behaviour resulting in the possibility of obtaining the hydrate stoichiometry of the hydrated samples from water mass gain and loss. The study of pharmaceutical hydrates have also included the use of Raman spectroscopy, Nuclear Magnetic Resonance and isothermal microcalorimetry and is reviewed by Khankari and Grant [161].

Also of interest is the dehydration process, as this may sometimes result in the formation of an unstable amorphous phase (Section 3.4.3). In the case where a solvent molecule such as ethanol is included into the crystalline structure, the material is described as a solvate. Detailed reviews for characterisation of solvates by thermal analysis [162] and spectral analysis [163] can be found elsewhere.

With over a third of pharmaceutical solids forming hydrates and solvates, this area of research is of major interest to many, due to their complex physicochemical behaviour. This section only serves as an introductory note to the voluminous literature available. In this thesis, it may suffice to report that paracetamol is known to be able to form solvate only when crystallised from dioxane [164] and also a trihydrate by slow cooling of an aqueous solution to 0 °C. This hydrate rapidly transforms to the anhydrous stable monoclinic form at 20 °C [165]. Meanwhile, no hydrates or solvates have been reported for aspirin and ibuprofen.

3.4.3 Amorphous

Mechanical actions during processing such as the act of milling, compaction and grinding of pharmaceutical solids are known to induce local crystalline disorder resulting in the creation of amorphous zones. Spray drying of a pharmaceutical solid, may also result in the creation of an amorphous state as in the well known case of α-lactose monohydrate [166]. The amorphous state is that of a liquid like solid, characterised by its disorder over the entire solid phase, and will exhibit no X-ray powder diffraction pattern due to a lack of long-range order within the solid. These materials are thermodynamically less stable than the crystalline phase and would eventually crystallise to the stable crystalline form. The time for such transformations from amorphous to crystalline states is a subject of great research importance.

The amorphous state possesses several solid-state characteristics which at times are desirable, such as better powder flowability and increased solubility. An important characteristic of the amorphous phase is its glass transition temperature, T_g. Below the T_g, the amorphous phase lacks molecular mobility, which is termed the glassy state which is mechanically brittle. Above the T_g, the solid behaves more like an elastomer and is termed the rubbery state. The T_g is said to provide an indication of

the storage temperature to suppress the recrystallisation, which can be approximated by $T_g \approx 0.7 - 0.85\ T_m$, where T_m is the melting point.

The recrystallisation of a hydrophilic amorphous phase can be accelerated in the presence of moisture. It has been reported that water allows surface reorganisation and acts as a plasticising agent which lowers the T_g of an amorphous solid [167]. The importance of water on the plasticisation of many food based organic solids is reviewed in detail by Roos [168]. Elevated temperatures are also known to accelerate this transformation, and have been described in the classic polymer literature. On the contrary, recrystallisation of amorphous indomethacin was reported to be inhibited by the presence of poly(vinylpyrrolidone) (PVP). A molecular dispersion of indomethacin and PVC was thought to increase its T_g and hence stability of the amorphous state [169]. Changes in T_g due to salt selection have also been reported for indomethacin [170].

The need to characterise and quantify the amorphous content of pharmaceutical solids is indispensable and essential in the understanding of their behaviour and properties. Techniques such as isothermal microcalorimetry, powder XRD and IR/Raman spectroscopy will give a bulk based amorphous content determination for materials and the detection limits are often in the order of 5-10 % [171]. The tendency for amorphous regions to form at the surface of a solid at low overall levels, often limits the usefulness of these particular techniques.

Microcalorimetry was successfully used in the determination of amorphous contents in the order of 1 % for a ball milled hydrophobic drug, where no difference were reported from DSC scans and XRD patterns [172]. Another useful technique for detection of very low amounts of disorder is vapour sorption. Amorphous contents will change the sorption behaviour of solid materials drastically, with reported

detection levels by sorption techniques down to as low as 0.05 % [173]. This enhanced sensitivity is due to the enhanced water take up by the amorphous phase, compared to a very low level of water uptake for crystalline solids.

This section is intended only as an introductory, and the reader is directed to the works of Zografi, Buckton amongst the many others. A comprehensive review is reported by Yu [174]. The T_g of paracetamol and aspirin are 302 K and 243 K respectively. Ibuprofen is reported to form an amorphous solid in the presence of PVP [175]. In the milling of these solids, it is possible that amorphous regions may be generated, albeit at very low levels, and consequent recrystallisation is thought to dominate within the timescale of the experiment.

CHAPTER 4 PREPARATION OF CRYSTALLINE SOLIDS AND EXPERIMENTAL METHODOLOGY

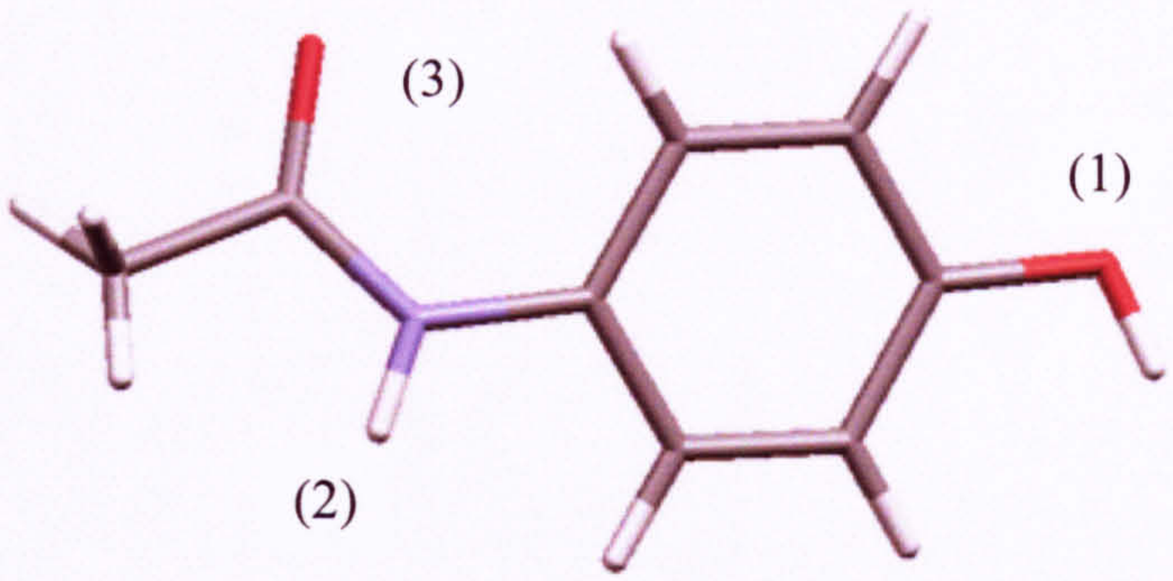
4.1 Introduction

Crystal growth can be induced via solvent evaporation, temperature reduction, sublimation and directly from the melt. The general approach employed here for the growth of macroscopic single crystals is described in this Chapter. Growth of macroscopic crystals enables the direct determination of facet specific surface properties. These properties are determined by contact angle analysis and reported in Chapter 6, and by X-ray Photoelectron Spectroscopy as reported in Chapter 7.

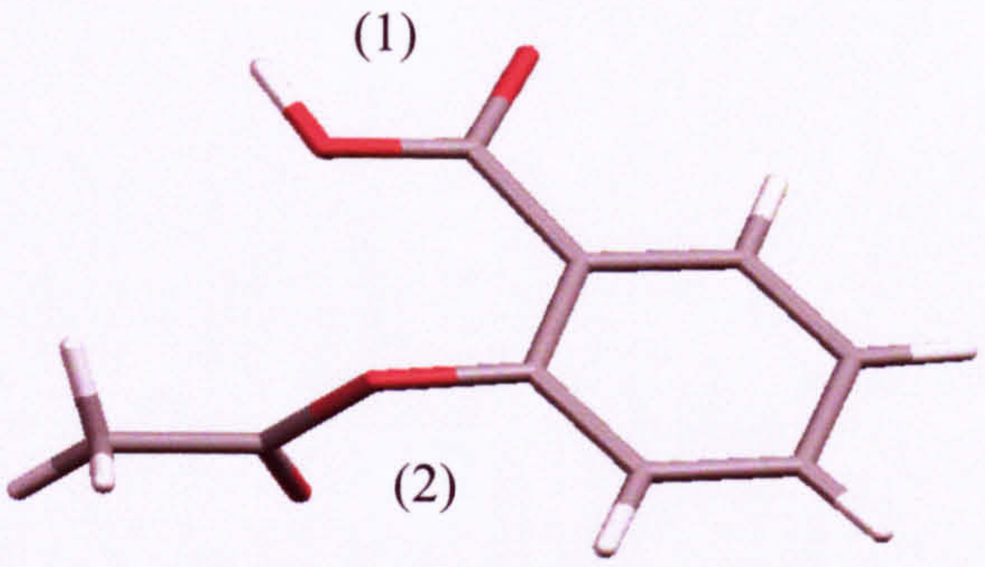
4.2 Materials

Paracetamol (4-acetamidophenol) (98% purity) and aspirin (acetyl salicyclic acid) >99.5% purity was obtained from Sigma-Aldrich (Poole, UK). Ibuprofen [2-(4-isobutylphenyl) propionic acid] was obtained from Shasun, U.K. and S-(+)-Ibuprofen [(2S)-2-[4-(2-Methylpropyl)phenyl]propionic acid] was obtained from Acros Organics (Geel, Belgium). The molecular structure of these materials is shown in Figure 4.1. Solvents methyl alcohol, ethanol and acetone were HPLC grade (>99.9% purity) obtained from Sigma-Aldrich (Poole, UK) and were used for the preparation of macroscopic crystals without further purification.

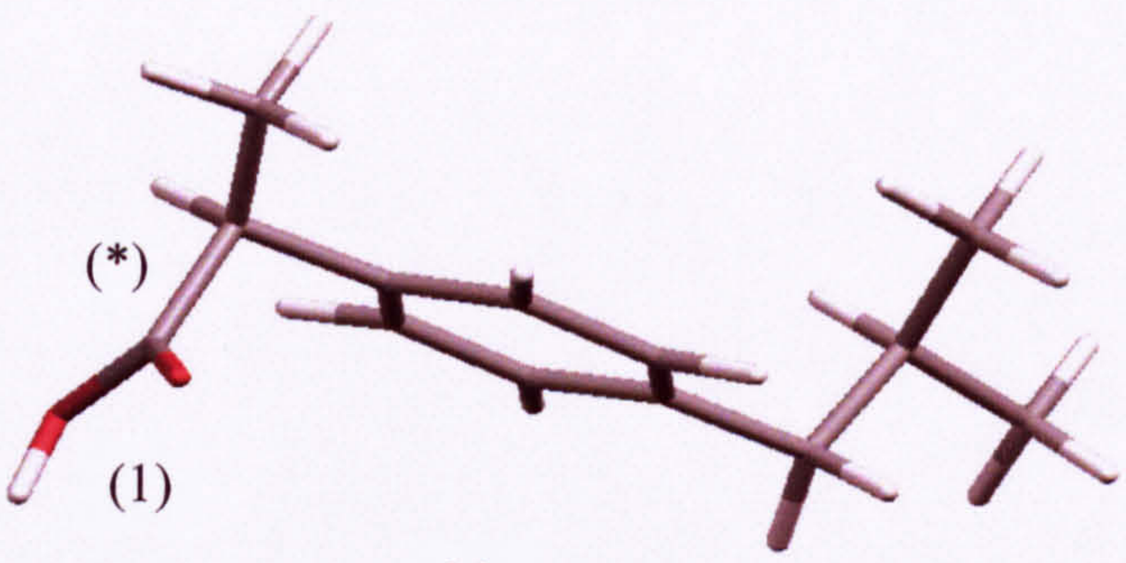
Figure 4.1: Molecular structure of (a) paracetamol with (1) hydroxyl, (2) amine and (3) carbonyl functional groups, (b) aspirin with the (1) carboxylic, (2) ester groups and (c) ibuprofen with the (1) carboxylic functionality while (*) denotes the chiral centre.



(a)



(b)



(c)

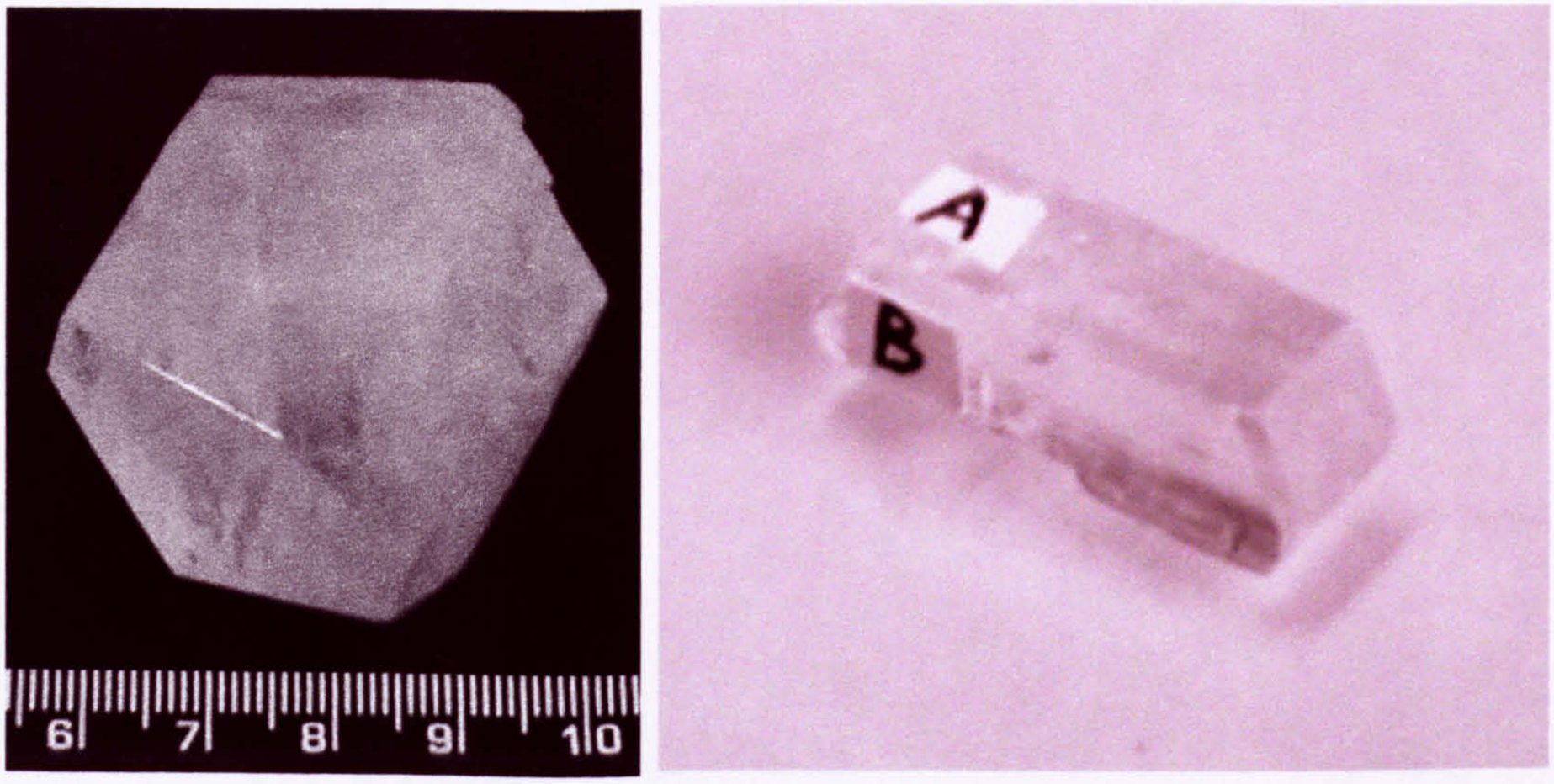
4.3 Crystal Growth

4.3.1 Growth of Thermodynamically Stable Macroscopic Crystals

Powders were typically dissolved in either methanol or acetone at 20 °C under continuous stirring. This step was repeated until the solubility limit was reached. At this limit, no further powder can dissolve and the solution is at its saturation level. If the solution is heated, more powder can be dissolved, however upon cooling back to the initial temperature, crystals do not always immediately precipitate. In this case, the solution is at a metastable thermodynamic state, and is known as a supersaturated solution. This metastable state can easily be overcome by seeding, which provides sites for crystallisation. Seed crystals of a few mm in size are typically obtained overnight via this method.

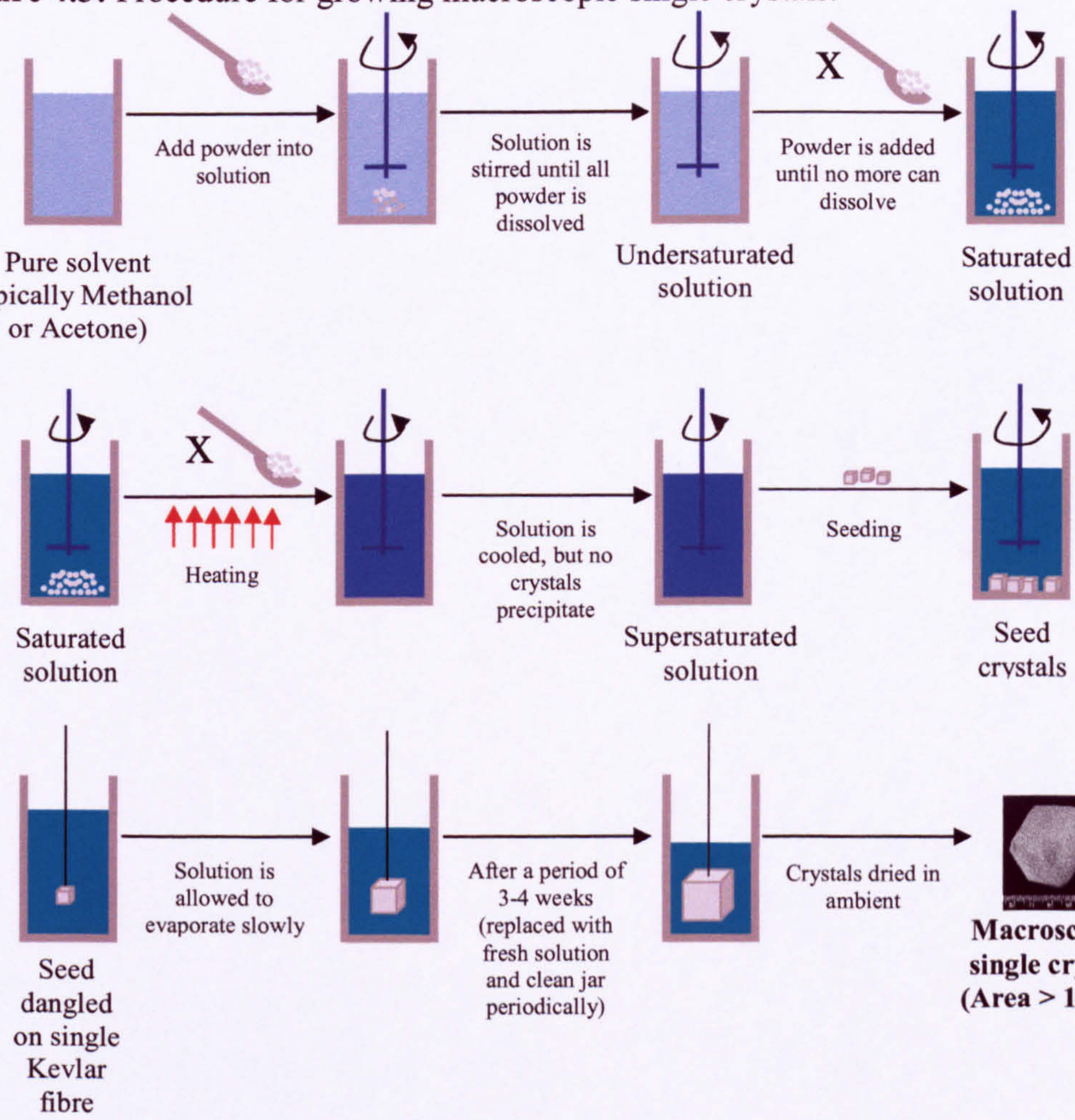
In our methodology, a single seed crystal is then tied with a single aramid fibre (diameter = 10 μm) and suspended in a saturated solution. The saturated solution is then allowed to evaporate slowly over a period of 20 - 30 days, resulting in the growth of a macroscopic single crystal. The crystal size is often > 1 cm in length and a typical one is shown in Figure 4.2. Crystal growth can be expedited by allowing the solvent to evaporate faster, but the quality of these crystals is often compromised.

Figure 4.2: Single crystals of (a) paracetamol (scale in cm) and (b) aspirin.



Upon removal of the crystal from solution, residual solvent on the crystalline facets will evaporate and cause crystals to nucleate on the surface. This secondary nucleation will result in a rough surface, and is overcome by either rinsing the crystals with an inert solvent or by gently dabbing the crystalline facets with soft tissues. The crystals are then left in an empty beaker to dry. Vacuum drying of the macroscopic crystals at elevated temperatures (60 °C) was found to result in roughened surfaces, possibly a thermally induced etching effect. This procedure for macroscopic growth is summarised in Figure 4.3.

Figure 4.3: Procedure for growing macroscopic single crystals.

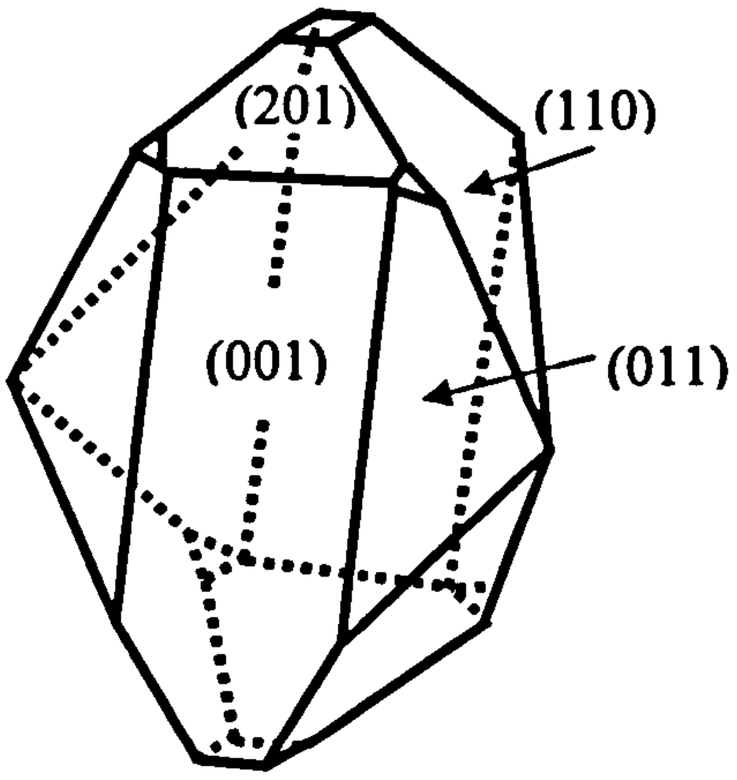


Macroscopic paracetamol form I (monoclinic, thermodynamically stable) crystals were grown by slow solvent evaporation from a saturated solution of methanol as described above. The solution was stirred constantly until the solubility limit was reached. However, heating of these solutions was avoided as paracetamol is reported to oxidize readily in warm alcohol solutions yielding a pink coloured solution [176]. It was observed that the solutions prepared here may also turn pinkish after exposure to light, so care was taken to avoid exposure to daylight. Fresh saturated solutions were prepared and replaced any saturated solutions which turned slightly pink. Macroscopic single crystals were obtained and their habit is shown in Figure 4.4. This crystal habit corresponds to those reported in literature [177] with major facets of (201), (001), (011) and (110). Crystals were dried under ambient conditions inside an empty beaker before conducting contact angle measurements.

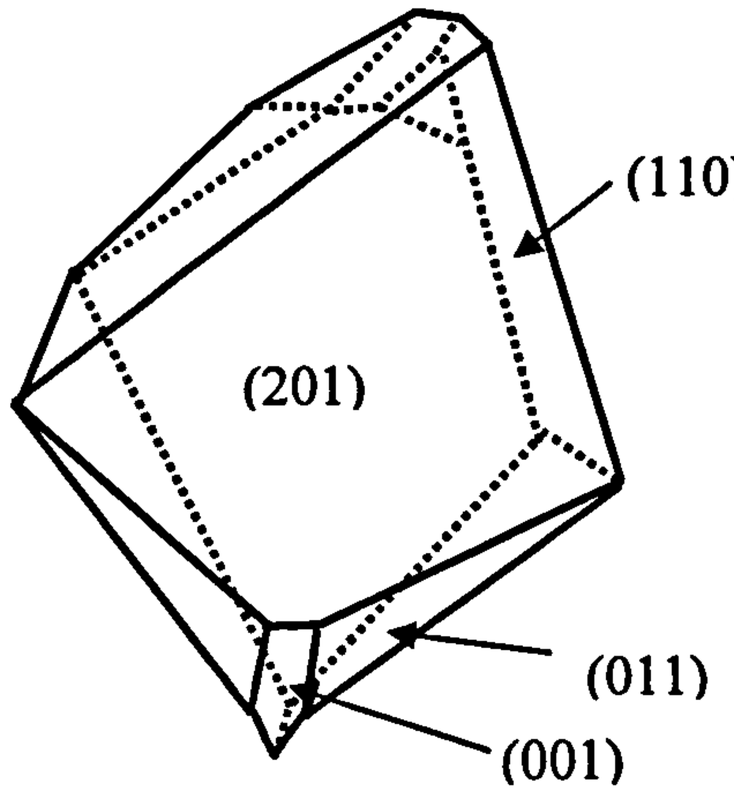
Crystallisation from a saturated acetone solution resulted in a different crystalline habit. The macroscopic crystals obtained here possessed identical major facets, but were of different morphological importance with greater significance of facet (201) as shown in Figure 4.4. The two habits however, exhibited identical bulk properties such as their melting point, vapour pressures and are indistinguishable by spectroscopic techniques.

Facet (010) has been reported as being the preferred cleavage plane of paracetamol, as the attachment energy of this crystal face is the lowest [178, 179]. This facet is thought to be the dominant face present in milled samples. Facet (010) was exposed by cleaving the macroscopic crystal perpendicular to the *b*-axis using a razor blade. Contact angles reported were obtained on the freshly cleaved surfaces for facet (010).

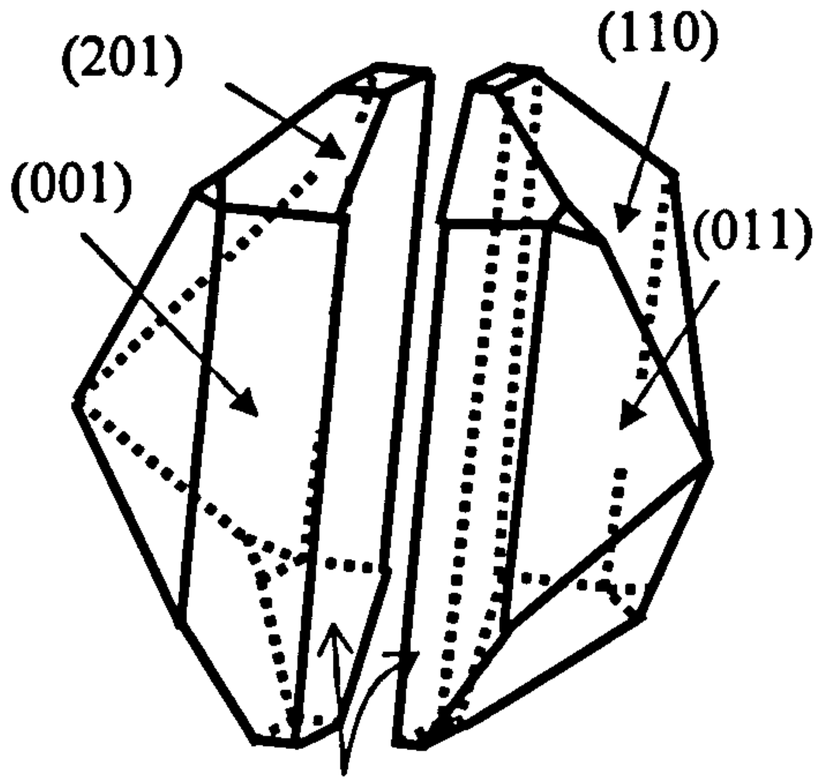
Figure 4.4: (a) Habit of macroscopic form I paracetamol single crystals grown from (a) methanol saturated solution, (b) acetone saturated solution and (c) the preferred cleavage plane.



(a)



(b)



(c)

The crystallisation procedure described here was also tested on several other common pharmaceutical solids. Macroscopic crystal growth was achieved successfully and was not limited to the case of paracetamol form I crystals. In this thesis, the growth of macroscopic single crystals of aspirin, racemic ibuprofen and S-(+)-ibuprofen are all reported. These crystals were crystallised in either methanol or ethanol and acetone, all resulting in different habits for the same crystalline systems illustrating the importance of crystallisation solvent. The habits for these systems are shown in Figure 4.5 to Figure 4.7.

The crystalline habit of aspirin was first reported by Yeesok et al. [180] and more recently by Mao et al. [181], with facet (001) the most dominant facet for growth from methanol solution. The habits of ibuprofen have been reported by [182] but no known literature is available on S-(+)-ibuprofen crystals.

Figure 4.5: Habit of aspirin crystals grown from (a) acetone solution and (b) methanol solution.

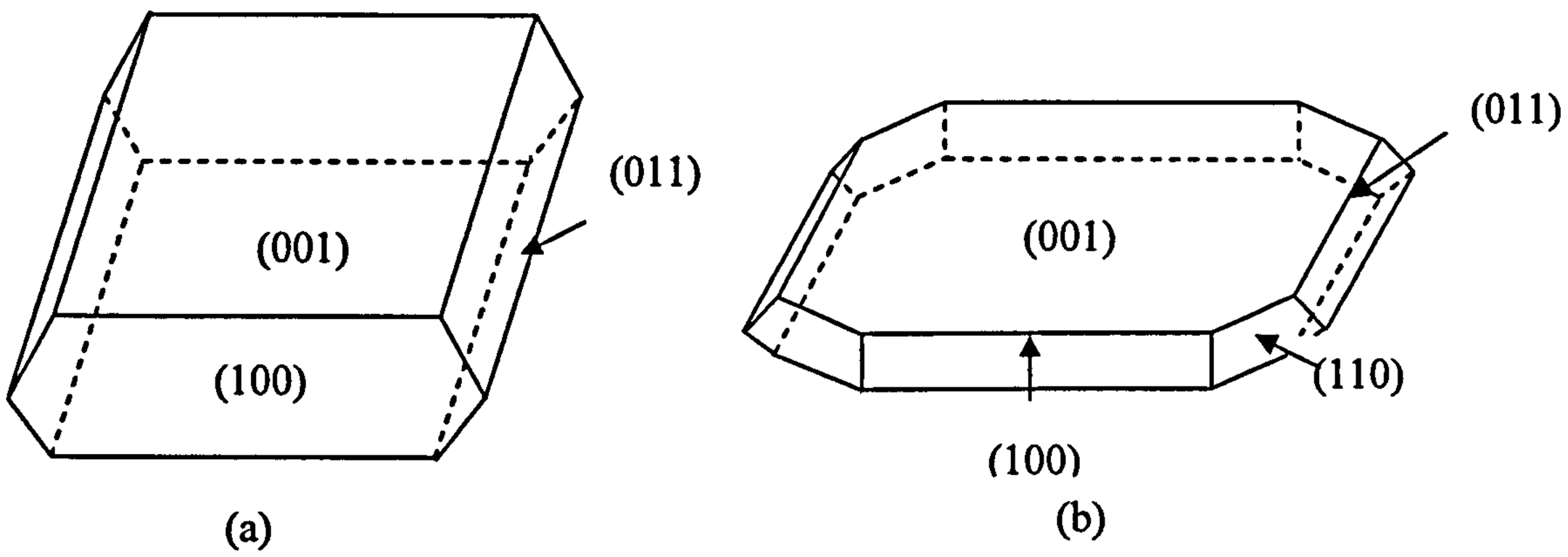


Figure 4.6: Habit of ibuprofen crystals grown from (a) acetone solution and (b) ethanol solution.

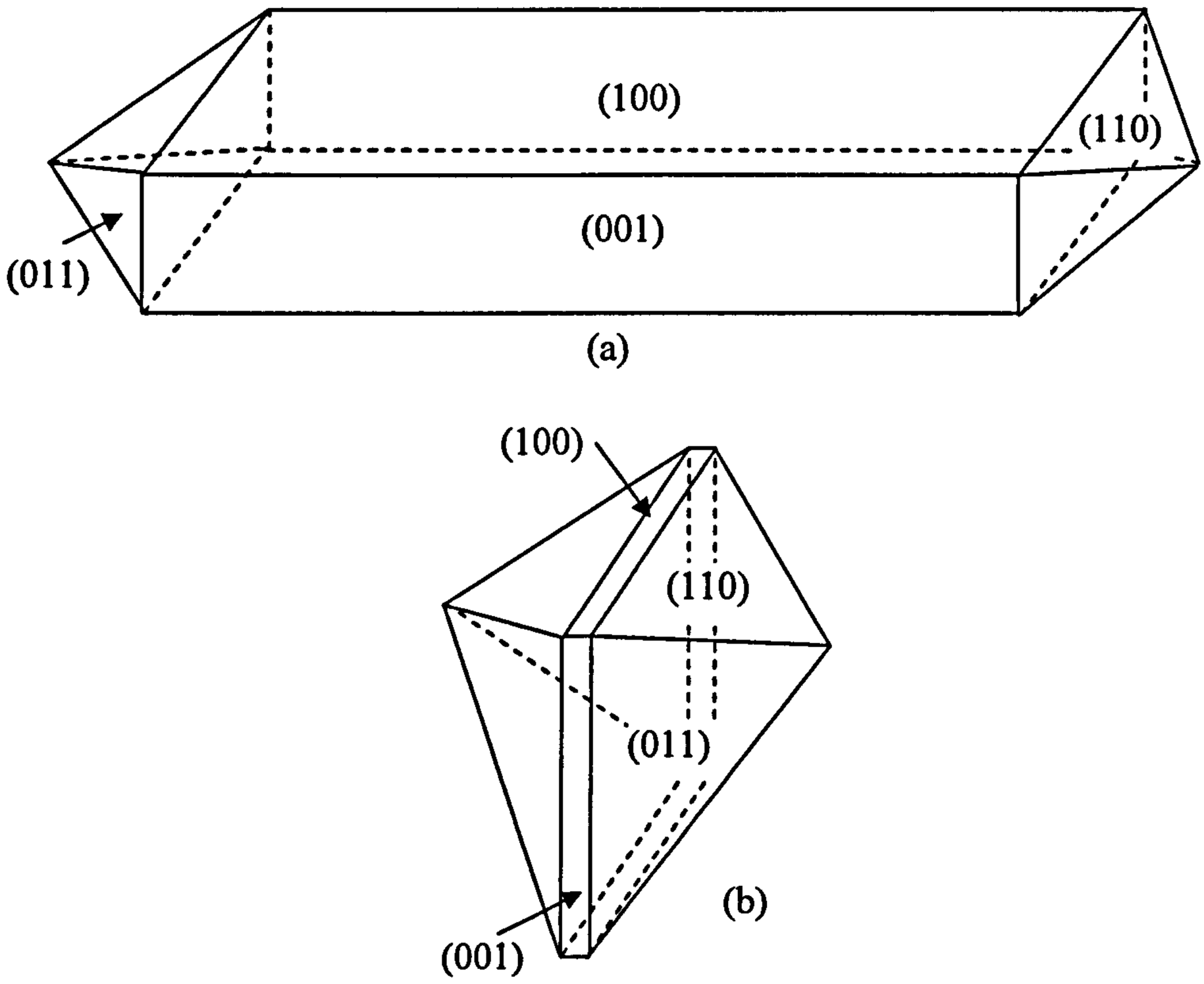
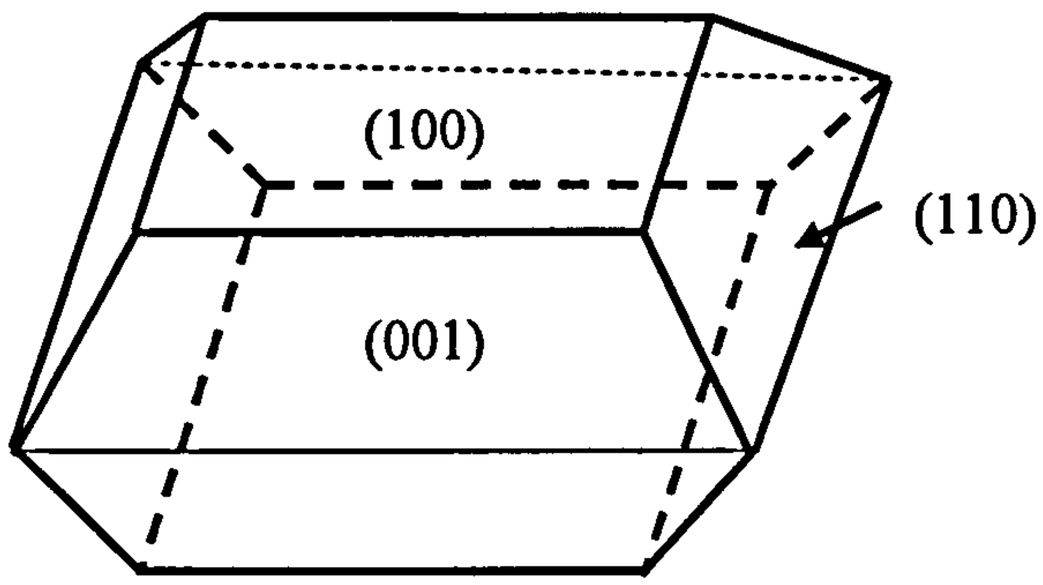


Figure 4.7: Habit of S-(+)-ibuprofen crystals grown from acetone solution.



4.3.2 Growth of Thermodynamically Metastable Macroscopic Crystals

For growing macroscopic form II (orthorhombic, thermodynamically metastable) paracetamol crystals, a controlled temperature drop approach was employed. Form II crystals could not be grown by seeding a saturated solution with form II seeds as conversion back to form I is favourable in solution, often a complete conversion occurred within 6 hours even at 0 °C [183].

The description of a method for the growth of macroscopic (> 1 cm) sized metastable form II single crystals was first reported by Mikhailenko [184]. A mixture of 25 g of paracetamol in 1 L of deionised water was prepared at 40 °C. The mixture was then heated to its boiling point to ensure that all powder was fully dissolved. This solution was continually boiled for 15 minutes and then filtered. The solution was then placed in a water bath at 40 °C for 24 hours before cooling at a rate of 3 °C/day until typically 0-4 °C. Form II crystals were formed at the bottom of the flask, with reported 95 % probability within 24 days [184].

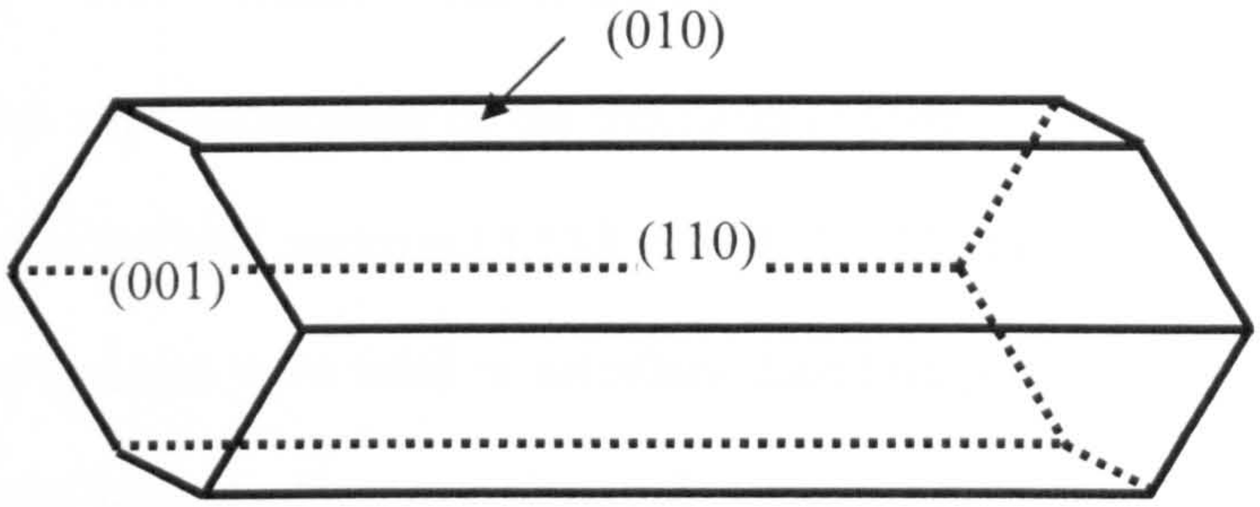
In any case when the supersaturated solution was contaminated, the form I re-crystallisation was favourable, as this provided sites for the thermodynamically stable form to crystallise. As such, the flask is sealed with parafilm to ensure that no

contaminant particles can enter the solution. All of the glassware used was initially washed with alcohol solvents and rinsed thoroughly with deionised water. In this research, it has been observed that crystallisation of form II can be expedited by directly cooling the solution from 40 °C to 4 °C. Crystals are typically formed within 48 hours as is shown in Figure 4.8.

Figure 4.8: Paracetamol (a) form II single crystals (scale in cm) and (b) its habit.



(a)



(b)

4.3.3 Cambridge Crystallographic Data Services

The crystallographic structure of the systems investigated here were obtained from the Cambridge Structural Database (CSD) [185]. The crystal structure of stable monoclinic and metastable orthorhombic paracetamol was solved by Haisa et al. [186, 187]. The unit cell parameters of the stable monoclinic form are as follows: a = 12.93 Å, b = 9.4 Å and c = 7.1 Å with $\beta = 115.9^{\circ}$ and of $P2_1/a$ space group. While for the metastable orthorhombic form, a = 11.805 Å, b = 17.164 Å and c = 7.393 Å and of Pcab space group. Paracetamol form I and form II were deposited in the CSD as HXACAN01 and HXACAN, respectively.

Aspirin crystallises in the monoclinic form with four (z = 4) molecules in each unit cell and of $P2_1/C$ space group. The unit cell parameters are as follows: a = 11.430

Å, b = 6.591 Å and c = 11.395 Å with β = 95.68 ° which is deposited as "ACSALA01" in the CSD.

In this research, both the racemic ibuprofen and the S enantiomer (dexibuprofen) were studied. The reported crystal structure of ibuprofen was refined at 100K and determined by single-crystal pulsed neutron diffraction [188]. Ibuprofen racemate crystallises in the monoclinic form with four (z = 4) molecules in each unit cell and of $P2_1/C$ space group. The unit cell parameters are as follows: a = 14.397 Å, b = 7.818 Å and c = 10.506 Å with β = 99.7 ° which is deposited as "IBPRA02" and obtained from the CSD. Dexibuprofen also crystallises in the monoclinic form, with unit cell parameters of a = 12.456 Å, b = 8.036 Å and c = 13.533 Å with β = 112.86 °.

The unit cell parameters for the systems were used to calculate their interplanar spacing and dihedral angles for facet identification, as reported in the following section. Crystallographic structure at specific facets is generated from these input files obtained from the CSD using Mercury (version 1.2.1, CCDC, Cambridge, U.K.). These structures at specific facets are shown in Figure 4.9 to Figure 4.13, for the systems investigated in this thesis.

Figure 4.9: Crystallographic structure of form I paracetamol (a) facet (001) and (b) facet (010). Inset are droplet profiles of water saturated with paracetamol on the crystalline facets showing large variations in droplet profiles.

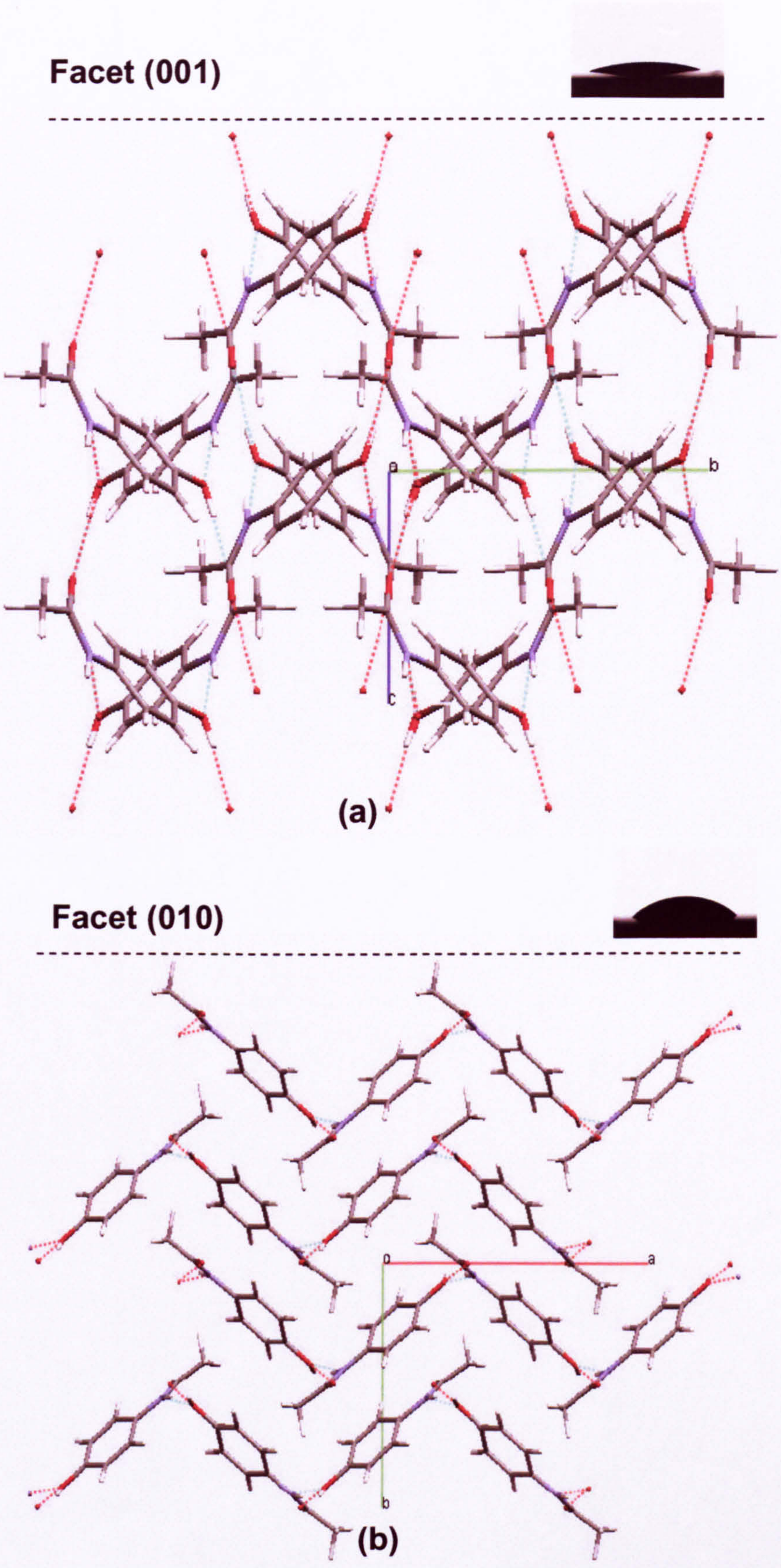


Figure 4.10: Crystallographic structure of the orthorhombic (form II) paracetamol crystals at (a) facets (010) and (b) facet (001).

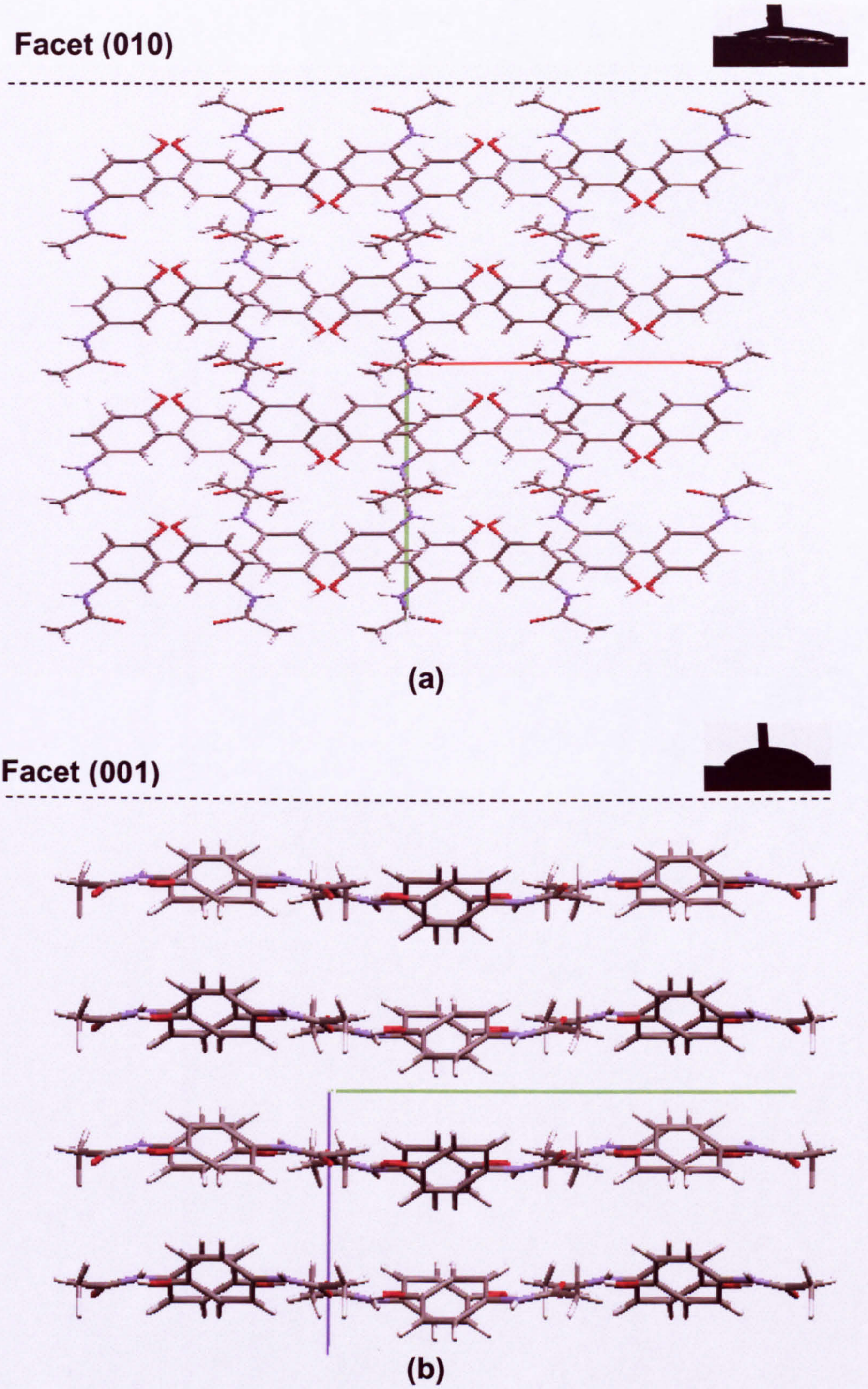
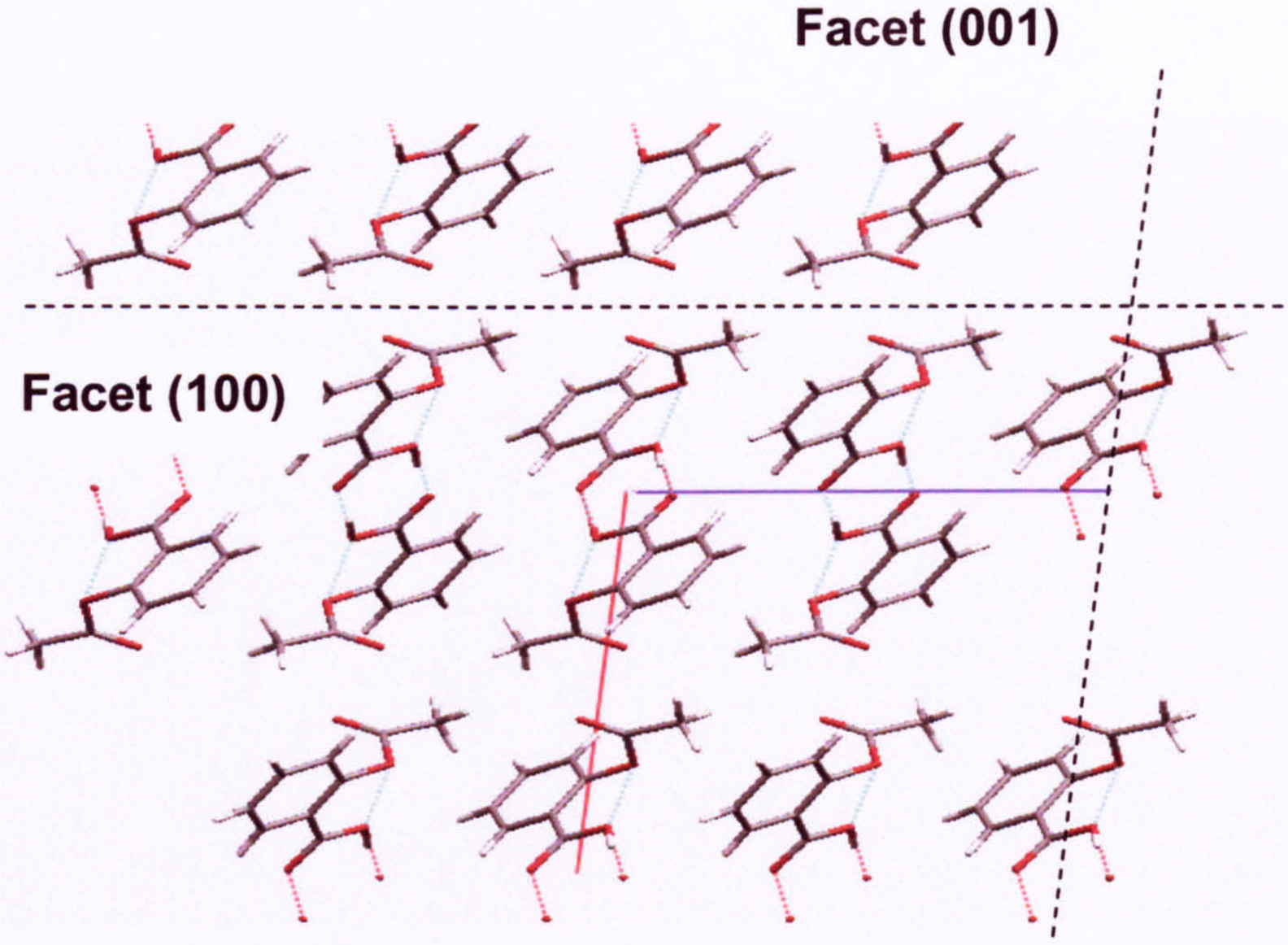
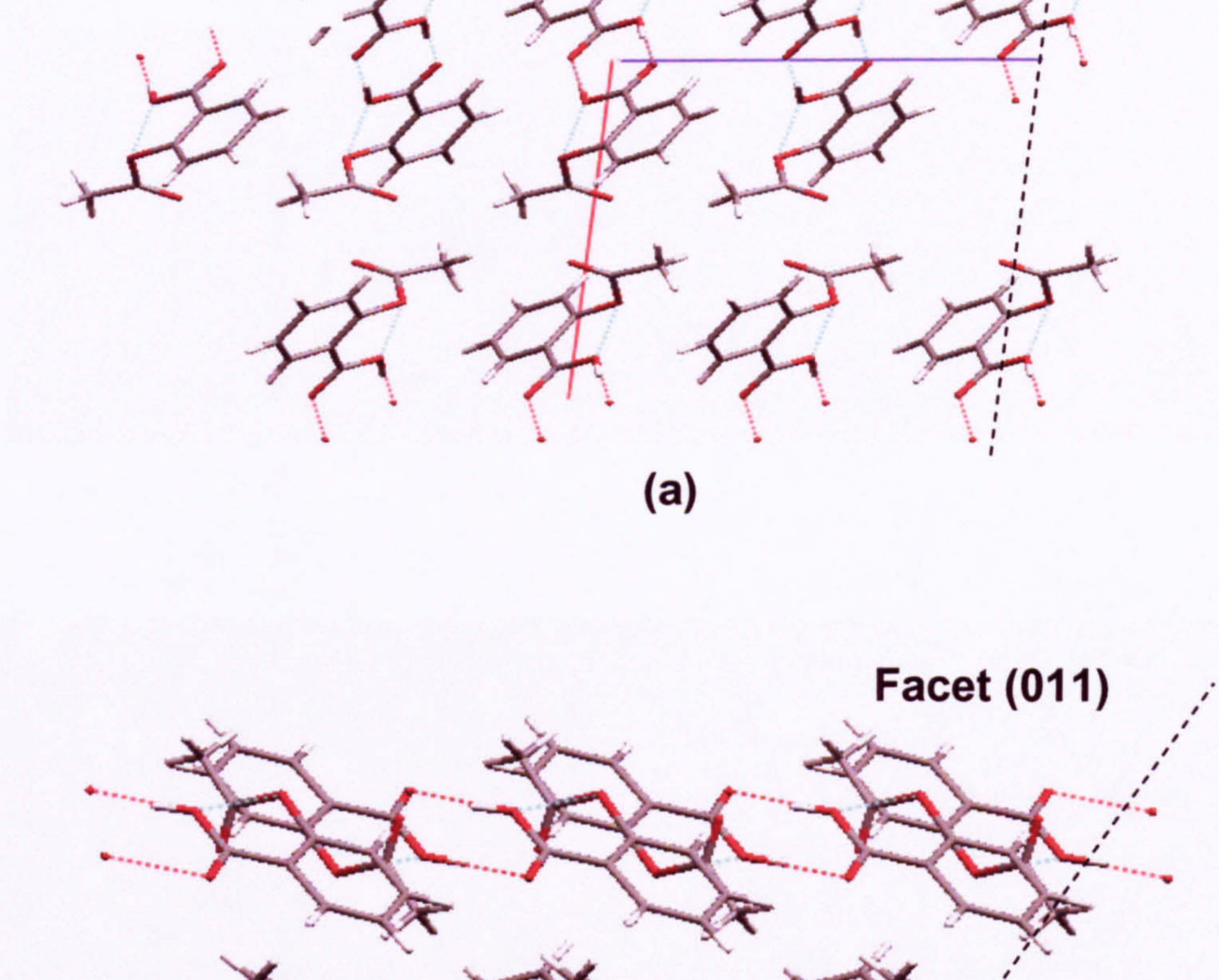


Figure 4.11: Crystallographic structure of aspirin crystals viewed along (a) b-axis and (b) a-axis.

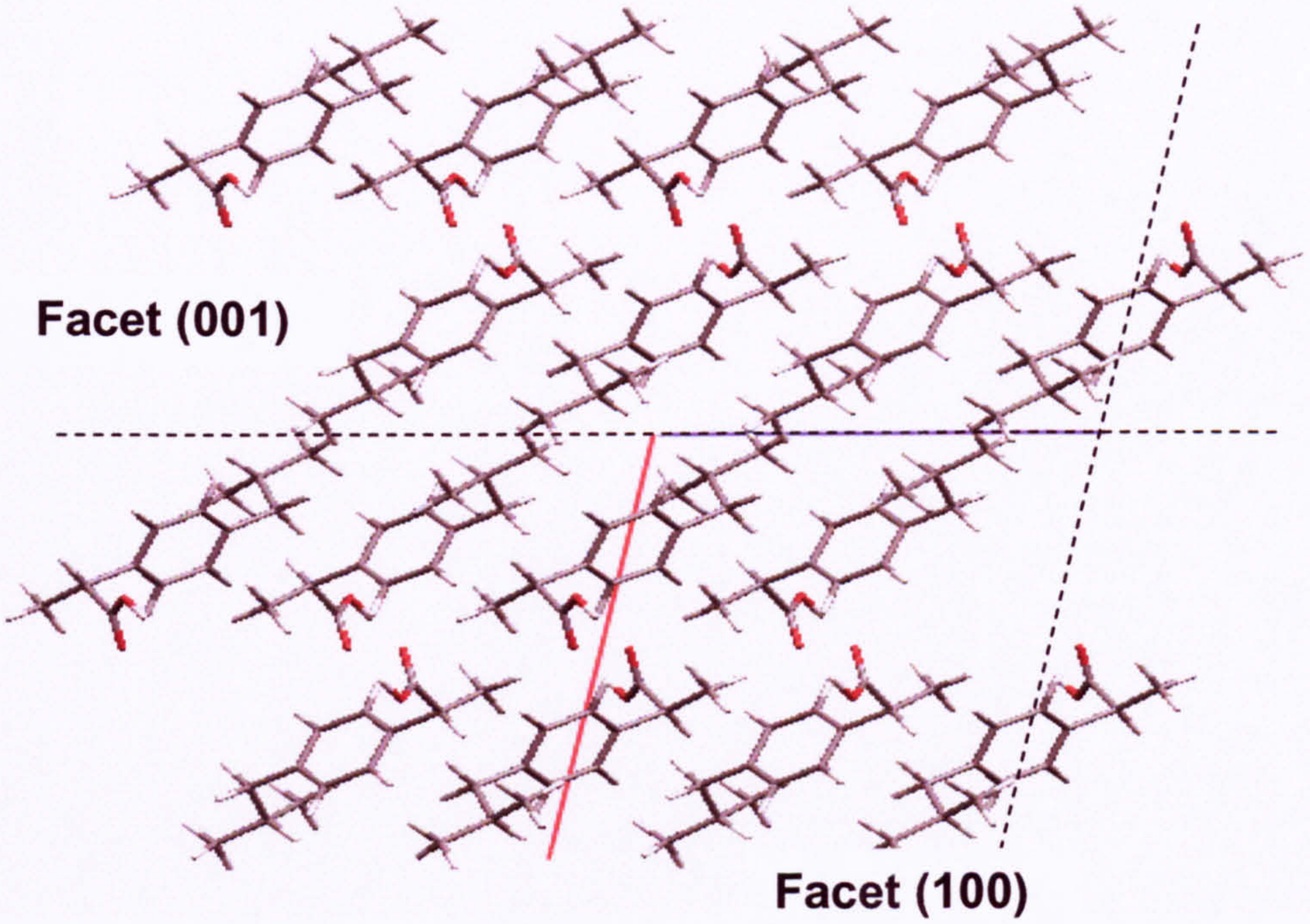


(a)

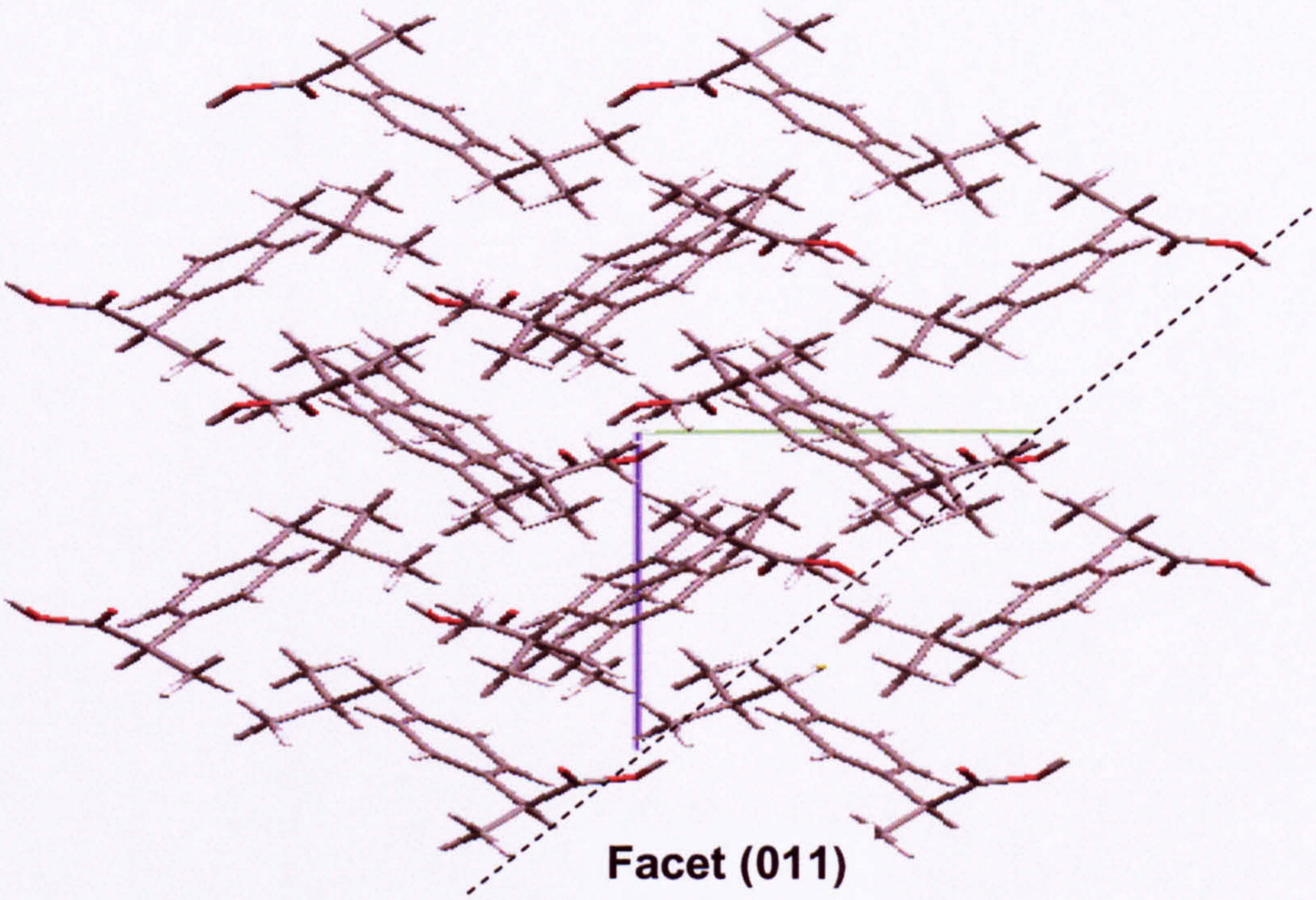


(b)

Figure 4.12: Crystallographic structure of racemic ibuprofen crystals viewed along (a) b-axis and (b) a-axis.

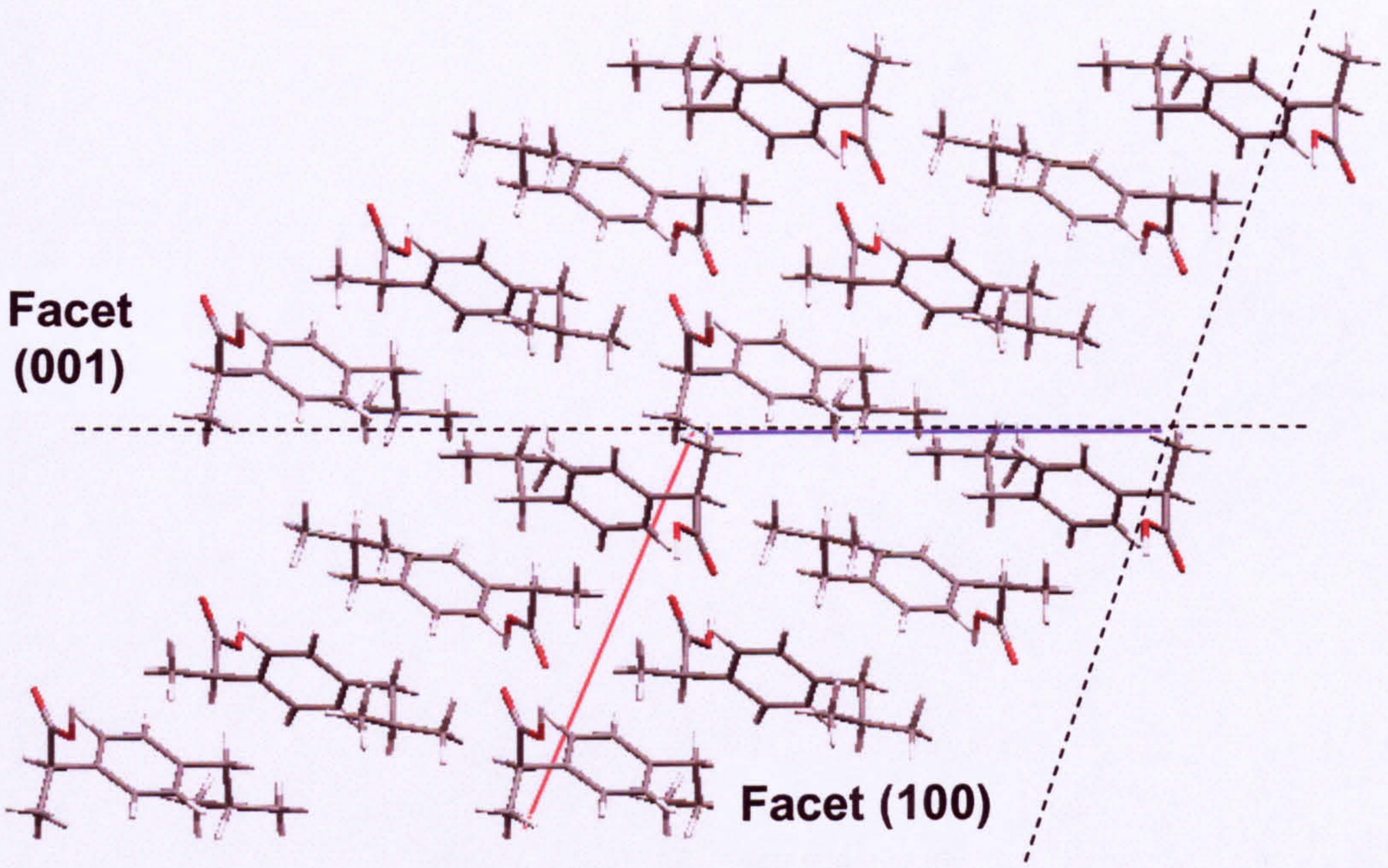


(a)

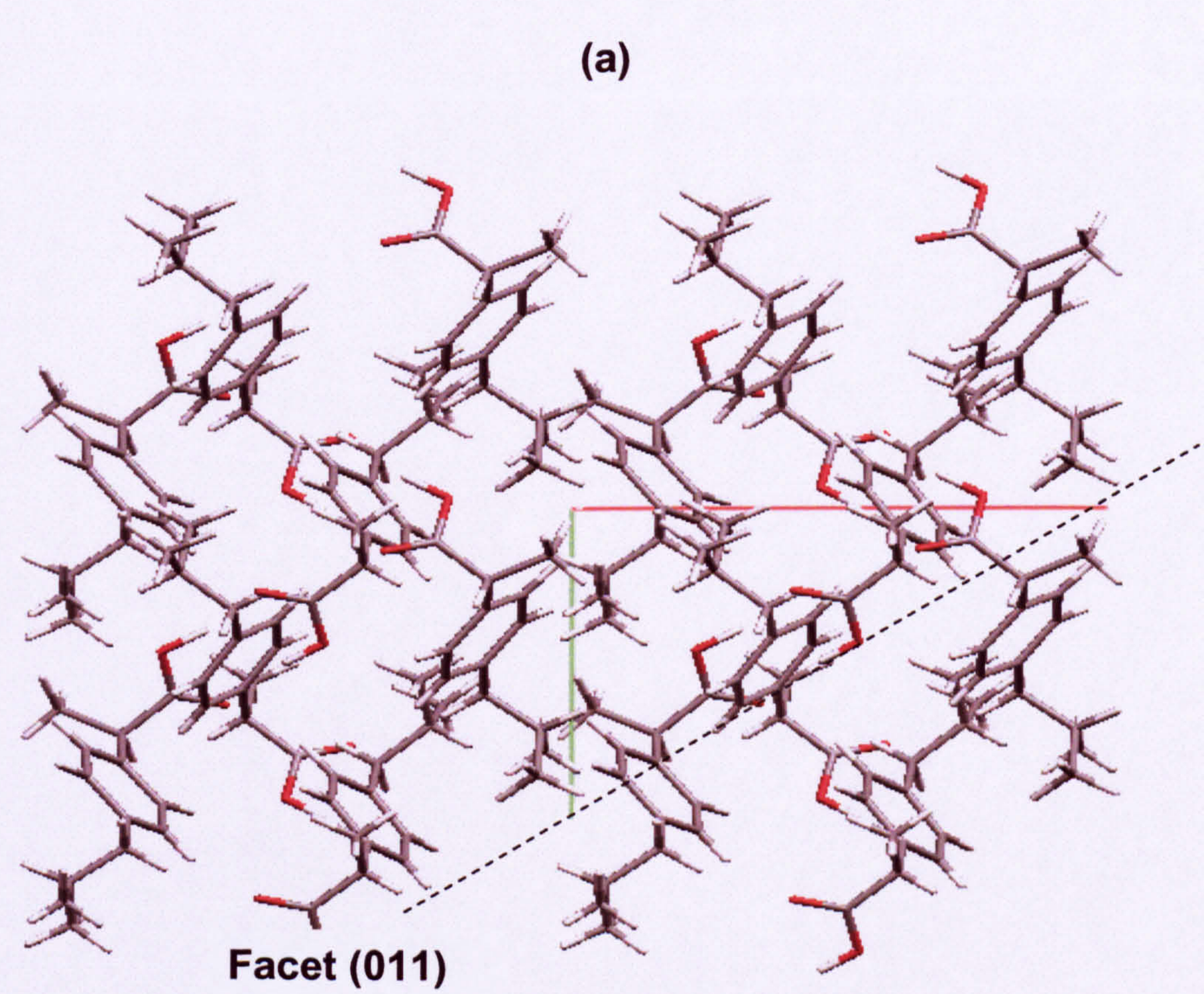


(b)

Figure 4.13: Crystallographic structure of dexibuprofen crystals viewed along (a) b-axis and (b) a-axis.



(a)



(b)

4.3.4 Facet Identification

The identification of crystalline facets was achieved by the measurement of the dihedral angles as described in Chapter 3. This angle can be measured with the aid of a goniometer, but the use a protractor (± 1 °) was sufficient for this study as the samples were macroscopic in size. The dihedral angles measured are reported in Table 4.1 to Table 4.5. The experimentally measured values were in good agreement with the calculated values based on the crystal lattice information obtained from the CSD. The dihedral angles for paracetamol facets (201)-(011) and ibuprofen facets (001)-(110) had larger errors, due to their shape making measurements for these facets more difficult. However, the angles obtained gave sufficient agreement for confirmation of facets with those reported in literature rather than for indexing purposes.

Table 4.1: Dihedral Angles for Paracetamol Form I (Monoclinic) Crystals

Facet i	Facet j	Calculated (°)	Measured (°)	% Difference
(001)	(201)	117.77	117	-0.66
(001)	(011)	145.81	145	-0.56
(001)	(110)	105.96	104	-1.85
(201)	(011)	112.67	104	-7.70
(201)	(110)	111.84	112	0.14
(011)	(110)	131.63	133	1.04

Table 4.2: Dihedral Angles for Paracetamol Form II (Orthorhombic) Crystals

Facet i	Facet j	Calculated (°)	Measured (°)	% Difference
(001)	(110)	90	89	1.11
(001)	(010)	90	90	0.00
(110)	(010)	104.13	103	0.96

Table 4.3: Dihedral Angles for Aspirin Crystals

Facet i	Facet j	Calculated (°)	Measured (°)	% Difference
(001)	(100)	95.69	98	2.41
(001)	(011)	120.17	122	1.52
(100)	(011)	92.86	93	0.15

Table 4.4: Dihedral Angles for Racemic Ibuprofen Crystals

Facet i	Facet j	Calculated (°)	Measured (°)	% Difference
(100)	(001)	99.37	104	4.66
(100)	(110)	118.59	124	4.56
(100)	(011)	95.58	98	2.53
(001)	(110)	94.47	102	7.97
(001)	(011)	126.68	131	3.41
(110)	(011)	138.65	140	0.97

Table 4.5: Dihedral Angles for S-(+)-Ibuprofen Crystals

Facet i	Facet j	Calculated (°)	Measured (°)	% Difference
(100)	(001)	112.87	112	0.78
(100)	(110)	125.00	123	1.61
(100)	(011)	102.16	99	3.78

4.3.5 Attachment Energies

Computed attachment energies for specific crystalline facets have been reported for paracetamol form I and form II, racemic ibuprofen, while the interaction energies are listed for aspirin facets [189-192]. These values are summarised in Table 4.6. Attachment energies were not reported for all of the crystals faces experimentally studied in this thesis. No reported attachment energy data is available for the S-(+)-ibuprofen crystal.

Table 4.6: Computed Attachment Energies for Pharmaceutical Crystals

Facet	Attachment Energies (kJ/mol)			
	Paracetamol Form I	Paracetamol Form II	Aspirin[1]	Racemic Ibuprofen
(001)	-47.6	-13.6	-10.0	-110.0
(100)	-	-19.1	-6.7	-50.3
(011)	-48.7	-	-	-80.6
(110)	-35.6	-	-	-73.4
(010)	-31.6	-	-	-
(201)	-35.4	-	-	-
(101)	-	-	-83.3	-
(111)	-	-17.5	-	-

[1] Denotes the interaction energy

4.4 Conclusions

The technique described here for the growth of macroscopic crystals was found to be successful. These macroscopic crystals enabled the measurements of liquid sessile drop contact angles and XPS on specific individual facets, and hence the direct description of their surface properties (Chapter 6 and Chapter 7, respectively). The dihedral angles measured confirmed the miller indices of the facets studied. Attachment energies reported in the literature for the materials studied in this thesis are summarised.

CHAPTER 5 EXPERIMENTAL DETERMINATION OF CRYSTALLINE SOLID SURFACE CHEMISTRY

5.1 Introduction

The wetting properties of solids are primarily governed by their surface energetics. Unlike liquid surfaces, the direct surface energy measurement for solids is not viable as solid surfaces are rigid. Almost all indirect approaches involve the use of known vapours [193, 194], liquids [45, 56] or solids [195-197] as probes for the solid materials under investigation. Amongst these approaches, the liquid sessile drop contact angle technique is one of the most common, and is sensitive to the outermost molecular layers of the solid surface. The contact angle is the angle between the solid surface and the tangent of the liquid drop surface, through the liquid phase at the three phase (solid-liquid-vapour) contact point (Figure 2.11), and is related to the surface energy of the solid via the Young's equation [1]. The solid surface energy is obtained by measuring the contact angles of various reference liquids and analysing the data with an appropriate theory. Wetting behaviour and related theories are reviewed in Chapter 2.

In this chapter, the various experimental techniques to evaluate surface properties in general and surface energy in particular, for solids will be reviewed. Numerous techniques, depending on the nature of the material, have been established for determining the surface energies of solid materials. Conventional methods include sessile drop, capillary rise in a powder bed, air-pressure techniques, Wilhelmy plate, sedimentation volume, film flotation and vapour probe techniques [198-211]. Most of these traditional methods of characterising solid materials rely on the use of a packed

powder bed. More recently, the use of atomic force microscopy has been employed by various workers [212, 213].

All of the techniques reviewed in detail here involve the use of chemical probes of known properties for characterisation of a solid with unknown properties. These characterisation techniques are undertaken by probing the unknown solid with (a) gas/vapour, (b) liquid, (c) solid or (d) electromagnetic radiation such as X-rays (the use of X-rays reveals only the surface chemical composition and not the surface energies). In each case, the knowledge of the interaction between the solid and the external probe may be analysed via an appropriate model in terms of properties of the solid of interest.

5.2 Sessile Drop

The sessile drop method is a simple, straight forward procedure which is sensitive to the first 10 Å (1 nm) of a surface [214]. A liquid drop is placed on a surface and a tangent aligned at the three phase point to obtain the contact angle as shown in Figure 2.11. Measurements are made optically and the use of computer programmes to fit drop profile dimensions using various models is now routine, via a number of commercial instruments.

A flat solid sample area of only a few square millimetres is required and small quantities of probe liquid are sufficient to obtain contact angle data. The probe liquid should be non-reactive with the solid surface and have a low volatility. In order to obtain the advancing contact angle, θ_a, the liquid front has to advance to wet fresh surface. This condition is achieved by increasing the drop volume slowly, then subsequently decreasing the volume to obtain the receding contact angle, θ_r.

Whilst this method is relatively straight forward, a surface which is smooth, flat and homogenous is ideally required. Without these requirements, the applicability of this method is further complicated by the existence of the contact angle hysteresis [85, 215-217], which is defined as the difference between the θ_a and the θ_r. This phenomenon occurs mainly due to roughness and heterogeneity of the surface [95, 218, 219], and has been reviewed in Chapter 2.

Contact angle determination of complex organic solids using the sessile drop method is traditionally performed on powder compacts or tablets. However, the fabrication of powder compacts under high pressures is reported to cause surface deformation [199], and thus the contact angles measured here may therefore not represent the true equilibrium surface energy of the particles. Furthermore, these compacts have a rough surface topography and are porous, leading to penetration of the liquid into the tablets and swelling effects [220]. However, this technique is still used extensively by many researchers even for the characterisation of pharmaceutical powders [199, 201, 220, 221], though doubts have been raised over the validity of such contact angle data.

The inability to measure contact angles directly on individual powder particles is due to the small size of powder particles, normally 100 μm or smaller. This limitation can in theory be overcome by the use of very small droplets, but μm diameter droplets vapourise quickly due to their high Laplacian pressure. The use of larger surfaces (millimeter scale) seems however to be a more feasible option. One possible way of obtaining surfaces large enough for the sessile drop technique is by growing macroscopic sized single crystals as described in Chapter 4. Such smooth and flat facets are ideal surfaces for the sessile drop method. This new and novel method is detailed extensively in Chapter 6 for the various crystalline systems investigated.

5.3 Capillary Rise

Washburn, Bartell and Osterhof [222] were pioneers on characterising the wettability of powders. Their work involves measuring the liquid penetration rate into a powder bed, or the pressure required to halt the penetration of such a liquid front.

A column packed with a sample powder is brought into contact with the surface of a liquid, and the rate the liquid penetrates or wicks into the powder bed is measured. The liquid should be non-reactive with the sample and a range of liquids with differing surface tension should be used. Characterisation of powders by capillary rise method is primarily based on the Washburn equation as shown below:

$$h^2 = \frac{r_{eff}\gamma_{LV}\cos\theta}{2\eta}\cdot t \tag{5.1}$$

where h is the distance travelled by the liquid in time t and r_{eff} the effective interstitial pore radius. γ_{LV} and η are the surface tension and viscosity of the liquid respectively. The model is derived in conjunction with the Hagen-Poisseuille equation and based on the assumption of a laminar flow of liquid, negligible gravitational effects and constant cylindrical pore geometry [214].

By measuring the mass gained, the Washburn equation can be expressed as [223]:

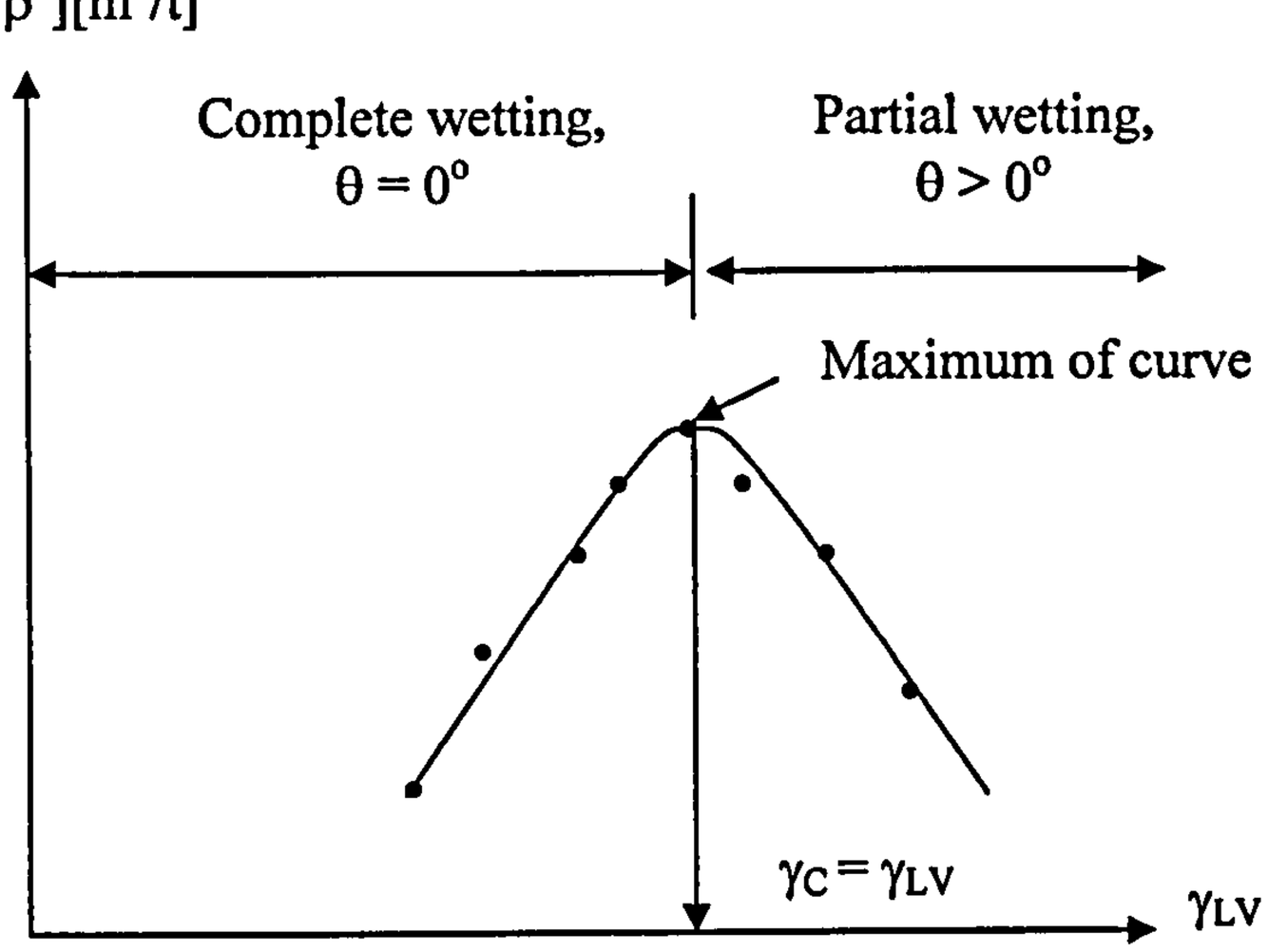
$$\frac{m^2}{t}\cdot\frac{\eta}{\rho^2} = K_C\gamma_{LV}\cos\theta \tag{5.2}$$

with K_C the capillary constant, representing the geometry of the porous network.

By plotting the normalised wetting rates, $[\eta/\rho^2][m^2/t]$ versus liquid surface tension, γ_{LV}, the capillary constant and contact angles can be calculated. Such a typical plot is shown in Figure 5.1. The capillary constant, K_C is calculated from the

complete wetting case where contact angle, $\theta = 0^{\circ}$ while the contact angles measured for the partial wetting case are calculated based on the K_C obtained.

Figure 5.1: Normalised ideal wetting plot.



The capillary rise techniques have been widely used to characterise fibres and powders, including pharmaceutical powders [209, 220, 224-226]. However, the reproducibility of column packing and poorly defined effective pore radius have often raised speculation on the accuracy of the experiments [227-229]. Swelling of the powder bed also affects the effective pore radius yielding higher contact angles compared to the results of Wilhelmy and sessile drop methods [223, 230].

Contact angles derived via the Washburn equation incorporate numerous assumptions, all of which are based on idealised conditions and may not be applicable to real particulate materials, especially for porous materials [231, 232]. Furthermore, penetration of liquid into the powder bed might cause swelling of the particles in the packed bed resulting in a sample temperature change and/or altering the effective

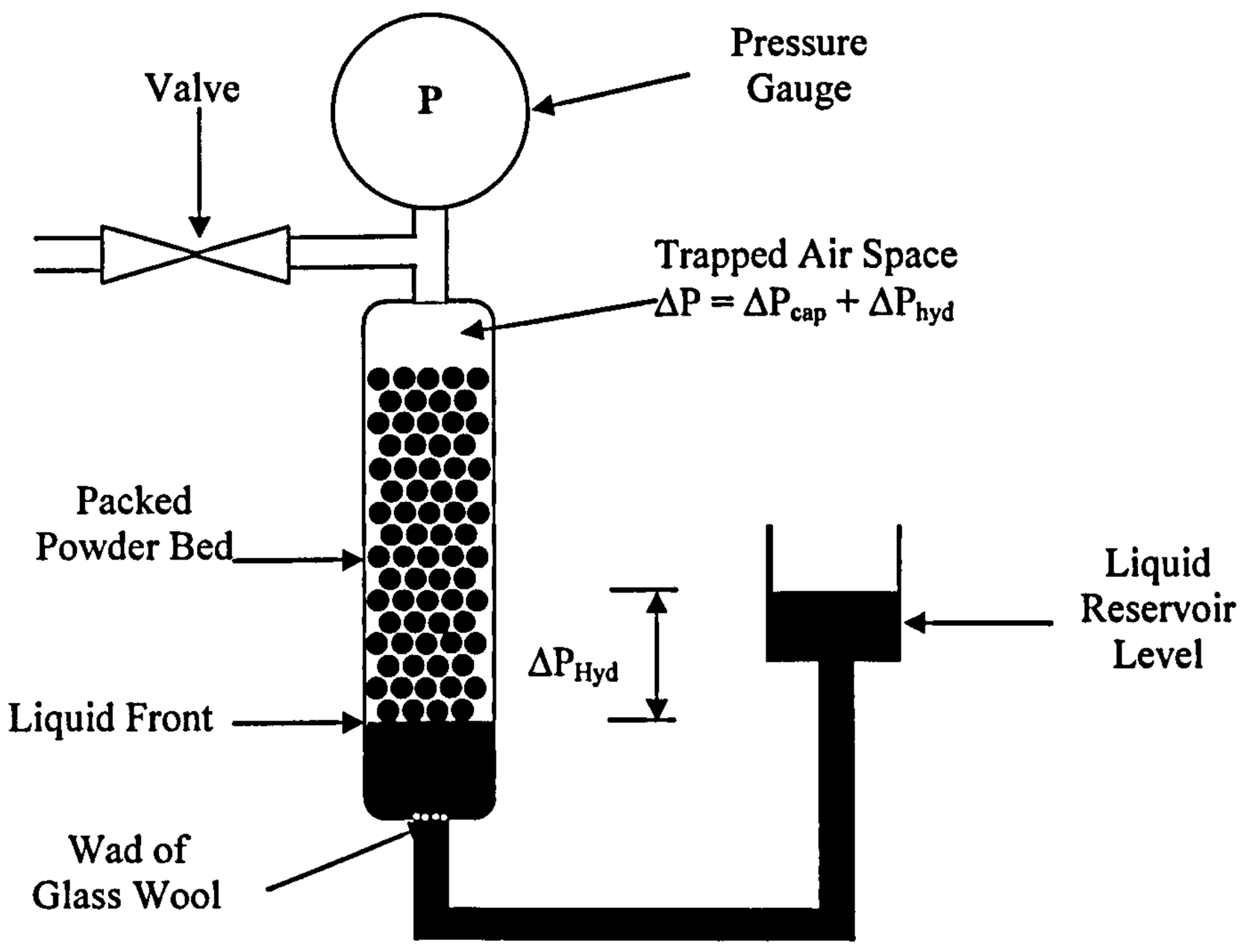
capillary radius of the bed. Shi and Gardner [230] introduced a new model to take into account of some of these changes for the characterisation of porous wood samples.

Wettability of powders can also be evaluated by measuring the air pressure required to halt capillary penetration as shown schematically in Figure 5.2 [207, 210]. This pressure is related to the contact angle and is given by the Laplace equation:

$$\Delta P = \frac{2\gamma_{LV}\cos\theta}{r_{eff}} \tag{5.3}$$

The use of pressure to halt penetration of liquid is a modified application of the capillary rise method. As with all other methods involving capillaries and packing, difficulties in measuring the properties of the powder bed are inevitable. Applicability of this technique is limited by the same constrains of the other capillary techniques.

Figure 5.2: Schematic of equipment for measuring capillary pressure generated by liquid rising through a packed powder bed.



5.4 Wilhelmy Plate

Wilhelmy (1863) developed a method to measure the downward force exerted on a vertical plate when it is brought into contact with liquid, as shown in Figure 5.3, and related this force to the contact angle between the plate and the liquid [233]. By measuring the wetting force of liquids with known surface tensions, γ_{LV}, and a known perimeter of the plate, p, the contact angle of the solid surface can be calculated by:

$$F_W = p_p \gamma_{LV} \cdot \cos\theta \tag{5.4}$$

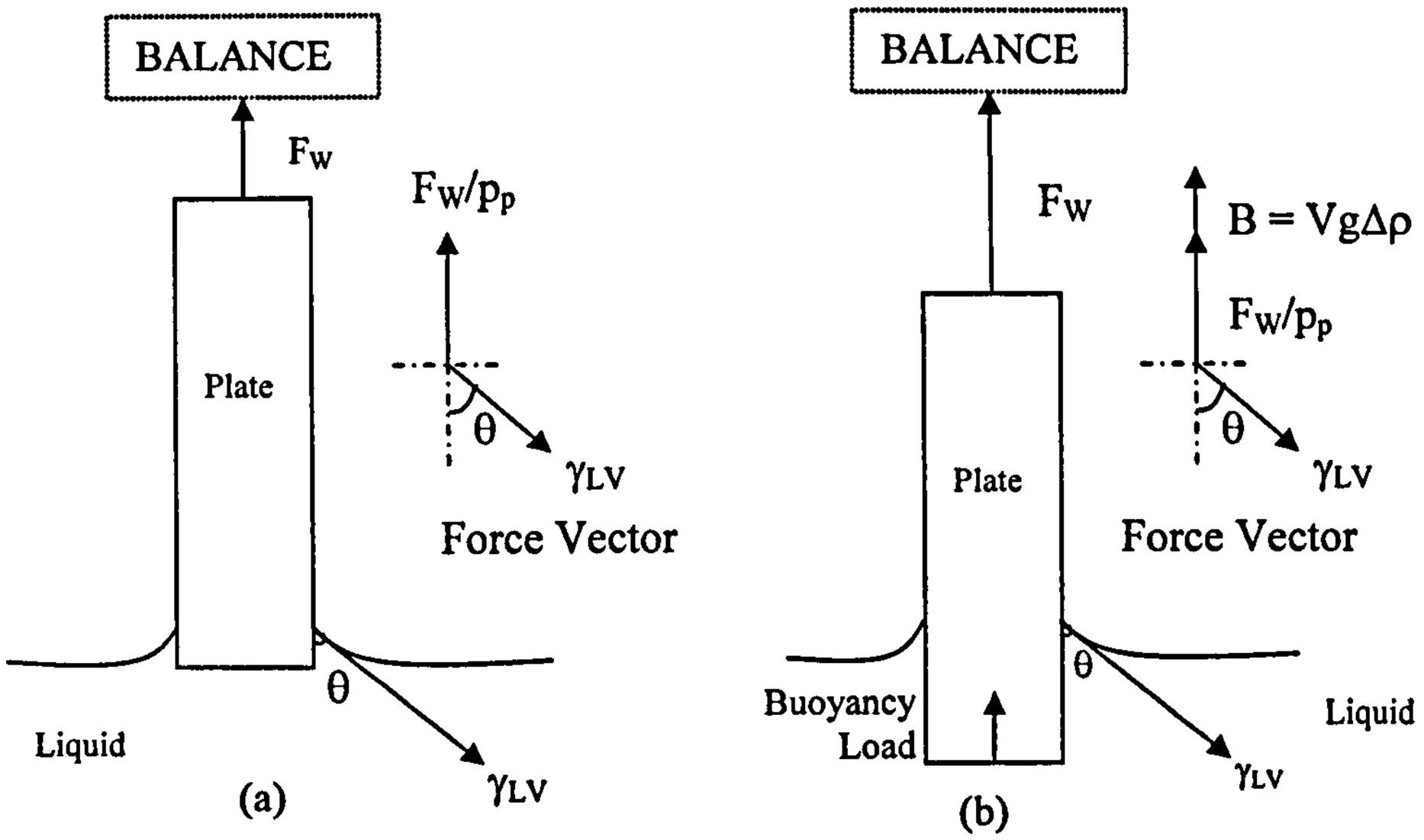
However, when the plate is immersed in the liquid, a reduction in force is measured due to the buoyancy force, notably in the case of a thick vertical plate. The contact angle can then be calculated by:

$$F_W = p_p \gamma_{LV} \cdot \cos\theta - Vg\Delta\rho \tag{5.5}$$

where V is the volume of displaced fluid and $\Delta\rho$ the density difference between the solid plate and the liquid and g is the gravitational force constant.

Dynamic contact angles can be obtained by advancing the plate or cylinder into the liquid to obtain θ_a and then retrieving the plate to obtain θ_r. The use of the Wilhelmy plate method might seem favourable and simple. However, the method works best with a smooth plate with constant or known perimeter. The plate should also have the same compositions on all surfaces [214, 234]. This technique has been usefully applied to fibres and thin films. Dynamic contact angles of powders can be obtained by either compacting powder into a flat plate or by adhering the powder particles to a glass slide coated with an adhesive.

Figure 5.3: Forces acting along Wilhelmy plate (a) zero net depth of immersion (b) finite depth of immersion.



Dove et al. [202] determined θ for compressed powder discs as well as for glass plates on which powder had been adhered, using the Wilhelmy plate approach. Glass slides were first sprayed with a liquid adhesive and powder was adhered on the slide by shaking slides briefly in a container of the test powder. Theophylline and caffeine powders were studied in this work. They found that the surface energy values obtained from the powder plates were more realistic compared to results obtained from compressed powder discs. This difference was attributed to possible changes in the surface properties of the powders during the preparation of the compacted powder discs. The effect of compression on surface chemistry has always been a point of concern for samples prepared in this manner. While the adhesion of powders onto slides overcome some difficulties faced by compacted samples, it introduces other variables such as surface roughness as well as a potential contribution by the adhesive to the results obtained.

For powder adhering onto a plate, the contact angle measured is of a composite surface. This contact angle is described by Cassie's Law [235];

$$\cos\theta = \sum_{i=1}^{n} f_i \cdot \cos\theta_i = f_{glue} \cdot \cos\theta_{glue} + f_{powder} \cdot \cos\theta_{powder} \qquad (5.6)$$

with f_i the surface fraction of species i and θ_i the contact angle of the liquid on the *i*th component. In the case of powder adhesion on an adhesive, the system might be represented by a two component species of the adhesive and adhered powder as shown in the equation above.

Surface roughness and perimeter of adhered particles on plates were adjusted by introducing an effective wetting parameter, p_{eff} [206, 236, 237]. Two apolar liquids with finite contact angles were used and a system of equations was solved simultaneously to obtain the contact angles on particles. However, the inability to measure the corrected parameter independently raises doubts on its validity. Suggestions that this effective parameter may be erroneous for non-polar liquids has been recently mentioned, resulting in alternative approaches being recommended [238]. Even with the problems outlined here, this technique is still used to characterise pharmaceutical powders, and their results are often accepted.

5.5 Inverse Gas Chromatography

Inverse gas chromatography (IGC) is a simple, yet versatile and robust technique for studying the physicochemical properties of particulate and fibrous materials. This technique was first developed in the 1950s, and early work focused on characterisation of catalysts, adsorbents and polymers [193, 194, 239, 240]. IGC is simply the inverse use of a conventional gas chromatography (GC), in which a column is packed with an *unknown* solid sample and *known* vapour probes are

injected into the column via an inert carrier gas. The retention time of the probe molecules is recorded by a GC detector, allowing the retention volume and then the partitioning co-efficient for the solid-vapour interaction to be determined. From this primary data, a wide range of physicochemical properties of solid materials such as surface energies, acid-base functionality of surfaces, diffusion kinetics, solubility parameters, surface heterogeneity and phase transition temperatures may be determined [241].

At infinite dilution, the retention behaviour of organic vapour probes has been successfully measured using IGC to study the surface energies of pharmaceutical solids [203, 204, 242-245]. With infinite dilution injections, only a small amount of probe (adsorbate) is injected and adsorption normally occurs in the linear Henry region of the adsorption isotherm. The retention behaviour of these injection pulses yields a net retention volume, V_R^0 which is a fundamental surface thermodynamic property of the solid-vapour interaction process. From this parameter, a wide range of surface properties, including surface energies can be derived. For infinite dilution IGC in the Henry's law region, the chromatogram peaks obtained are symmetrical (Gaussian). The net retention volume, V_R^o is given by:

$$V_R^o = \frac{j}{m} \cdot F \cdot (t_R - t_o) \cdot \frac{T}{273.15} \tag{5.7}$$

where T is the column temperature in Kelvin (K), F is the carrier gas exit flow rate at standard temperature and pressure (STP), t_R is the retention time for adsorbing probe and t_o is the mobile phase hold-up time (dead-time) and j is the James-Martin correction factor, which corrects the retention time for the pressure drop along the column bed.

V_R^o can be related to the free energy of adsorption by Equation 5.8:

$$\Delta G^o = RT \ln V_R^o + K = N_A \cdot a_m \cdot W_A \tag{5.8}$$

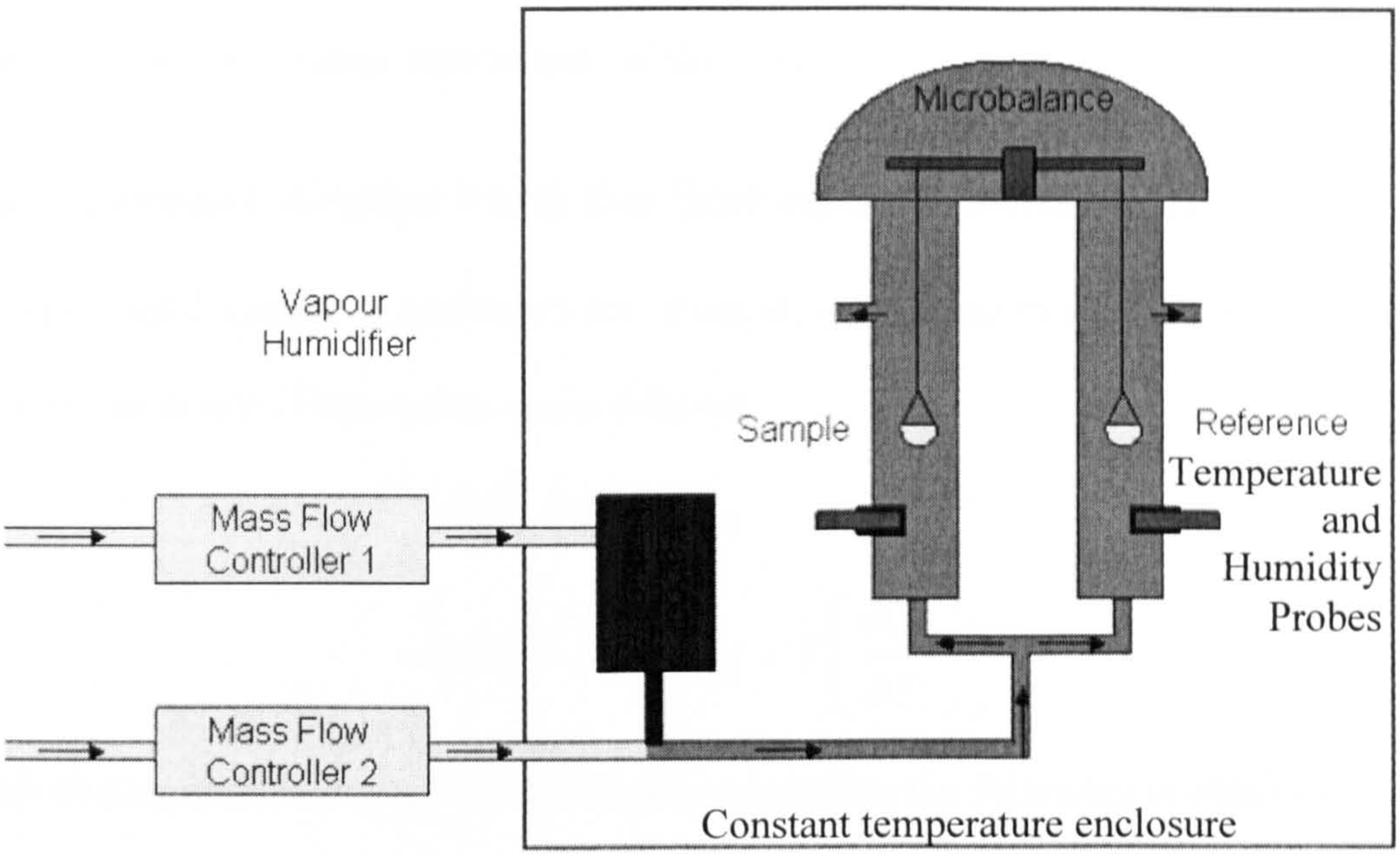
where R is the universal gas constant, K a constant, N_A the Avogadro's number, a_m the cross sectional surface area of the adsorbed molecule and W_A is the work of adhesion [239].

IGC has been used to study a range of materials; catalysts, food and cosmetics including pharmaceuticals. The robustness of the IGC technique is exemplified by the increasing wide scope and range of applications including for pharmaceutical solids, reviewed in Chapter 8. This information could be used to evaluate performance or stability of products as well as suitability of pharmaceutical delivery systems [200]. The evaluation of the dispersive component of the surface energy and the acid-base properties of the solid from the retention volumes are described in Chapter 8.

5.6 Gravimetric Vapour Sorption

Vapour sorption isotherms were traditionally evaluated by placing a sample in a controlled environment at specific relative humidities and regularly measuring sample masses until equilibrium is reached. This static technique requires a large amount of sample (a few grams) and lengthy time (a few weeks) to reach equilibrium [46]. Inaccuracies occur as samples have to be removed from controlled environment to be weighed. The introduction of a highly sensitive and accurate flow control for determination of sorption isotherms rapidly, has enabled such measurements of higher precision to be obtained (Figure 5.4). In turn, properties such as the surface energy of powders can also be determined with confidence [246].

Figure 5.4: The Dynamic Vapour Sorption equipment used for gravimetric vapour sorption experiments.



The work of adhesion as described by the Young-Dupre (Equation 1.2) assumes a negligible spreading pressure ($\pi_e = 0$). Such an assumption is widely accepted for the case of partial wetting when contact angles, θ are greater than 10°. However, for liquids which completely wet a solid ($\theta = 0^o$), the spreading pressure may be significant and work of adhesion can be described as follows:

$$W_A = 2\gamma_{LV} + \pi_e = 2\sqrt{\gamma_S^d \gamma_L^d} + 2\sqrt{\gamma_S^p \gamma_L^p} \tag{5.9}$$

From Gibb's surface tension equation, Equation 2.106 is obtained and thus, the spreading pressure can be calculated by:

$$\pi_e = \frac{RT}{\sigma} \int \Theta \cdot d \ln p \tag{5.10}$$

where σ is the specific surface area and Θ is the total amount adsorbed.

Therefore, by measuring the adsorption isotherm of the vapour for a completely wetting liquid, we may be able to determine the π_e and estimate the W_A including surface energy components of the solid.

5.7 Contact Angles from the Enthalpy of Immersion

When a solid surface is immersed into a liquid, the change in the Gibbs free energy and the enthalpy of immersion are as follows:

$$-\Delta G_i = \gamma_S - \gamma_{SL} \tag{5.11}$$

$$-\Delta H_i = \gamma_S - \gamma_{SL} + T\left(\frac{\partial G_i}{\partial T}\right)_P \tag{5.12}$$

Substituting Equation 5.12 with the Young's equation, the following is obtained:

$$\Delta H_i = -\gamma_{LV}\cos\theta - (\gamma_S - \gamma_{SV}) - T\cdot\left[\frac{\partial(\gamma_{SL})}{\partial T} - \frac{\partial(\gamma_S)}{\partial T}\right]_P \tag{5.13}$$

The above equation is normally simplified by assuming that $\gamma_S \approx \gamma_{SV}$ (that is to assume that the π_e is negligible) and that surface energy is independent of temperature, $\frac{\partial(\gamma_S)}{\partial T} \approx 0$. The relationship of γ_{SL} to temperature is given by $\frac{\partial(\gamma_{SL})}{\partial T} \approx 0.07 \pm 0.02$ mJ $m^{-2} K^{-1}$ [247]. This results in a simple relationship as shown:

$$\cos\theta = \frac{-0.07\cdot T - H_i}{\gamma_L} \tag{5.14}$$

where the enthalpy of immersion is easily measurable with a microcalorimeter.

The measurement of heat of immersion for the determination of contact angles and surface energy is known to work well for low energy monopolar surfaces, such as Teflon [248] and fluorinated hydrocarbons [249], including pharmaceutical solids [250]. Although samples need not be prepared in a specific manner for immersion

experiments, contamination from moisture adsorption for example can drastically affect the results. Furthermore, this technique suffers from the assumption of $\gamma_S \approx \gamma_{SV}$, which may not be applicable if θ of the probe liquid is low.

5.8 X-ray Photoelectron Spectroscopy

When X-rays irradiate a surface, surface electrons are ejected in what is known as the photoelectric effect, first noticed by Hertz in 1887. In the first of three very important and significantly ground-breaking papers, Einstein described and explained this photoelectric effect which heralded the birth of the quantum theory, and which also resulted in him winning the Nobel prize for Physics in 1921. This year marks the centennial anniversary of the publication of these papers and is appropriately named as the Einstein year. It is this photoelectric principle which forms the basis of the X-ray Photoelectron Spectroscopy (XPS), also known as Electron Spectroscopy for Chemical Analysis (ESCA).

XPS is a technique in which the surface of a sample kept under high vacuum is bombarded by high energy X-rays, resulting in the emission of core shell electrons. X-rays will typically penetrate deep (a few mm) into the sample, but only a small fraction of the excited electrons, typically from the outer surfaces ($\approx$ 5 nm) are successfully ejected and their energy analysed. A detector measures the kinetic energy of these electrons, and if monochromatic X-rays are used, the photoelectron binding energies can be calculated. The binding energies of core shell electrons are very specific and dependant on the state of the element from which the electrons are ejected. This results in the resolution of chemical information and elemental composition of a solid surface. It is this ability to distinguish chemical functionalities and coupled with its surface sensitivity which has been the major strength of XPS.

The XPS instrument consists of an electron source and an anode for generation of X-rays, an ultra high vacuum chamber for the sample and an electron energy analyser as shown in Figure 5.5. The design and selection of these parts and its theories are described in further detail in Chapter 7. Reviews of the technique and their application can be found elsewhere [251-253]. Figure 5.6 shows the photoelectron ejection process on which XPS is based.

Figure 5.5: The schematic diagram of the XPS equipment.

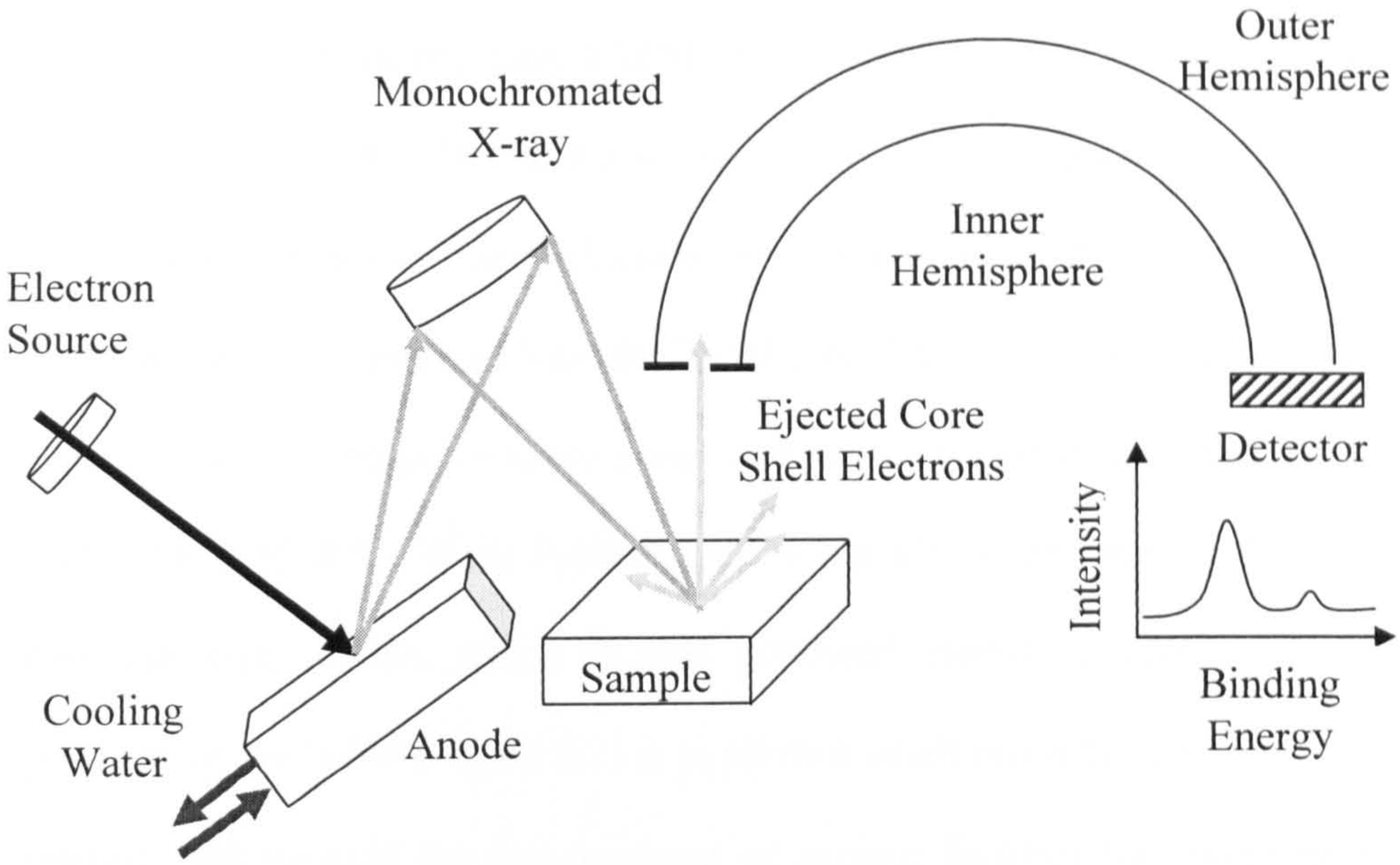
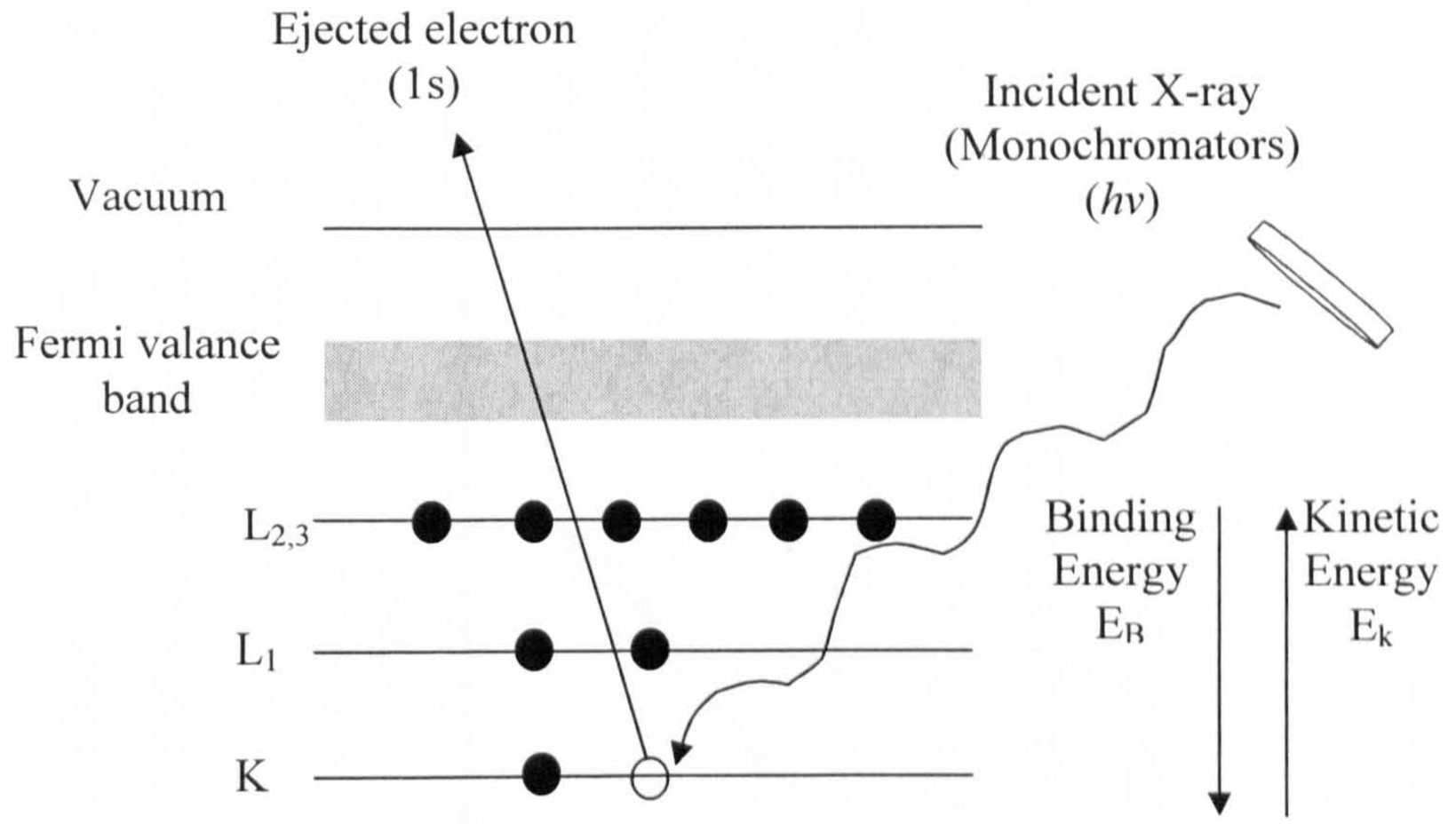


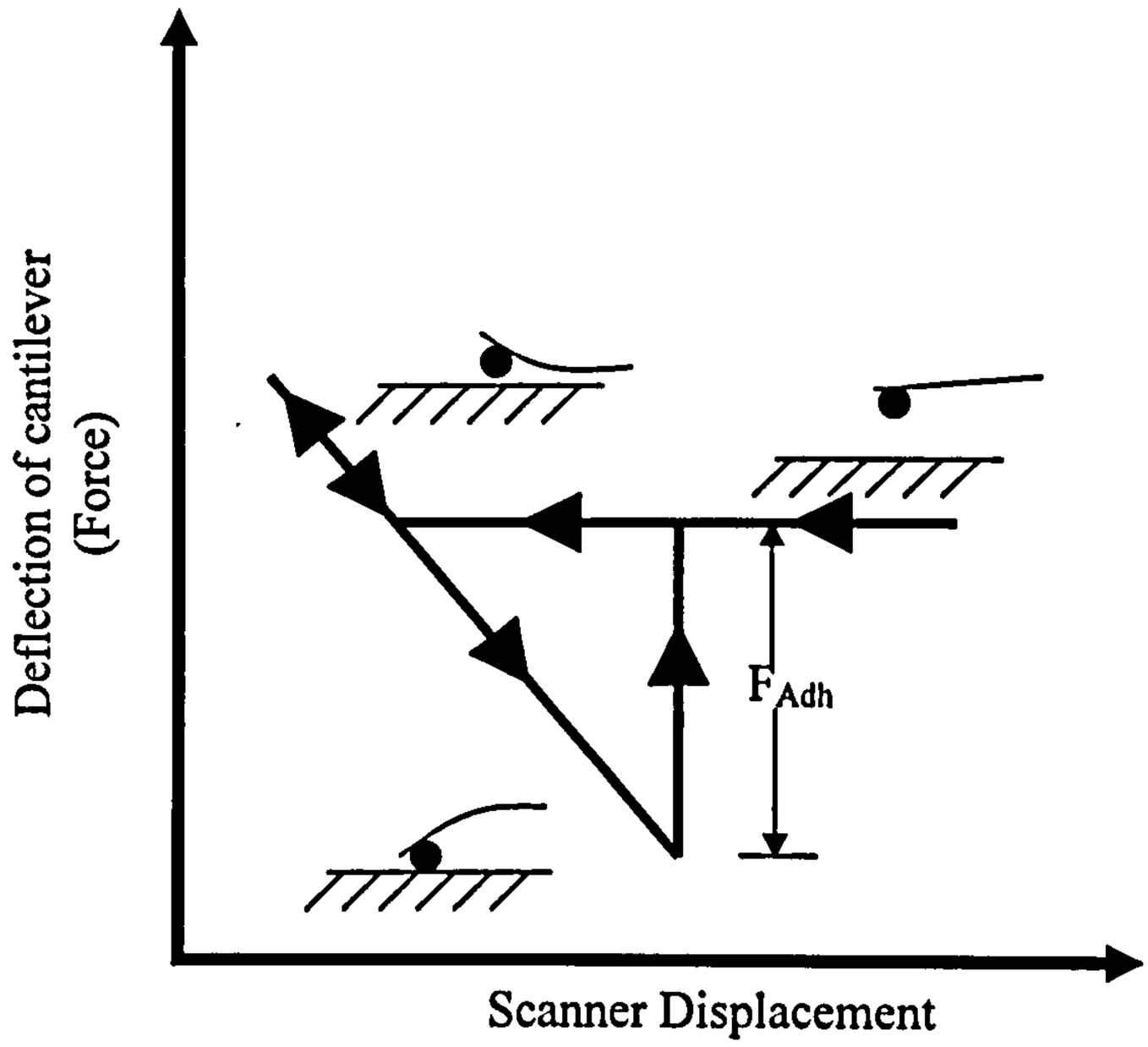
Figure 5.6: Schematic of the photo-ejection process of the core shell electron by X-rays for XPS analysis.



5.9 Atomic Force Microscope

The atomic force microscopy (AFM) was invented by 1986 Physics Nobel Prize winners Binnig et al. [254], and used initially as an imaging tool, but has since gained wide spread use in the characterisation of particulate interactions. Its applications vary from the measurements of van der Waals, double layer, specific forces in various media for a wide range of applications and have been reviewed by many researchers elsewhere [255-259]. More recently, AFM has also been employed in the study of pharmaceutical solids, which is also reviewed elsewhere [260-262]. The basic principle of the AFM (Figure 5.7) is to allow a small probe to scan across a sample of interest, and permits the measurement of surface features by observing the probe-sample interactions, which is capable of imaging features down to the atomic scale.

Figure 5.7: Schematic of the cantilever deflection with respect to scanner displacement on approach to and from the solid surface. As the cantilever approaches the solid surface, the cantilever bends upwards due to repulsive forces. The cantilever is bent downwards as the particle is attracted to the surface. As the scanner is moved further away from the surface, the particle is detached from the surface with the force equals to the F_{Adh}.



Molecular resolution images of organic molecules with well defined crystal structures were first reported by Yamada and Nakayama [263]. AFM images were obtained for both the cleaved surfaces of polydiacetylene and a molecular film of liquid crystals on graphite. The molecular spacing obtained by AFM was in good agreement with the predicted unit cell dimensions, which were of the order of a few nm. Surface roughness is also routinely obtained by AFM. Surface roughness characteristics were evaluated by various imaging techniques by Seitavuopio et al. on potassium chloride and sodium chloride tablets [264]. Li and Park proposed the use of fractal analysis to describe the surface roughness of pharmaceutical particles from profiles obtained by AFM [265]. Nanocrystalline particles shape and structural information were also successfully obtained by the use of an AFM which were not available by classical light scattering techniques [266]. These studies, to mention but a few, demonstrate the ability of the AFM as a tool to image both qualitatively and quantitatively the surface features of solid surfaces and have led to studies on growth, dissolution and etching behaviour of crystalline solids.

Surface restructuring during the growth of crystalline solids or the effects due to solvent supersaturation [267], applied magnetic fields [268], additives [269, 270], relative humidity [271, 272] have been studied with the AFM, with in-situ observations first reported for trichosanthin crystals [273]. The individual dissolution rates of aspirin crystalline facets (001) and (100) were measured by AFM by Danesh et al.. It was reported that the (100) face dissolves six times faster in 0.05 M HCl solution at room temperatures [274]. AFM was also utilised to study solid-liquid interactions by observing the effects of solvent and additives on the etching patterns of individual facets of paracetamol single crystals [275-277].

Particle-particle interactions are vital in the formulation of pharmaceutical drug delivery systems such as the dry powder inhaler (DPI) [278]. These interactions can also be determined from the measurements of adhesion forces by AFM as reported by Louey et al. [279] for a common excipient, lactose obtained by the colloidal probe technique. Sindel and Zimmerman investigated the forces between individual single crystalline particles and tablet surfaces [280]. They concluded that although AFM is suited for determination of surface forces, surface roughness and contact area of probe-substrate may influence the magnitude of the measured forces. Such factors including the effects of surface chemistry, have been evaluated by several researchers [281-285]. As such, a qualitative ranking of intermolecular forces is plausible while the determination of an absolute value may prove to be a greater challenge.

The adhesion of a particle on a solid surface occurs via a range of complex intermolecular forces. The two most commonly used models for the approximation of such interactions are the Johnson-Kendall-Roberts (JKR) [36] and Derjaguin-Muller-Toporov (DMT) [37] approaches, and are detailed in Chapter 2. The measurement of the adhesion force, F_{Adh} by AFM has been utilised by several investigators to study surface energetics of pharmaceutical solids.

Two polymorphic forms of cimetidine; form A and B were successfully discriminated by AFM scans acquired under tapping mode [286, 287]. A stronger attractive force between tip and surface of form A compared to form B was obtained, in agreement with lower contact angles of water on form A. Cao and co-workers [288] attributed the contrasting adhesion force of silicon nitride tips on facet (020) of form I and facet (002) to the chemical end groups exposed at the respective surface, and related these to their wettability.

Relini et al. [213] recently measured the adhesion force of streptavidin functionalised polystyrene beads with the crystal surface of streptavidin under liquid. They reported that the Bradley equation is more applicable than the JKR approach for their experiments, with surface energies of 0.16 ± 0.04 mJ/m^2 obtained (the surface energy quoted here is not for one in equilibrium with a vapour, but for a solid immersed in liquid). The authors claim that AFM measurements are in good agreement with values obtained from analysis of crystal growth morphology. Davies and co-workers quantitatively investigated the surface energies of milled and unmilled budesonide by both AFM and inverse gas chromatography [285]. The variations and wide range of surface energies obtained by AFM were attributed to surface features, variation in contact geometry including crystal face orientation resulting in exposure of dissimilar chemical moieties. The effects of surface chemistry on adhesion forces were reported for facets (001) and (100) of aspirin single crystals [135]. On the more hydrophobic (001) face, -CH_3 terminated probes had a greater degree of interaction while –COOH terminated probes interacted stronger with the hydrophilic (100) face.

5.10 Experimental Comparison of Characterisation Techniques

In the following sections, conventional techniques and their suitability for characterising crystalline pharmaceutical solids were investigated. Both liquid and vapour probe techniques were employed on powdered and macroscopic single crystalline samples. For powder bed samples, the capillary rise through a powder bed and sessile drop measurements on compacted powders were used, as these are the two most frequently used techniques and are thought to provide representative characterisation of the powder bed techniques as a whole. Vapour probe investigations were conducted with inverse gas chromatography (IGC) operated under

infinite dilution conditions. Contact angles on macroscopic single crystals were determined using the sessile drop technique and this work is reported in detail in Chapter 6. The choice of these techniques has enabled some degree of comparison between these well reported powder techniques with our single crystal techniques proposed in this thesis, for wettability studies on complex organic materials [289]. It is known that the accurate knowledge of the surface energetics are vital to improving crystallisation techniques and powder processing operations [290, 291].

5.11 Experimental Section

5.11.1 Materials

For the capillary rise and IGC measurements reported in this chapter, the pharmaceutical powders were used as received. Contact angle measurements were carried out with deionised water, diiodomethane (>99 %,Arcos Organics, Belgium), formamide (>99.5%, Arcos Organics, Belgium) and ethylene glycol (>99 %, Sigma-Aldrich, England). Diiodomethane was purified by passing through chromatographic columns of silica (Merck, Silica gel for column chromatography, 70-230 mesh) and basic alumina (Sigma-Aldrich England, STD Grade, activated basic, 150 mesh). Properties of contact angle probe liquids are listed in Table 5.1.

Table 5.1: Properties of Contact Angle Liquid Probes Used

Liquids	Purity (%)	Density at 20 °C (kg/m^3)	γ_{LV} (mJ/m^2)	γ_{LV}^{d} (mJ/m^2)	γ_{LV}^{p} (mJ/m^2)
Diiodomethane	>99	3325	50.8	50.8	0.0
Water	Deionised	998	72.8	21.8	51.0
Ethylene Glycol	>99	1109	48.0	29.0	19.0
Formamide	>99.5	1139	58.0	39.0	19.0

5.11.2 Powder Compact Preparation

Powder compacts were prepared with a Lloyds Beal Compression machine (Ammtek, U.S.A.) with a 20 mm diameter stainless-steel die and punch (Specac, U.K.). Approximately 3 g of powder was poured into the die for compaction, and the cell assembly was tapped for 1 minute to minimise density distribution within the cell. The crosshead was lowered at a controlled speed of 5 mm/min, with compression forces of 10 kN, 20 kN, 30 kN and 40 kN applied by a force transducer (Sensotec Inc., U.S.A.). Ejection of the compact was achieved by applying a corresponding maximum compression force with the crosshead speed again of 5 mm/min. Scanning electron microscope (Jeol Ltd. U.K.) images were obtained for the compacts with an accelerating voltage of 20 kV. Prior to examination, the samples were gold coated.

5.11.3 Capillary Rise Measurements

Capillary rise of liquid into a powder bed was measured with a tensionmeter (K100, Krűss GmbH, Germany). An FL12 Powder Cell (Krűss GmbH, Germany) was filled with 1 g of paracetamol powder. A fine wire mesh was placed at the bottom of the cell to stop the powder escaping from the cell. Consistent slow tapping of the cell over a period of 1 minute was performed to ensure that the particles were evenly distributed within the cell and to ensure reproducible column packing. The cell was fixed onto a clamp within the tensionmeter. A glass beaker was filled with the probe liquid and placed within a crucible, held at a constant temperature of 293 K by an external water bath. The mass of the cell plus sample was tared before the probe liquid was brought slowly towards the sample, until about 1 mm from the cell edge. The z-stage is then set to move automatically upwards until a small wetting force is detected. At that moment, the wetting measurement starts ($t = 0$ s and $m = 0$ mg) and the liquid level is held at position without any further immersion of cell. The weight gain of the sample

was measured as a function of time until a steady state mass was obtained. The beaker was then lowered with residual mass indicating the total mass of liquid retained by the sample [292]. Data was recorded by the Krűss software (version 2.0.1, Krűss GmbH, Germany). Experiments were repeated at least 8 times for each liquid probe used. Liquid properties were as shown in Table 5.2.

Table 5.2: Capillary Rise Liquid Properties

Test liquid	γ_{LV} [mN/m][a]	ρ_l [g/cm^3] [b]	η_l [mPa.s] [a]
n-Hexane (HPLC Grade)	18.40	0.649	0.313
n-Heptane (99%)	20.14	0.684	0.416
n-Octane (>99.0%)	21.68	0.703	0.489
Ethanol (>99.7%)	22.38	0.789	0.998
Methanol (>99.9%)	22.45	0.792	0.588
Cyclohexane (99+%)	25.24	0.779	0.860
n-Dodecane (99+%)	25.35	0.751	1.288
n-Tetradecane (99+%)	26.56	0.765	1.978
Chloroform (99.9%)	27.32	1.489	0.514
n-Hexadecane (99%)	27.47	0.774	2.801
Toluene (99.8%)	28.52	0.866	0.523
p-Xylene (99%)	28.54	0.861	0.574
Decan-1-ol (>99%)	28.88	0.830	9.638
Mesitylene (99%)	28.80	0.865	1.154
Decalin (>98%)	31.03	0.883	2.312
Tetralin (97+%)	35.50	0.973	2.202
Tetrachloroethane (97+%)	36.21	1.594	1.456
α-Bromonaphthalene	44.40	1.482	5.107
Ethylene Glycol	28.43	1.109	21.84
Diiodomethane (>99%)	50.80	3.325	2.762
Formamide (>99.5%)	57.45	1.139	3.645
Water (Deionised water)	72.80	0.998	1.002

Source: [a] J. J. Jasper, J. Phys. Chem. Ref. Data, 1:842 (1972) at 20 °C
[b] Perry's Chemical Engineering Handbook (density at 20 °C)

5.11.4 Sessile Drop Measurements

The contact angle formed by liquid probes on the solid surface defines solid-liquid interactions according to the Young-Duprè equation. Initial drops of about 5 μL were dispensed onto solid surface and their droplet profiles fitted. By continuously adding liquid into the droplet, the advancing contact angle was obtained using the Krüss Drop Shape Analysis (DSA 10, Krüss GmbH, Hamburg, Germany) instrument. The needle remained immersed within the top half of the droplet during measurements. Measurements were conducted in the open air at room temperatures of 293 ± 2 K. Contact angles were obtained on powder compacts and on macroscopic single crystals. At least 8 contact angle measurements were taken for each probe liquid on the compacts and the single crystals. Measurement of contact angles on tablets were immediately carried out after powder compaction.

5.11.5 Inverse Gas Chromatography

Paracetamol and ibuprofen powder was packed into pre-silanated glass columns (4 mm ID) with silanated glass wool at its ends to avoid powder movements during the experiments. The sample was pretreated at 303 K, 0 % RH for 2 hours by flowing 10 standard cubic centimetres (sccm) of helium gas, to remove any residual moisture and solvent. A series of alkane vapours (undecane, decane, nonane and octane) was selected and used as dispersive surface energy probes. Methane gas was used as a non-interacting probe to determine the dead-time of the column. The injected probes were at infinite dilution (4 $\%p/p_o$) for a peak maximum analysis and chromatograms were obtained with an SMS-iGC 2000 (Surface Measurements Systems Ltd., London, UK) instrument. The surface energy of paracetamol and ibuprofen was calculated

according to the Schultz et al. [293] method by the SMS-iGC analysis software (version 1.2, Surface Measurements Systems Ltd., London, UK).

5.12 Results and Discussion

5.12.1 Capillary Rise

Figure 5.8 and Figure 5.9 show the weight gain curves for hexane (apolar probe liquid) and 1-decanol (polar probe liquid) respectively. Liquid penetration into the cell occurs immediately after contact with the probe liquid. For the apolar probe liquids, increments in mass due to liquid capillary rise occur over the next several seconds until they level off. When no further change in mass is detected, the liquid was drained from the cell and a drop in mass is observed. This final mass is the liquid mass uptake or liquid retention by the powder. The [m^2/t] is obtained by fitting a linear regression to m^2 versus t, during the initial mass increase.

Figure 5.8: Weight gain curves for n-hexane as a function of time measured for paracetamol powders.

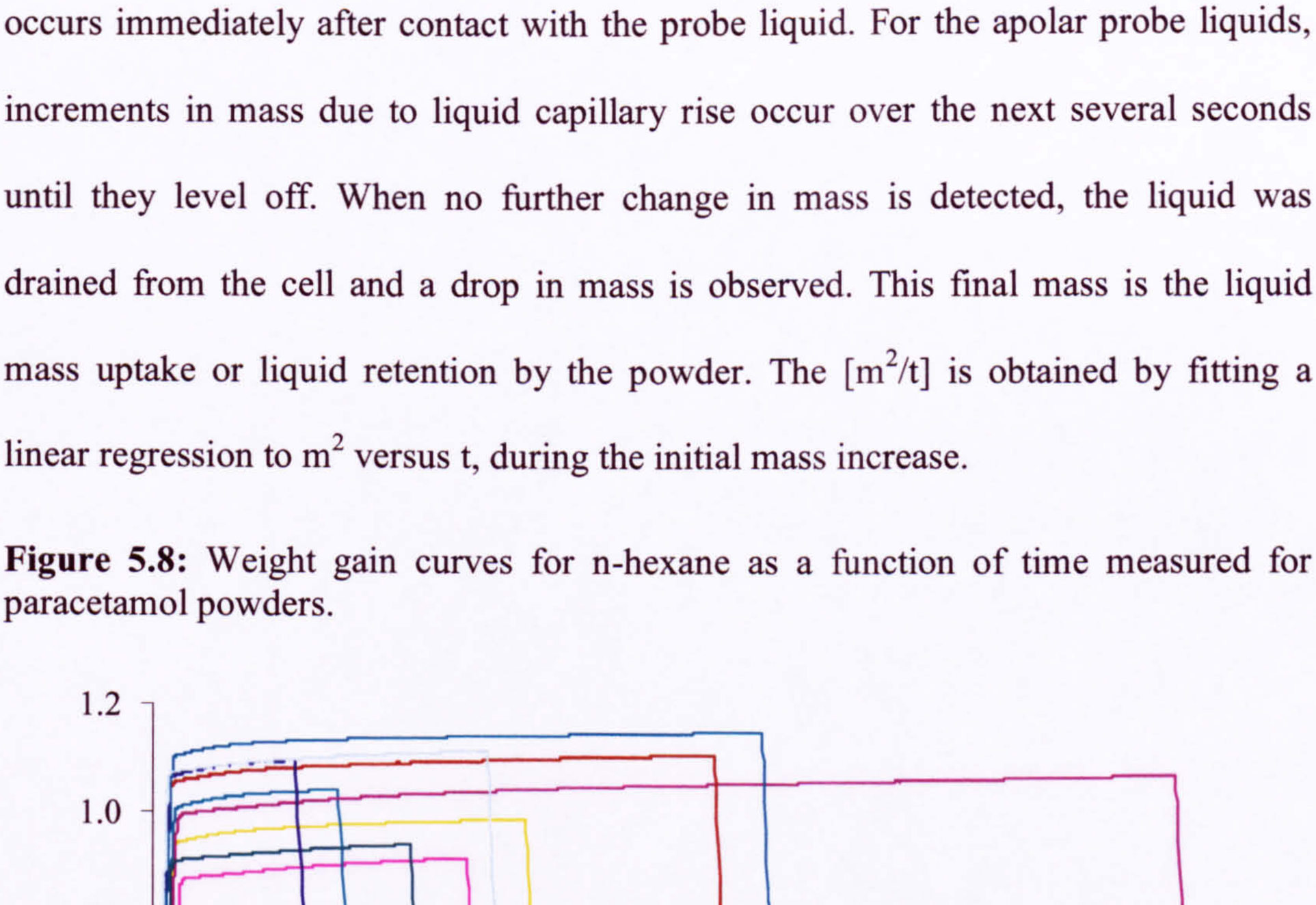
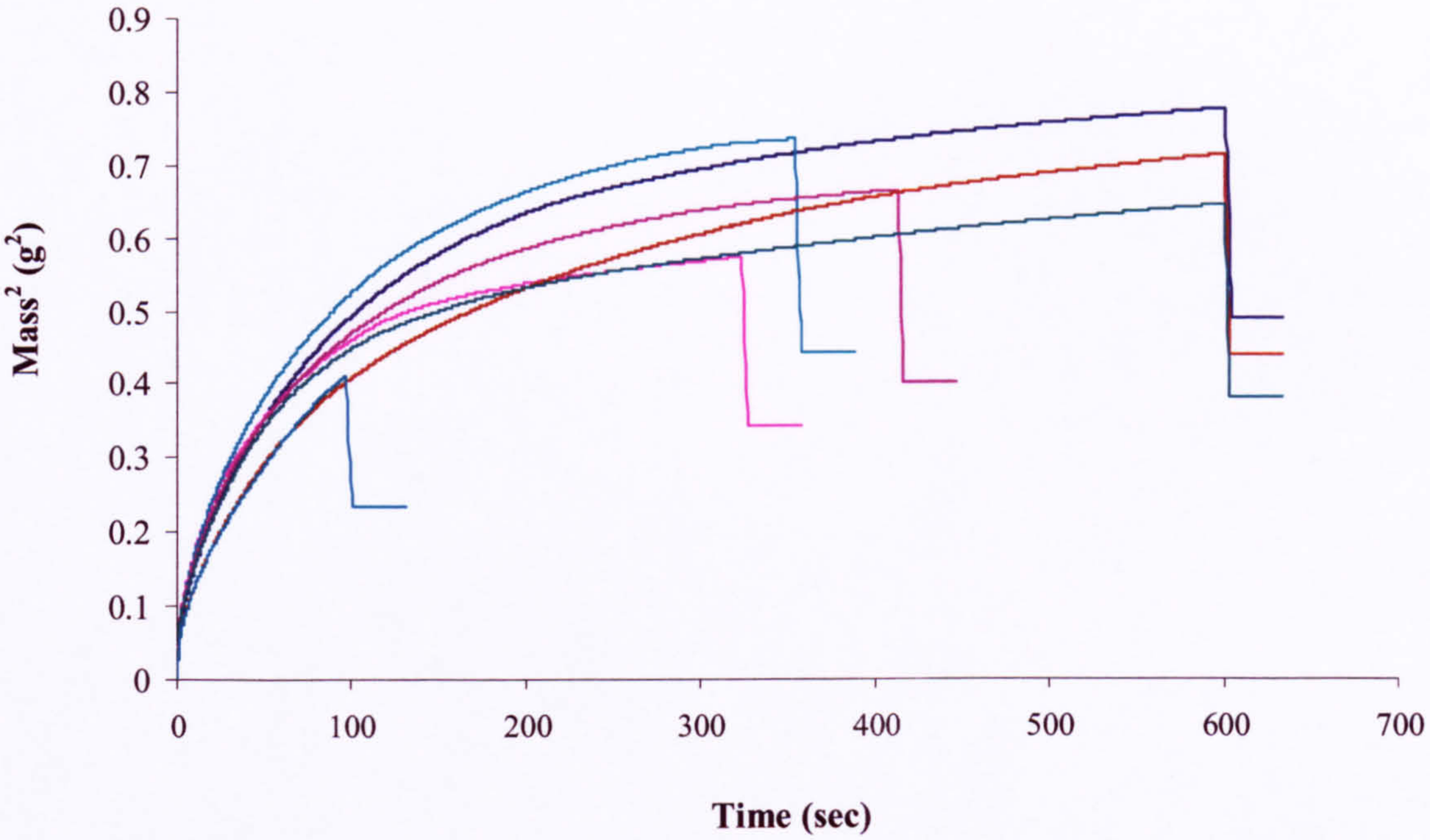


Figure 5.9: Weight gain curves for 1-decanol as a function of time measured for paracetamol powders.

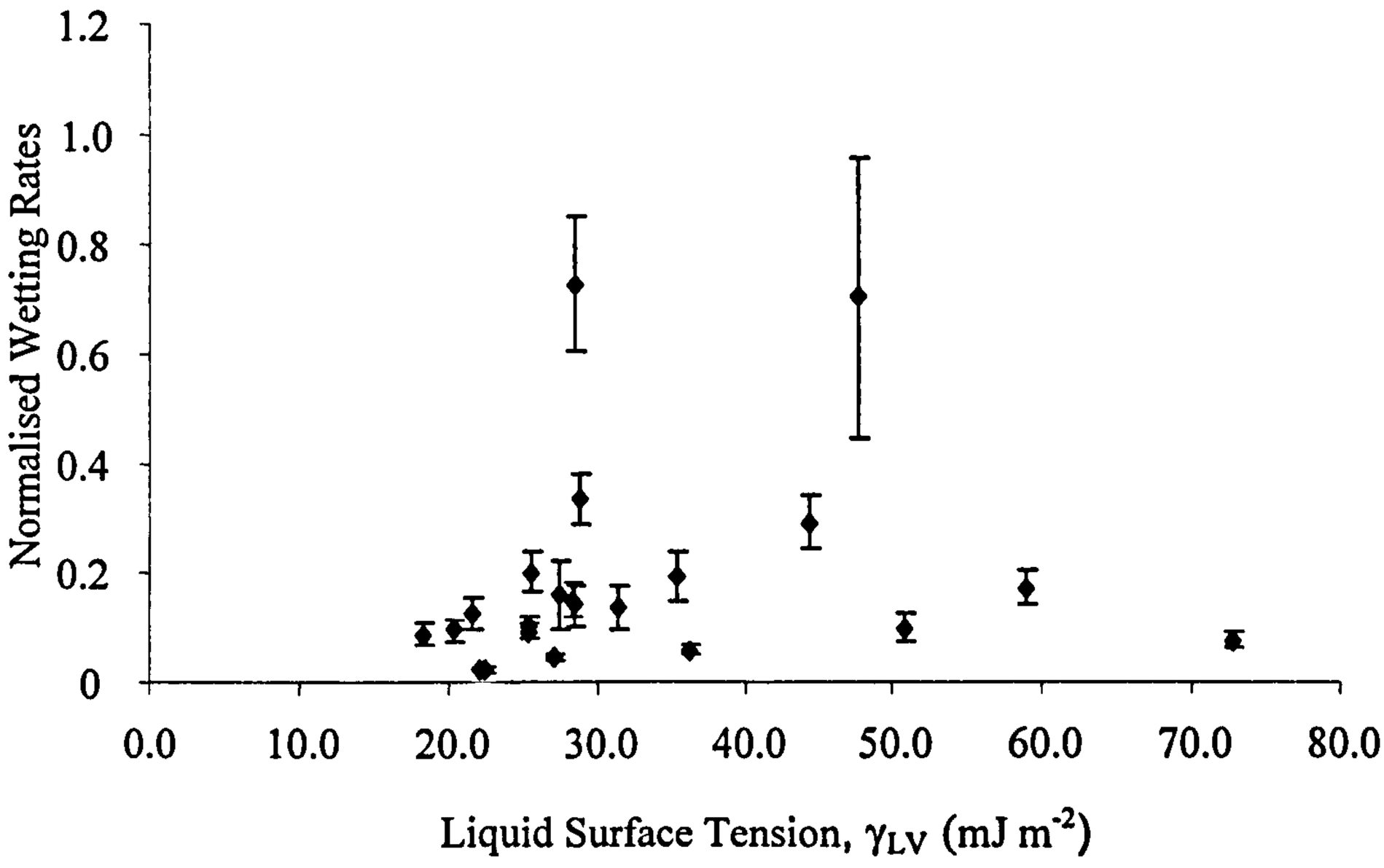


For some polar probes, a decrease in rate of mass uptake by the column was observed. This is possibly due to dissolution of the powder bed by the liquid resulting in a reduction of material available in the column. [m^2/t] is obtained by fitting the curve and differentiating with respect to time at t = 0 s. It is assumed that dissolution has not occurred when the powder bed was initially brought into contact with liquid.

The weight rise curves obtained are quite reproducible considering that a new powder sample is used for each measurement. Concerns about the reproducibility of the powder beds, which may compromise the quality of the measurements, do not appear to be an issue here. The surface energy of solid particles is then obtained by plotting a normalised wetting rates plot, analogous to Zisman's approach. The scattered points on a normalised wetting rates plot may be due to the inappropriate use of such an analysis (Figure 5.10). Based on the normalised wetting plot, it is postulated that the use of the plot does not accurately describe the surface energies of

complex organic materials, while ruling out the contributions of an irreproducible column. However, if the packed columns were to behave in an irreproducible manner, then the points would show larger deviations on the Y-axis and not a random scattering as observed. The use of equation of states based analysis may not be suitable to assess the surface energy of complex organic materials, and this point is examined in some detail in Chapter 9.

Figure 5.10: Normalised wetting rates for paracetamol powder bed.



To analyse the dispersive surface energy component, γ_{SV}^{d}, the normalised wetting rates for only apolar liquids were plotted. This approach incorporates Fowkes' assumptions that same type of interactions occur between phases, with plot of apolar liquids indicative of the apolar nature of the solid phase [21]. Figure 5.11 and Figure 5.12 shows the normalised wetting rate for paracetamol and ibuprofen, respectively. In this analysis of γ_{SV}^{d} of paracetamol and ibuprofen powders, only aliphatic hydrocarbon probes are used for the fully wetted section while both α-bromonaphthalene and diiodomethane were used for the non-wetting part. The points

are Gaussian fitted with the maximum giving surface energy of the particulate sample. The γ_{sv}^{d} of paracetamol and ibuprofen powder was found to be 40.0 mJ/m^2 and 32.5 mJ/m^2 respectively.

Figure 5.11: Normalised wetting rates for apolar probe liquids for paracetamol powder bed.

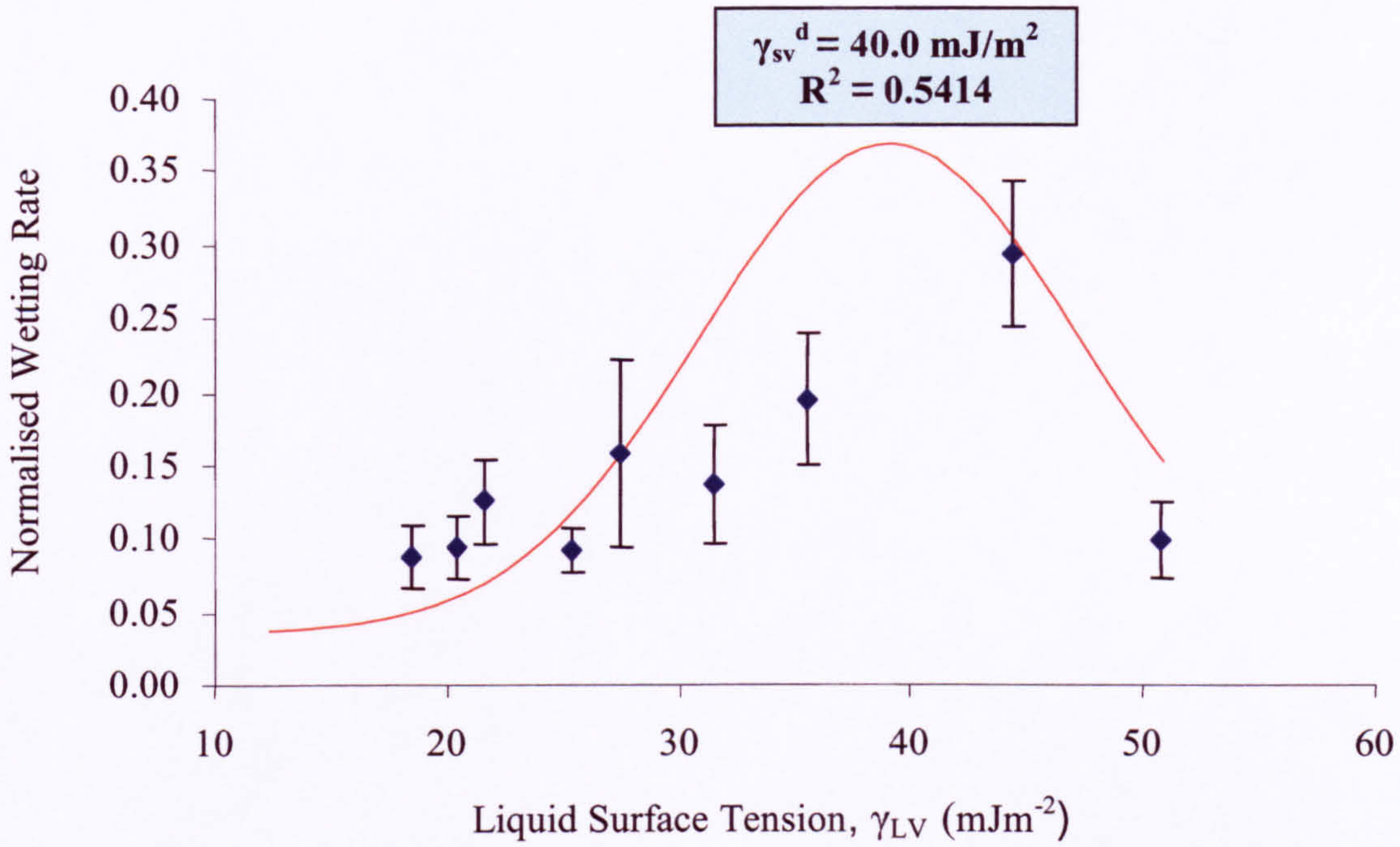
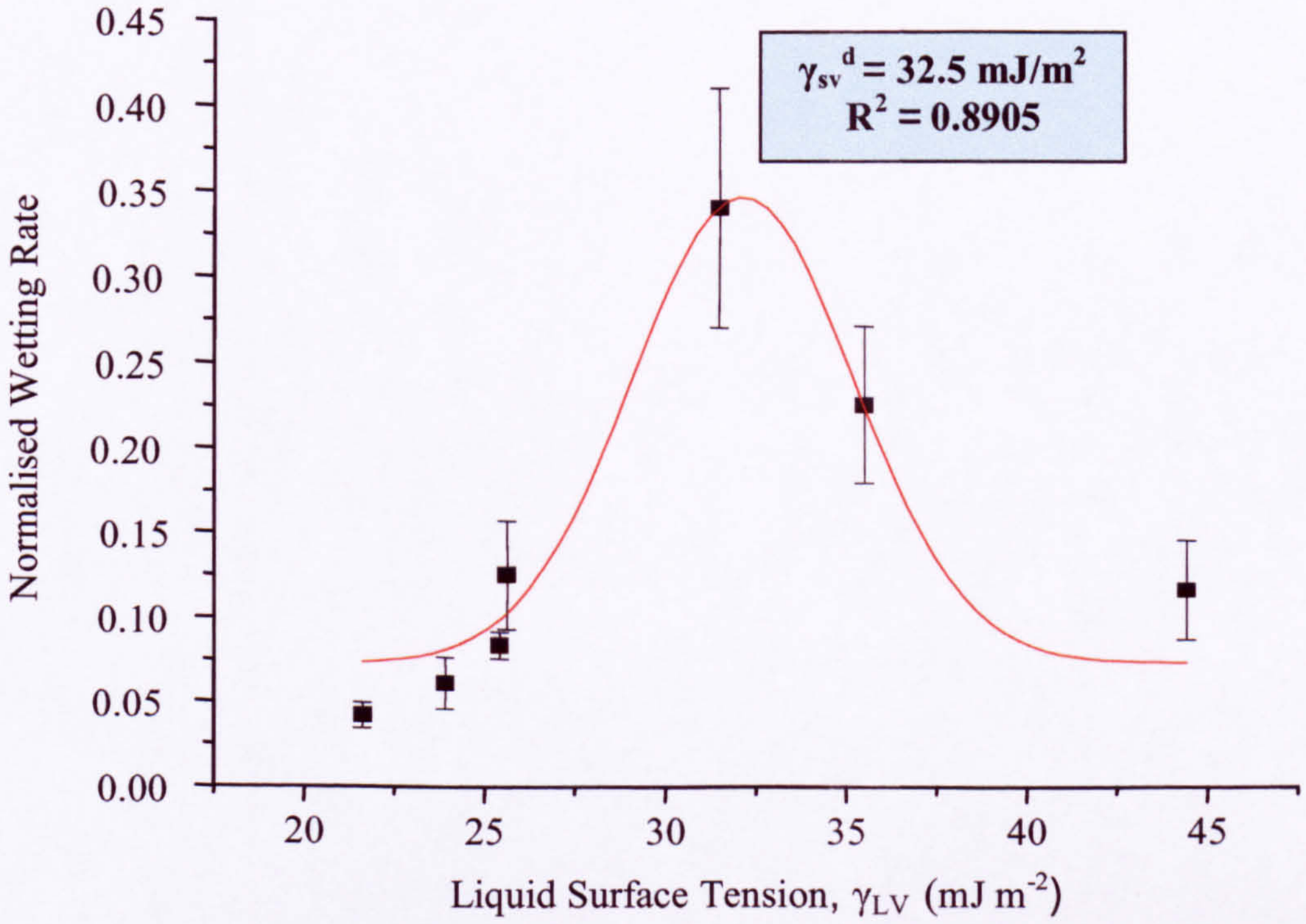


Figure 5.12: Normalised wetting rates for liquid capillary rise into ibuprofen powder bed for apolar probe liquids.



5.12.2 Sessile Drops on Powder Compacts

Powder was compacted under high pressure to form tablets for characterisation by the sessile drop technique. As previously noted, pressure induced compaction may result in deformed particle surfaces. Surprisingly, results for powder compacts are still reported by other workers as to be sensible and comparable with other techniques, with one such case for paracetamol. The γ_{sv} was reported to be 46 ± 2 mJ/m^2 for both capillary rise and sessile drop on compacts. However, this observation has not been confirmed in the current study, and all attempts to measure contact angles on paracetamol tablets, compacted at 10 kN, 20 kN, 30 kN and 40 kN were unsuccessful.

In this study, the liquid drops of water and diiodomethane on compacted tablets penetrated almost immediately upon contact and no contact angle was measurable. A series of liquid drop penetration pictures on a tablet formed under 20 kN compaction pressure is shown in Figure 5.13. In other studies, it has been reported that dramatic change in contact angle of water on paracetamol compacts is observed, with a change from 35 ° to 0 ° in 40 seconds [199]. This study reports that a complete penetration of the test liquids occurs within the first five seconds, with increasing penetration times into the tablets formed at higher compaction pressure. SEM images (Figure 5.14) confirm suggestions that tablets surfaces are porous, leading to the liquid penetration. The rates of liquid imbibition on compacts are thought to be dependent on the particle arrangements within the tablet. The porosity and the density distribution within the tablet are affected by the tabletting process including the punch geometry [294].

Figure 5.13: Penetration of water droplet into 20 kN paracetamol compacts at (a) 0 mS, (b) 450 mS, (c) 950 mS, (d) 1450 mS, (e) 1950 mS and (f) 2450 mS.

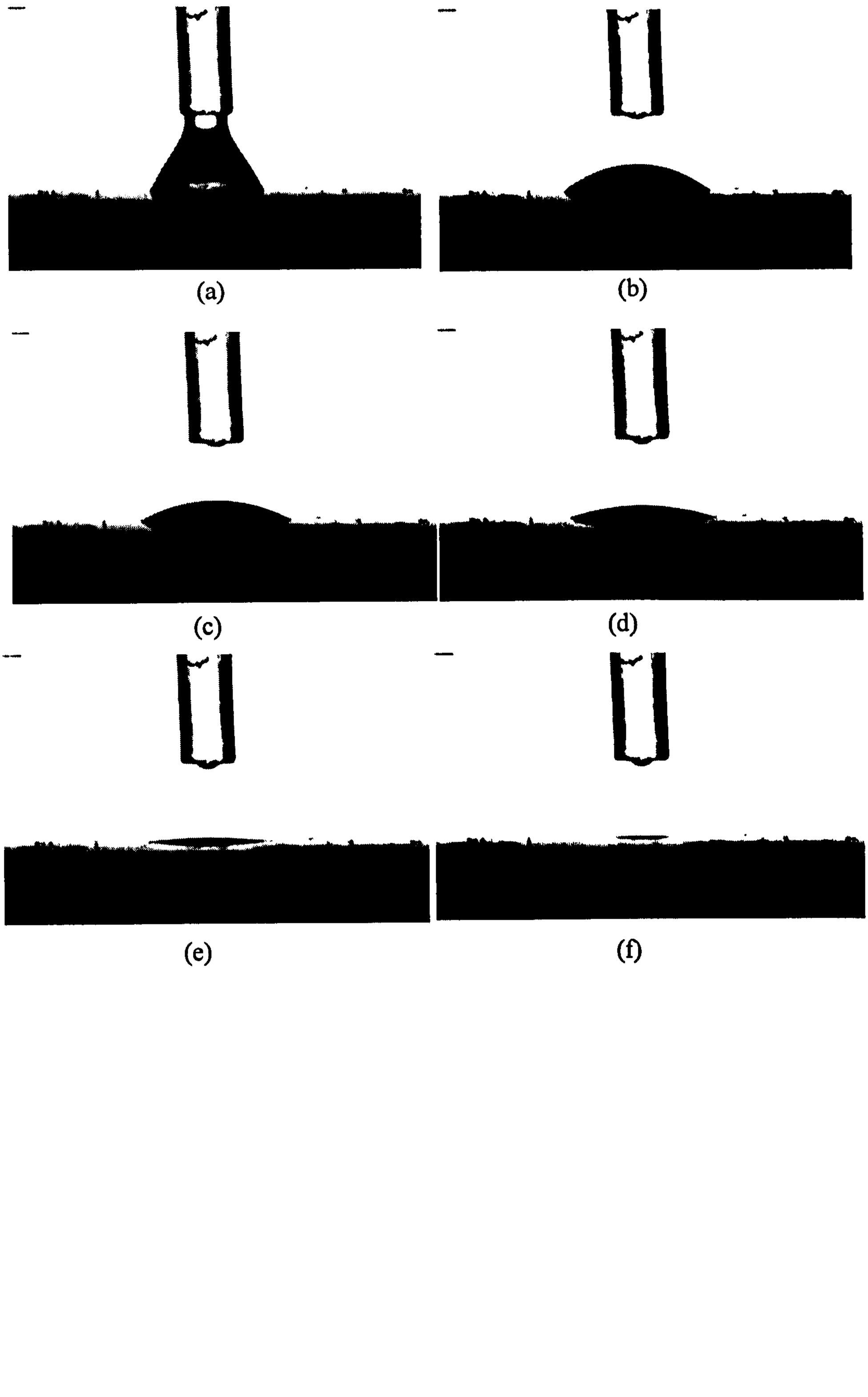
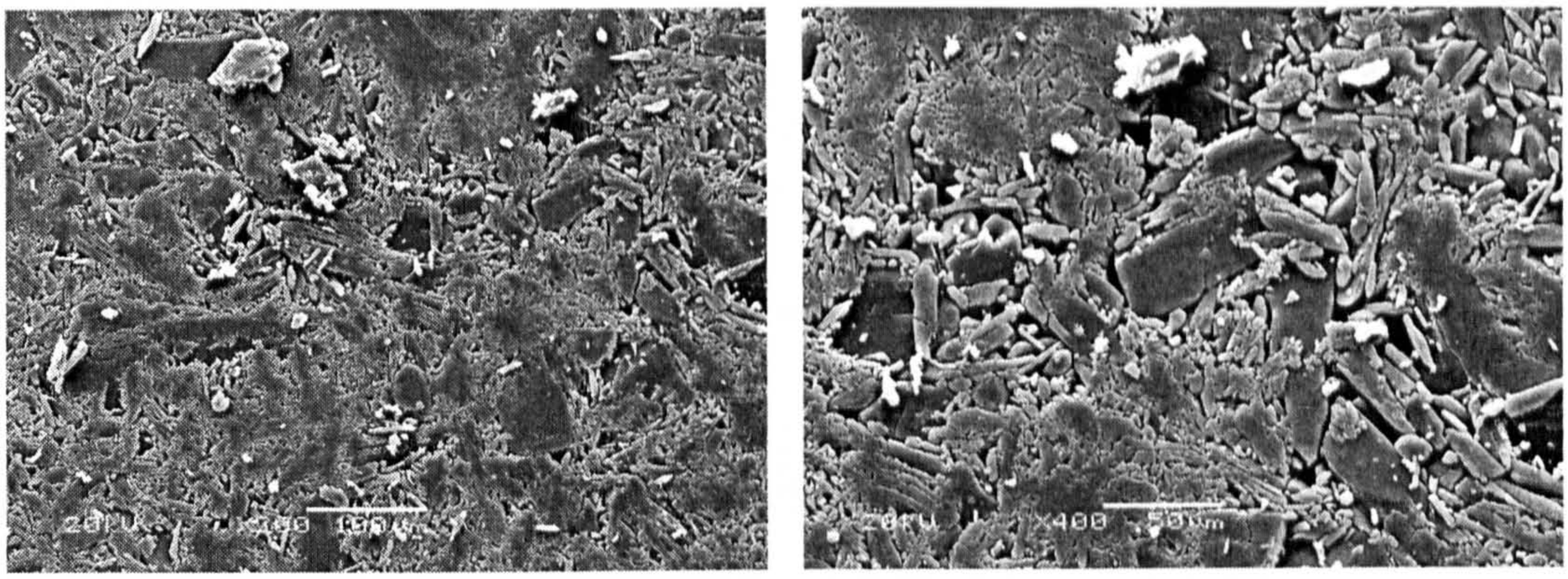


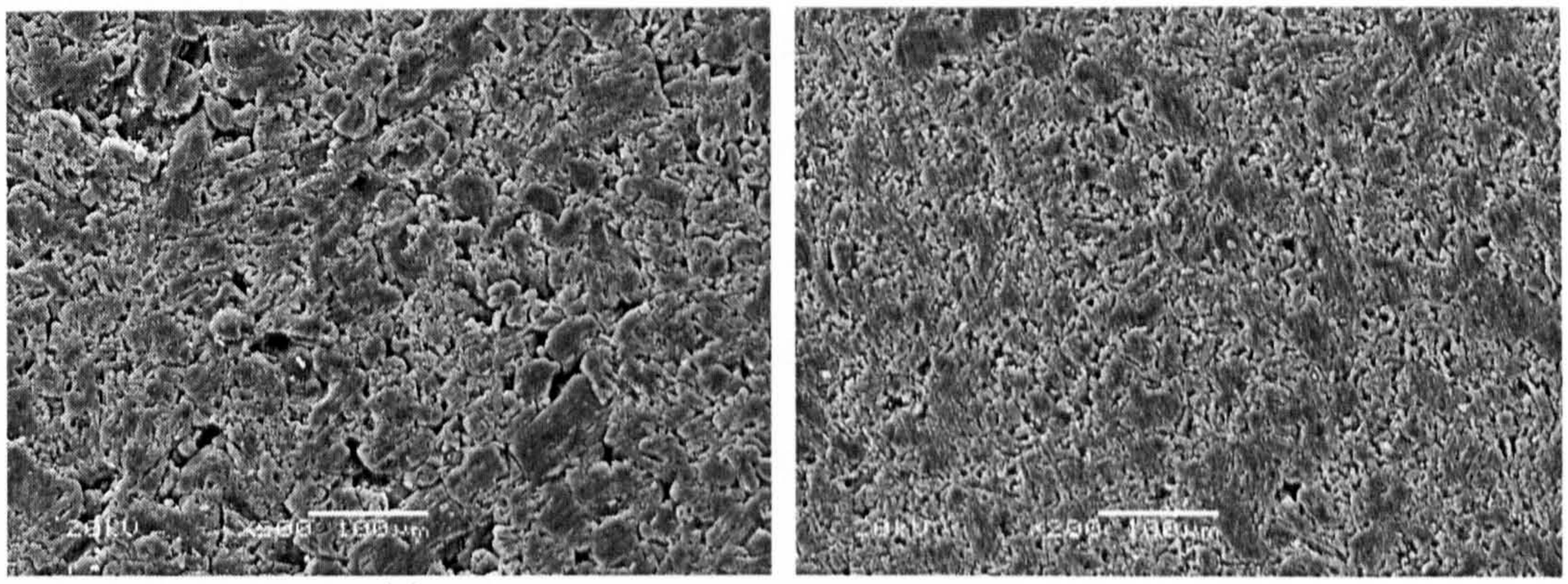
Figure 5.14: Scanning electron micrographs of paracetamol tablet compacted at 20 kN (a) 200 x and (b) 400 x magnification.



(a) (b)

In the case of ibuprofen compacts, contact angles were measurable for the advancing case. This difference could be due to ibuprofen being more compactable compared to paracetamol [182], although both these materials exhibit very poor compaction properties (Figure 5.15). Another more probable factor which may have hindered instantaneous liquid penetration is due to the surface chemistry of ibuprofen, which is hydrophobic. As such, high contact angles are expected, reducing the propensity for liquid to penetrate into the tablet capillaries. The θ_a results are shown in Table 5.3.

Figure 5.15: Scanning electron micrographs of ibuprofen tablet at (a) 10 kN and (b) 20 kN compaction pressure, 200 x magnification.



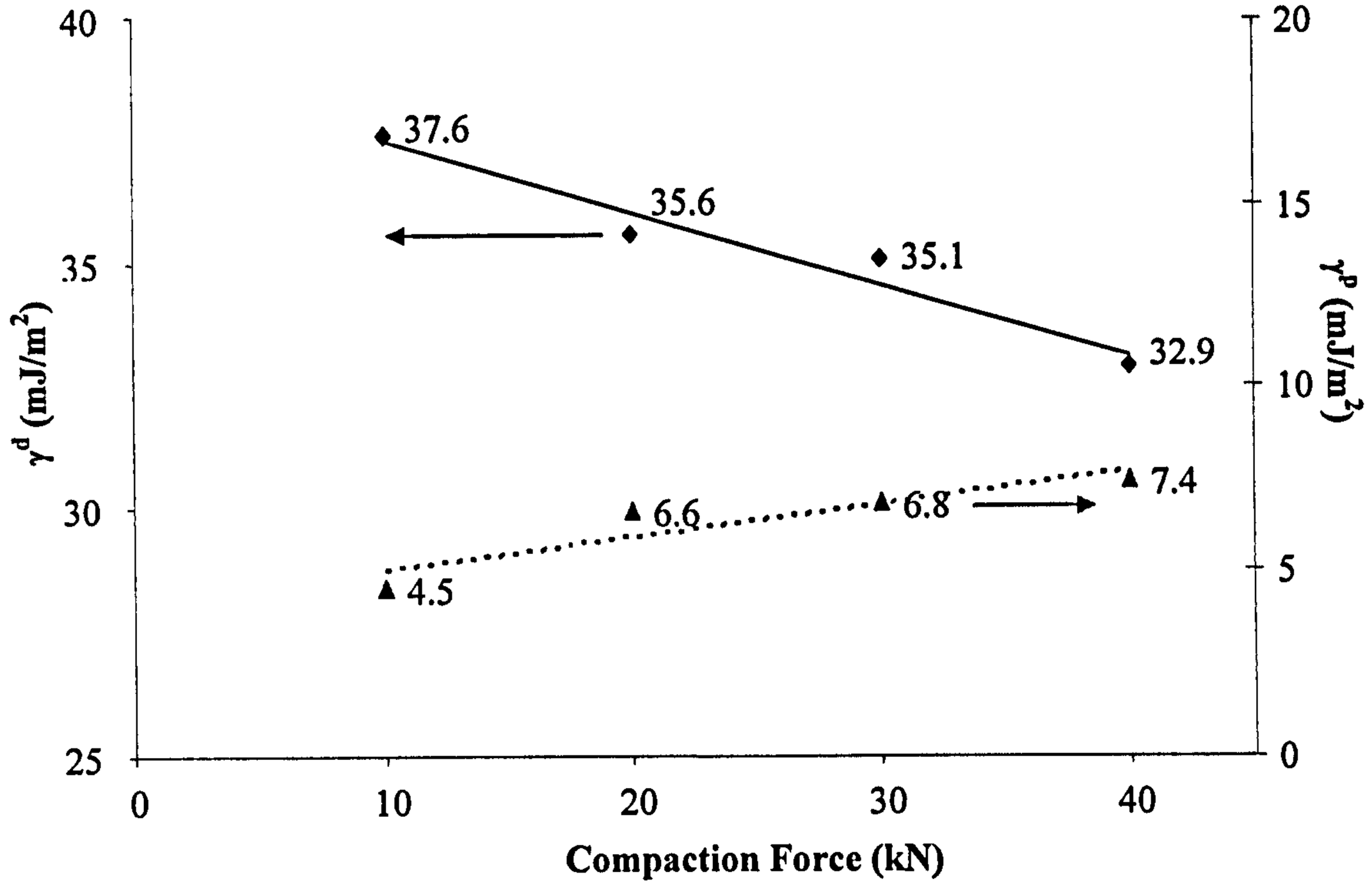
(a) (b)

Table 5.3: θ_a (°) on Ibuprofen Tablets

Compaction Force	Diiodomethane	Water	Ethylene Glycol
10 kN	43.2 ± 1.0	78.0 ± 0.8	41.6 ± 2.5
20 kN	45.1 ± 2.3	73.3 ± 1.0	41.2 ± 2.4
30 kN	45.4 ± 2.2	73.0 ± 1.3	42.6 ± 2.0
40 kN	48.5 ± 4.3	72.7 ± 4.4	46.3 ± 2.6

The surface energies of ibuprofen compacts computed by the classical Owens-Wendt method are shown in Figure 5.16 as a function of compaction pressure. It is rather interesting to note the correlation between surface energies and compaction pressure. The dispersive component indicates a decrease in value with increasing compaction pressure. It is reasonable to expect that at higher compaction pressures, the porosity of the tablet is reduced and will result in reduced penetration of liquid. This may have given higher contact angles as observed for the diiodomethane. If this is the case, and ibuprofen being a hydrophobic material, this must surely reduce the imbibition of water even more, and expected to reveal larger contact angles of water, with increasing compaction pressures. However, a lower contact angle for water was obtained, indicative of a greater polar component and this experimental observation contradicts the suggested interpretation. Without further experimental validification, it will be proposed that this observation may well be reflective of the possible surface chemistry modification due to compression. It is postulated, that the carboxylic end groups of the ibuprofen dimers may have been exposed under higher compaction pressure regimes. This analysis however, necessitates further investigation to fully understand the phenomenon and may well be just a reflection of the degree of gross deformation at the surface.

Figure 5.16: Surface energy of ibuprofen tablets as a function of compaction pressure.



Buckton and Newton [201] assessed the wettability of barbiturate powders prepared using different tablet compression forces and found that the contact angles measured decreased with increasing compression force until a limiting contact angle was achieved. This variation was attributed to plastic deformations at the tablet surface and indicates that the changes in contact angles were related to the extent of mechanical deformation, and thus may not represent a true surface equilibrium state of the material. Muster and Prestidge [221] exploited the time-dependence of sessile drop contact angles on compacts to characterise sulfathiazole crystals. The results obtained were found to be dependent on pre-saturation conditions, humidity, surface roughness, particle size and shape including polymorphic form. Liquid penetration effects were overcome by pre-saturating the compact with the probe liquid, but this can lead to swelling or dissolution effects. The imbibition of liquid on porous surfaces

is also governed by hydrodynamics and internal pore structures which complicates this technique [295].

For both cases of paracetamol and ibuprofen, the SEM imaged compacted surfaces indicate that plastic deformations have occured, being more pronounced at higher compaction pressure. This deformation will render such surfaces unsuitable for characterisation by the sessile drop method. As such, even a measurable contact angle on a tablet surface may not represent the characteristics of the real paracetamol or ibuprofen surface but that of a deformed surface. However, characterisation using this method on tablets continues to be reported, and hence results from such methods should be treated with caution.

5.12.3 Vapour Probe Characterisation - IGC

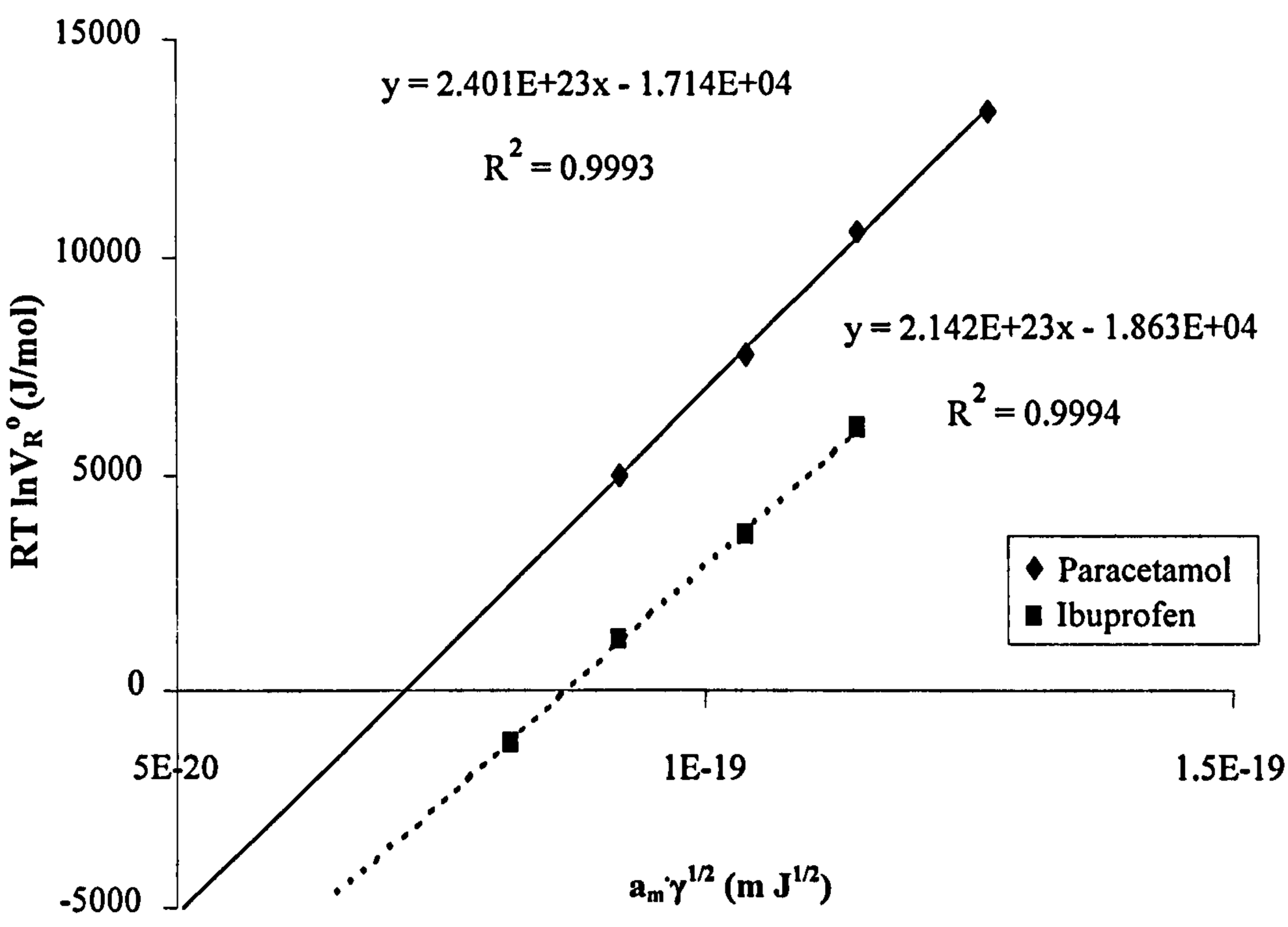
The surface properties of both paracetamol and ibuprofen powder were measured by inverse gas chromatography (IGC) at infinite dilution via pulse injections of the vapour probes. The vapour retention behaviour and the amount of vapour adsorbed within the infinite dilution regions are governed by linear adsorption isotherms. As such, the retention volume is independent of the injection size. The IGC technique is reviewed in detailed in Chapter 8.

The method of Schultz et al. was used to calculate the dispersive surface energy, γ_{SV}^{d} of paracetamol. A plot of RT ln V_R^{o} vs $a_m(\gamma_{LV}^{d})^{1/2}$ is shown in Figure 5.17 with the slope giving γ_{SV}^{d}. The γ_{SV}^{d} of paracetamol and ibuprofen were 39.8 mJ/m^2 and 31.7 mJ/m^2, respectively. It is expected that experiments conducted using the pulse method at infinite dilution should reflect interactions between the low concentrations of vapour probe with highest energy surface sites. This expectation may be true for high surface area materials such as catalysts with very high surface areas (>300 m^2/g). However, vapour probes are believed to interact not only with the

highest energy sites in the particulates studied here. This occurrence is due to the very low surface area (σ = 0.25 m^2/g and 0.14 m^2/g for paracetamol and ibuprofen, respectively), as determined by nitrogen BET adsorption experiments. As such, the surface coverage even at infinite dilution may cover sites in addition to the preferential high energy sites.

It is evident that the γ_{SV}^d values from the IGC technique for paracetamol and ibuprofen are similar to those obtained from the liquid capillary rise technique. In a powdered sample, it is expected that the weakest attachment energy surface is being exposed with greater propensity as the particle size is reduced (see Chapter 8). These γ_{SV}^d values are compared to those obtained from direct contact angle measurements on the weakest attachment energy facets.

Figure 5.17: Free energy of adsorption (RT ln V_N) as a function of dispersive energy of probe vapour, γ_{SV}^d for paracetamol and ibuprofen.



5.12.4 Sessile Drop on Single Crystals

The contact angles of probe liquids on the specific facets of crystalline organic solids and detailed analyses of the wetting behaviour of paracetamol are reported in Chapter 6. In this chapter, the property of the weakest attachment energy facet is reported. Facet (010) is the weakest attachment energy for paracetamol, while facet (100) is the weakest attachment energy facet [192] for ibuprofen crystals. The surface energies by the classical Owens-Wendt method are calculated for the weakest attachment energy facets, and shown in Table 5.4. The detailed θ_a's and γ_{SV} are reported in Chapters 6 and 9, respectively. The γ_{SV}^d was found to be in excellent agreement with those obtained from capillary rise and IGC techniques.

Table 5.4: Surface Energy Analysis Using the Classical Owens-Wendt Approach for Paracetamol and Ibuprofen Single Crystals

Facet	γ_{SV}^d (mJ/m^2)	γ_{SV}^p (mJ/m^2)	γ_{SV} (mJ/m^2)	$\gamma_{SV}^p/\gamma_{SV}$
Paracetamol (010)	39.5	6.9	46.4	0.15
Ibuprofen (100)	36.7	5.1	41.8	0.122

5.13 Discussion

Three fundamentally very different techniques were investigated; the sessile drop contact angle technique, the capillary rise and a vapour sorption technique. While it may not be necessary to list all the theoretical and experimental difficulties of these techniques again, several conclusions will be drawn.

The sessile drop technique has long been acknowledged as ***the*** most surface sensitive technique. With the inability to measure contact angles of droplets on

individual particles, compaction of powders to a tablet form was thought to provide an alternative substrate for measurement. Such tablets are typically prepared under high pressure but were found to have deformed surfaces, which were rough and porous, especially for those compacted under very high pressures. These rough and porous surfaces caused liquid drops to penetrate into tablets within seconds of contact as in the case of paracetamol compacts. No equilibrium contact angles were obtained for tablets compacted between 10 - 40 kN. For ibuprofen compacts, the contact angles were found to be dependant on the compaction pressure. The effects of a reduced porosity did not concur with experimental results. It is thought that this was due to molecular reorientation, but this supposition cannot be confirmed. However, if one conclusion were to be drawn here, it will be that powder compacts are not suitable for the evaluation of surface energy of complex organic solids.

For the commercial paracetamol and ibuprofen powders, γ_{SV}^{d} by both the capillary rise and inverse gas chromatography techniques were found to be in good agreement with values obtained for direct θ_a measurements on the weakest attachment energy facet. The similarity, with available data (Chapter 6) on the variations in contact angles for a range of crystalline facets, is that the γ_{SV}^{d} measured on powders were probably reflective of the weakest attachment energy facet. This conclusion is reasonable as commercial powders typically undergo a step involving particle size reduction, and hence resulting in the exposure of the weakest attachment energy facet. The dependence of γ_{SV}^{d} on particle size is reported in Chapter 8.

5.14 Conclusions

The measurements of crystalline powders yield one surface energy value, possibly a bulk or an average property of the value of a dominant facet.

It is thought that the values obtained on powders are reflective of the weakest attachment energy facet as obtained by sessile drop contact angle measurements on single crystals (Chapter 6).

In view of the complications of powder bed characterisation techniques, this thesis will advocate the characterisation on specific facets of crystalline pharmaceutical crystals. However, one may argue that it may not be always viable to grow macroscopic crystals. In this very likely event, a choice of techniques has to be made for characterisation of powdered samples and a vapour sorption technique such as the IGC is recommended (Chapter 8). The interactions between a gaseous probe and a solid surface are better understood and the experimental techniques are certainly more robust. The IGC technique has been reported to be able to differentiate production, processing and environmental conditions on powders.

CHAPTER 6 CONTACT ANGLES AND SURFACE ENERGETICS OF MACROSCOPIC CRYSTALLINE PHARMACEUTICAL SOLIDS

6.1 Overview

The first detailed systematic experimental investigation of the anisotropic surface chemistry of crystalline pharmaceutical solids is reported in this chapter. The systems investigated and reported in this chapter were the two polymorphic forms of paracetamol; thermodynamically stable monoclinic form and the metastable orthorhombic form, aspirin, racemic ibuprofen and S-(+)-ibuprofen single crystals. This study aims to directly measure contact angles and determine the surface properties for different facets on a single macroscopic crystal in order to obtain a comprehensive description of its surface thermodynamic properties.

6.2 Introduction

The surface energy governs a range of important solid-liquid or solid-vapour interactions of materials [296]. The wetting properties of solid state materials are of both fundamental and practical importance in the performance of particulate materials such as pharmaceutical and fine chemicals. In the case of pharmaceuticals, these include their dissolution behaviour, mixing performance, powder performance including the possibility of controlling crystal habit by varying crystallisation solvents or compositions [297].

The final delivery of the majority of drugs is as solid state dosage forms such as tablets and capsules [298], and a detailed knowledge of particulate surface properties is thus invaluable. This information will help to predict processing stability, surfactant adsorption, adhesion, solubility, colloid stability, powder flow, mixing performances and product performance including the rate of drug release [197, 199, 220, 290, 291]. However, until a complete understanding of wetting phenomena is possible, the ability to tailor these properties for optimised formulation and manufacture will remain an elusive goal.

Traditional methods of characterising the wettability of particulate solid pharmaceuticals have relied on powder bed techniques. Whilst these approaches might be valid for low energy flat surfaces such as polymers, their applicability is more problematic for complex crystalline organic materials, such as pharmaceutical solids. An evaluation of the suitability of the capillary rise and sessile drop on powder compacts is reported in Chapter 5.

Duncan-Hewitt and Nisman [220] have examined the wettability of paracetamol and adipic acid powders using a range of experimental techniques including the Washburn capillary rise method and sedimentation volume methods, as well as sessile drop determinations on compacts, films and single crystals. It was concluded that current powder characterisation techniques have limitations. The major problems are the sample preparation, data interpretation and imprecision of the experimental methodology. They suggested that the contact angle measurement for powders for surface energy evaluations should be abandoned in favour of measurements on films or single crystals. However, these potentially important conclusions were not supported by detailed data on either films or single crystals, with only one contact angle data being reported for the single crystal samples. Moreover,

only limited information on the sample's surface chemistry were presented as the surface energy calculations were based on the equation of state analysis [220]. However, despite these conclusions, powder bed techniques are still used extensively by many researchers for characterising the wettability of pharmaceutical powders.

The availability of an accurate and a reliable contact angle measurement technique would facilitate a more complete understanding of pharmaceutical powder surface properties. Such a technique could be applied to real industrial problems in powder wetting such as wet powder granulation [290]. Surface energy information would assist in predicting the likelihood of binder spreading and hence lead to the successful prediction of wet granulation or explain manufacturing related problems such as dissolution, surfactant adsorption, drying, coating or compaction.

The basis of the current work, whereby the sessile drop technique is used to characterise crystals of large facet sizes and normal sessile drops of a few mm in diameter, is reported in this chapter.

6.2.1 Anisotropic Wettability

Very little work has been reported on the anisotropic surface energetics and wettability of crystalline solids based on contact angle data. Contact angles on single crystals of inorganic minerals [299-303] have been measured with interesting observations. Anisotropic wetting behaviour has been observed for the wetting of liquid pure metals on diamond [301] and MgO single crystals [304] by Nogi and co-workers. In the first case the wettability of (100), (110) and (111) facets of diamond were characterised using sessile drops of Sn, Bi, Ag and Pb between 773 K and 1773 K. Small differences in θ were observed which were indicative of anisotropic surface properties. In the case of MgO crystals, larger anisotropic variations in θ of up to 40°

were reported for liquid Sn, Pb and Bi. However, the authors were unable to establish any clear relationship between crystal structure and anisotropic wettability.

Muster and Prestidge have investigated the wettability of a N,n-octyl-D-gluconamide and sulfathiazole crystals [305]. They reported face specific contact angles for water for both systems, as well as a correlation between surface hydrophobicity and the presence of alkyl surface groups as detected using TOF SIMS. The same group has also reported that morphine sulfate crystals exhibit facet dependant contact angles [209]. However, no other θ's were reported.

6.3 Experimental Section

The growth of macroscopic crystals was described in Chapter 4. Contact angle liquids are given in Table 6.1 and measurement methods are reported in Chapter 5.

Table 6.1: Properties of Liquid Probes Used

Liquids	Purity (%)	Density (kg/m^3)	γ_{LV} (mJ/m^2)	γ^{LW}	γ^{AB}	γ^+	γ^-
Diiodomethane	>99	3325	50.8	50.8	0.0	0.0	0.0
Water	Deionised	998	72.8	21.8	51.0	25.5	25.5
Ethylene Glycol	>99	1109	48.0	29.0	19.0	1.92	47.0
Formamide	>99.5	1139	58.0	39.0	19.0	2.30	39.60

γ^{LW} is taken to be similar to Fowkes' γ^d as Keesom and Debye interaction terms in condensed phases are assumed to be negligible. γ^+ and γ^- values are those proposed by C. J. van Oss (Colloids and Surfaces A **1993,** 78, 1-49).

6.4 Results and Discussion

6.4.1 Paracetamol Form I

Paracetamol, also known as *p*-hydroxyacetanilide or acetaminophen, was discovered by accident about 100 years ago when chemists tried to modify the toxic form of acetanilide while retaining its analgesic properties. Today, paracetamol is widely accepted as an antipyretic and analgesic, as well as being used as an intermediate in the manufacture of azodyes and photographic chemicals, and therefore its physicochemical properties are of considerable practical interest. In this study, paracetamol is taken as a model drug to study the wettability behaviour of a complex organic crystalline solid.

Three polymorphs of paracetamol have been reported in the literature [306]; a thermodynamically stable monoclinic (form I), a metastable orthorhombic (form II) and a very unstable form III. This third form has only been observed during fusion experiments and is reported to be so unstable that isolation of the crystals is impossible, thus no physicochemical characterisation data has been reported. The monoclinic form I is the commercially used form due to its thermodynamic stability at room temperature and is the subject of this current work.

Paracetamol is a complex organic compound, with functional end groups of hydroxyl, carbonyl, amine as well as a benzene ring. The basic molecular structure is shown in Figure 4.1. With the aid of crystallographic graphical imaging software (Mercury, CCDC, Cambridge, UK), crystallographic structure diagrams have been generated for the monoclinic (I) and orthorhombic (II) forms. Form I has pleated sheets stacked along the *b*-axis, creating a relatively rigid structure. Since the molecular structure of form I lacks a crystallographic slip plane, it displays poor powder compaction behaviour. However, form II has parallel hydrogen-bonded sheets

along the *c*-axis, resulting in slip planes which can accommodate mechanical deformations during compaction. Consequently, chemical additives need be added to form I powders prior to tabletting in order to facilitate the compaction process. Such an additional process is both timely and costly [190]. The possibility for direct compression of paracetamol form I into tablets has been investigated [164] but remains industrially unfeasible.

The hydroxyl, carbonyl and amine functional groups found within paracetamol molecules are capable of forming intermolecular hydrogen bonds. This leads to a crystal structure in which the paracetamol molecules align themselves into hydrogen bonded chains of molecules packed in a criss-cross configuration. The crystallographic structure of a typical external face, facet (001) of the macroscopic crystal and a cleaved internal facet (010) are shown in Figure 4.9.

6.4.1.1 Form I Identification

The detection of potentially oxidised paracetamol was achieved using DSC and FTIR. DSC measurements were performed using a Pyris 1 (Perkin-Elmer Cooperation, Boston, USA) differential scanning calorimeter. Sample masses of not more than 10 mg were sealed in aluminium pans with an empty pan used as the reference. DSC curves were obtained under nitrogen purge of 20 ml/min at a heating rate of 10 °C/min from 30 – 200 °C to determine the crystal melting endotherm. Curves were analysed by the Perkin Elmer Thermal Analysis software.

FTIR spectra were obtained using an Equinox 55 (Bruker Optics, England) spectrometer with a liquid nitrogen cooled mercury cadmium telluride (MCT) detector and a KBr beam splitter. The background measurements for all spectra were collected for a clean dry ATR crystal with air at the measured interface. A total of 32 individual scans were signal-averaged using an optical resolution of 4 cm^{-1}. The

sample crystal was ensured to be in good contact with the spectroscopic ATR diamond crystal so as to obtain strong absorbance. The incident angle was 45 ° and spectral range from 4000 – 600 cm^{-1} was recorded.

DSC curves reveal a melting point onset of 170 °C and an enthalpy of fusion of 188 J/g. ATR-FTIR spectrums obtained for both commercial paracetamol and recrystallised samples were similar. These results are comparable and in agreement with DSC [159] and FTIR [307] published data for the stable monoclinic form I of paracetamol. No evidence of sample oxidation could be detected by the thermal and spectroscopic experiments.

6.4.1.2 Contact Angles for Monoclinic Paracetamol

θ_a data for the paracetamol crystal facets are summarised in Table 6.2, while the θ_a and θ_r data for diiodomethane is reported in Table 6.3.

Table 6.2: θ_a (°) Results for Paracetamol Crystals

Facet	Diiodomethane	Water	Ethylene Glycol	Formamide	Saturated Paracetamol Water Solution[a]
External Facets of Form I Paracetamol Crystals					
(201)	48.8 ± 2.2	38.1 ± 4.6	-	13.3 ± 1.2	37.3 ± 3.7
(001)	49.8 ± 3.2	15.9 ± 3.1	-	-	18.4 ± 4.3
(011)	50.7 ± 2.9	29.8 ± 5.7	10.9 ± 2.5	14.5 ± 2.5	31.0 ± 3.7
(110)	50.2 ± 2.4	50.8 ± 4.9	15.7 ± 2.2	17.6 ± 3.0	49.6 ± 5.8
Internal Facet of Form I Paracetamol Crystals					
(010)	27.8 ± 2.5	67.7 ± 2.5	42.5 ± 3.2	46.9 ± 2.4	72.7 ± 6.4

[a] Contact angles of water saturated with paracetamol at 20 °C.

Table 6.3: θ_a and θ_r Data for Diiodomethane on Paracetamol Crystals

Facet	θ_a	θ_r	$\Delta\theta$
(201)	48.8 ± 2.2	26.9 ± 5.7	22
(001)	49.8 ± 3.2	26.4 ± 5.3	23
(011)	50.7 ± 2.9	30.4 ± 4.3	20
(110)	50.2 ± 2.4	23.8 ± 3.0	26
(010)	27.8 ± 2.5	13.4 ± 2.0	14

There are several well established phenomena which can contribute to contact angle hysteresis. They are surface roughness, surface dissolution, chemical heterogeneity, material swelling, surface restructuring as well as other non-equilibrium effects [308]. It is however the first two phenomena which are the most commonly encountered for crystalline solids. In this work specific experiments were performed to establish the significance of surface roughness, crystal dissolution, non-equilibrium effects and local surface chemistry to the contact angle data obtained.

To establish the importance of surface roughness, crystal facets were splutter coated with 100 nm thick films of gold, and θ_a were measured for water and di-iodomethane on both coated and uncoated facets (Table 6.4). This thin gold coating will mask any effects of facet surface chemistry, whilst retaining the gross surface topographical features which might contribute to surface roughness. All coated facets exhibited the same θ_a for both liquids, within an experimental error of typically 4°. This contrasts with the θ_a variations reported for the uncoated facets which were greater than 50 ° for water droplets. This data clearly confirms that the surface roughness has a negligible role on the θ_a differences reported in this study.

Table 6.4: θ_a and R_a Data for Native and Gold Coated Single Crystal Facets of Paracetamol Crystals

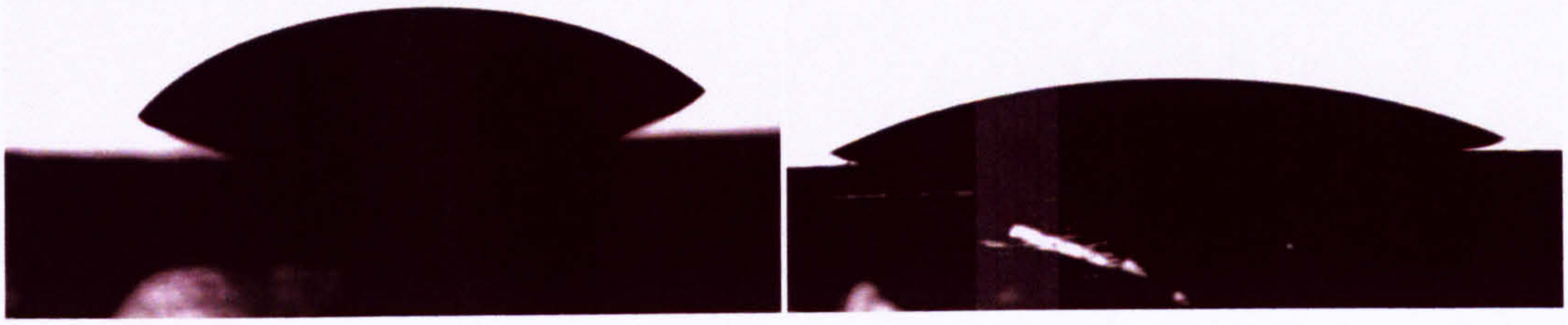
	θ_a for Water (°)		θ_a for Diiodomethane (°)		R_a(μm)
Facet	Single Crystals	Gold Coated Crystals	Single Crystals	Gold Coated Crystals	Single Crystals
(201)	38.1 ± 4.6	78.7 ± 4.1	48.8 ± 2.2	40.8 ± 2.5	0.16
(001)	15.9 ± 3.1	68.6 ± 5.8	49.8 ± 3.2	34.7 ± 2.5	0.19
(011)	29.8 ± 5.7	72.8 ± 3.2	50.7 ± 2.9	38.7 ± 3.7	0.32
(110)	50.8 ± 4.9	69.8 ± 4.2	50.2 ± 2.4	39.0 ± 4.4	0.29
(010)	67.7 ± 2.5	73.1 ± 3.6	27.8 ± 2.5	38.0 ± 2.5	0.20

In addition, the surface roughness of crystal facets was determined using non-contact optical laser surface profilometry. The purpose built instrument utilizes a Rodenstock RM 300 non-contact laser system with a height resolution of 5 nm, incorporated into a xyz motion control system with a position resolution of 100 nm. Surface topography maps based on a scan area of typically 100 μm x 100 μm were reported for all facets with a 256 x 256 raster scan. The measured R_a's for all sample facets were very similar at about 0.2 μm, close to accepted estimates of 0.1 μm whereupon roughness is known to have a negligible impact on θ_a measurements [309].

To establish the significance of crystal dissolution, θ_a was measured for both water and paracetamol saturated water solutions. Although paracetamol has low solubility with water (solubility at 20 °C, $C_S = 12.78 \pm 0.05$ g/kg H_2O) [310], the potential effects of the presence of dissolved paracetamol on the measured contact angles were unknown and could be significant. Specifically, it is known that impurities present in the contact angle fluids can affect the results by either adsorbing at the solid-liquid interface and/or the liquid-vapour surface. However, measured values of θ_a were also found, within experimental error, to be same for both water and

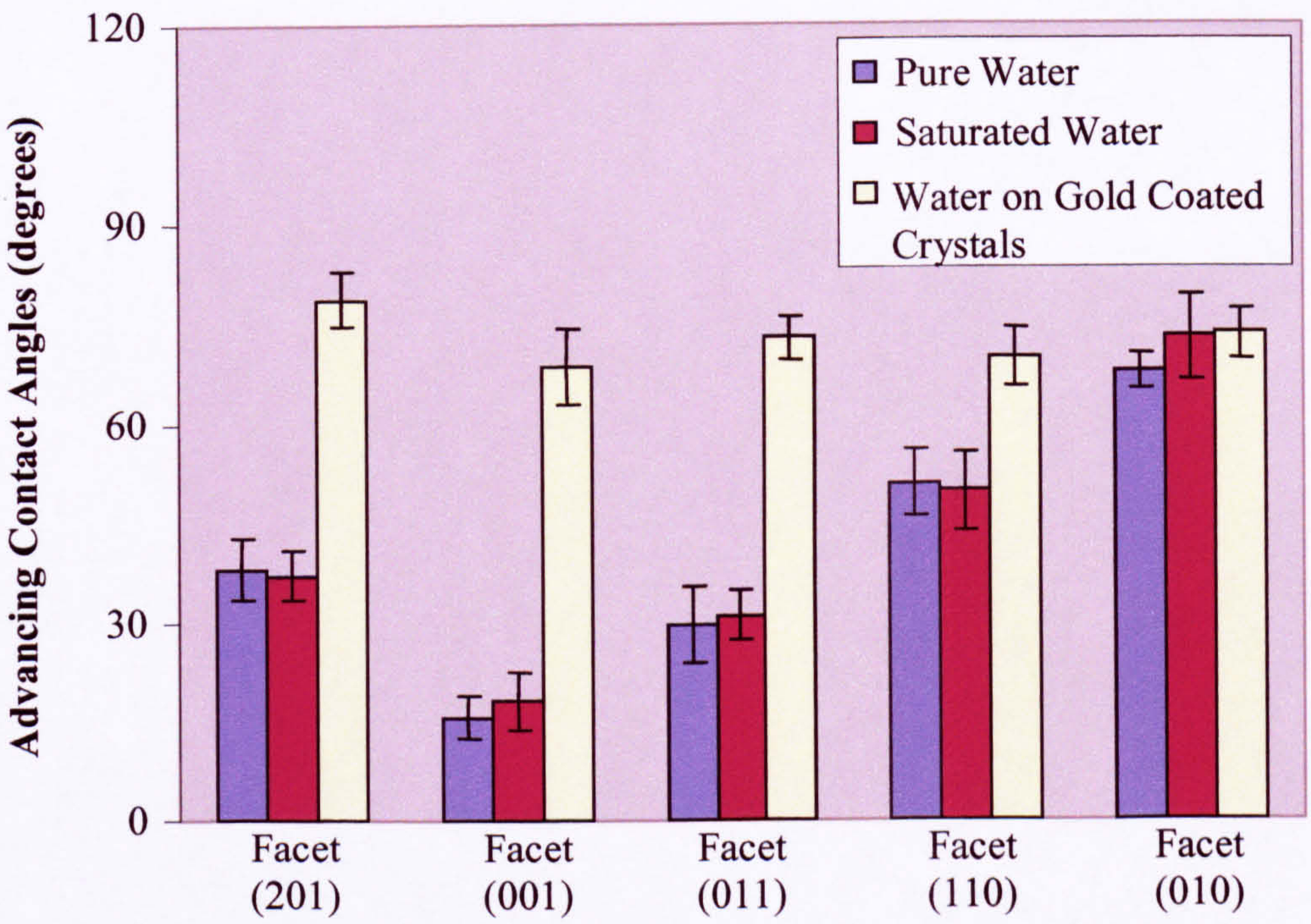
paracetamol saturated solutions (Table 6.2). It was thus concluded that any dissolution of paracetamol that might occur during the measurements with water, was inconsequential with respect to measured θ_a's (Figure 6.1 and Figure 6.2).

Figure 6.1: Droplet profile of water saturated with paracetamol at 20 °C on (a) facet (010) and (b) facet (011).



(a) (b)

Figure 6.2: θ_a of water and water saturated with paracetamol on specific facets of form I paracetamol crystal, and of water on gold coated surfaces.



Different workers have reported on a range of non-equilibrium effects which can influence contact angle determinations. In this study, swelling of the solids was assumed to be unlikely. Furthermore, no time dependant contact angle phenomena were observed. It is therefore concluded that time dependant non-equilibrium effects did not make a significant contribution to the measured contact angles. It can therefore be safely inferred that the variations in contact angles reported in this study must be a consequence of surface chemical heterogeneities present on the specific crystal facets.

The solid-liquid interactions between diidomethane, a purely dispersive van der Waals liquid, and the surfaces examined will consist of purely dispersive non-specific van der Waals interactions. However, water (H_2O), ethylene glycol (HO CH_2CH_2OH) and formamide ($HCONH_2$) liquid probe molecules are postulated to interact with the solid surfaces via both the non-specific and specific intermolecular interactions. It is hypothesised that the interfacial interaction of these liquid probes will vary depending on the nature of each surface characterised, and more specifically their local surface chemistry, orientation of molecules and density of end-groups exposed at the surface. This difference is postulated to transcribe to a difference in contact angle measurements of the same probe liquid on different facets.

From θ_a results shown in Table 6.2, a number of clear and significant trends can be observed. Firstly, θ_a for diiodomethane on the four major external facets of the macroscopic crystal were very similar; all between 49 – 51 °. These results indicated similar long-range dispersive interactions for these four facets, and thus similar γ^d values. Secondly, θ_a of polar probes (water, ethylene glycol and formamide) vary significantly for the different external facets, with θ_a data for water exhibiting the largest variation; from 16 – 51 °. Ethylene glycol did not exhibit finite contact angles

on the facets (201) and (001), while formamide drops wetted on the (001) facet only. On all other facets, ethylene glycol and formamide gave low, but finite, contact angles. The wetting behaviour of both ethylene glycol and formamide on facet (001) would indicate that this surface interacts strongly with the polar probes while facet (201) interacts slightly less strongly as only ethylene glycol wets this surface. No other significant differences were observed in the measurable contact angles of both ethylene glycol and formamide.

θ_a for diiodomethane on internal facet (010) is 27.8 ± 2.5 °, about half the observed θ_a for any of the external facets. This result is indicative of stronger van der Waals dispersive interactions on the cleaved facet and thus a higher value of γ_{sv}^d. On the other hand, θ_a of all polar probe liquids on facet (010) were much higher than those observed for the external facets signifying less significant specific interactions for this facet and thus greater hydrophobicity. θ_a of water was found to be 67.7 ± 2.5 °. It is known that facet (010) is the preferred cleavage plane due to its low attachment energy [178, 179] and this is fully consistent with the hydrophobic surface we have observed here.

Based on the water contact angle results (Table 6.2), an order of hydrophilicity for paracetamol form I facets can be proposed, which is:

$$(001) > (011) > (201) > (110) > (010)$$

From the contact angle data for diiodomethane (Table 6.2), the van der Waals type of interactions for the paracetamol facets can be ranked as:

$$(010) > (001) = (011) = (201) = (110)$$

The effects of milling on single paracetamol crystals will lead to fracture, exposing predominantly the facet (010). As particle size reduces, the prevalence of

this facet is expected to increase, resulting in an increasing hydrophobic nature of the milled paracetamol powders. Such surface chemical behaviour may have a significant bearing on the performance of the subsequent wet powder granulation of milled powders which is common practice in industry and is reported in Chapter 8 [311].

6.4.2 Paracetamol Form II

In this section, the experimental evaluation of the influence of crystal packing and the resulting surface chemistry on the wettability of crystalline solids is reported. This is achieved by comparison of the wetting behaviour between form I (monoclinic) and form II (orthorhombic) paracetamol crystals. This work reports the first systematic investigation of an anisotropic wetting behaviour influenced by local surface chemistry of two polymorphic forms of organic paracetamol.

6.4.2.1 Paracetamol Polymorphs

Etching patterns are governed by the crystal network and interactions between solvent and solid surface. It has been observed that etching patterns were dependent on the solubilizing ability of the solvents, which is affected by both the solvent and surface properties [277]. Recently, Mikhailenko et al. observed different initial dissolution etching patterns on specific facets of both paracetamol monoclinic and orthorhombic forms [312]. Such unlike features were attributed to the dissimilar crystalline structure and also the surface chemistry of the crystalline facets.

6.4.2.2 Crystal Habits

Monoclinic paracetamol crystallised from saturated methanol solution resulted in prismatic shaped crystals, while the orthorhombic crystals were rod like with hexagonal cross sections (Figure 4.8). Form II crystals possess facets (001), (010) and

(110), with facet (001) being the preferential slip plane. This study aims to understand these surface chemistry differences.

6.4.2.3 Contact Angles for Orthorhombic Paracetamol

As shown in Table 6.5, the contact angles of water varied across all facets for both form I and form II paracetamol crystals. This data is again indicative of an anisotropic wetting behaviour for organic solids. Measured θ_a were as low as 15.9 ° to as high as 67.7° on facet (001) and (010) of form I respectively. A very different behaviour was observed for wetting on the metastable form II. The chemical groups on each crystal facet vary as facets slice through the crystal at different planes and angles, resulting in an exposure of dissimilar chemical groups. It is postulated that the anisotropic wetting phenomenon is governed by the local surface chemistry; the different availabilities and proportions of functional groups at the specific facet including the packing of molecules within the crystal lattice. Differences in etching patterns on both form I and II paracetamol crystals for the same etching agents were reported recently, and are consistent with observed variations in surface properties [312].

Table 6.5: θ_a (°) Results for Form I and II Paracetamol Crystals

Facets	θ_a for Diiodomethane (°)		θ_a for Water (°)	
	Form I	Form II	Form I	Form II
(201)	48.8 ± 2.2	-	38.1 ± 4.6	-
(001)	49.8 ± 3.2	34.5 ± 1.2	15.9 ± 3.1	64.5 ± 3.5
(011)	50.7 ± 2.9	-	29.8 ± 5.7	-
(110)	50.2 ± 2.4	51.6 ± 3.2	50.8 ± 4.9	16.6 ± 1.4
(010)	27.8 ± 2.5	53.6 ± 2.3	67.7 ± 2.5	17.9 ± 2.5

In the monoclinic form, the -OH accepts hydrogen bonds from the -NH and donates to the C=O, of an adjacent molecule and thus forms a corrugated sheet along the ac plane (Figure 4.9). These sheets are held together by weak intermolecular van der Waals forces. On facet (010), the hydroxyl group of the paracetamol molecule appears to be sterically hindered. Furthermore, the carbonyl and amine functionality of the adjacent molecule form hydrogen bonds with the hydroxyl group, by behaving as donors and acceptors respectively. This results in almost negligible hydrogen bonding potential on facet (010) and as such give rise to the hydrophobic nature of this surface and thus a high θ_a for water. In contrast, on facet (001), hydroxyl functional groups are exposed resulting in the low observed θ_a with water. Detailed surface spectroscopic analysis of each individual facet of paracetamol and quantitative determination of functional groups by X-ray photoelectron spectroscopy are reported in Chapter 7 [289].

The same hydrogen bonding pairing exists within the orthorhombic form, but is formed between –OH with C=O and –NH of two different adjacent molecules. This results in 2-D sheets parallel to the ab plane (Figure 4.10). For the facet (001), the paracetamol molecule lies parallel to the ab plane, with the –OH, -NH and C=O functional groups being exposed. However, the formation of hydrogen bonds amongst these groups with neighbouring molecules leaves almost negligible hydrogen bonding potential with foreign molecules. This presumption agrees very well with contact angle observations, which reveal that (001) for form II is the most hydrophobic facet, although the polar functionalities were present. On both facets (010) and (110), the functional groups C=O, –NH and –OH are also present. On facet (010), the C=O does not form hydrogen bonds within the crystalline structure and as such is free to interact with foreign molecules while–NH forms hydrogen bonds with –OH. This

conformation, and with the orientation of the molecule to face inwards at the surface, leaves the –NH group with negligible hydrogen bonding potential for interaction with foreign molecules. The –OH group may still form hydrogen bonds which give rise to the hydrophilicity of facet (010). Only slight differences in wetting behaviour were seen for facet (110) as compared to facet (010). This trend may be due to the similar configuration of functional groups and hydrogen bonding potential. One may conclude that the small difference may be due to the orientation of the C=O groups and also their densities at the surface. The crystallographic structure for facets (001) and (110) for form II paracetamol is shown in Figure 4.10.

Although within the bulk of each crystalline form, the solid is composed of the same molecule, the availabilities and proportion of functional groups at the surface appears to be very dissimilar. This data is again indicative that this anisotropic wetting behaviour, is very dependent on the localised surface chemistry.

From the measurement of θ_a of water in this study, a hydrophilicity ranking of a surface can be determined. The hydrophilicity order for form II is:

$$(010) \approx (110) > (001)$$

It has to be noted that facet (001) of form I paracetamol appears to be the most hydrophilic face while the same Miller indexed face for form II appears to be the most hydrophobic. On the other hand, facet (010) appears as the most hydrophobic facet of form I but have opposite properties for form II, again another rather contrasting feature for both polymorphic forms. In the case of form I, the weakest attachment energy plane is the (010) facet [178], while (001) for form II is known to be the preferential slip plane [157]. Interestingly, for both forms, the most hydrophobic surface was also the weakest attachment energy plane.

6.4.3 Aspirin Single Crystals

Aspirin (acetyl salicyclic acid or 2-(acetyloxy)-benzoic acid) is a common and widely used analgesic, first synthesized in 1897 by F. Hoffmann at Bayer. The crystal structure of aspirin was initially solved by Wheatley and later refined by Kim and co-workers [313].

The crystal structure of aspirin is based on centrosymmetric carboxylic acid dimers, where two molecules of aspirin are held together by two hydrogen bonds. The hydrogen bonds are formed between carboxylic acid functionalities of two molecules forming dimers. Ab initio studies of aspirin molecules have been reported and describe the intermolecular and intramolecular interactions [314-316]. Claims of the existence of aspirin polymorphs have been originally based on the differences in solubility rates for different crystal facets [317], for aspirin crystals prepared from ethanol and hexane solutions. Such claims of polymorphism remains unproven as no supporting X-ray diffraction data are available. The observed differences in solubility could well be a manifestation of the different habits being studied [18]. It has been widely reported that recrystallisation from polar and apolar solvents may result in different crystal habits [192]. The dissolution rates as measured by Atomic Force Microscopy of facet (100) in presence of 0.05 M HCl was found to be 6 times greater than that of facet (001) [274].

Differences in etching patterns reported [318] coupled with face dependant dissolution rates of aspirin single crystal facets suggest that the surface chemistry on specific facets may be of major importance.

6.4.3.1 Contact Angles for Aspirin

Experimentally measured θ_a of probe liquids diiodomethane, water, ethylene glycol and formamide on aspirin facets are summarised in Table 6.6. θ_a for diidomethane was found to be fairly constant (< 20% differences) over all three major facets examined. θ_a of polar liquids on aspirin varied significantly (> 50% difference between highest and lowest contact angles) from facet to facet. Such behaviour is indicative of anisotropic specific interactions.

Table 6.6: θ_a (°) Results for Aspirin Crystals

Facet	Diiodomethane	Water	Ethylene Glycol	Formamide
(001)	47.6 ± 4.3	60.7 ± 3.5	51.2 ± 5.4	48.7 ± 2.8
(100)	48.0 ± 2.5	52.9 ± 2.5	48.9 ± 2.9	40.2 ± 6.3
(011)	41.1 ± 4.6	42.9 ± 4.8	31.0 ± 3.2	17.5 ± 2.1

Figure 6.3: Aspirin saturated water droplets on (a) facet (001), (b) facet (100) and (c) facet (011).

(a) (b)

(c)

The differences in contact angles on various facets of aspirin single crystals may be argued to arise from dissolution of the material into the probe liquid. It has been reported that aspirin is poorly soluble in water with solubility of < 5 g/L of water at 20 °C [319], and as such any dissolution effects on the surface tension of probe liquid may be negligible. Furthermore, contact angles reported here are the dynamic advancing contact angles whereby liquid is continuously added and allowed to wet new surfaces which have not been dissolved. However, in order to eliminate doubts completely, contact angles of water saturated with aspirin were measured. The same hydrophilicity order (011) > (100) > (001) on various facets of aspirin crystals was also found in this case (Figure 6.3).

Water contact angles were found to be higher on facet (001) than on facet (100), indicating that facet (001) is more hydrophobic than facet (100). This observation is consistent with reported dynamic chemical force microscopy experiments where AFM probes were coated with –COOH and $–CH_3$ terminated self assembled monolayers. The –COOH coated probes gave higher interactions with the (100) facet [135], reflective of the differences in the hydrophilic nature of the facets. The crystal structure of aspirin for both facets (001) and (100) along the b-axis is shown in Figure 4.11.

Facet (100) can be formed via two separate processes: one plane passes through the hydrogen bonds between the carboxylic functionalities of the dimers while another does not. The former will reveal a surface with carboxylic end groups while the latter exposes the carbonyl functionality of the ester. A molecular orbital study of the intermolecular interaction energies reveals that the first configuration is more than 30 times more energetic than the other [191]. Thus, it is expected that facet (100) will be formed by the less energetic plane as crystal growth would tend to

minimise its total surface free energy per unit volume [320]. This viewpoint is supported by the high contact angles obtained with water as probe liquid, signifying less strong interaction between the surface and its surroundings.

The surface chemistry of facet (001) differs slightly from that of facet (100). Facet (001) exposes both the carbonyl functionality and the ester, $H_3C\underline{O}(C=O)$-. The oxygen of the $H_3C\underline{O}(C=O)$- ester group is thought to form an intramolecular bond with the carboxylic acid group. Hydrogen bonds are formed between the carboxylic functionality within the crystalline structure in the form of dimers. As such, there is no contribution of hydrogen bonding at the surface with external moities.

On facet (100), assuming that the facet is formed by the less energetic plane, only the carbonyl functionality is available for hydrogen bonding with foreign molecules. The carbonyl group is electron rich and will accept hydrogen bonds and may result in facet (100) being a slight Lewis basic surface. The aspirin molecules are arranged in a repeated structure along the b and c axis.

Both facets (001) and (100) expose hydrophobic methyl and ester functionalities, albeit at different orientations, and with the dimers normal to facet (100) but parallel to facet (001). The carboxylic functionalities are fully bonded leaving no residual hydrogen bonding potential. The orientation of the molecules however, results in differences in the unit area of the facets as the unit cell dimensions along the a-axis are almost double the unit length of the b-axis. Ester functionality ($H_3C\underline{O}(C=O)$- and $H_3CO(C=\underline{O})$-) at facet (001) and carbonyl ($H_3CO(C=\underline{O})$-) at facet (100) can potentially form hydrogen bonds with foreign molecules, with different degrees of interactions. It must be noted that the hydrogen bonding between donors and oxygen acceptor atoms of carbonyl, ether and ester may also vary [321].

θ_a of water on facet (100) was found to be 52.9 °, significantly lower than facet (001) θ_a of 60.7 °. These noticeable differences in contact angles may be attributed to the molecular orientation, densities of chemical groups present at the surface. These factors may have resulted in the slight difference in polarity of facet (001) as compared to facet (100), although both facets may possess similar end groups. Quantification of the availability and proportion of surface functionalities is carried out by X-ray photoelectron spectroscopy and is discussed in Chapter 7.

θ_a of water on facet (011) was approximately 20 ° lower than θ_a on facet (001). On this facet, the carboxylic acid functionalities may not be fully engaged in internal hydrogen bonding, and as such the presence of these non-dimerised molecules will possess the potential to form hydrogen bonding at the surface. This results in facet (011) being relatively more hydrophilic. The crystallographic structure for facet (011) is shown in Figure 4.11, and the presence of hydrogen bonding potential from its carboxylic functionality is evident. θ_a of both ethylene glycol and formamide probe liquids were also found to give the lowest θ_a on facet (011), consistent with the results observed for water. The contact angles of all polar probe liquids were lowest on facet (011), followed by facets (100) and (001) respectively, reflective of the specific interaction strengths for each facet.

From the measurement of θ_a of water on aspirin crystals, a hydrophilicity ranking of a surface is determined as:

$$(011) > (100) > (001)$$

Static contact angle values of water have been reported for facets (001) and (100) with the θ greater on the (001) facet [322, 323]. These results are consistent with data obtained from this work. These workers explained the anisotropic wettability of aspirin based on the electrophilicity of different crystalline planes, with

the (100) face appearing to have a more electrophilic moieties. The authors successfully related computed electrophilicity to wettability. The growth of macroscopic aspirin crystals from aspirin saturated acetone solution however has enabled facet (011) to be characterised for the first time.

6.4.4 Ibuprofen Crystals

The molecule structure of ibuprofen [2-(4-isobutylphenyl) propionic acid] possesses an asymmetric carbon which gives rise to its chirality. A sample is considered as an enantiomer when the chirality of the molecules is the same throughout, while an equimolar mix of both enantiomeric forms results in a racemic species. The racemic ibuprofen has quite different thermodynamic properties compared to the S-(+)-ibuprofen. Perlovich et al. [324] reported that heats of sublimation of the racemic form and S forms of ibuprofen were 116 kJ/mol and 107 kJ/mol, respectively. This difference is indicative that the former is thermodynamically more stable.

Recrystallisation of ibuprofen from solution has resulted in various crystal habits being created, with higher aspect ratio crystals formed from non-polar solvents. X-ray diffraction studies have revealed similar patterns excluding polymorphic modifications [325]. Prismatic shaped crystals often possess more favourable tabletting and particulate flow rates as opposed to the needle shaped crystals [182, 326, 327]. It has been proposed that these differences in crystal habits are due to the interactions between crystal and solution from which they are crystallised [328]. A strong relationship illustrating these differences in intermolecular interaction is provided by the dissolution rates of different ibuprofen habits [329].

As ibuprofen is a complex organic compound, containing a carboxylic acid group and a benzene ring, one can expect both non-specific and specific intermolecular interactions to exist. The molecule has one hydrophobic end while the

other end is very hydrophilic. Surface energies of the facets were evaluated from θ_a of the droplets via various semi-empirical analyses (Chapter 9). The wetting behaviour of ibuprofen is interpreted based on the surface chemistry of the specific facets.

6.4.4.1 Contact Angles for Racemic Ibuprofen Crystals

θ_a of diiodomethane and water obtained for racemic ibuprofen single crystals are shown in Table 6.7. θ_a of diiodomethane were found to be highest at 45.5 ° on facet (100) and about 36 °, approximately 20 % lower on facets (001) and (011). Water contact angles showed the largest variations over the three facets with the highest θ_a on facet (100), followed by (001) and (011), with the θ_a 40 % lower. As in the wetting behaviour of the other crystalline solids examined, the anisotropic behaviour is also observed for ibuprofen crystals.

Table 6.7: θ_a (°) Results for Ibuprofen Crystals

	Racemic Ibuprofen		S-(+)-Ibuprofen	
Facet	Diiodomethane	Water	Diiodomethane	Water
(100)	45.5 ± 3.0	77.2 ± 4.0	31.2 ± 3.0	70.7 ± 3.1
(001)	36.9 ± 3.5	68.5 ± 4.8	38.4 ± 2.7	64.5 ± 3.9
(110)	-	-	39.5 ± 3.5	48.4 ± 4.0
(011)	35.0 ± 3.4	46.9 ± 5.5	-	-

The crystallographic structure of ibuprofen facets (100), (001) and (011) is shown in Figure 4.13. For facets (100) and (001), the carboxylic functionality is not available to form hydrogen bonds at the surfaces of these facets. The carboxylic functionality forms a pair of hydrogen bonds (by donating and accepting) with an adjacent molecule's carboxylic functionality in a dimer formation. Although they

appear to be closer to the surface at facet (001), this did not translate to a dramatically more hydrophilic property due to the negligible residual hydrogen bonding potential of the dimers.

Although θ_a for water on facets (100) and (001) was approximately within experimental errors, θ_a for diiodomethane were rather different. Winn and Docherty [192] calculated the attachment energies for various facets of crystalline ibuprofen and reported the lowest value for facet (100). This concurs very well with the measured contact angles and calculated surface energies (reported in Chapter 9). Assuming that the two facets had almost identical polar components (based on contact angles of water), the difference between the two faces will be the dispersive surface energy. The γ_{SV}^{d} of facet (100) which is the predicted weakest attachment energy face, was found to be about 10% lower than facet (001).

The crystallographic structure of (011) is shown in Figure 4.12. θ_a for water on this face was found to be relatively lower than facets (100) and (001). On this facet, the carboxylic functionalities do not form hydrogen bonded dimers, and thus may contribute to hydrogen bonding interactions at the surface.

Based on the contact angle results for water, we can propose an order of hydrophilicity for racemic ibuprofen crystalline facets which is:

$$(011) > (001) > (100)$$

From the contact angle data for diiodomethane, we can prepare an order of the van der Waals type of interactions for racemic ibuprofen crystalline facets which is:

$$(011) = (001) > (100)$$

6.4.4.2 Contact Angles for S-(+)-Ibuprofen Crystals

θ_a of diiodomethane and water for S-(+)-ibuprofen single crystals are shown in Table 6.7. θ_a of diiodomethane were found to be about 40 ° on facets (001) and (110) and

about 30°, approximately 25% lower on facet (100). Water contact angles were found to be different on all three facets with the lowest θ_a on facet (110), followed by (001) and (100).

Like the racemic ibuprofen crystals, the carboxylic functionality of the ibuprofen molecule forms hydrogen bond pairs in a dimer conformation. No hydrogen bonding potential at the surface of facets (100) and (001) is evident as shown in the crystallographic structure of ibuprofen (Figure 4.13). On the other hand, the crystallographic structure of facet (110) suggests that carboxylic functionality present may be able to participate in the interactions with foreign molecules at the surface.

The S-(+)-ibuprofen single crystals have also been observed to be rather brittle and to fracture easily at both planes (100) and (001). However, there has not been any reported literature on the mechanical properties of S-(+)-ibuprofen crystals. As such, one will predict the fracture purely based on its crystallographic structure. Due to the similarities between the two mirror image molecules, the unit cell for both racemic and S-(+)-ibuprofen are also very similar. One would therefore be inclined to predict that their fracture planes may also be analogous. The racemic crystalline ibuprofen has a weakest attachment energy facet at its (100) plane. Adopting this assumption for the S-(+)-ibuprofen crystalline structure as well, θ_a of water is found to be the highest on facet (100). This observation concurs well with our hypothesis that the weakest attachment energy facet for crystalline pharmaceutical solids is the most hydrophobic surface, which has been observed for all the other crystalline systems investigated in this thesis.

Based on the contact angle results of probe liquid water, we can propose an order of hydrophilicity for S-(+)-ibuprofen crystalline facets which is:

$$(110) > (001) > (100)$$

From the contact angle data for diiodomethane, we can prepare an order of the van der Waals type of interactions for S-(+)-ibuprofen crystalline facets which is:

$$(100) > (001) = (110)$$

6.5 Conclusions

In summary, contact angle measurements on macroscopic single crystals have demonstrated that the wettability of a crystalline organic solid is anisotropic. This behaviour is attributed to the facet specific local surface chemistry, which is determined by the presence of different functional groups, their ability to interact with foreign molecules including their concentrations as well the molecular orientation.

For paracetamol form I crystals, facets (201), (001), (011) and (110) had very similar values for θ_a of diiodomethane, though values for (010) were much lower. Values for θ_a of water, varied significantly for all faces, though the values for (010) were the highest. The hydrophilicity order for form I paracetamol, as determined from the θ_a with water is:

$$(001) > (011) > (201) > (110) > (010)$$

In this study, the first contact angle measurements for two macroscopic crystals of different polymorphs, at specific crystalline facets were performed. From this experiment, it is clearly shown that the wetting behaviour of polymorphs is also different. On facets where functional groups of –NH, C=O or –OH groups are present and able to form hydrogen bonds, a low water θ_a was obtained, reflective of the surface hydrophilicity. On facets where formation of hydrogen bonds with foreign molecules is not possible, a high water θ_a was obtained, reflective of the surface hydrophobicity Exposure of different availabilities and proportions of functional groups on various facets is a direct result of the orientation of crystalline planes. As could be anticipated, for polymorphs of which the crystallographic structures of like

molecules are different, their wetting phenomena were found to be very dissimilar. This phenomenon is influenced by the packing of molecules within the crystal lattice, confirming the importance of the local surface chemistry and has been reported experimentally in this thesis.

The wetting behaviour of crystalline solids and their Miller indices are not related. Facet (001) was found to be most hydrophilic facet of the monoclinic form but appeared to be the most hydrophobic face for the orthorhombic form. Also, on facet (010), a high θ_a of water was obtained on the monoclinic form but a low θ_a of water for orthorhombic form. The hydrophilicity order for form II paracetamol, as determined from the θ_a with water is:

$$(010) \approx (110) > (001)$$

The wettability of aspirin single crystals is also found to be anisotropic with θ_a of water differing by up to 50 % on various crystalline facets. As in the case of paracetamol, this result was also very much influenced by the functional groups, the orientation and their densities at the facets examined. The hydrophilicity order for aspirin, as determined from the θ_a with water is:

$$(011) > (100) > (001)$$

The contact angle measurements for both ibuprofen (racemic and S enantiomer) single crystals, at specific crystalline facets were also performed. As in the other crystalline systems, the wettability of ibuprofen (racemic and S enantiomer) single crystals was found to be anisotropic with θ_a of water differing by up to 40% for various crystalline facets. On facets where the carboxylic functionality is able to form hydrogen bonds, a hydrophilic behaviour was observed. The hydrophilicity order for both racemic ibuprofen and S-(+)-ibuprofen, respectively, as determined from the θ_a with water are:

$$(011) > (001) > (100)$$

$$(110) > (001) > (100)$$

θ_a of diiodomethane and water on facets for racemic ibuprofen and S-(+)-ibuprofen were similar, unlike those of paracetamol polymorphs. This result is due to their very similar packing within the crystal lattice. However, from these experiments, it is shown that the variation in atomic orientation within a molecule will still result in a different wetting behaviour, albeit subtle for this ibuprofen system.

From the ranking of the hydrophilicity of the crystalline facets of the systems investigated, an interesting correlation can be drawn. It is clear that the weakest attachment energy facet was also the most hydrophobic facet, an observation not reported before. This property for the weakest attachment energy facet may have serious implications on manufacturing processes of pharmaceutical solids, such as milling (Chapter 8).

CHAPTER 7 QUANTIFICATION OF SURFACE CHEMISTRY

7.1 Introduction

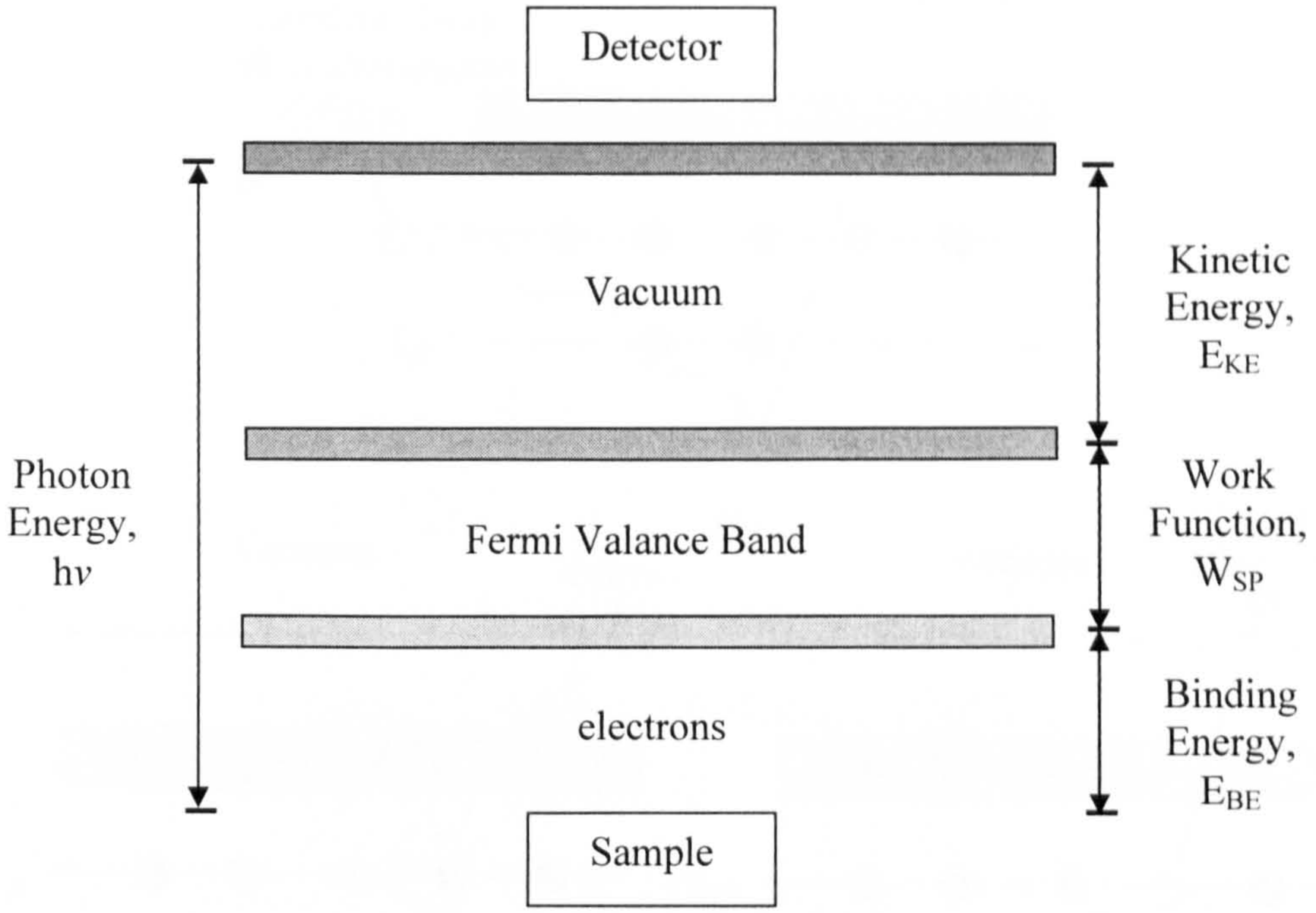
Unlike most spectroscopic techniques, XPS is a surface sensitive technique which enables precise evaluation of atomic surface chemical composition. This ability has resulted in the widespread use of XPS in characterising polymers, for example in studies involving surface modification and grafting [330, 331] and catalysis [332, 333]. More recently, XPS experiments have also been employed to study processing influence and formulation of pharmaceutical solids [334, 335]. In this chapter, the use of XPS to quantify the presence of chemical functionalities on specific facets of crystalline pharmaceutical solid is performed, to assist in elucidating the anisotropic wetting behaviour reported in previous chapters.

7.1.1 Theory

The absorbance of an X-ray by a solid surface results in the transfer of energy to its atom, more specifically the electrons. Where the energy of the X-ray, $h\nu$ is greater than the binding energy, E_{BE} of the electrons, these electrons will be ejected in what is described as the photoelectric effect. The ejected electrons will travel across a vacuum to a detector where its kinetic energy, E_{KE} is measured. This kinetic energy of the ejected electron is a property dependant on the energy level of the photons. It is the binding energies which are specific to the element, and are calculated taking into account of the spectrometer work function, W_{SP} (Figure 7.1). Applying the conversation of energy laws, the relationship between these energies is shown as:

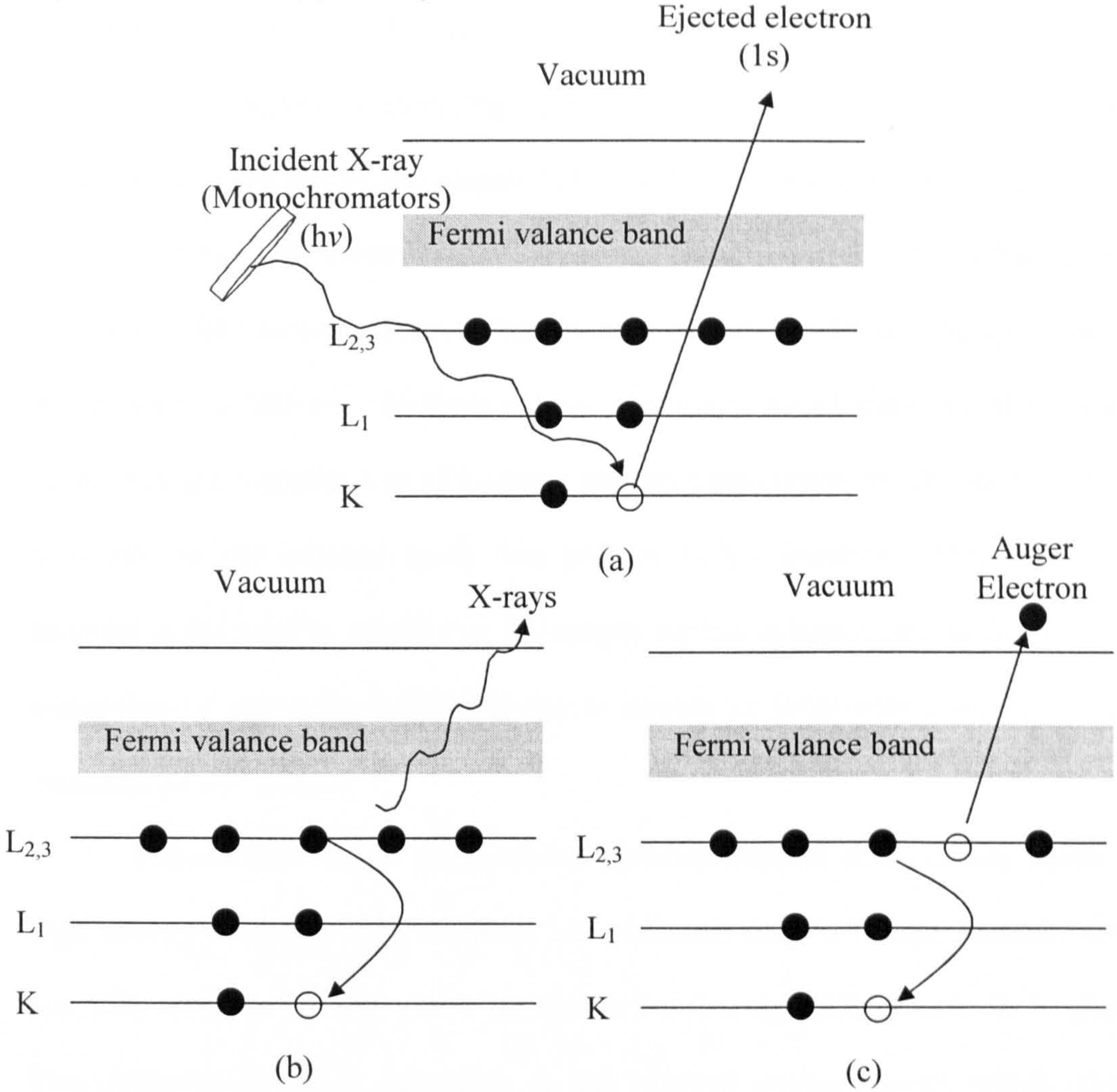
$$E_{BE} = h\nu - E_{KE} - W_{SP} \tag{7.1}$$

Figure 7.1: Energy levels.



Electrons which are excited and escape without energy loss will contribute to the spectrum recorded. However, in most cases, electrons will undergo inelastic scattering which contributes to the background of the spectrum. An ionised atom losing its core shell electron will relax in one of the following, X-ray fluorescence or the Auger electron. When an outer orbital electron fills the vacancy, the energy is released in the form of photons or transferred to another electron resulting in its ejection which forms the basis of the Auger Electron Spectroscopy (AES) (Figure 7.2).

Figure 7.2: (a) Ejection of a core shell electron and its resulting relaxation by (b) X-ray fluorescence or (c) an Auger electron.



The ionisation of the atom will inevitably result in excitation of electrons both from the core shell and from valance bands. Whilst the core shell electrons have a specific energy with respect to their chemical states, the valence electrons do not and require additional treatment.

7.1.2 The XPS System

The main parts of the XPS consist of the vacuum system, the electron and X-ray source and the detector system (Figure 5.5). A comprehensive introduction to XPS is provided by Watts and Wolstenholme [251], and is briefly described in this section.

A typical XP spectrum is measured at pressures of 10^{-8} -10^{-10} mbar, achieved by use of either the ion pumps, turbomolecular pumps or diffusion pumps. The ultra-low pressure is necessary for three primary reasons; to avoid scattering of spectra due to remaining molecules, loss of intensity and noise minimisation. The loss of intensity is related to the reduced mean free path at higher pressures. More importantly however is the need to ensure that the sample surface is kept clean, as the monolayer adsorption of contaminating molecules is known to form within seconds even at pressures of 10^{-6} mbar.

The incident X-rays are produced by bombardment of a suitable anode with high energy electrons. The electrons are produced from a heated filament source, normally tungsten but sometimes lanthanum hexaboride (LaB_6) due to its brightness. The choice of anodes is dependent on the required photon energy, which must be greater energy than the electrons to be ejected, with aluminium and magnesium commonly used. Aluminium and magnesium anodes produce photons of 1486.6 and 1253.6 eV with full-width half-maximum (FWHM) of 0.9 and 0.7, respectively. By increasing the electron energy, the photon flux also proportionally increases but this benefit is greatly hindered by heat generated at the anode. This heat produced is typically dissipated by the use of cooling water at the anode. The X-rays produced are monochromatised due to the favourable qualities such as a smaller FHWM, smaller spot-size including removal of satellite peaks. This improvement is achieved by diffraction within a crystal lattice, typically the $10\bar{1}0$ face of a quartz crystal.

Analysers often used are the cylindrical mirror analysers (CMA) and hemispherical sector analyser (HSA). The HSA is also known as the concentric hemispherical analyser (CHA) or the spherical sector analyser (SSA) and is normally used in the XPS due to its higher resolution. The HSA is made up of two hemispherical electrodes with a gap in between them which forms the passage of the electrons. The electrons ejected from the sample surface enter the HSA tangentially, and are retarded by a series of electrostatic lens as their kinetic energy is normally too large for the analysers. These electrons are further subjected to some user defined energy as they pass through the analyser, known as the pass energy. Typical pass energy of 100 eV is used for a wide scan while in the region of 20 eV for high resolution scans. In most spectrometers, the electrons arriving at the detectors are counted individually by electron multipliers such as channel electron multipliers or channel plates.

7.1.3 Photoelectron Emission

Electrons from a molecule can be ejected due to excitement by a monochromatic beam of X-rays, in a process which is known as the photoelectron emission. These electrons originate from various energy levels within the molecule, typically from the valence band and core shell electrons. For organic molecules, the binding energies of the core shell electrons are typically between 200 – 700 eV while the valence band photoelectron has a range of between 5 – 50 eV. The valence electron's spectra require additional detailed data analysis. The valence electrons may be useful for detailed studies of band structures and photoelectron emission threshold. These spectra are obtained by the use of radiation sources with energies of only 10 – 45 eV, typically UV radiation forms the basis of the Ultraviolet Photoelectron Spectroscopy technique.

The core shell electrons have specific energies with respect to their chemical states. For an unfunctionalised carbon (methylene), the C 1s binding energy is 285 eV, which can vary by several eVs due to a chemical shift exerted by the presence of functionalities bound to the C atom of interest. The shift is reflective of the electronegativity of these adjoining atoms, and some typical examples for C 1s shifts are shown in Table 7.1. It is this uniqueness of the core shell electrons binding energies, coupled with their small escape depths, which makes XPS a very powerful surface analysis technique.

Table 7.1: C 1s Binding Energies for Methylene and Its Functionalised Derivatives

Functionality	Binding Energy (eV)
Methylene (CH_x)	285.0
C-O-R	285.4
C-Cl	287.0
C=O, C-F	287.8
COOR	288.9
$\pi - \pi^*$	291.7
CF_3	292.7

7.1.4 Application of XPS

Sometimes, it is desirable to obtain information from very small sample areas, say about 10 μm^2. The XPS can be operated in two ways to achieve this; either by limiting the region from which the photoelectrons are collected, or by focusing the X-ray beams to a very small spot. The first is achieved by using an aperture so that only limited photoelectrons can reach the analysers, whilst the latter utilises a quartz crystal to focus the electrons so that a monochromatic X-ray with narrow width is produced. If an array of small area scans is assembled, a two dimensional mapping of the sample

showing the distribution of elements can be produced. This approach has been used to study failure mechanisms at an interface due to localised features [336, 337].

The surface sensitivity of the XPS technique is due to the small escape depths of the photoelectrons, which is dependent on the angle of electron emission according to the Beer-Lambert equation. Therefore, by collecting the photoelectrons at different angles to the sample surface normal, a quasi depth profile can be obtained. When different anodes are used, the X-rays generated by bombardments of electrons will possess different energy, which ultimately results in a different penetration depth of the sample evaluated. This angle-resolved approach is experimentally easier and has been used to examine properties of thin film interfaces [338-340].

7.2 Experimental Section

7.2.1 XPS on Single Crystals

XP spectra were recorded on crystal facets using a high-vacuum XPS instrument (Kratos AXIS HSi, England) equipped with charge neutraliser and Mg K_α X-ray source. C, N and O 1s spectra were acquired at a 40 eV pass energy with two-point energy referencing employed using adventitious carbon at 285 eV and the valence band for paracetamol crystals. On aspirin crystals, only C and O 1s spectra were recorded, at a normal emission using analyser pass energy of 20 eV, X-ray power of 144 W and were energy referenced to the valence band and adventitious carbon. All spectra were Shirley background-subtracted and fitted using a Duniach-Sunjic profile deconvoluted with a Gaussian/Lorentzian (4:1) mix. Similar line shapes were employed for all C, N and O 1s components with FWHM of 1.65, 1.69 and 1.76 eV, respectively unless otherwise stated. Fitting was performed using CasaXPS Version 2.0.35 using the minimum number of peaks required to minimise the R-factor.

7.3 Results and Discussion

7.3.1 XPS Analysis on Paracetamol

XP spectra were recorded on individual facets of the macroscopic single crystals. A detailed analysis of the relative contributions of the functional groups is presented here to qualitatively compare the chemical properties of these facets. High-resolution scans of the C, O and N 1s XP spectra for paracetamol external facets (201), (001), (011) and (110) and weakest attachment energy facet (010) are shown in Figure 7.3 to Figure 7.5. The surface atomic compositions of each facet were determined by XPS and are presented in Table 7.2. In all cases the surface compositions were comparable to the theoretical values for bulk pure paracetamol of ~73 % C, 9 % N and 18 % O.

Table 7.2: Atomic Composition of C, N and O on Various Crystalline Paracetamol Facets

Facet	C atomic %	N atomic %	O atomic %
Theoretical	72.7	9.1	18.2
(201)	75.7	5.6	18.7
(001)	78.9	2.8	18.3
(011)	80.0	2.4	17.6
(110)	79.8	3.5	16.7
(010)	77.2	6.4	11.1

Figure 7.3: C 1s XP spectra for various facets of form I paracetamol crystal.

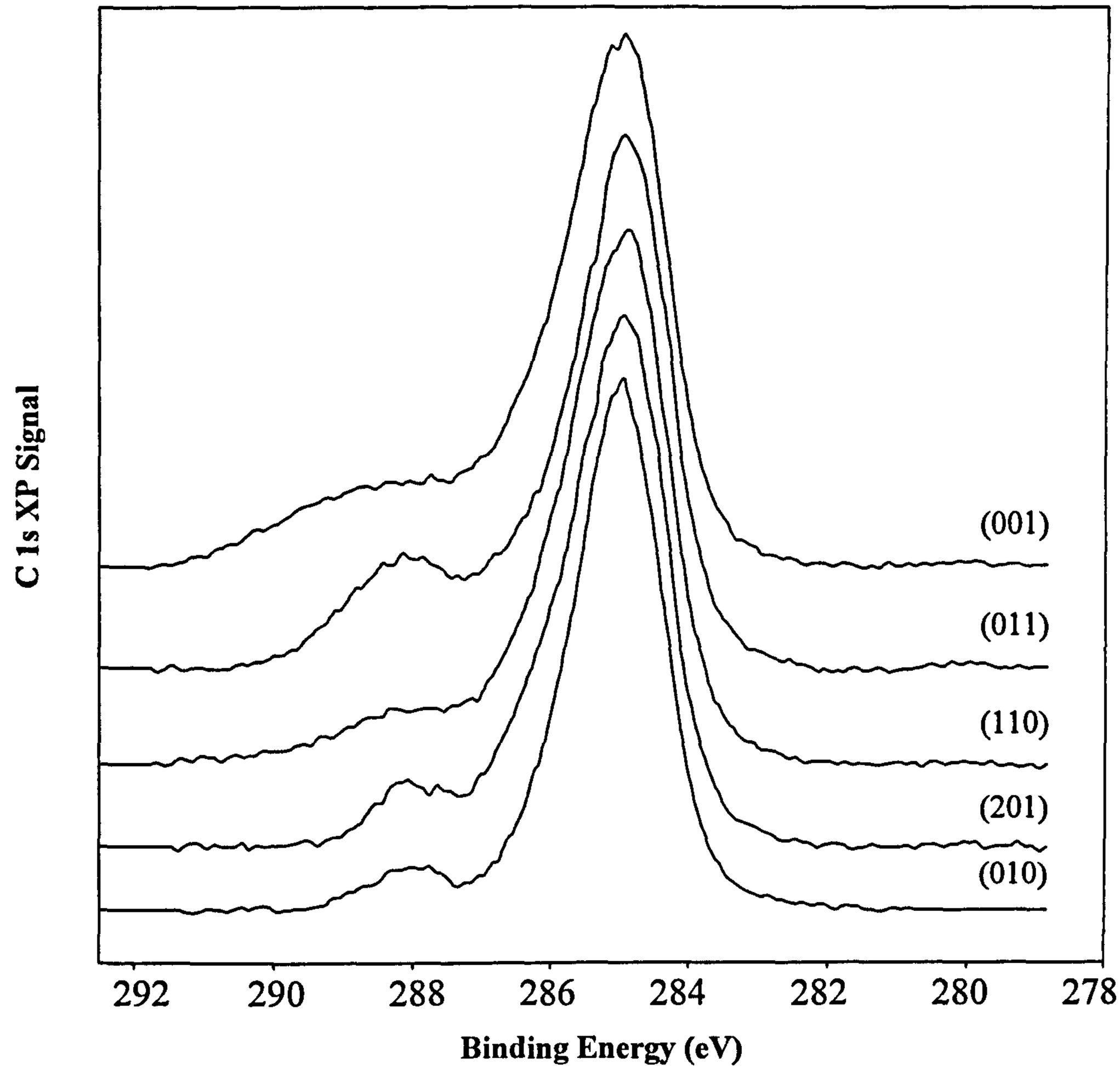


Figure 7.4: O 1s XP spectra for various facets of form I paracetamol crystal.

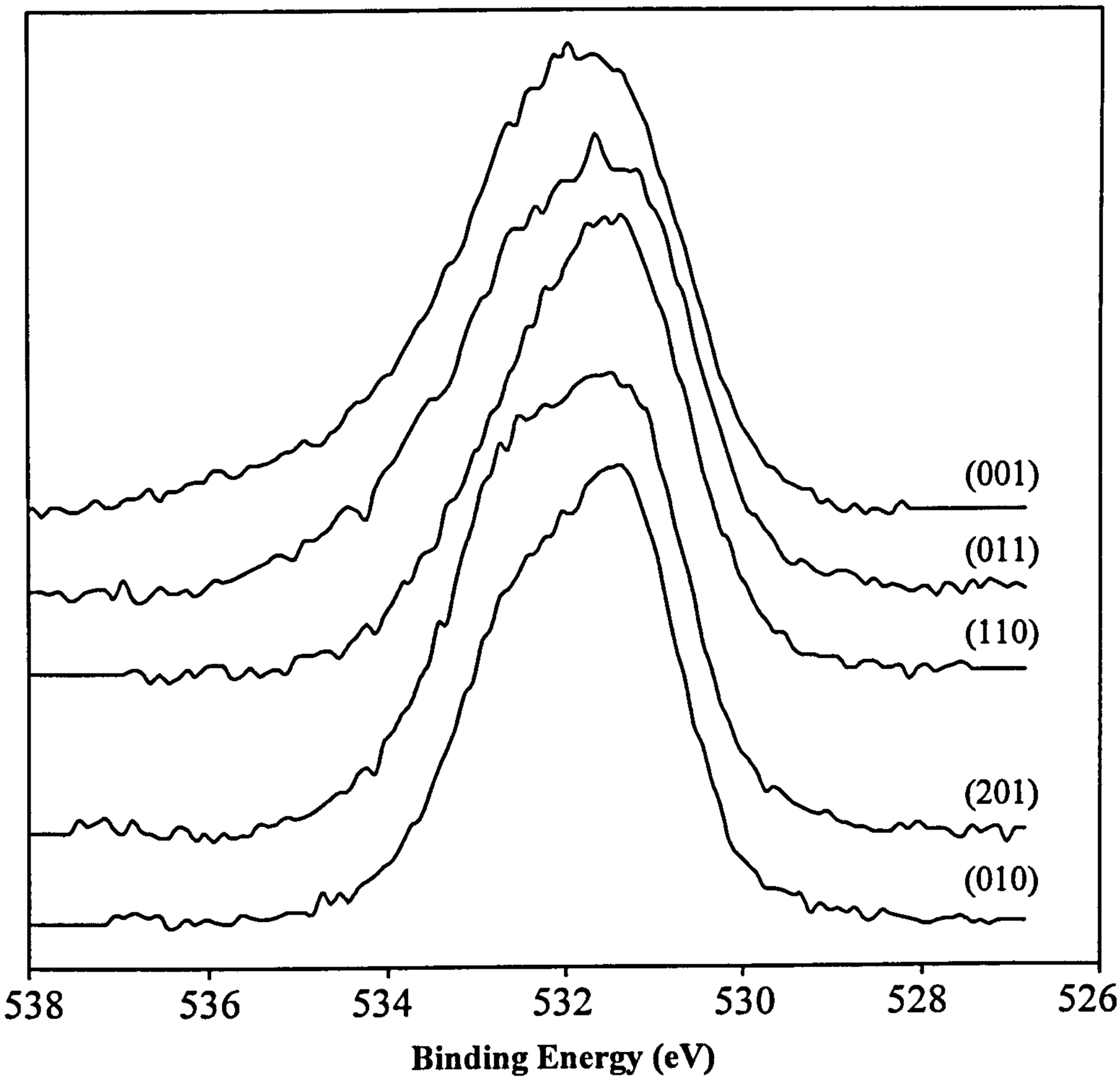
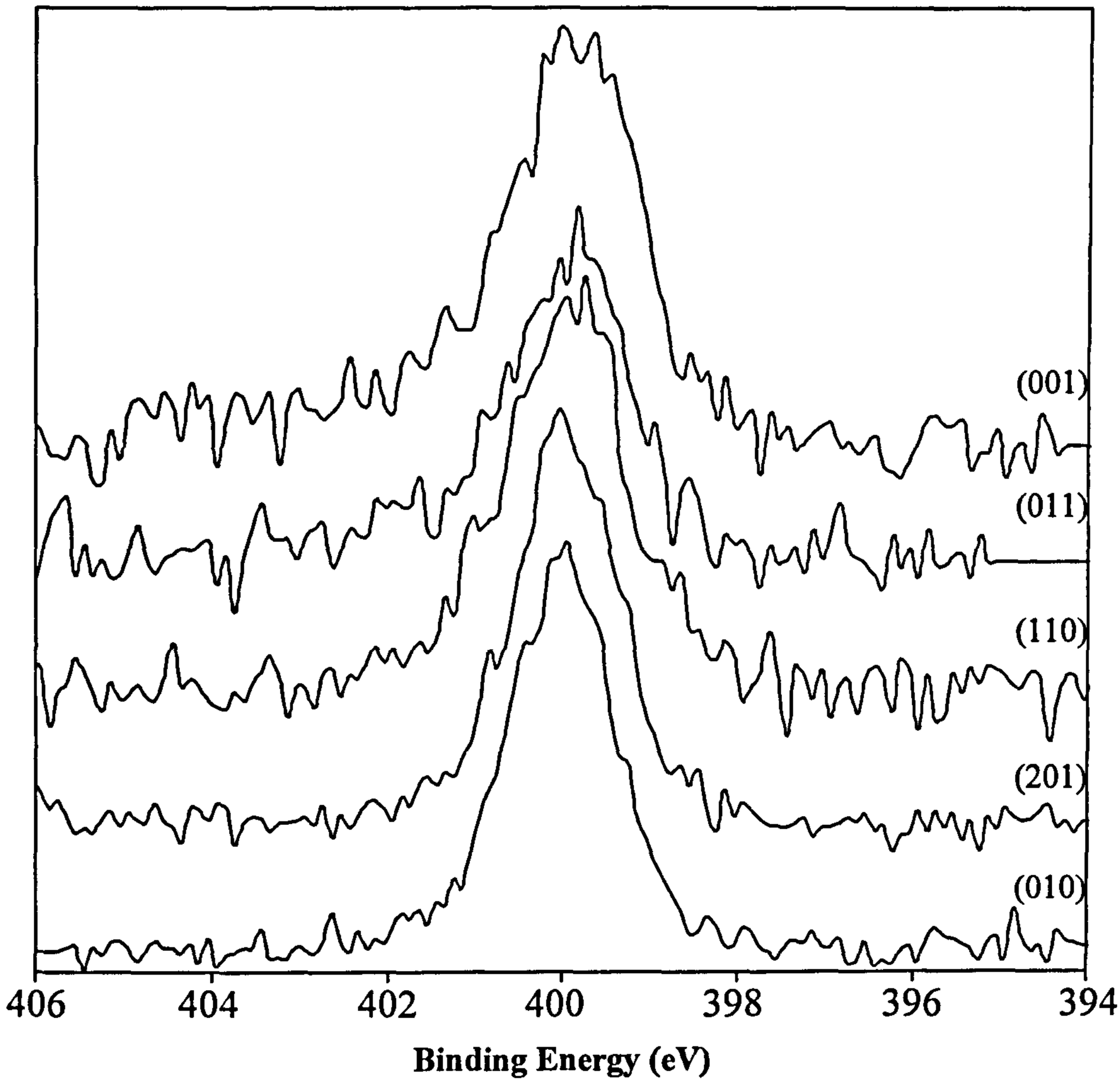


Figure 7.5: N 1s XP spectra for various facets of form I paracetamol crystal.



In contrast, both the C and O 1s spectra (Figure 7.3 and Figure 7.4) reveal multiple chemical environments, at different proportions which were facet specific. The contributions for the carbon region is attributed to methyl and aromatic moieties at around 285 eV while the C-OH and –C=O functionalities at 286.8 and 288.8 eV, respectively. The contributions from the hydroxyl and carbonyl functionalities were also revealed in the oxygen region at 531.3 and 532.8/534.6 eV, respectively. A single nitrogen environment was observed at binding energy (E_{BE}) of 400 eV for all surfaces, in good accordance with literature values for NHR_2 groups and consistent with the single amine group present in paracetamol. The binding energies are available online from the National Institute of Standards and Technology (NIST), USA.

Figure 7.6 and Figure 7.7 show the C and O 1s deconvulated spectra. The full-width half-maximum (FWHM) of the small 288 eV C 1s component peak observed for facet (010) is 0.82 eV, exceeding the limiting resolution of the instrumentation of 0.70 eV. This peak could not be fitted to either the carbonyl (289 eV) or the hydroxyl (286.5 eV) components which were observed to be present on other facets. However, this observation suggests that facet (010) has an environment predominantly terminated with CH_3 groups, and any polar carbon environments are indeed buried deeper away from the surface.

The relative intensity ratio of (C=O + C-OH):CH_x groups determined from the C 1s spectra varies greatly, being highest for the facet (001) and an order of magnitude lower for the facet (010). The facets (011), (201) and (110) likewise contain a relatively high number of C=O and C-OH groups; although the concentration of such moeities on the (110) surface is only ~35 % that of the most polar facet (001) (Figure 7.8). This demonstrates there are significant differences in the distribution of surface groups over the different facets of paracetamol crystals.

Figure 7.6: Deconvoluted C 1s XP spectra for (001) and (010) facets of form I paracetamol crystal. Note 288 eV component required fitting with FWHM = 0.82 eV.

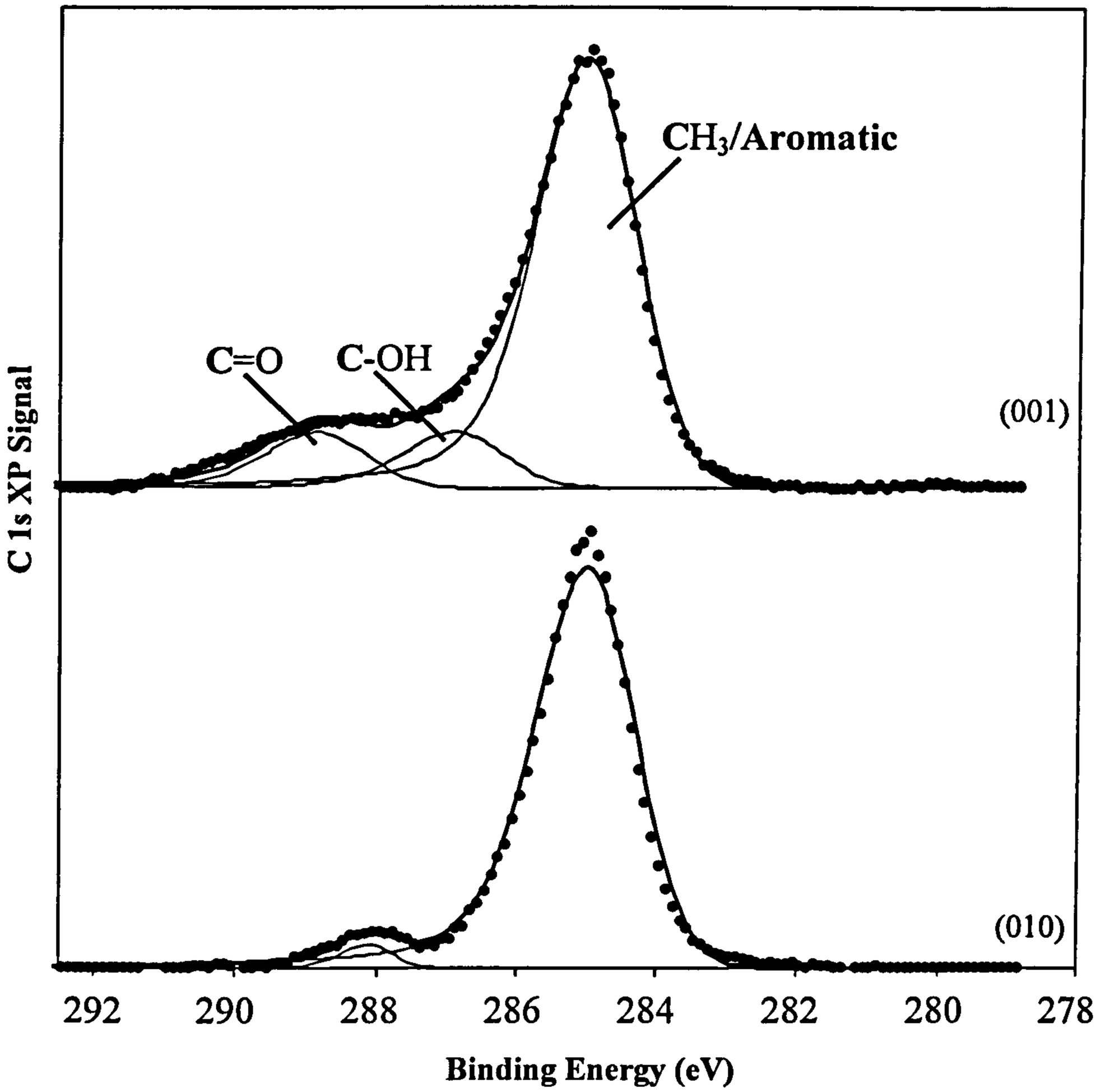


Figure 7.7: Deconvoluted O 1s XP spectra for (001) and (010) facets of form I paracetamol crystal.

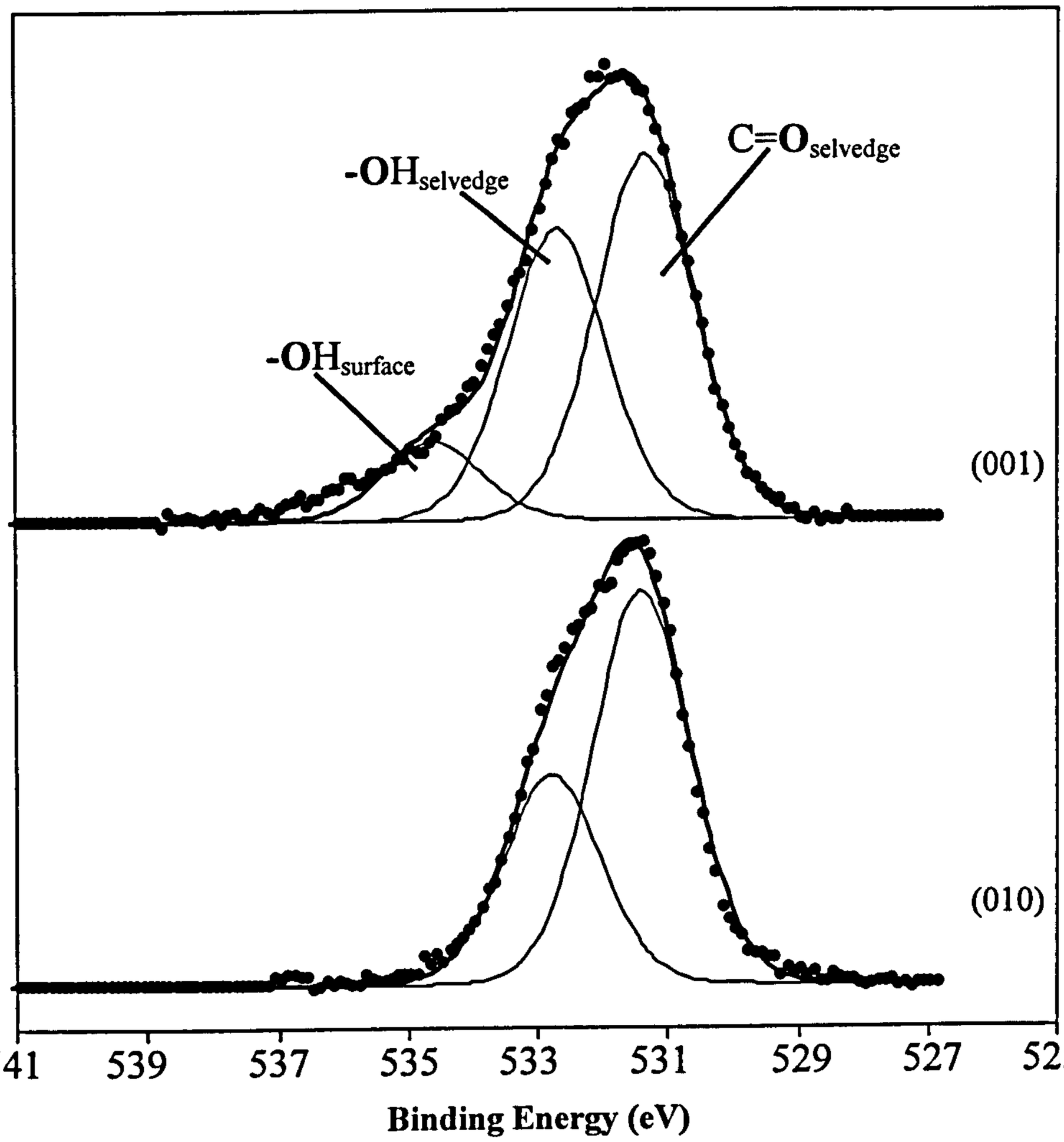
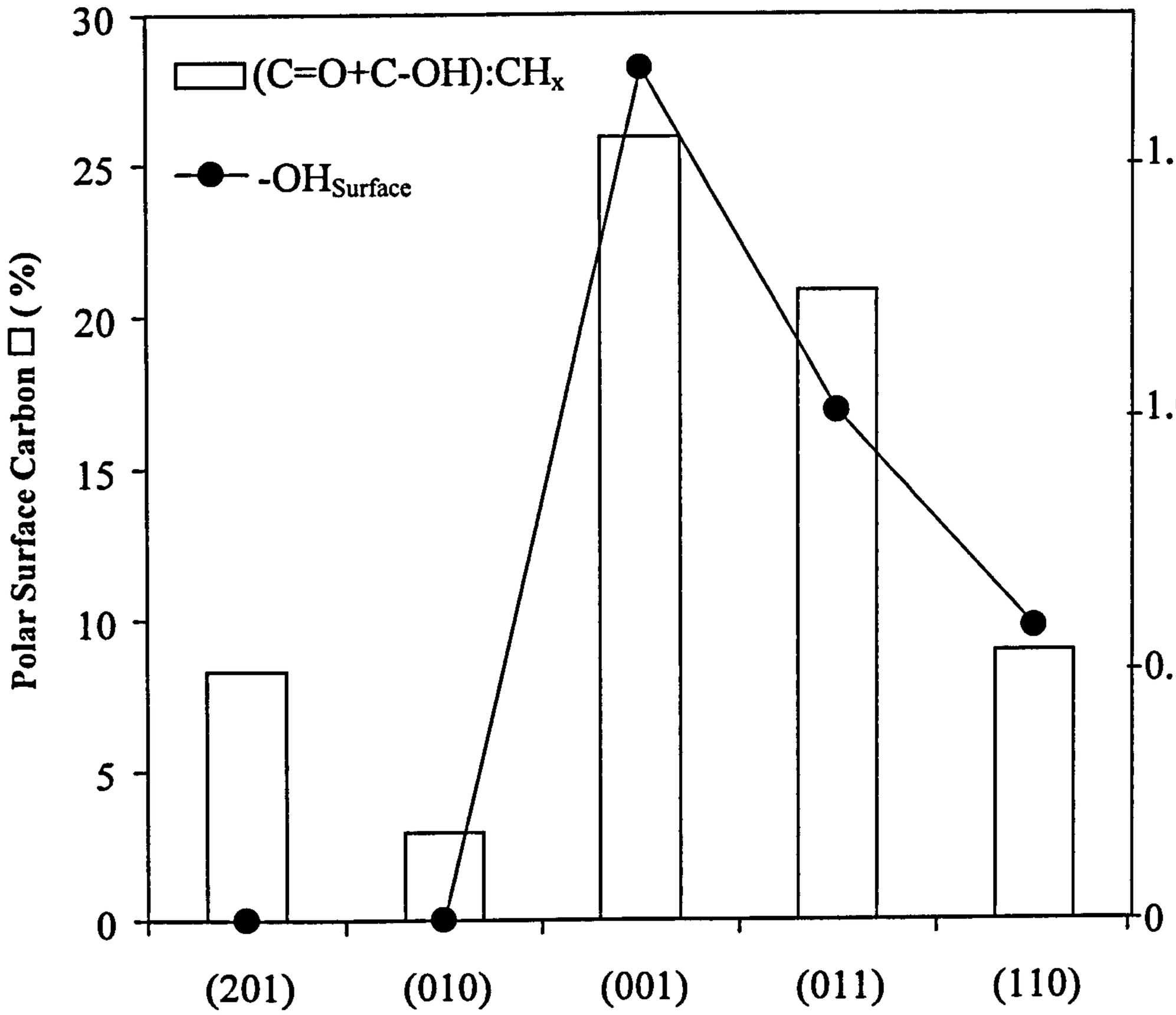


Figure 7.8: Variation in surface composition of polar groups for different facets of form I paracetamol crystal as determined from C 1s and O 1s XP peak-fitting. Surface -OH intensities taken from 534.6 eV component in Figure 7.7.



From this experiment, we verified that the anisotropic wetting behaviour of crystalline solids is attributed to the availability and variation of surface functional groups. The order of polarity by XPS for paracetamol single crystals is:

$$(001) > (011) > (201) > (110) > (010)$$

The order by XPS is in excellent agreement with the hydrophilicity order as predicted by θ_a of water. In order to establish their correlation, a comparison between the polarity as determined by XPS and surface energy polarity is prepared and presented in Chapter 9.

All the O 1s spectra obtained contained two principal components that can be readily associated with the unique carbonyl and alcohol environments within paracetamol. In view of the longer inelastic mean free path of the O 1s photoelectrons (~1.5-2 nm), the influence of subsurface –OH is also expected. The latter state (534.6 eV) corresponding to the surface hydroxyl was found to be strongest on the most polar facet (001) and is reflective of the surface terminated hydroxyl groups. In contrast, no such high energy binding energy component was revealed on the non-polar (010) facet, representative of the methyl-terminated surface. On the other external facets of (011) and (110), the surface hydroxyl contribution was also present, wherein the intensity of the O 1s 534.6 eV state clearly tracts that of the C=O + C-OH C1s intensities, with the exception of facet (201) (Figure 7.8).

Although the O 1s spectra predict that facet (201) should be significantly less polar than the facet (110), the carbon spectra suggest that they are of comparable polarity; this discrepancy remains to be further explored. One possible explanation is the abundance of the carbonyl functionalities on facet (201), resulting in its polarity not being solely representative of the hydroxyl density. However, it is admittedly

difficult to predict the properties of the various facets, but is envisaged that the C 1s spectra may be more representative of the polarity of facet (201).

This correlation confirms both our peak assignments and provides direct, unambiguous confirmation for anistropic surface termination of form I paracetamol crystals. With confidence, the surface polarity of paracetamol facets determined by XPS is therefore predicted to decrease in the order of:

$$(001) > (011) > (201) > (110) > (010)$$

The dominant role of surface hydroxyls in regulating surface polarity is also confirmed in accordance with our contact angle based surface energy analysis and first-order surface hydroxyl density determination from crystallographic data reported in Chapter 9.

7.3.2 XPS Analysis on Aspirin

The C 1s XP spectra of all the low index facets were very similar containing two main features centred around 285 and 289 eV binding energy (E_{BE}). Figure 7.9 shows representative spectra for each surface. Spectral deconvolution and peak fitting reveals the presence of three unique chemical environments at 285, 286.5 and 289.3 eV corresponding to CH_x, ether/alcohol and carbonyl of the carboxylic acid/ester functionalities respectively, in excellent agreement with the molecular structure of aspirin. One should note that the C-O-C and C-OH functional groups and the carbonyl (C=O) functionality within ester (COO-R) and carboxylic acid (COOH) groups possess identical binding energies prohibiting their unique identification from the C 1s spectra alone.

The surface composition of these facets, ranged between 63 and 73 % atomic carbon, all close to the theoretical bulk aspirin composition of 69 atom% carbon

(Table 7.3). Facet (001) was found to be the most carbon-rich and the (011) the most oxygen-rich. These differences reflect the presence of significant additional CH_x moeities on the more apolar (001) surface, as expected for a surface termination parallel to the methyl/phenyl rings, as depicted by crystallographic structure (Figure 4.11). In turn the distribution of COH (COC):C=O species in the more oxygen-rich (011) facet is close to that predicted for a polar, carboxylic acid terminated surface.

Confirmation of the composition and termination of each facet was provided by the O 1s XP spectra as shown in Figure 7.10. All three surfaces exhibited a broad partially resolved feature centred ~532.5 eV, which could be readily deconvoluted into 2 states at 532 and 533.5 eV. These correspond to the respective carbonyl ((H)COC=O), and ester/acid hydroxyl ((H)COC=O) environments. Comparison of the O 1s carbonyl:ester/OH ratio reveals it is close to 1:1 for the (011) plane, confirming the exposure of acid functional groups at the surface (Table 7.4). This suggests the (011) facet cuts through the crystal to expose the non-dimerised carboxylic acid group.

Figure 7.9: C 1s XP spectra of the (001), (100) and (011) facets showing the deconvoluted C environments.

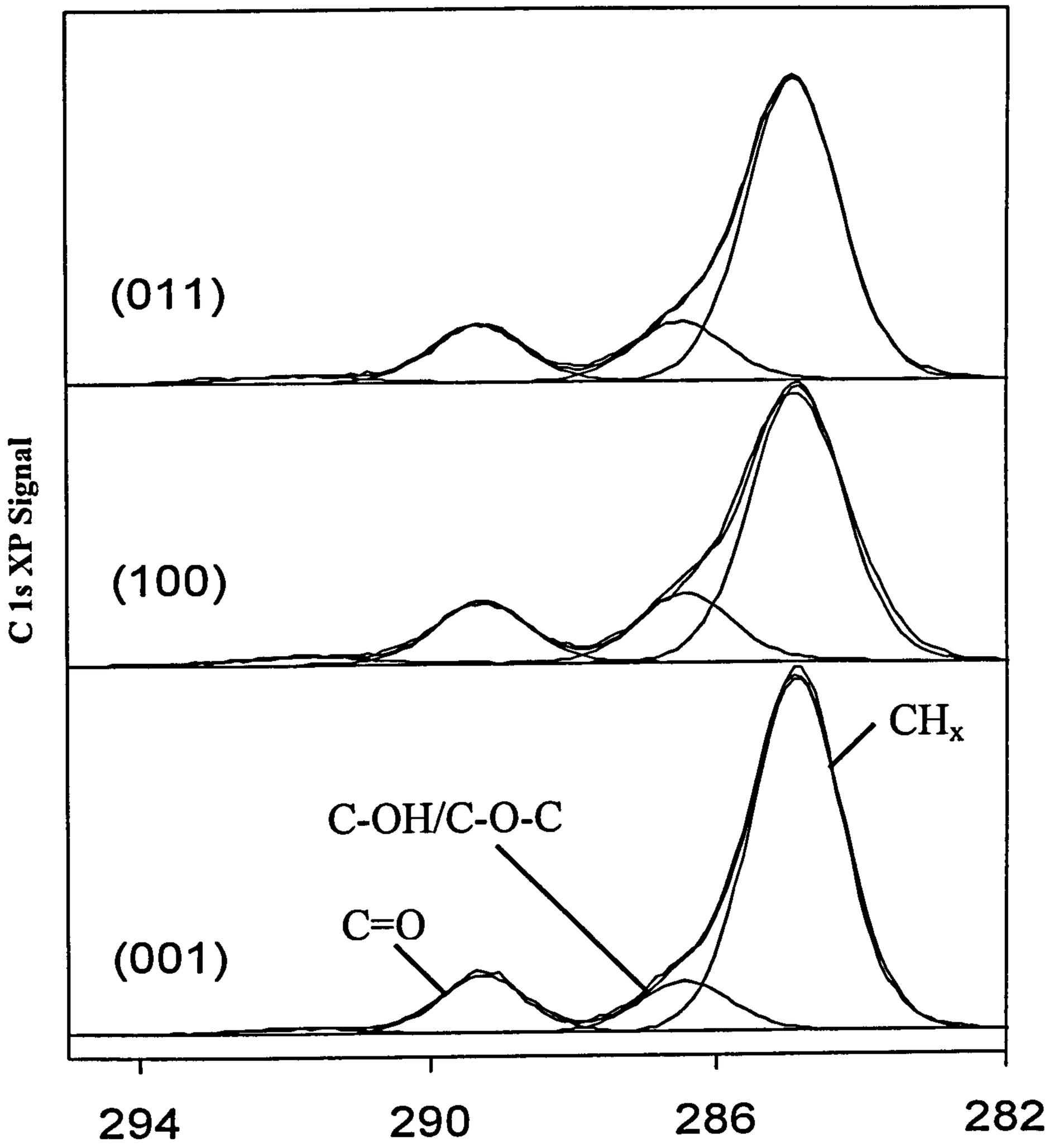


Figure 7.10: O 1s XP spectra of the (001), (100) and (011) facets showing the deconvoluted O environments.

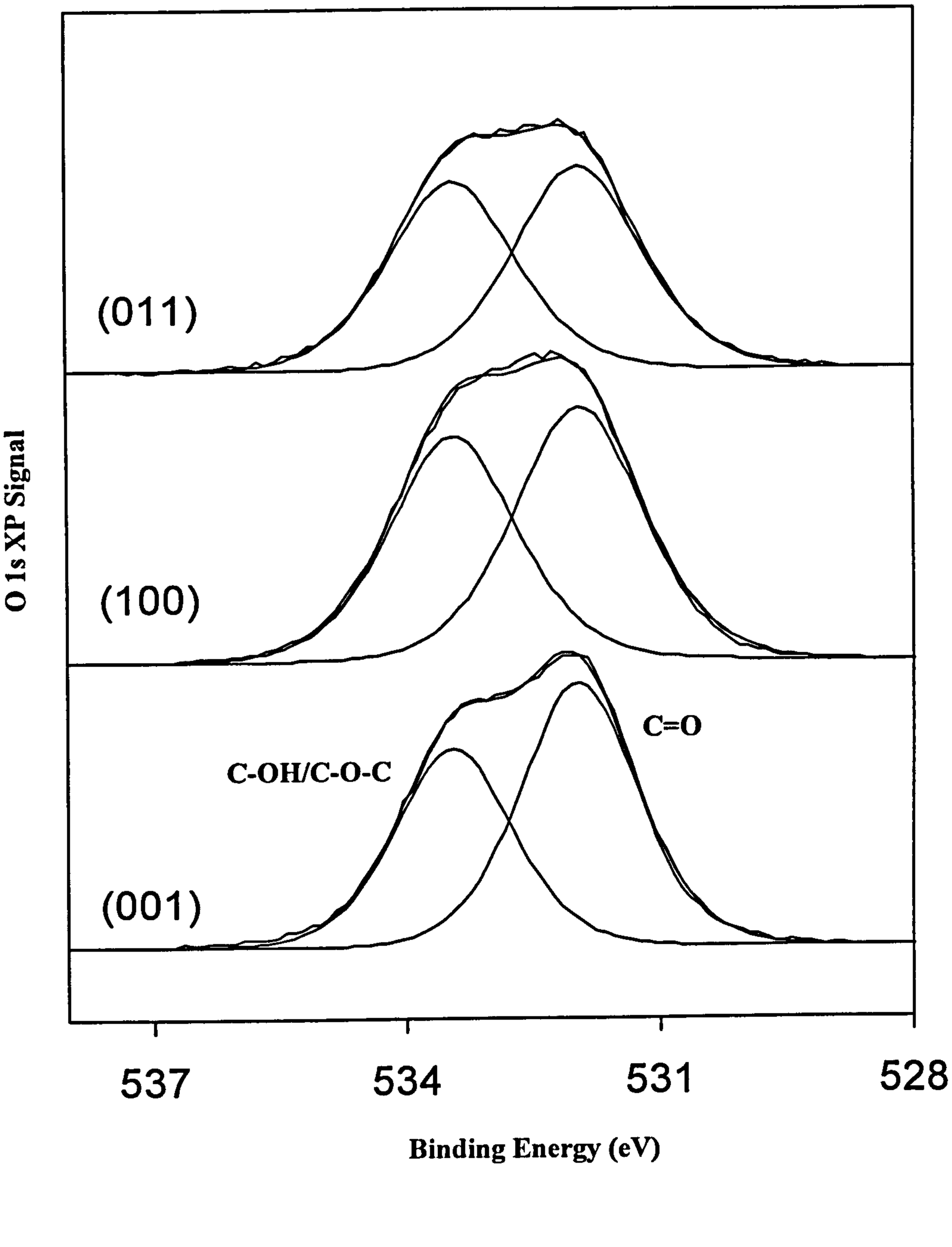


Table 7.3: Surface Composition of Crystal Facets from XPS

Facet	Carbon (atom %)	Oxygen (atom %)
(001)	73.2	26.8
(100)	68.3	31.7
(011)	62.8	37.2

Table 7.4: Distribution of O 1s Surface Environments from XPS (atom %)

Facet	C=O	COH (COC)
(001)	56.5	43.5
(100)	52.4	47.6
(011)	51.3	48.7

This observation fits nicely with the reported higher acidity and polarity of the (011) facet determined from contact angle measurements (Chapter 9). In contrast the (100) facet exhibits a proportionally higher C=O content, consistent with surface terminations that preferentially expose the ester group and thus the C=O functionality as shown above. This finding again supports the stacking and terminations which expose both ester methyl and carbonyl functionality for the (100) facet resulting in a less polar and more basic surface.

In summary, C and O 1s XP spectra reveal the (011) surface as the most polar facet being carboxylic acid terminated, while the (100) facet also exposes significant polar hydroxyl and ester/acid surface functions (albeit less than facet (011)). In contrast the (001) facet is significantly more apolar with a larger fraction of the acid and ester groups trapped subsurface. The polarity of aspirin facets is in the order of:

$$(011) > (100) > (001)$$

7.4 Conclusions

From this study, XPS data has successfully related and exemplified the influence of surface chemistry at specific planes of a complex organic crystalline material in governing their wetting behaviour. For paracetamol single crystals, XPS identified strong variations in the surface termination of each facet and the concentration of exposed polar (notably surface -OH) groups. A predicted surface polarity of paracetamol facets determined by XPS is proposed to decrease in the order (001) > (011) > (201) > (110) > (010), which is in excellent agreement with contact angle analysis.

For aspirin crystals, the hydrophobicity order of the facets is (011) < (100) < (001). Facet (011) was found to be more acidic than both facets (001) and (100) due to a surface termination preferentially exposing the carboxylic acid functionality. The hydrophobicity of the (001) facet reflects the reduced accessibility of surface acid, ester and hydroxyl groups and concomitant exposure of the aromatic aspirin backbone groups.

CHAPTER 8 SURFACE PROPERTIES OF MILLED AND UNMILLED PHARMACEUTICAL SOLIDS

8.1 Introduction

In this chapter, the surface energies of paracetamol, aspirin and ibuprofen as a function of particle size of single unmilled crystals and milled macroscopic crystals were investigated by the Inverse Gas Chromatography (IGC) technique. Their surface energies were evaluated and compared with liquid sessile drop contact angle data on macroscopic single crystals. The differences in surface energy trends are investigated and analysed from contact angle data as reported in earlier chapters. The IGC technique is also reviewed in this section.

8.2 Background

A range of experimental techniques are in current usage for characterising surface chemical properties of organics materials, including pharmaceutical solids. Fourier transform infrared (FTIR) and Raman spectroscopy reveal predominantly bulk as well as some surface chemical information. Much more surface sensitive information is revealed using secondary ion mass spectrometry (SIMS) and X-ray photoelectron spectroscopy (XPS) [251]. Spectroscopic techniques will normally yield analytical information on solid state materials such as what is present, where is it present and how much is present. This data contains little, if any, thermodynamic information.

A more robust technique for determining solid surface thermodynamics and related physicochemical information is by the use of vapour phase molecules as

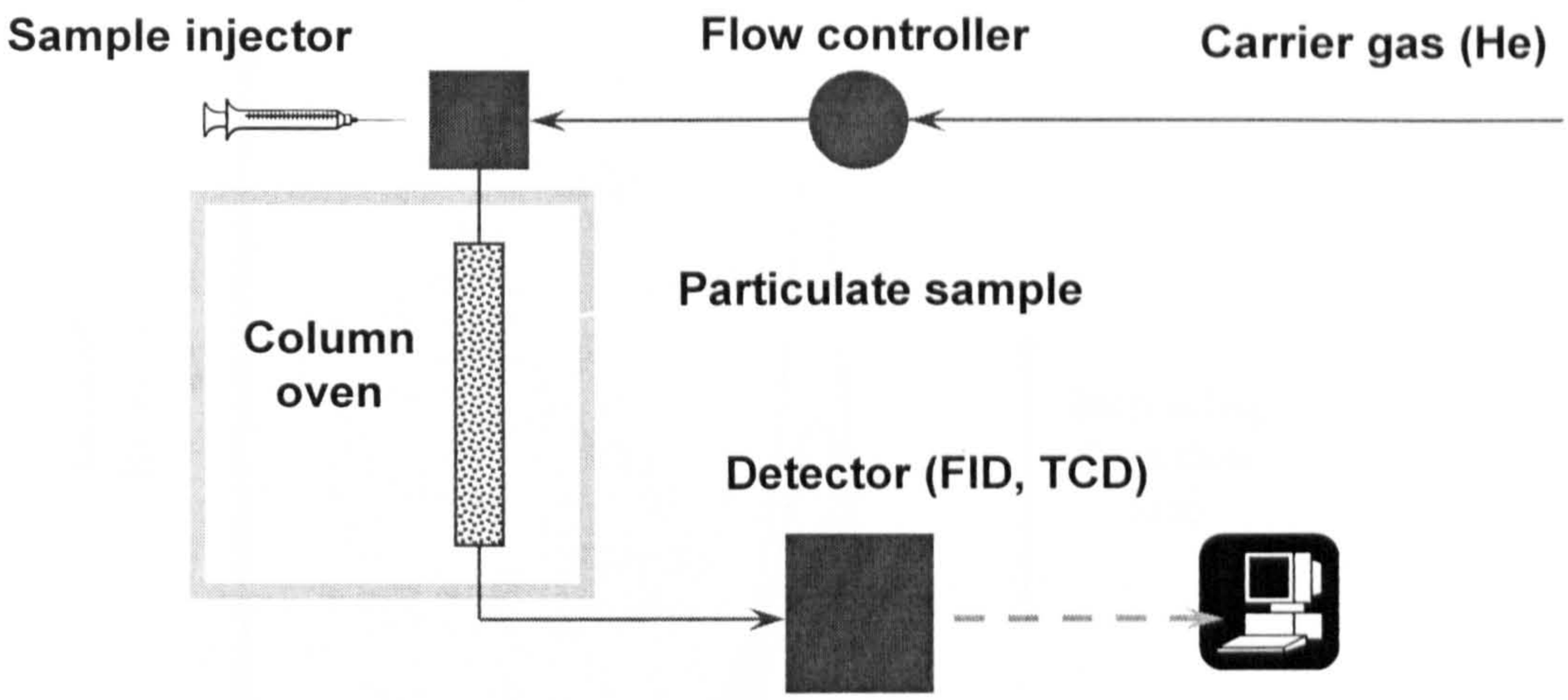
molecular probes for studying, in detail, gas-solid interactions. Not only are these the most naturally relevant probes, but their size results in sensing volumes that are appropriate to the scale of surface chemical information required, sub-nanometer. Techniques which use vapour phase probes offer a number of significant advantages over traditional analytical or spectroscopic approaches including:

- Samples can be studied under real world conditions i.e. ambient temperature and pressure
- Probe molecules can be chosen with appropriate or relevant chemical properties to the information required or problem to be addressed
- Both bulk and surface properties can be elucidated as molecular probes can diffuse into materials giving an insight into internal molecular structure
- Vapour phase molecular probes are extremely sensitive probes for determining the surface chemistry at sub-monolayer coverages for particulate materials
- Typically both kinetic and equilibrium thermodynamic data can be obtained using molecular probe techniques.

8.3 Inverse Gas Chromatography

Gas molecules are injected into a carrier gas which passes over the sample solid, sorbing on the surface with a distribution coefficient, $K_S = V_R^{\circ}/W_S$ where V_R° is the net retention volume and W_S is the mass of the sample. V_R° is the volume of carrier gas required to elute the injection solute through the column, and is a measure of how strongly the probe solute molecules interact with the solid sample. This forms the basic principal of this technique whereby molecules are used as probes, and the nature of the molecular interaction can be directly studied. It is from V_R° that a wide range of surface and bulk properties can be calculated. These are described in further detail in the following section while an instrumentation schematic is shown in Figure 8.1.

Figure 8.1: The Inverse Gas Chromatography (IGC) schematic diagram.



8.4 Theoretical Aspects of IGC

8.4.1 Infinite and Finite Dilution

Infinite and finite dilution experiments are determined by the injection size of the vapour used. Infinite dilution refers to very small solute injection sizes, where the surface coverage is low, and is referred to as adsorption at zero surface coverage of the adsorbate. Within this portion of the adsorption isotherm, Henry's Law is applicable where the amount of vapour adsorbed is governed by a linear relation to the injection concentration. The chromatogram peaks obtained for infinite dilution IGC experiments are typically symmetrical and Gaussian in shape. The retention time, t_R of the probe will be independent of the injection size, as shown in Figure 8.2. For higher solute concentrations or finite dilution experiments, Henry's Law is no longer applicable and Langmuirian (Type I) or sigmoidal isotherms (Type II or III) will be encountered, resulting in a concave or convex chromatograms (Figure 8.3). The analysis of such chromatograms is reported elsewhere [239].

Figure 8.2: Retention times of probe molecules with increasing injection size for the infinite dilution regime.

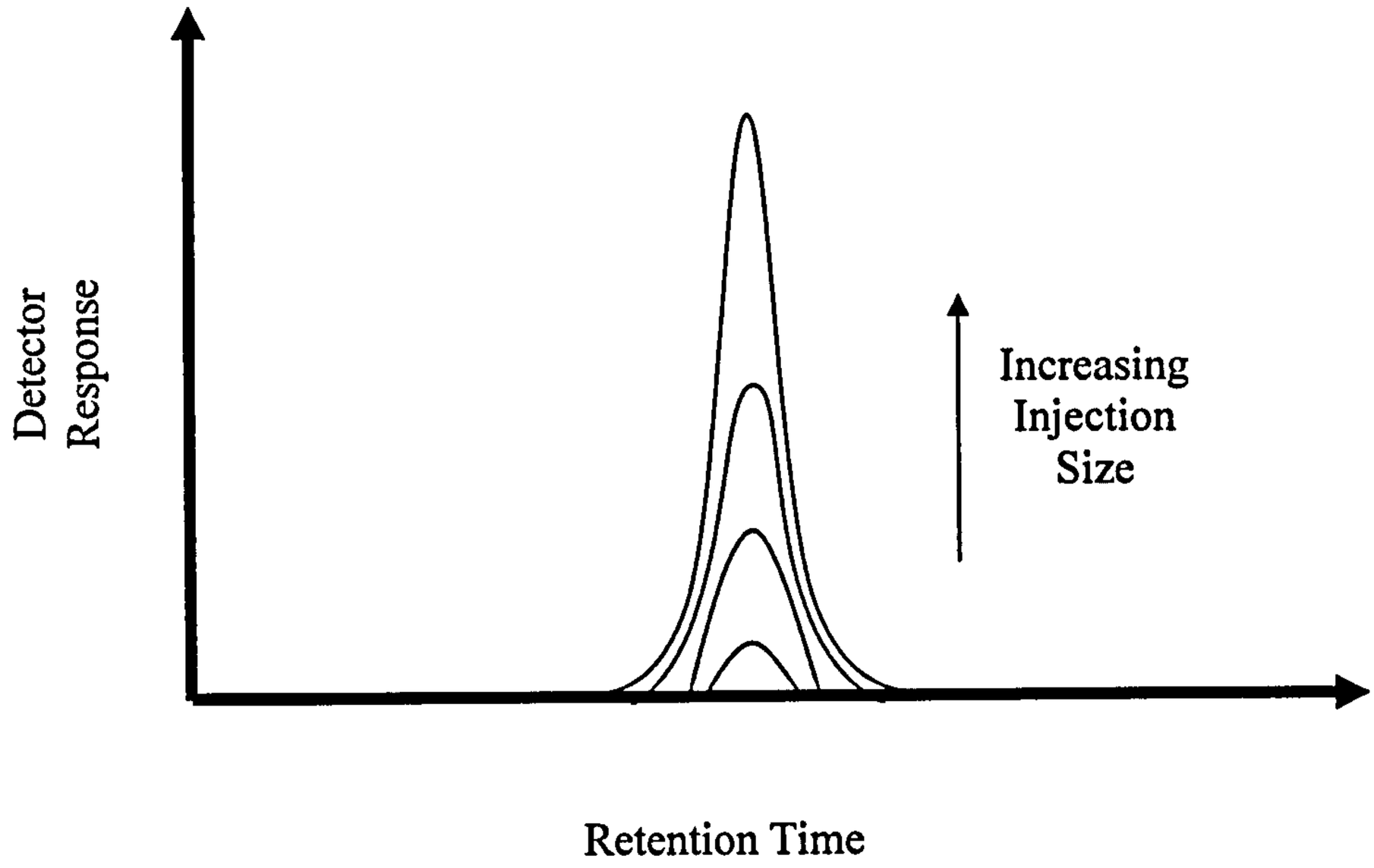
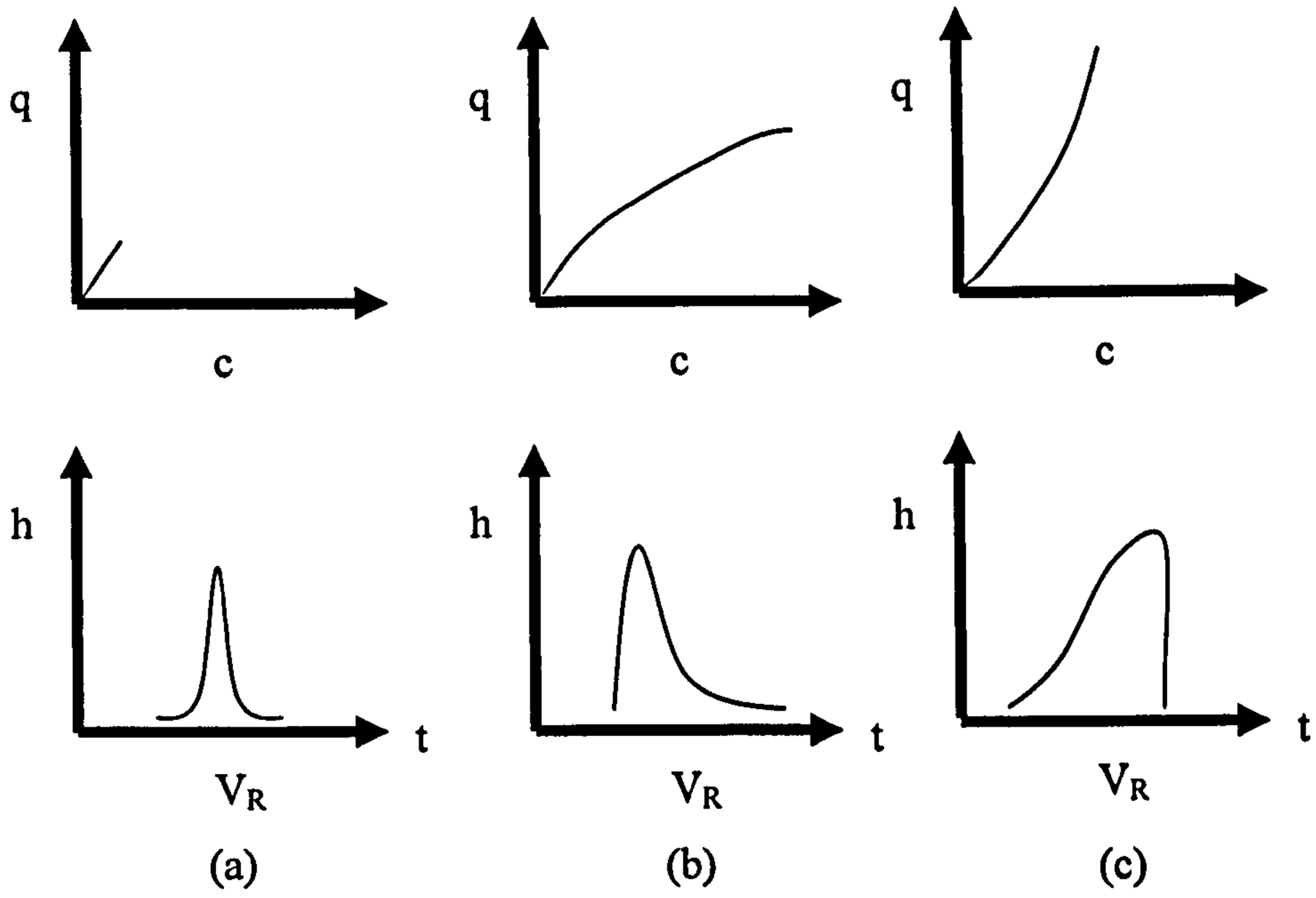


Figure 8.3: The isotherms and chromatographic peaks for (a) the infinite dilution case where Henry's Law is valid, (b) the Langmuir case and (c) the type II and III adsorption isotherm cases.



At infinite dilution, the information obtained about surfaces or bulk materials are at low surface coverages of probe molecules, normally within the Henry's law region. The solute molecules are expected to behave independently of process conditions. Information obtainable from such experiments includes:

- Surface Energies
- Acid-base Interactions
- Phase and Morphology Changes
- Adsorption thermodynamics: enthalpy, entropy and free energies

At finite concentration, solute-solute interactions result in non-linear effects. The following information may be determined, depending upon experiment design:

- Isotherm measurements
- Competitive Adsorption Phenomena
- Surface Areas
- Gas Phase reactions eg. surface titrations
- Porosity (micro & meso)
- Solubility, Diffusion and Permeability

Both infinite and finite dilution studies have been successfully undertaken using IGC by a number of research groups to study the surface properties of pharmaceutical solids.

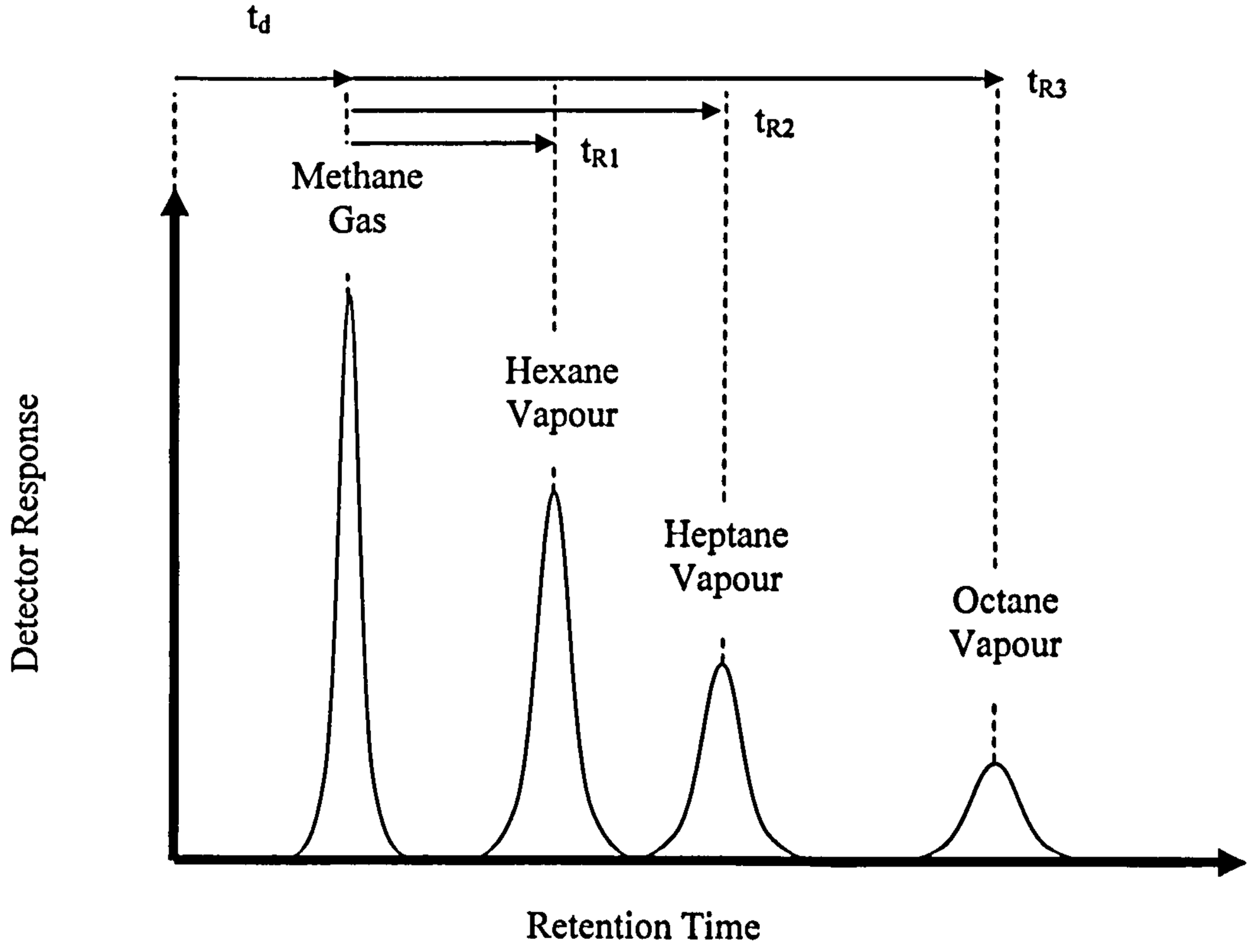
8.4.2 Determination of Retention Time

The retention time, t_R allows the retention volume, V_R^0 of any vapour probe to be evaluated. To calculate t_R for any vapour probe from the maxima of the chromatogram is straight forward for a symmetrical peak, with a Gaussian profile. For a symmetrical peak, the centre of mass will be the same as the point of maximum peak height, and therefore;

$$t_R = t_{max} \tag{8.1}$$

where t_{max} is the time for the peak maximum. The t_R is a measure of the strength of molecular interaction between the vapour probe and the solid surface of the column packing. Therefore t_R will increase with increasing chain lengths of probes, such as for an homologous series of alkanes (Figure 8.4). However, in some cases, such as heterogeneous solids, the resulting IGC peaks are often skewed. This skewing is especially true for cases involving the use of acidic and basic vapour probes. The skew ratio, η is then used to define the measure of asymmetry, with unity representing a perfect symmetric peak [239]. Alternative methods for determination of t_R have been suggested by Conder and co-workers [239, 341].

Figure 8.4: Retention time as a function of increasing chain lengths for a series of n-alkane injections.



8.4.3 Determination of Retention Volumes

From the retention time, t_R, the retention volume, V_R^0 of any vapour probe may be evaluated. V_R^0 is a fundamental thermodynamic property (Equation 5.7), from which a wide range of equilibrium surface thermodynamic properties are derived.

The James-Martin correction factor, corrects the retention time for the pressure drop along the packed column. This correction factor was derived based on assumptions of Darcy's law and Boyle's law by relating the column length and gas flow rates to pressures and is defined by:

$$j = \frac{3}{2}\left[\frac{\left(\frac{P_i}{P_o}\right)^2 - 1}{\left(\frac{P_i}{P_o}\right)^3 - 1}\right] \tag{8.2}$$

where P_i is the column inlet pressure and P_o is the column outlet pressure. This correction factor is always equal to or less than unity in conformity with Darcy's Law.

8.4.4 Determination of Thermodynamic Properties

The net retention volume, V_R^0 can be related to the equilibrium distribution of the gaseous phase and the stationary phase, both at the surface and in the bulk, as shown in Equation 8.3:

$$V_R^o = K_s A + K_b V \tag{8.3}$$

where K_s and K_b are the surface and bulk partition coefficient respectively, with A and V the total surface area and volume of the stationary phase respectively. For an infinite dilution injection, Equation 8.3 can be reduced to Equation 8.4 where free energy change, ΔG_A^o, the enthalpy change, ΔH_A^o and entropy change, ΔS_A^o due to adsorption can be determined.

$$V_R^o = K_s A \tag{8.4}$$

It is from Equation 8.4 that the free energy change, ΔG_A^o, the enthalpy change, ΔH_A^o and entropy change, ΔS_A^o due to adsorption can be determined. For a known sample surface area, A, the partition coefficient of a series of probes can be determined defining the absorbate-absorbent interactions.

The free energy of adsorption and desorption can be related to the partition coefficient and retention volumes as follows:

$$\Delta G_A^o = -RT \ln\left(\frac{K_s p_{s,g}}{\pi_s}\right) \tag{8.5}$$

$$\Delta G_D^o = -\Delta G_A^o = RT \ln\left(\frac{V_R^o p_o}{Am\pi_o}\right) \tag{8.6}$$

where $p_{s,g}$ is the adsorbate vapour pressure in the gas phase and π_s is the spreading pressure at standard states, while π_o is the adsorbed film to a reference state defined by partial pressure, p_o. A is the specific surface area and m the mass of the absorbing phase. Equations 8.5 and 8.6 can be further simplified to:

$$\Delta G_A^o = -RT \ln(K_s) + C_1 \tag{8.7}$$

$$\Delta G_D^o = -\Delta G_A^o = RT \ln(V_R^o) + C_2 \tag{8.8}$$

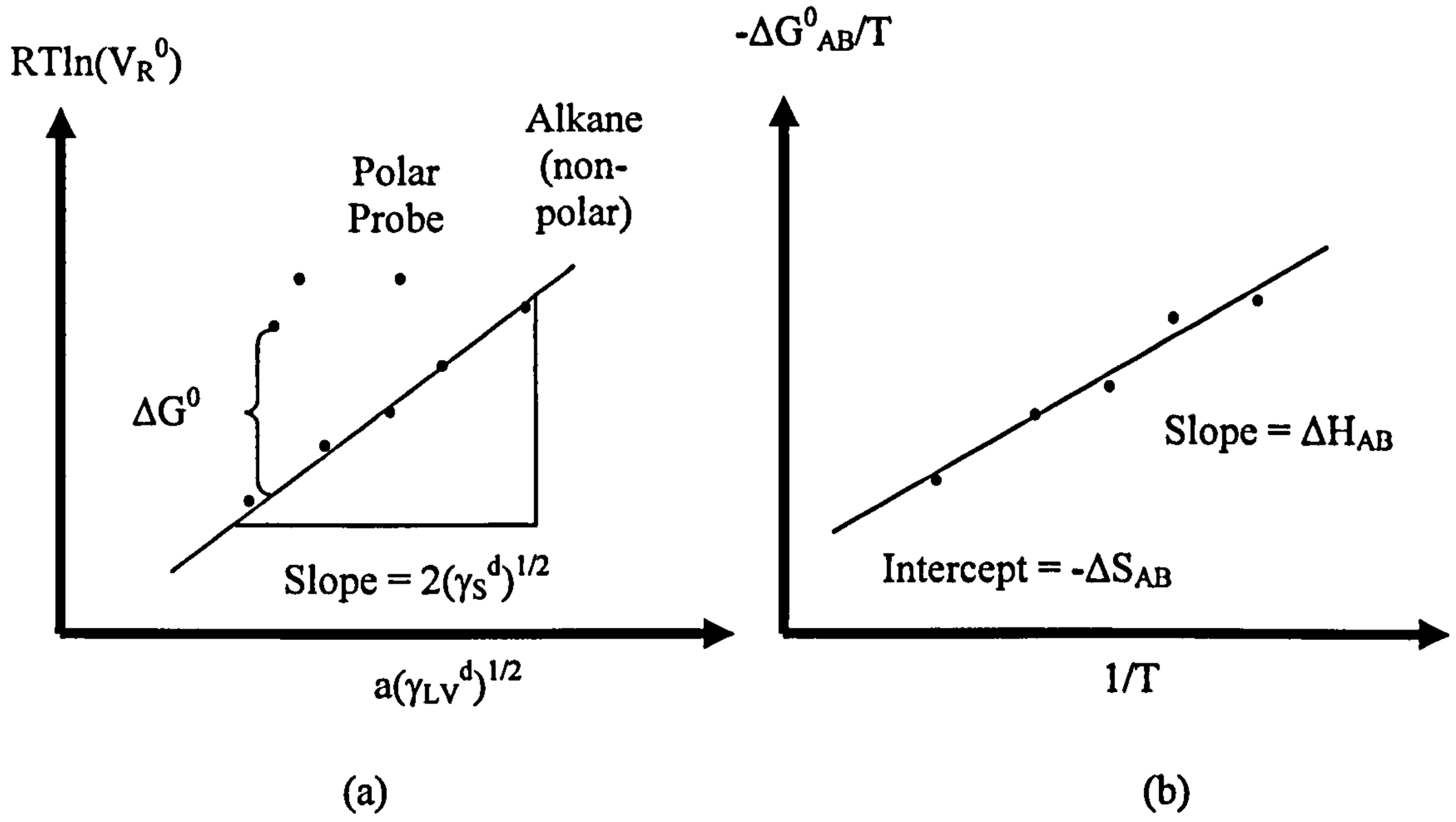
Using van Hoff's relation, the enthalpy of adsorption is obtained by the variation of experimental temperature (Figure 8.5) and is given by:

$$-\Delta H_A^o = q_d = R \cdot \frac{d \ln(K_s)}{d\left(\frac{1}{T}\right)} = R \cdot \frac{d \ln(V_R^o)}{d\left(\frac{1}{T}\right)} \tag{8.9}$$

Whereas the entropy term is given by:

$$-\Delta S_A^o = -\frac{\left(q_d + \Delta G_A^o\right)}{T} \tag{8.10}$$

Figure 8.5: (a) A typical net retention volume plot versus vapour surface property for the determination of solid surface dispersion energy and (b) determination of enthalpy of adsorption.



8.4.5 Determination of Surface Energy

The free energy of adsorption and the corresponding work of adhesion are related to the net retention volume, V_R^o, by Equation 5.8. The dispersive component of a solid, γ_{SV}^d is described by Schultz et al. and can be determined by plotting $RT\ln(V_R^0)$ versus $a(\gamma_{LV}^d)^{1/2}$ (Figure 8.5) [293]. Dorris and Gray suggested a similar approach which took into account the contribution of a methylene group in the alkane series to the free energy of desorption [342]. Surface energy results of polycarbonates using both methods were found to be very similar [343].

In the determination of γ, prior knowledge - or estimation - of vapour probe physical properties, such as the vapour pressure, boiling temperature and cross

sectional surface area of the molecule are required. Amongst these properties, the molecular cross sectional area of the adsorbed probe molecules on the solid surface is of major interest. Emmett and Brunauer proposed Equation 8.11 to estimate the cross sectional area of the adsorbate occupies based on an average cross sectional area of a molecule [344].

$$a_m = (4)\cdot(0.866)\left(\frac{M}{4\cdot\sqrt{2}\cdot N_A\rho_L}\right)^{\frac{2}{3}} \tag{8.11}$$

where a_m is the area occupied, M the molecular weight, ρ_L the density of the adsorbate with N_A the Avogadro constant.

When using polar probes such as ethanol, values of V_R^0 may be considered to consist of a dispersive as well as an acid-base component. With knowledge of γ_L^d for the polar probes used, the dispersive component of V_R^0 may be plotted. Then the difference between the $RT\ln(V_R^0)$ values obtained and the dispersive line equates to the acid-base adsorption energy contribution, ΔG_{AB}^o, as shown in Figure 8.5. By taking measurements at different temperatures, the enthalpy of adsorption can be calculated. This specific interaction of polar probes with known electron acceptor (AN) and electron donor (DN) numbers is used to evaluate the acid-base characteristics of the solid by Gutmann's equation [62]. K_A and K_B constants of the solid surface are obtained from the slope and intercept respectively of the $\Delta H_{AB}^o/AN^*$ versus DN/ AN* plot. These methods are detailed in Chapter 2.

8.5 Experimental Conditions

At infinite dilution conditions, the calculated surface energy should be independent of experimental conditions. Planinsek et al. evaluated the influence of carrier gas flow

rates and column dimensions (material, diameter, length and material) and found little effect of these conditions on the γ_{SV}^{d} of lactose and for those columns diluted with Chromosorb W [345]. They reported however, that the acid-base property was more dependent on these experimental conditions. It was further confirmed by Planinsek and Buckton that the γ_{SV}^{d} for of a range of powders with varying degrees of hydrophobicity, hydrophilicity, aqueous solubility and crystalline content were also found to be independent of packing mass or carrier gas flow rates [346], as would be expected.

The IGC can also be undertaken at specific relative humidities (%RH), with reports of the γ_{SV}^{d} for carbamazepine and paracetamol as a function of %RH [347]. Sunkersett et al. reported that γ_{SV}^{d} did not change significantly but the specific component of the free energy decreased by up to 10 % for variations of %RH. The increase in %RH was thought to have led to water molecules present competing with the polar probes to adsorb on surface sites resulting in an apparent decrease in the free energy of adsorption. This result was however probe and the material dependent, explained by the preferential interactions of each vapour probe with the solid state drug molecules.

The use of %RH was also extended to differentiate two batches of amorphous spray-dried cefditoren pivoxil samples. These samples are known to possess stability differences but these could not be distinguished by powder X-ray diffraction patterns and even had similar T_g's. By using the IGC to investigate the stability of these two samples at different %RH, Otha and Buckton showed that the two samples had different surface properties [348]. They explain their differences in physical stability from molecular orientation at the surface, which may have affected their moisture sorption mechanisms and resulted in the observed stability variations.

8.6 Determination of Properties of Crystalline Solids

8.6.1 Crystalline Forms

The IGC has been used by various workers to evaluate the variation in surface properties for various crystalline forms. Tong et al. investigated the surface property differences for two polymorphs of salmetero xinafoate (SX-I and SX-II) and a micronized SX (MSX). As expected, the milled sample possessed the highest γ_S^d of 38.3 mJ/m^2, while SX-II and SX-I forms possessed γ_{SV}^d of 28.6 and 32.5 mJ/m^2 respectively. The K_A and K_B values of the unmilled forms were however higher [349]. Although the authors tried to reason the higher γ_{SV}^d values from crystallographic structure data, they acknowledged that further molecular modelling was necessary to validate their claim.

The IGC has also been used to investigate the surface properties of DL and a βL optical forms of mannitol. Grimsey et al. found that the γ_{SV}^d and basic probes interaction values were higher for the DL form [350]. With the aid of molecular modelling, differences in densities of the dispersive and acidic sites for the DL and βL forms were observed. The acidic site concentrations of the DL and βL forms were 0.038 and 0.031 sites Å^{-2} and dispersive site concentration are 0.056 and 0.034 sites Å^{-2} respectively, in excellent agreement with the IGC interaction results.

In a similar study, the various forms of tocopherols; α, β, δ and γ which are structurally similar except for the number and patterns of methyl substituents in the phenolic ring, were evaluated by infinite dilution by IGC. The IGC was used to characterise the tocopherols in terms of dipolarity and polarizability, hydrogen bond acidity and basicity, and lipophilicity [351]. From the IGC experiments, and the Abraham equation of state, the various forms of tocopherol isomers were successfully discriminated.

8.6.2 Crystalline Habits

Crystalline solids may have characteristic shapes, influenced by the growth rates of individual facets, with the slowest growing facet being most dominant. These crystal facets are Miller indexed, depending on how the planes intersect through the crystal lattice resulting in dissimilar axes intercepts. This will very likely result in an exposure of dissimilar proportions and orientations of chemical groups, and as such may have very different surface properties. The crystal shape (commonly known as its habit) is often influenced by factors such as the crystallising solvent [352], degree of supersaturation [353] and presence of additives [270]. As such, a different shaped crystal does not necessarily indicate a different polymorph.

Several workers have investigated the dependence of ibuprofen habit on crystallisation environment [326-329]. Recrystallisation of ibuprofen from solutions has resulted in various forms of crystal shapes or habits, with higher aspect ratios of crystals from non-polar solvents but no differences were revealed from X-ray diffraction studies [325], ruling out a polymorphic conversion. Storey investigated the surface properties of ibuprofen recrystallised from methanol, acetonitrile and hexane by IGC. Both the γ_{SV}^{d} and acid-base surface properties were found to be dependent on the crystal habit [354]. These studies show that surface property variations in crystalline habits were distinguishable by IGC. The ability to measure such differences may be potentially useful as crystal habit will influence tabletting and powder flow performance.

8.6.3 Amorphous and Glass Transition

The IGC has been used successfully to distinguish the crystallinity and amorphous content of various powders, including the determination of their T_g's and several

examples are highlighted here. The reduction in particle size of crystalline materials is achieved via several methods, including milling. However, the common view is that milling may also induce amorphisation of material, especially at the surface of the particles. IGC has been used by several researchers to quantify this local disorder where bulk characterisation techniques such as X-ray diffraction, differential scanning calorimetry (DSC) and Raman or FTIR spectroscopy revealed no differences.

Newell et al. prepared three different batches of lactose; a crystalline form, a spray dried amorphous form and a ball milled form, and their surface properties were evaluated by IGC. γ_{SV}^{d} was found to be 31.2, 37.1 and 41.6 mJ/m^2 for the crystalline, amorphous and ball milled lactose respectively [242, 355]. γ_{SV}^{d} for the milled samples was higher than the fully amorphous material and the authors suggested that this could be due to the different orientation and spacing between surface molecules resulting in the different energy states. However, for a physical mix of 99 % crystalline and 1 % amorphous, γ_{SV}^{d} was 31.5 mJ/m^2. The authors argued that the mixture was a weighted average of the two components and the weighted γ_{SV}^{d} average was calculated to be 31.3 mJ/m^2. Therefore, they concluded that such an observation was evidence of an amorphous surface and a crystalline bulk for milled lactose samples.

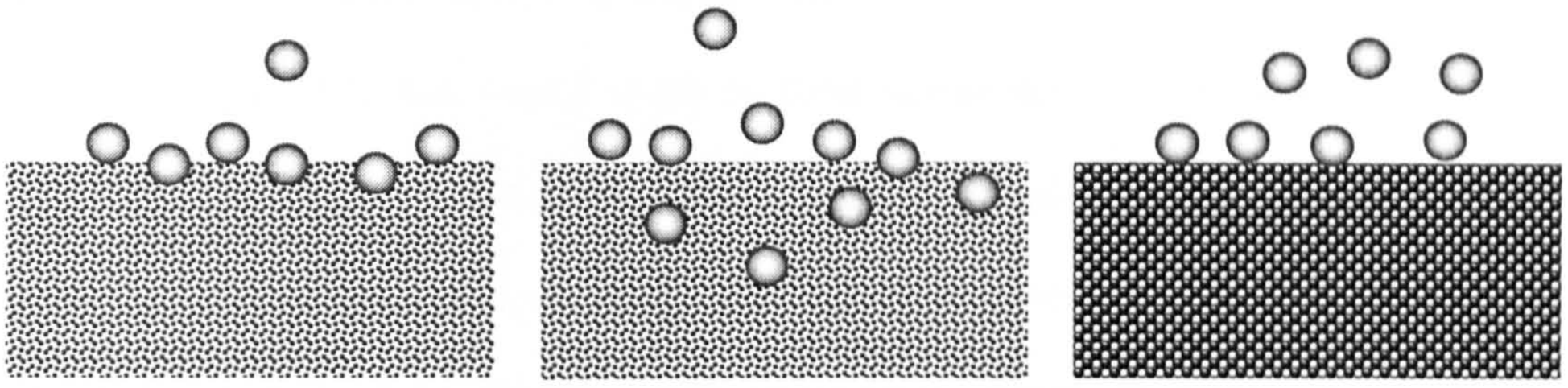
Micronised batches of salbutamol sulphate were found to possess higher γ_{SV}^{d} than unmicronised samples. The acid-base properties were slightly different, with the unmicronised samples amphoteric while the relative basicity (K_D/K_A) for the micronised sample was observed to increase. Feeley et al. attributed to the exposure of basic functional groups present at the preferred slip plane of the crystal lattice [356]. The increase in both γ_{SV}^{d} and relative basicity after milling was also observed for DL-propranolol hydrochloride. It was suggested that the increase in basicity was due to preferential cleavage along the lowest attachment facet which was rich in π-electrons

from molecular modelling [357]. They found no difference in γ_{SV}^{d} for unmilled and milled α-lactose monohydrate even after blending, but an increase in surface acidity was observed by IGC [358]. The dependence of γ_{SV}^{d}, K_A and K_B as a function of %RH for cefditoren pivoxil revealed basic surfaces with decreasing crystallinity, resulting in a direct relationship between amorphous content induced during milling being established [359].

The effects of emulsifiers, lecithin and polyglycerol polyricinoleate, on the surface properties of sucrose particles was also investigated by IGC. The γ_{SV}^{d} for jet milled sucrose was higher than for granulated sucrose, as milling is expected to create higher energy surface sites. Coatings on both jet milled sucrose and granulated sucrose revealed similar γ_{SV}^{d}, indicating a uniform change of surface properties. The emulsifier coating resulted in a decrease of surface acidity as the acid sites of sucrose were possibly masked. Differences in basicity for both coated samples were attributed to the molecular structure of the emulsifiers [360]. This study shows that IGC is capable of detecting small amounts of surface coatings.

For amorphous materials which are heated through the glass transition region, a z-shaped temperature dependant retention plot is obtained due to changes in the molecular retention mechanism above and below the T_g (Figure 8.6). In region I, retention by surface adsorption dominates while in region III where conversion to the rubbery state is complete, retention by both surface and bulk sorption mechanisms dominates. In region II, where the glassy and rubbery states coexist, the retention mechanism is a combination of surface adsorption and bulk sorption. The deviation from linearity in region 1 represents the T_g (Figure 8.7).

Figure 8.6: Sorption mechanisms of amorphous and crystalline solids.

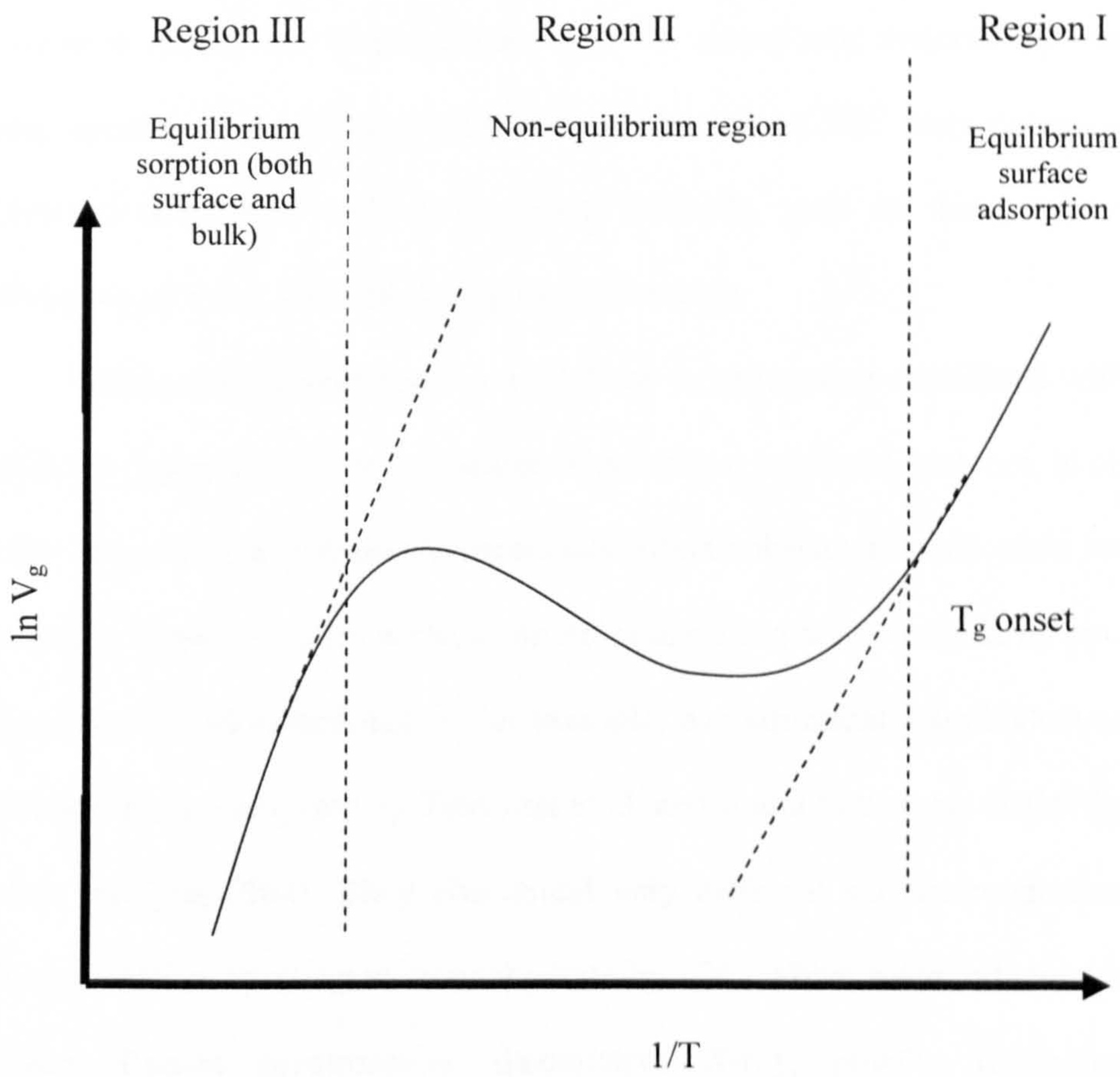


Amorphous- Glassy Solid
$T < T_g$
Surface and local bulk adsorption
Fast elution

Amorphous- Rubbery Solid
$T > T_g$
Deep bulk sorption
Slow elution

Crystalline
No T_g
Surface adsorption
Fast elution

Figure 8.7: Determination of glass transition temperature, T_g for amorphous solids [361].



Surana et al. investigated the T_g of amorphous sucrose and co-lyophilised sucrose-PVP mixtures by IGC and DSC. The T_g of the dry phase as determined by both IGC and DSC was found to be in good agreement. Under increasing relative humidities, the T_g predicted by the Gordon-Taylor equations for plasticised materials were found to be in good agreement with those determined experimentally using IGC [361]. In another study, Buckton and co-workers extrapolated the critical relative humidities and their corresponding T_g's to 0 % RH, and the T_g obtained for indomethacin was found to be in good agreement with literature values [362].

Williams and Thielmann have also reported on the use of IGC to determine the T_g of partially amorphous organic materials as a function of %RH. For a maltose sample, increasing moisture content (at higher %RH's), resulted in the predicted decrease in the T_g due to plasticisation of the amorphous material by water [363]. These authors suggested and illustrate that the use of IGC may overcome several difficulties associated with conventional methods, such as those relating to the disturbance of water sorption during sample heating.

Often, small disruptions or alterations to processing conditions will result in significant material property changes. One major industrial concern is changes in surface properties which may dramatically affect subsequent particulate handling or processing. However, such surface variations are often not detectable by conventional bulk characterisation techniques. For example, two structurally equivalent salbutamol sulphate were investigated by Ticehurst et al. and found to possess distinctly different surface energies [364]. They also found very different surface properties for four different batches of α-lactose monohydrate by IGC, which were indistinguishable by FT-laser Raman spectroscopy, quantitative X-ray, powder diffraction, DSC, thermogravimetric analysis (TGA) and surface area measurement techniques [365].

8.7 Materials and Methods

8.7.1 Materials

IGC vapour probes were generated from HPLC grade undecane, decane, nonane, octane, ethanol, acetone, ethyl acetate, acetonitrile and dichloromethane obtained from Aldrich (Poole, UK). The properties of these probes are listed in Table 8.1.

Table 8.1: Acid-Base Numbers of Probe Molecules Used in IGC

Probes	$a_m(\gamma_{LV}^d)^{1/2}$ [1] $m^2(J/m^2)^{1/2}$	DN [2] kJ/mol	AN* [3] kJ/mol
n-Undecane	1.27×10^{-19}	-	-
n-Decane	1.15×10^{-19}	-	-
n-Nonane	1.04×10^{-19}	-	-
n-Octane	9.19×10^{-20}	-	-
Ethanol	5.13×10^{-20}	79.80	43.26
Acetone	4.37×10^{-20}	71.40	10.50
Ethyl acetate	4.62×10^{-20}	71.82	6.30
Acetonitrile	3.56×10^{-20}	59.22	19.74
Dichloromethane	3.83×10^{-20}	0.00	16.38

[1] Values obtained from the SMS-iGC analysis software (version 1.2).
[2] Donor numbers according to Gutmann.
[3] Acceptor numbers according to Fowkes.

8.7.2 Preparation of Fine Crystalline Particulates

Paracetamol powder was dissolved in methanol and acetone respectively for the preparation of saturated solutions at 15 °C. These saturated solutions were then heated to 30 °C and more paracetamol was added until the solubility limit was reached. The warm solutions were then allowed to cool quickly to ambient room temperature at constant stirring rates. Seed crystals were added resulting in nucleation of a fine crystalline powder. Upon harvesting these seeds from the bulk solution, the crystals were washed in cold (4 °C) water to remove any residual solvents. The washed fractions were then decanted and dried by suction filtration. It was observed that the crystals nucleated from acetone saturated solutions favoured the formation of agglomerates as reported in literature [366]. Aspirin fine crystals from acetone solution were also prepared in the same manner. However, the use of water resulted in ibuprofen crystals forming agglomerates. The ibuprofen fine crystal fractions were washed in cold hexane followed on by the same drying procedures.

Large macroscopic crystals grown from saturated solutions of methanol and acetone were milled with a ball-mill in a porcelain pot (Pascall Engineering, Suffolk, UK) with ceramic balls for 4 hours.

All powders were then sieved for 30 minutes using a test sieve shaker through a series of stainless steel test sieves (Pascall Engineering, Suffolk, UK). Typically the following sieved fractions were obtained; 32–75 μm, 75–150 μm, 150–250 μm, 250–425 μm, 425–600 μm and >600 μm were collected for paracetamol, aspirin and ibuprofen powders. The powders were than characterised by IGC, as described in Chapter 5.

8.8 Results and Discussion

8.8.1 Dispersive Surface Energy of Milled Paracetamol Crystals

As crystalline materials are milled, resulting in a decrease in particle size, it is reasonable to postulate that the crystals will fracture along their weakest attachment energy facet. It has to be acknowledged that this will not be the only mechanism for fracture, but one would expect it to be the dominant mechanism. For paracetamol, this should result in the exposure of facet (010). The surface chemistry of facet (010) was found to be hydrophobic with a higher γ_{SV}^{d} from liquid sessile drop contact angle experiments. As such, one can expect the γ_{SV}^{d} of milled paracetamol to be inversely related to the particle size.

The γ_{SV}^{d} of two milled materials as a function of particle size are shown in Table 8.2. The increasing γ_{SV}^{d} with a decrease in particle size is observed for both sets of milled samples while γ_{SV}^{d} was independent of particle size for unmilled samples as shown in Table 8.3.

Table 8.2: γ_{SV}^{d} of Milled Macroscopic Single Crystals Grown from Saturated Paracetamol in Methanol and Acetone Solution

Particle Size (μm)	Milled Macroscopic Crystal Grown from Methanol Solution	Milled Macroscopic Crystal Grown from Acetone Solution
32 – 75	39.6	41.0
75 – 125	38.9	39.3
125 – 150	39.3	39.6
150 – 250	37.8	37.8
250 – 425	36.6	37.6
425 – 600	34.8	34.0

Table 8.3: γ_{SV}^{d} of Unmilled Single Crystals Grown from Saturated Paracetamol in Methanol and Acetone Solution

Particle Size (μm)	Single Crystals Grown from Methanol Solution	Single Crystals Grown from Acetone Solution
75 – 125	-	31.26
125 – 150	33.16	30.67
150 – 250	35.96	31.20
250 – 425	33.89	32.32
425 – 600	33.57	32.91

The growth of form I paracetamol macroscopic crystals from different solvents, methanol and acetone solution resulted in crystal different habits (Figure 4.4). However, similar (within experimental error of ± 1 mJ/m^2) γ_{SV}^{d} values are obtained for the same particle size fractions of both sets of milled samples. This indicates that as the particle size is reduced, the crystal fractures preferrentially along the weakest attachment energy facet. This fracture results in the weakest attachment energy facet to start being the dominant facet in the powder material. Indeed the γ_{SV}^{d} values obtained from IGC for the smallest milled size fractions of 39.6 and 41.0 mJ/m^2 are within experimental error, of 39.6 mJ/m^2 for γ_{SV}^{d} of the (010) faces as determined by contact angle analysis. It may thus be concluded that surface properties of the milled material are dominated by the weakest attachment energy facet with decreasing particle size. γ_{SV}^{d} is found to be independent of the starting habit of the macroscopic crystal.

It is however plausible that this increase in γ_{SV}^{d} might be due to the presence of an amorphous surface zone, as has been reported for milled lactose monohydrate. T_g of paracetamol is approximately 300K; room temperature. Therefore any

amorphous material created during milling, especially at room %RH, will have sufficient molecular mobility to crystalline quickly. As the milled samples were normally aged for a couple of weeks prior to measurements, amorphous contributions to surface properties can be safely ruled out. Thus, the increasing values of γ_{SV}^{d} were consistent with an increasing presence of the (010) facet as the particle size was reduced.

8.8.2 Dispersive Surface Energy of Unmilled Paracetamol Crystals

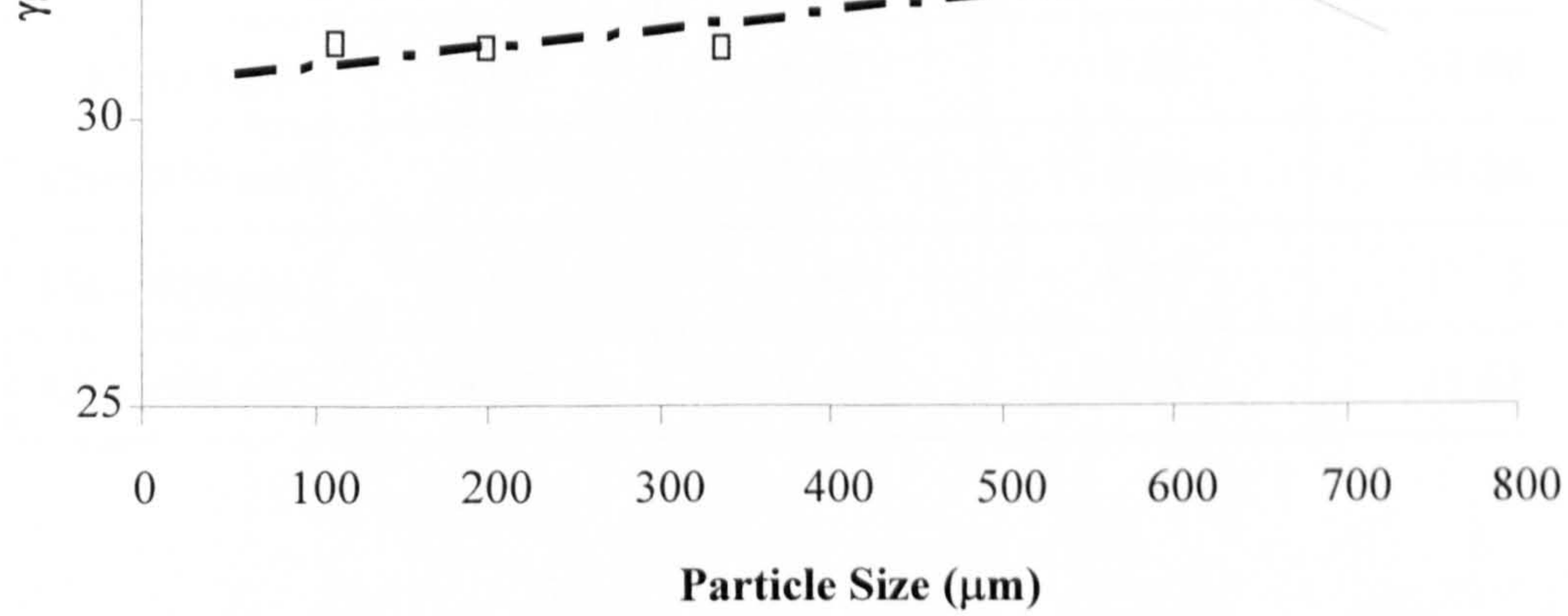
The γ_{SV}^{d} of paracetamol fine crystals grown from different solutions as a function of their particle size are shown in Table 8.3. In the case of the single crystals grown from solution, small differences in γ_{SV}^{d} are observed for crystals grown from methanol and acetone solutions. These γ_{SV}^{d} values are however very similar of those obtained by liquid sessile drop contact angle measurements on the external facets of a macroscopic single crystal. γ_{SV}^{d} of the external facets of paracetamol crystal as measured by contact angles of 31.2 mJ/m^2 [289].

Unlike the milled samples, γ_{SV}^{d} of both sets of fine crystals grown from methanol and acetone solution were found to be independent of their particle size. At all size fractions, their γ_{SV}^{d} values were lower than those of the milled samples. This reconfirms that facet (010) was not initially present in the native crystal, and it is only exposed upon milling. The variation in γ_{SV}^{d} for milled and unmilled paracetamol crystals are compared and shown in Figure 8.8.

It may appear that γ_{SV}^{d} for the unmilled crystals grown in acetone is marginally lower than γ_{SV}^{d} for the unmilled crystals grown from methanol. Furthermore, γ_{SV}^{d} for the former appears to be on the decrease with decreasing particle size. Since the variations in these values are within experimental errors, no

additional conclusions are appropriate. However, if one was to speculate, it would be suggested that these slight differences are due to the shape or habit of the crystals.

Figure 8.8: Variation in γ_{SV}^{d} for milled and unmilled paracetamol crystals as a function of particle size.



8.8.3 Acid-Base Properties of Paracetamol Crystals

The free energy of desorption, ΔG^{AB} of polar probes; ethanol, acetone, ethyl acetate and acetonitrile were obtained as described in Figure 8.5. The acid-base properties of milled and unmilled crystal fractions are found to be dissimilar. ΔG^{AB} for polar vapour probes on paracetamol crystallised from methanol and acetone are shown in Table 8.4 and Table 8.5, respectively. By comparing the values of ΔG^{AB} and the calculated acid-base numbers, a number of conclusions may be drawn.

Table 8.4: Free Energy of Desorption for Paracetamol Crystals Grown From Saturated Methanol Solution.

Sample	Free energy of desorption (kJ mol^{-1})			
	Ethanol	Acetone	Ethyl Acetate	Acetonitrile
Fine Single Crystals				
150 -250 μm	7.57	6.10	7.62	9.68
250 - 425 μm	8.68	6.60	8.17	10.30
425 - 600 μm	6.64	4.93	6.69	8.42
600 - 800 μm	6.19	5.10	6.67	7.29
Milled Macroscopic Single Crystals				
32 - 75 μm	10.45	8.13	9.94	11.79
75 -125 μm	10.08	8.12	9.79	11.49
125 - 150 μm	9.93	8.03	9.66	11.46
150 - 250 μm	9.30	7.57	8.84	11.26
250 - 425 μm	9.50	7.80	8.72	11.75
425 - 600 μm	9.33	7.69	8.83	11.61

Table 8.5: Free Energy of Desorption for Paracetamol Crystals Grown From Saturated Acetone Solution.

Sample	Free energy of desorption (kJ mol^{-1})			
	Ethanol	Acetone	Ethyl Acetate	Acetonitrile
Fine Single Crystals				
75 - 150 μm	4.95	4.58	6.23	8.22
150 -250 μm	5.86	5.18	6.80	8.36
250 - 425 μm	7.08	6.05	7.30	9.55
425 - 600 μm	7.40	6.46	7.49	9.74
600 - 800 μm	6.73	6.60	5.52	9.04
Milled Macroscopic Single Crystals				
32 - 75 μm	10.30	7.61	9.96	10.39
75 -125 μm	11.14	8.00	9.98	11.89
125 - 150 μm	10.17	7.29	9.11	10.85
150 - 250 μm	10.86	7.86	9.49	11.71
250 - 425 μm	8.17	6.35	7.91	9.79
425 - 600 μm	9.91	7.27	8.46	11.61

The acid-base numbers of milled paracetamol crystal grown from methanol and acetone solution are shown in Figure 8.9 and Figure 8.10. The K_A for milled macroscopic crystals grown from methanol solution was fairly constant with values of 0.11 for the larger fractions, increasing slightly to 0.13 with a reduction in particle sizes. Similarly, for the milled macroscopic crystals from an acetone solution, the K_A for the larger fractions was 0.10 and increasing with decreasing particle sizes until a maximum of 0.13. However, a much broader variation in the K_B was found for both samples with K_B varying from 0.12 to 0.02. The trend was less predictable in both sets of samples, but in general the K_B was lower for the smallest particle size fractions.

Figure 8.9: Acid-base numbers for milled macroscopic paracetamol crystals grown in methanol solution as a function of particle size.

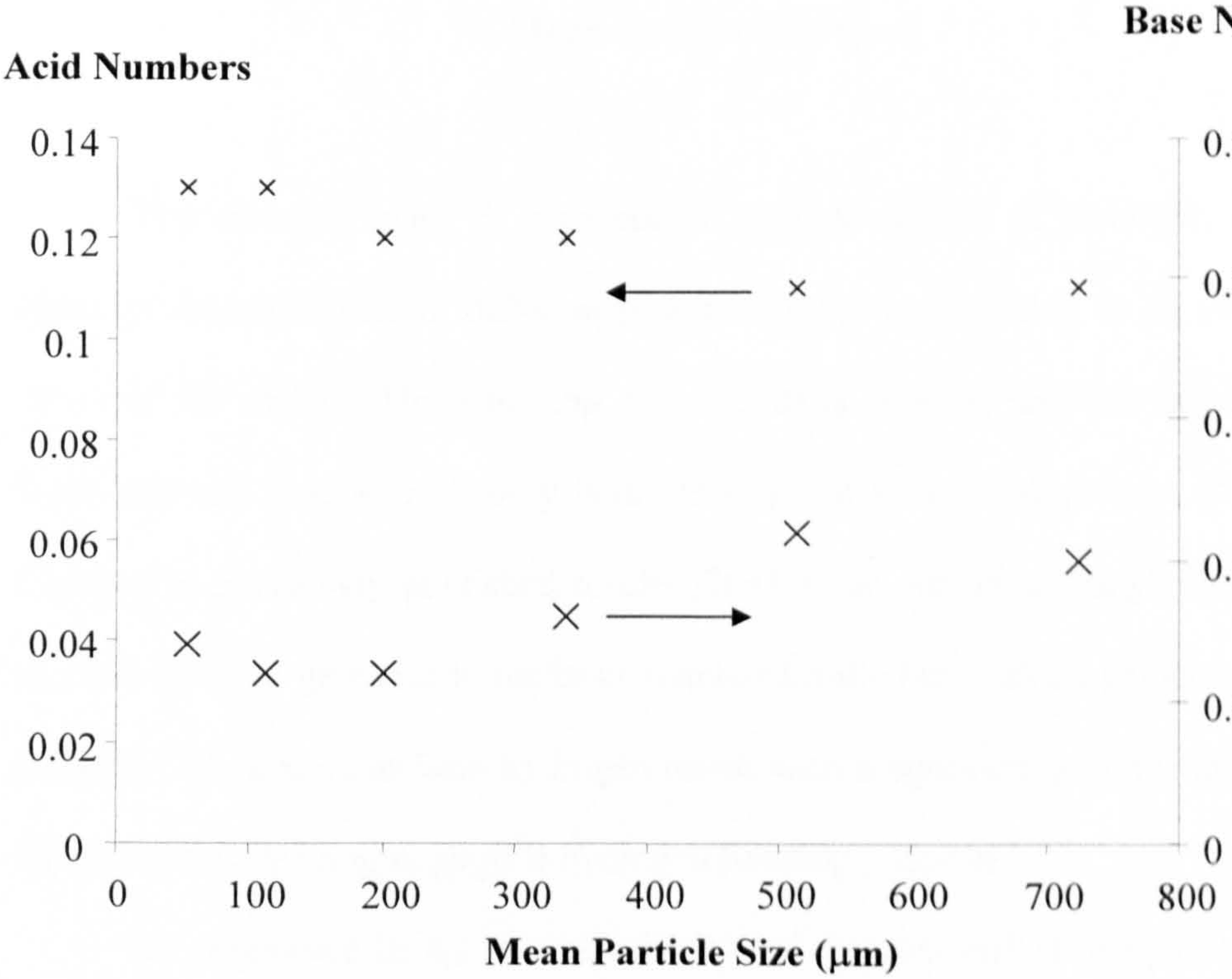
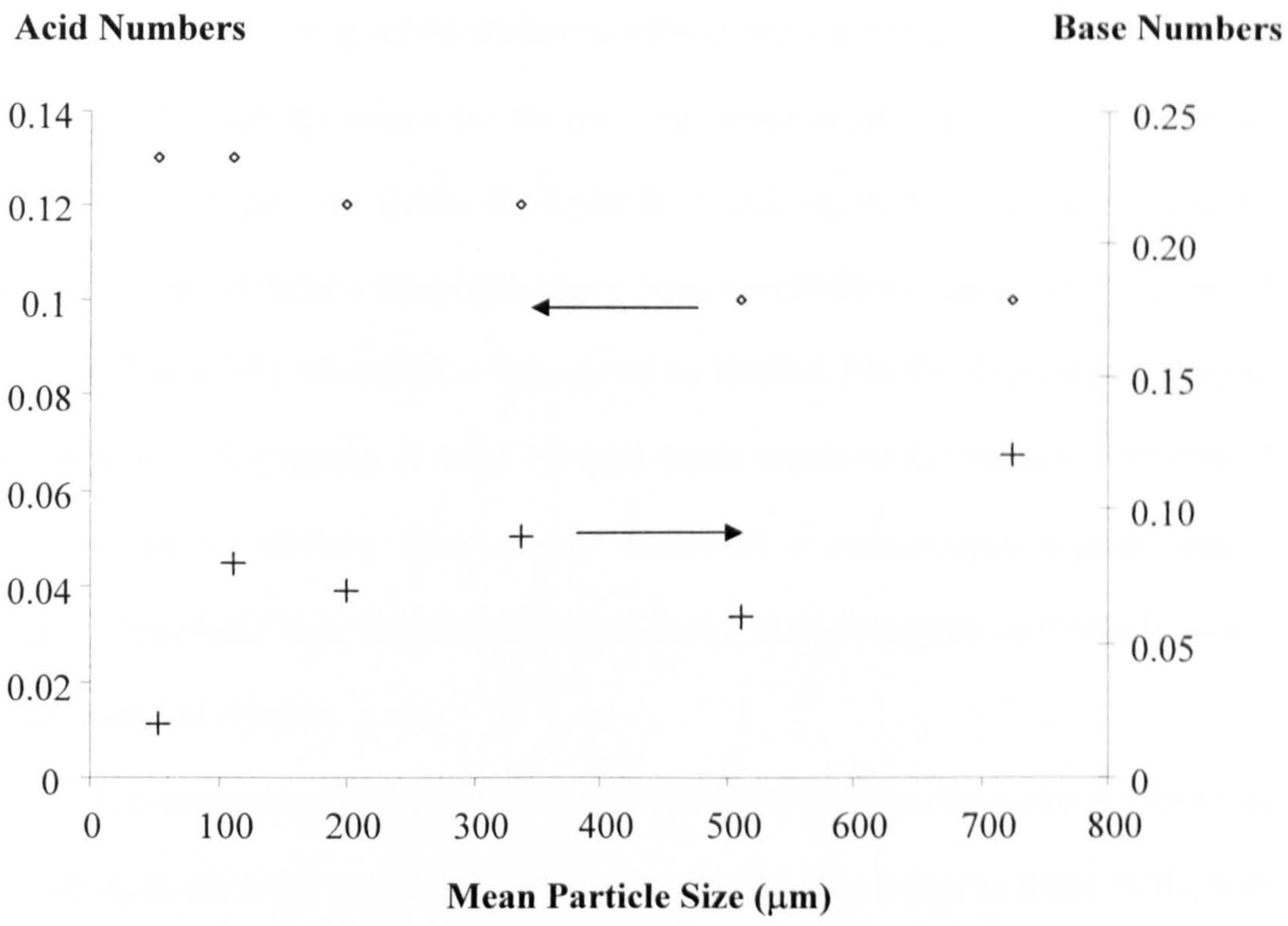


Figure 8.10: Acid-base numbers for milled macroscopic paracetamol crystals grown in acetone solution as a function of particle size.



The external facets of paracetamol crystals consist of carbonyl, amine and hydroxyl functionalities in different proportions but contributing to an overall basic nature of the surface. Upon milling, facet (010) is exposed and this facet lacks any functional end-groups, with only benzene ring moieties being present at this facet. Contrary to previously published results [204], there are no carbonyl functionalities on facet (010) to give rise to the basic nature of milled crystalline paracetamol as the phenolic OH appears to form hydrogen bonds with neighbouring amine and carbonyl functionalities, leaving negligible hydrogen bonding potential.

No difference in K_A was noted between the two milled samples confirming that milling exposes an acidic facet (010) while the variability in K_B highlights the potential importance of secondary fracture. For both sets of samples, the effect of

milling on form I paracetamol crystal is found to slightly increase the relatively acidic nature of the material. This indicates an increase in the acidic nature of crystalline paracetamol crystal irrespective of starting habit of the macroscopic crystal.

The K_A and K_B values for the unmilled single crystals grown from methanol and acetone solution are shown in Figure 8.11 and Figure 8.12. These K_A and K_B values are indicative of a marginally more basic contribution compared to the milled samples. The acidic contribution appears to be similar. For the unmilled crystals of paracetamol, it is expected that the external facets dominate the surface chemistry of the particulate materials. The external facets of a macroscopic crystal contain carbonyl functionalities, which the internal facet lacks, giving rise to the basic nature of the unmilled crystals.

The correlation between the K_A and K_B values and particle size are however less obvious, for both milled and unmilled samples. The irregular trend in K_B with decreasing particle size (for the milled samples) is thought to be due to the presence of secondary fracture mechanism of the crystal. The weakest attachment energy facet (010) will preferentially fracture when force is applied. However, as the aspect ratio of the crystal changes, the crystal may preferentially fracture along the (201) or (001) facets for example. This implies that for a crystal plate with sides of facet (010); a fracture exposing facet (201) is preferred if the slab is elongated along the b-axis or facet (001) if elongated along the c-axis. As such the dependence of K_B on particle size reduction due to milling will be harder to predict. For unmilled samples, the ratio of facet areas (crystal habit) may influence the K_A and K_B trend. The ability to map such profiles is advantageous, and is the focus of another research project within the group.

Figure 8.11: Acid-base numbers for unmilled fine paracetamol crystals grown from methanol solution.

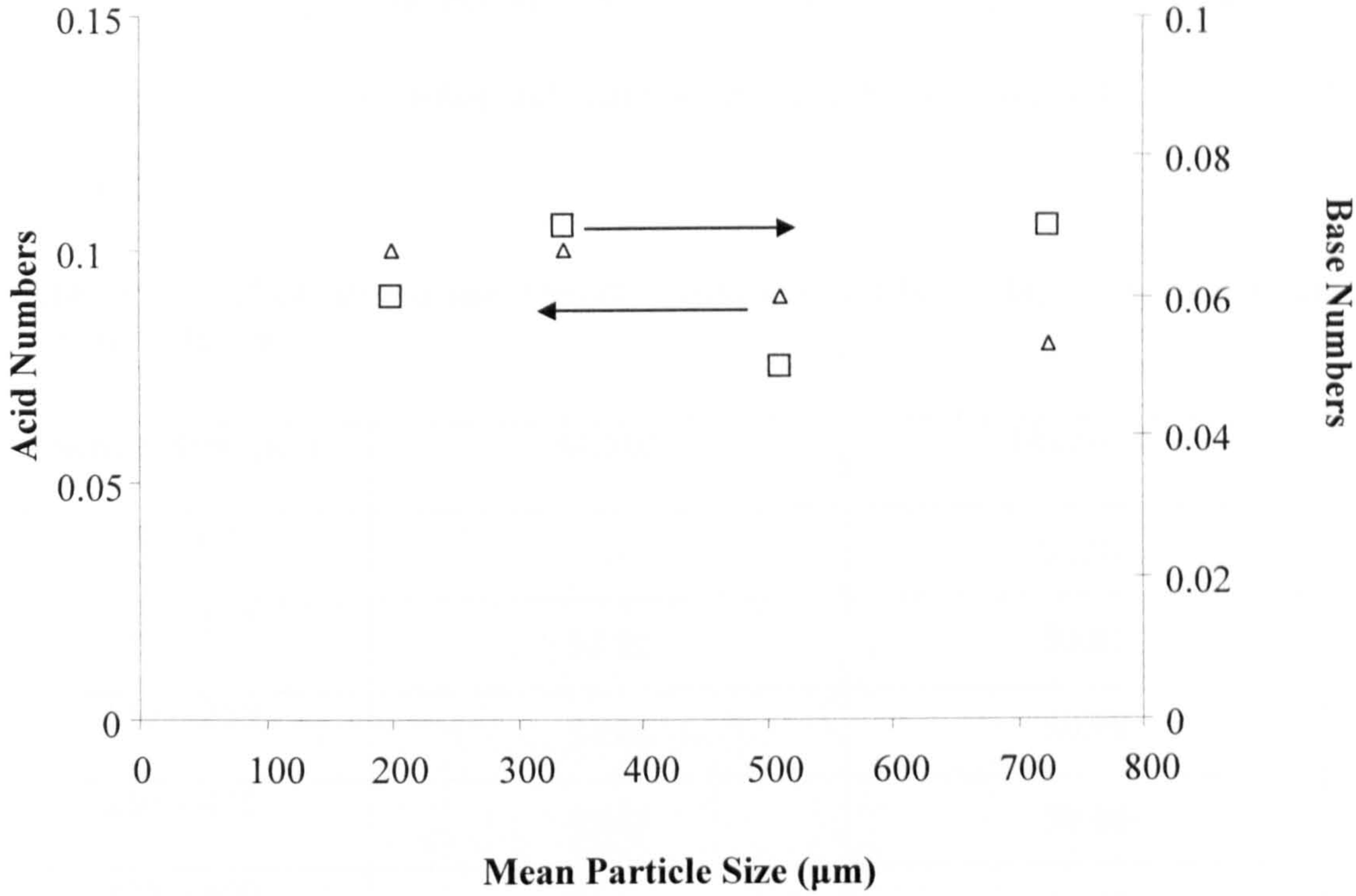
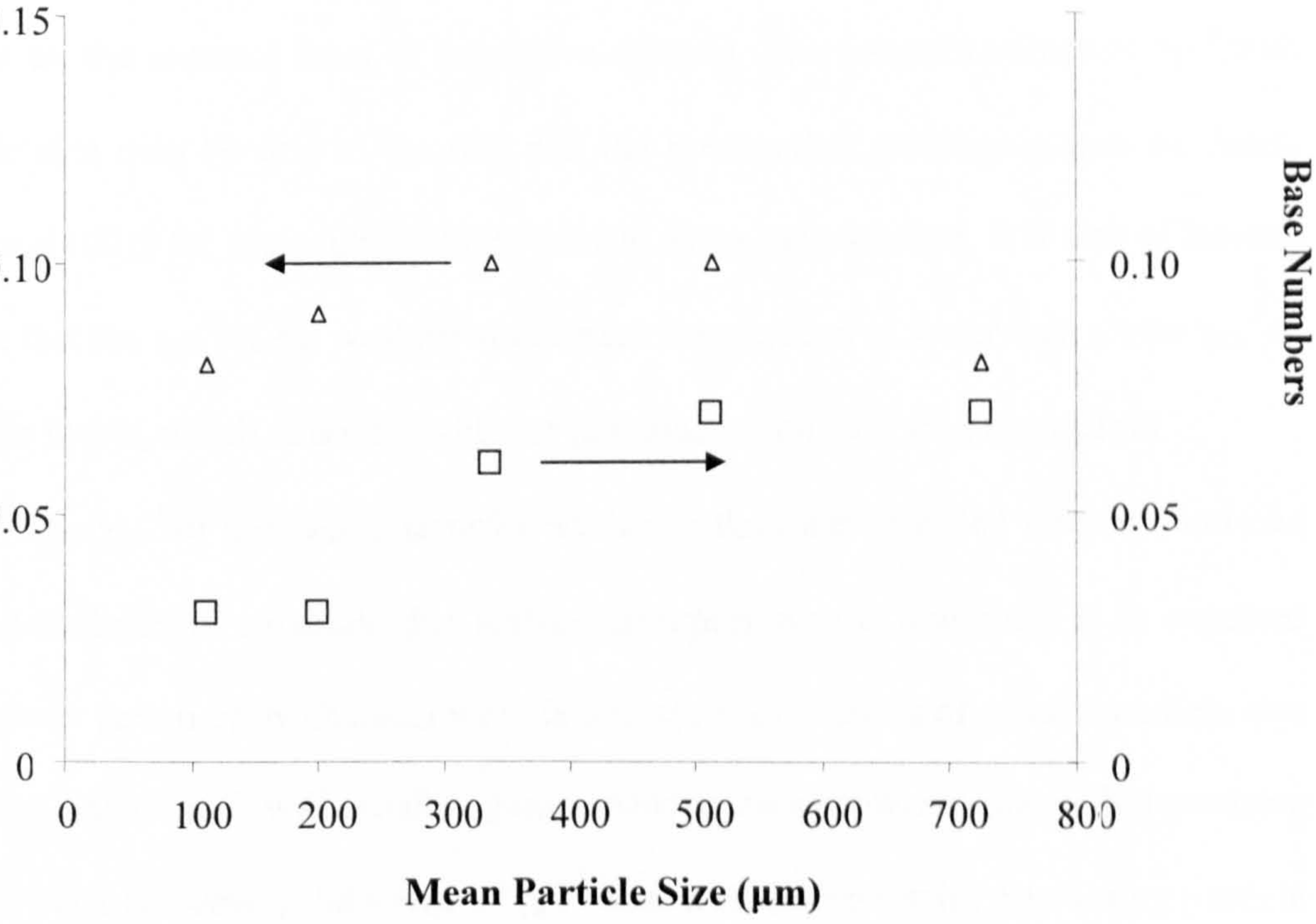


Figure 8.12: Acid-base numbers for unmilled fine paracetamol crystals grown from acetone solution.



8.8.4 Dispersive Surface Energy of Aspirin Crystals

The γ_{SV}^{d} of milled and unmilled aspirin crystals grown in acetone solution is shown in Table 8.6. For both sets, milled and unmilled samples, γ_{SV}^{d} is found to be independent of particle size.

Table 8.6: γ_{SV}^{d} of Milled and Unmilled Single Crystals of Aspirin Grown From Acetone Solution

Particle Size (μm)	Milled	Unmilled
75 – 125	-	31.81
125 – 150	34.02	30.83
150 – 250	34.43	30.99
250 – 425	35.33	30.66
425 – 600	35.37	31.47

Unlike paracetamol, the weakest attachment energy facet of aspirin crystals is present on the external facet of the native crystals. The constant values of γ_{SV}^{d} with particle size may be due to the fact that the preferential cleavage planes of, facets (100) and (001) for aspirin, is initially present as an external face. It is also of interest to note that the γ_{SV}^{d} of the weakest attachment energy facet is lower than all the γ_{SV}^{d} of all other facets, which contrasts with our previous conclusion for paracetamol.

The γ_{SV}^{d} of the milled samples are larger than the unmilled samples, and one may be inclined to conclude that surface amorphisation is dominant. It is expected that greater action of mechanical work is necessary in creating of smaller particle size fractions, and as such will possibly generate more amorphous regions with decreasing particle size. However, the value of γ_{SV}^{d} does not increase with decreasing particle

size for the milled fractions. This trend, in the case of milling of aspirin crystals, will indicate that amorphisation is not an issue.

γ_{SV}^{d} of milled aspirin crystals were found to be in the region of 35 mJ/m^2 while those of the unmilled fractions were about 31 mJ/m^2. Although one may predict that the weakest attachment energy facet be more dominant in the milled sample, this did not translate to a γ_{SV}^{d} representative of the particular facet. These results are however indicative that the surface properties of the unmilled samples are possibly dominated by the facets (001) and (100) while those of the milled fractions had contributions from facet (011) as well.

8.8.5 Acid-Base Properties of Aspirin Crystals

ΔG^{AB} for polar vapour probes on aspirin fine crystals and milled fractions are shown in Table 8.7. The K_A and K_B were evaluated without taking into account the contributions from ethanol. As ethanol is an acidic probe, and the surface properties of aspirin crystals are expected to be acidic in nature (only carboxylic functionality present at facet (011)), the interactions between ethanol probe and the crystal are rather weak and as such are susceptible to larger errors. The K_A and K_B values obtained by the Gutmann relationship are shown in Table 8.8.

Table 8.7: Free Energy of Desorption for Aspirin Fine Crystals Grown From Saturated Acetone Solution and Milled Fractions of Macroscopic Crystals

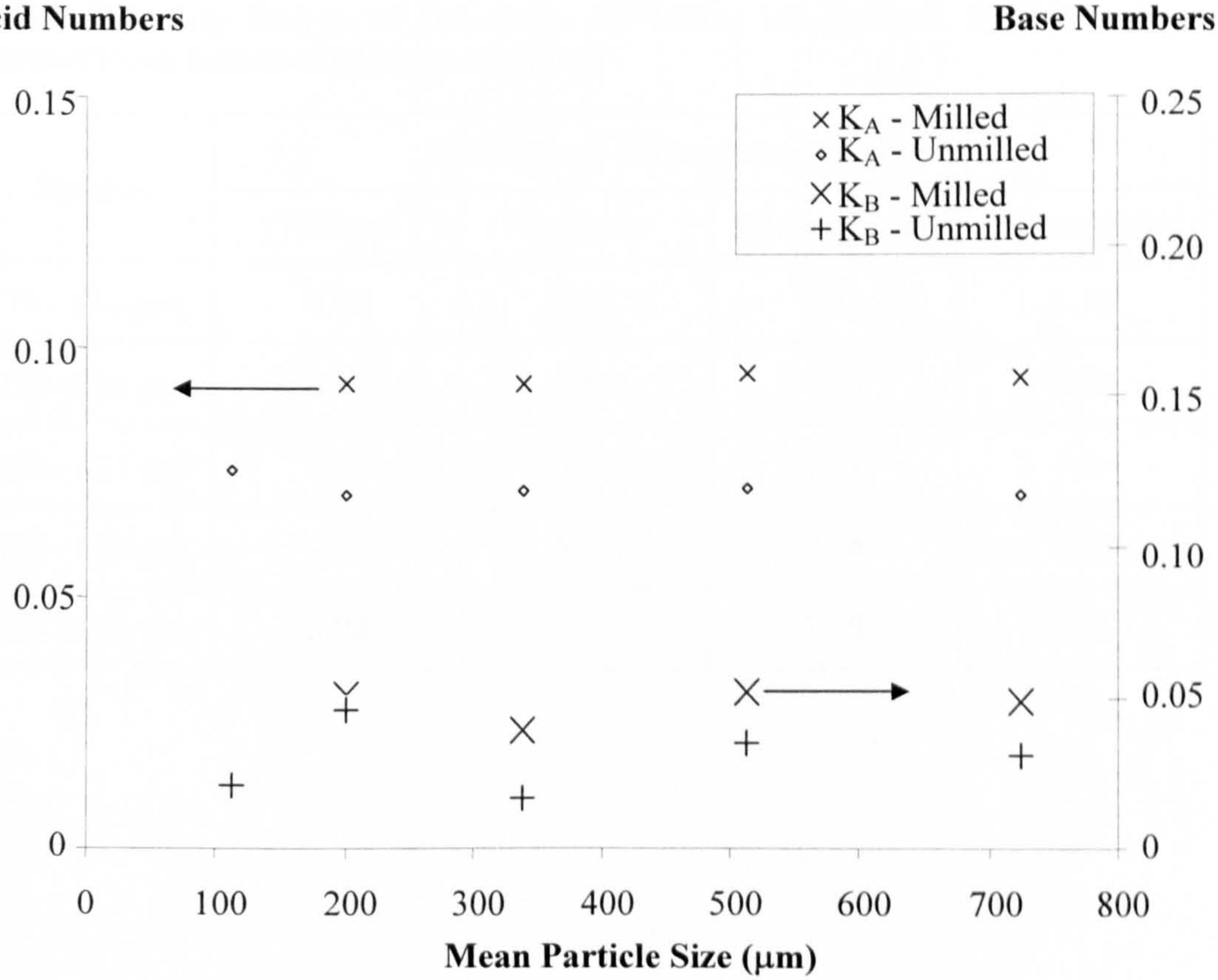
Sample	Free energy of desorption (kJ mol^{-1})			
	Ethanol	Acetone	Ethyl Acetate	Acetonitrile
Fine Single Crystals				
75 - 150 μm	3.77	3.87	6.00	6.65
150 -250 μm	3.61	3.73	5.79	6.53
250 - 425 μm	3.45	3.52	6.31	6.31
425 - 600 μm	3.83	4.09	5.82	6.61
600 - 800 μm	3.94	7.08	5.80	6.88
Milled Macroscopic Single Crystals				
150 -250 μm	5.95	5.80	7.35	7.90
250 - 425 μm	5.73	5.64	7.27	7.69
425 - 600 μm	5.93	5.94	7.48	8.03
600 - 800 μm	5.78	5.84	7.37	7.63

Table 8.8: Acid-Base Numbers for Aspirin Fine Crystals Grown From Saturated Acetone Solution and Milled Fractions of Macroscopic Crystals.

	Aspirin Acetone (Milled)		Aspirin Acetone (Unmilled)	
Sample	K_A	K_B	K_A	K_B
75 - 150 um	-	-	0.0754	0.0215
150 -250 um	0.0929	0.0519	0.0706	0.0464
250 - 425 um	0.0928	0.03985	0.0712	0.0172
425 - 600 um	0.0948	0.0525	0.072	0.03585
600 - 800 um	0.0936	0.049	0.0705	0.0309

The surface properties of specific facets of aspirin are described in detail in Chapter 6. The ester functionality ($H_3C\underline{O}(C=O)$- and $H_3CO(C=\underline{O})$-) at facet (001) and carbonyl ($H_3CO(C=\underline{O})$-) at facet (100) can contribute to hydrogen bonding potential by accepting a hydrogen bond, while on facet (011), the carboxylic acid functionality is non-dimerised and may not be fully bonded. As such, the –COOH functionality may be present at facet (011) and is able to accept and donate hydrogen bonds. It is postulated that upon milling, the facet (011) is exposed and as such reveals a slightly different surface chemistry. The exposure of this facet may have resulted in the relatively acidic nature of the aspirin milled fractions. At all particle size fractions, the K_A and K_B values of the milled samples are larger than those of the unmilled samples (Figure 8.13).

Figure 8.13: Acid-base numbers for milled and unmilled aspirin crystals.



8.8.6 Ibuprofen Crystals

The surface characteristics of ibuprofen crystals are similar to those of aspirin. The weakest attachment energy facet is also present as an external facet in the native crystal grown from acetone solution, with a γ_{SV}^{d} which is lower than all other facets (Chapter 9). However, this facet is of very low morphological importance, or may be not present if the crystal were grown from methanol. Macroscopic crystals grown from methanol were used in this study.

As in the case of aspirin, ibuprofen is thought to be relatively acidic as only the carboxylic functionality is present. The ΔG^{AB} of polar probes are shown in Table 8.9, but the ethanol value is neglected in the evaluation of the K_A and K_B values. The dispersive energy and K_A and K_B surface properties as obtained by the IGC technique are shown in Table 8.10.

Table 8.9: Free Energy of Desorption for Milled Macroscopic Ibuprofen Crystals Grown From Saturated Methanol Solution

Sample	Free energy of desorption (kJ mol^{-1})			
	Ethanol	Acetone	Ethyl Acetate	Acetonitrile
75 - 150 μm	4.98	5.63	7.32	8.18
150 -250 μm	4.94	5.64	7.39	8.30
250 - 425 μm	4.71	5.27	7.11	7.99
425 - 600 μm	4.66	5.25	7.14	8.00
600 - 800 μm	5.04	5.60	7.50	8.31

Table 8.10: Surface Properties of Milled Ibuprofen

Sample	γ_{SV}^{d}	K_A	K_B
75 - 150 um	37.75	0.0909	0.0642
150 -250 um	38.30	0.0916	0.0654
250 - 425 um	38.29	0.0882	0.0578
425 - 600 um	38.18	0.0888	0.0542
600 - 800 um	39.55	0.0937	0.0582

Upon milling of the macroscopic crystal of ibuprofen, it is postulated that the weakest attachment energy facet will become dominant as particle size reduces. This point is evident from the slight reduction in γ_{SV}^{d} as particle size is reduced. This is in contrast with results for milled paracetamol fractions and neither supports the notion of amorphisation. Clearly, such a trend is a manifestation of the surface properties of the facets present. In the case of macroscopic ibuprofen grown from methanol solution, facet (100) is not initially present. Although facet (100) has the lowest γ_{SV}^{d} values, its dominance as particle size is reduced is apparent.

The acid-base properties indicate that ibuprofen is acidic. However, a slight decrease in K_A is noted while K_B increases marginally as particle size is reduced. This trend can be attributed to the presence of the carboxylic functionality on facet (011) and indicative of the increased dominance of facet (100) upon milling.

8.9 Conclusions

The surface energetics of milled crystalline paracetamol was representative of the weakest attachment energy facet, being more dispersive in nature confirming the dominance of the weakest attachment energy facet with decreasing particle size. γ_{SV}^{d} of milled materials were also found to be independent of starting macroscopic crystal habit. In unmilled single crystals, γ_{SV}^{d} was lower compared to the milled samples and representative of the energetics of the external facets of a single crystal. These were in good agreement with contact angle measurements by liquid sessile drop methods.

The exposure of the weakest attachment energy facet during the milling of macroscopic crystals gave rise to an acidic nature of milled materials. K_A of the milled materials was found to be fairly consistent while K_B may be indicative of the secondary fracture of the crystalline material. An overall increase in the relative acidity was found due to milling, as a change in surface functionalities is proposed when the dominance of external facets are replaced by the (010) facet. In unmilled paracetamol crystal, the presence of carbonyl functionalities on the external facets contributed to the basic character. The habit of planar crystals with dominant (201) facets was seen to be more basic than the prismatic crystals.

In the case of aspirin crystals, γ_{SV}^{d} of both milled and unmilled fractions were independent of the particle size fractions. This tendency is due to the presence of the weakest attachment energy facet as an external facet of the native crystal. Furthermore, γ_{SV}^{d} of the milled fractions were higher than those of the unmilled fraction, possibly due to the secondary fracture mechanisms exposing facet (011). Milling also resulted in the slightly greater acidic nature for these samples. It is not thought that the presence of any amorphous regions contributed to the values obtained. However, this trend is attributed to the dominance and distribution of the

various crystalline facets in the native crystals and in the milled fractions, illustrating the importance of the surface chemistry.

The γ_{SV}^{d} of milled ibuprofen samples (grown from methanol) decreased slightly with decreasing particle size. This illustrates further that the weakest attachment energy facet will dominate as particle size is reduced. However it may be harder to predict the trend exactly as starting habits, location of weakest attachment energy facets and fracture mechanisms are all thought to be contributing factors to the final surface exposed.

Overall, the effect of milling is found to expose a hydrophobic surface, which may have serious implications to following manufacturing processes such as wet granulation. The IGC is found to be a robust technique, sensitive to very small variations in surface properties of crystalline materials.

CHAPTER 9 DISCUSSION

9.1 Surface Energy Evaluation

In this chapter the contact angle data has been analysed using both the classic Owens-Wendt [49] polar approach as well as the more recent acid-base approach suggested by van Oss and co-workers [50]. The use of the older Owens-Wendt analysis was to facilitate the subsequent comparison between wettability and XPS data (Chapter 7). The theoretical basis of these analyses and other semi-empirical relations for determination of surface energies has been recently reviewed in detail [297] and was reported in Chapter 2.

9.1.1 Paracetamol Form I and Form II

The calculated surface energy data for form I paracetamol, obtained using both of these approaches are summarised in Table 9.1 and Table 9.2. Both approaches indicated similar trends in the surface energies of the various external facets, with the dispersive components being marginally different on each facet of the macroscopic crystal but the polar and acid-base components varying significantly. Both the dispersive and the polar/acid-base components results for the cleaved facet (010) were at variance with those obtained for the external surfaces. The crystallographic structure for form I is shown in Figure 4.1.

The surface composition by XPS is reported in Chapter 7, and the surface polarity is calculated based on the ratio of the intensities of the polar components to the total intensity. The surface energy polarity is calculated as the ratio of the polar component, γ_{SV}^{p} to the total solid surface energy, γ_{SV}^{T}. Although no direct relationship

between XPS intensity and surface energy is presently available, this convention serves merely as a qualitative comparison. It is seen that this convention directly correlates the XPS polarity with the polarities based on the wettability measurements Figure 9.1.

Table 9.1: Results of Surface Energy for Paracetamol Using the Classical Owens-Wendt Approach

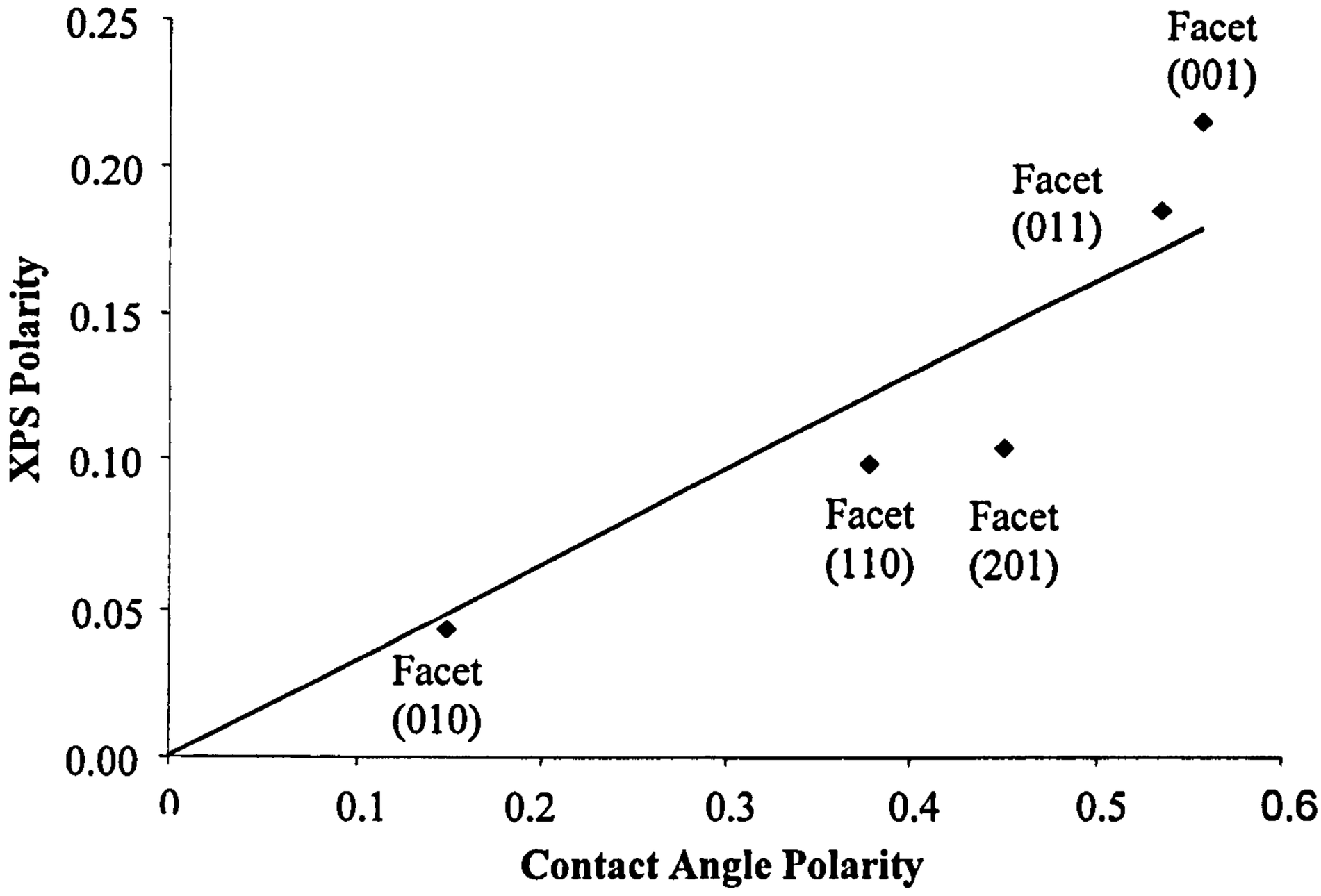
Facet	γ_{sv}^{d}	γ_{sv}^{p}	γ_{sv}	$\gamma_{sv}^{p}/\gamma_{sv}$
External Facets of Form I Paracetamol Crystals				
(201)	33.5	27.6	61.2	0.45
(001)	30.5	38.4	68.9	0.56
(011)	28.0	32.2	60.3	0.53
(110)	32.8	19.9	52.7	0.38
Internal Facets of Form I Paracetamol Crystals				
(010)	39.5	6.9	46.4	0.15

Table 9.2: Results of Surface Energy for Paracetamol by the van Oss et al. Acid-Base Approach

Facet	γ_{sv}^{LW}	γ_{sv}^{+}	γ_{sv}^{-}	γ_{sv}^{AB}	γ_{sv}
External Facets of Form I Paracetamol Crystals					
(201)	34.9	3.6	30.5	20.9	55.9
(001)*	34.9	2.8	49.2	23.4	58.2
(011)	34.5	1.5	46.6	16.8	51.4
(110)	34.9	2.5	22.4	15.1	50.0
Internal Facets of Form I Paracetamol Crystals					
(010)	45.3	0.02	12.9	1.0	46.2

* Calculation of acid-base property was performed with the assumption that $\theta_a \approx 0^\circ$ for formamide probe liquid.

Figure 9.1: Surface polarity of paracetamol crystalline facets determined by XPS and contact angle measurements.



In the following section we provide a simple quantitative analysis based on the paracetamol crystallographic structure. Table 9.3 gives information on the form I unit cell for paracetamol, as well as estimated "free" surface group concentrations for the hydroxyl groups. The concentration of "free" or non-hydrogen bonded hydroxyl groups has been estimated by examining molecular configurations for the individual crystal facets via the Mercury software, and estimating the number of "free" hydroxyl groups per unit area for each facet. Each hydroxyl group was examined and a decision was made as to whether the group was "free" and thus sufficiently labile to interact with a liquid for example, or not. In the case of a hydroxyl group fully engaged in hydrogen bonding, that is behaving as both an electron donor (O) and as an electron acceptor (H), then the hydroxyl group was considered to be not labile and was not counted in the "free" hydroxyl group concentration. In the case where it was free to act as either a hydrogen bond donor or acceptor or both, it was considered to be labile

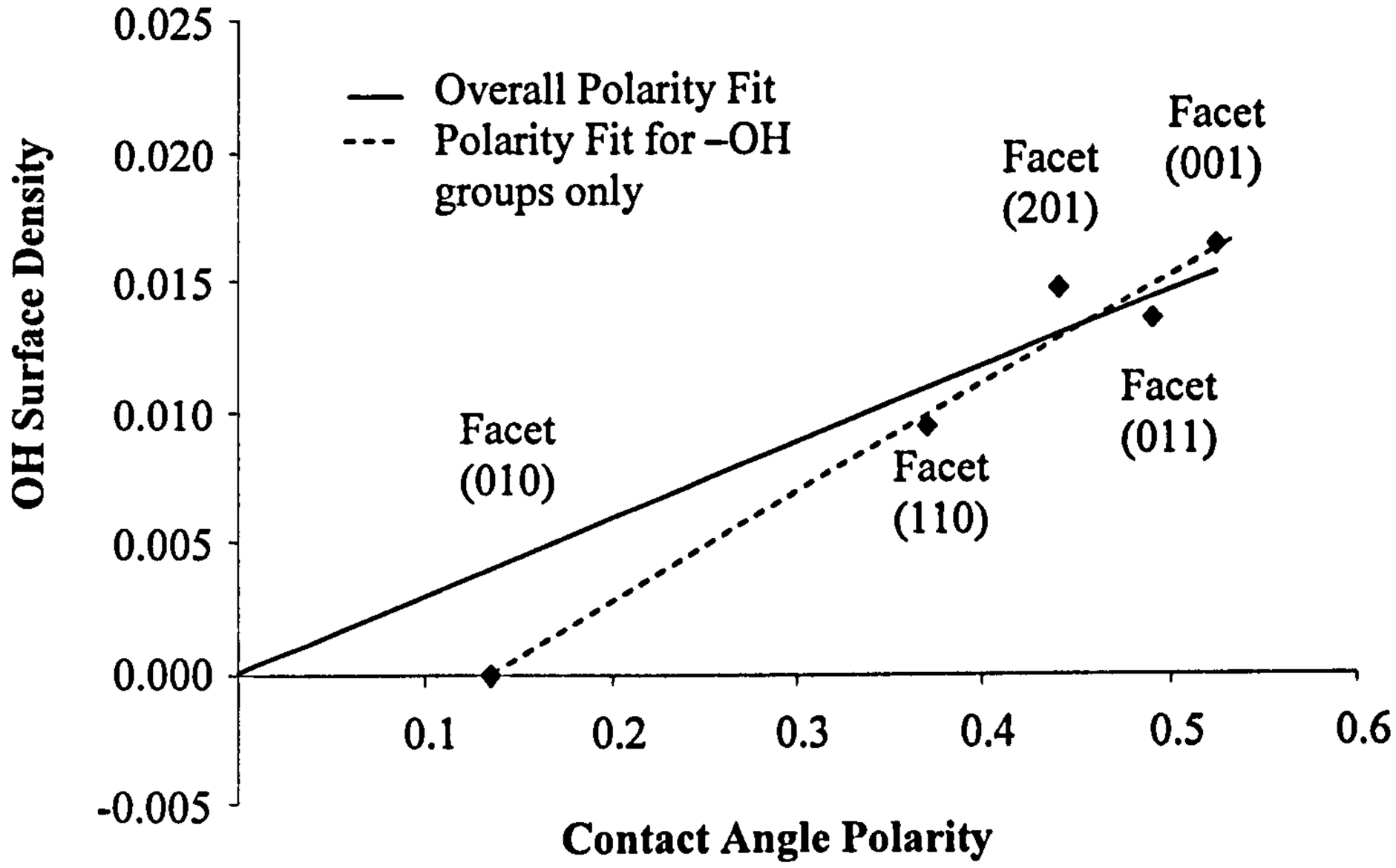
and such groups were counted as a part of the "free" hydroxyl group concentration. Though this classification is rudimentary, it does provide a first order estimation of potential contributions of hydroxyl groups to the surface chemistry of paracetamol facets. Table 9.3 shows that the number of hydroxyl groups per unit cell area free to interact with an external medium varies significantly from facet to facet.

Table 9.3: Unit Cell Information for Form I Paracetamol and Predicted Free Hydroxyl Group Surface Concentrations

Facet	Unit Cell Length (Å)	Unit Cell Depth (Å)	Unit Cell Angle (°)	Unit Cell Area ($Å^2$)	No. free OH Groups	OH Group Density ($Å^{-2}$)
(201)	14.44	9.4	90	135.7	2	0.0147
(001)	12.93	9.4	90	121.5	2	0.0165
(011)	11.78	12.93	74.74	146.9	2	0.0136
(110)	15.99	7.1	69.31	106.0	1	0.0094
(010)	12.93	7.1	64.1	82.59	0	0.0000

In Figure 9.2 we can see a good first order correlation between the surface polarity as given by the contact angle based surface energy analysis, and the predicted "free" OH surface group concentrations. Thus, we may conclude the wettability of these crystal faces is directly linked to the number of hydroxyl groups present on the crystal surface. This result, though intuitive, has not been previously reported for organic crystalline solids.

Figure 9.2: Comparison between contact angle polarity and predicted free OH surface group concentration for various facets of form I paracetamol.



This correlation is however based on a first order analysis with a number of limitations. The surface chemical contributions of the amide and carbonyl groups are considered to be much less significant than those of the hydroxyl groups due to both the relatively high acidity and basicity of the hydroxyl groups compared to amide groups, as well as their amphoteric nature. The orientation of the hydroxyl groups at the crystal surface as well as their molecular accessibility are also not considered in this calculation.

The predicted surface hydroxyl group density based on crystallographic data and contact angle measurements were in good agreement. It is concluded that, the facet specific wettability of paracetamol was significantly determined by the number of hydroxyl groups present on the surface (Figure 9.2).

The acid-base approach was also used to evaluate surface energy components for facets (201), (011), (110) and (010). For calculating the acid-base properties of facet (001), θ_a with formamide was assumed to be zero. The properties as calculated

by van Oss et al. scale are shown in Table 9.2, and the surface energies calculated by the Della Volpe scale are shown in (Table 9.4). The acid-base surface energy components by the van Oss et al. scale often over estimate the surface basicity [73]. The choice of water as a reference with the ratio of the acid part, γ^+ to the basic part, γ^- equal to unity has been criticized and other ratios are proposed assuming that water is more acidic in nature [58]. It is outside the scope of this thesis to comment on the choice of ratios, and these will not be discussed here. This analysis shows that the surfaces are predominantly basic (electron donor). However, the ratio of acidity to basicity depends on the probe liquid scales used [58]. Although acid-base theories provide the most detailed information about the composition of a surface, no conclusion can be reached. This model may be potentially useful but further work is still needed.

Table 9.4: Results of Surface Energy for Paracetamol by the Della Volpe Acid-Base Approach

Facet	γ_{sv}^{LW}	γ_{sv}^{+}	γ_{sv}^{-}	γ_{sv}^{AB}	γ_{sv}
External Facets of Form I Paracetamol Crystals					
(201)	35.5	1.8	19.9	11.8	47.4
(001)*	34.8	1.4	29.1	12.9	47.7
(011)	34.6	1.5	24.3	12.2	46.2
(110)	35.8	1.8	14.0	10.0	45.8
Internal Facets of Form I Paracetamol Crystals					
(010)	45.6	0.0	5.2	0.2	45.8

* Calculation of acid-base property was performed with the assumption that $0_a \approx 0^0$ for formamide probe liquid.

Facets (201), (001) and (011) have similar functional group contributions and the slight differences may be due to the differences in densities of the functional groups and their orientation at the surface. The polarity on facet (110) was lower than all other external facets although amine, carbonyl and hydroxyl functionalities are present, but may not be free to interact with external molecules. These differences may give rise to different interactions. This trend was further confirmed by dissolution kinetics experiments by Prasad et al. [367], who reported similar dissolution rates observed for facets (201), (001) and (011) but different rates for facet (110).This indicates that dissolution may well be thermodynamically controlled, and that surface energies give similar trends to those based on solubility of crystalline facets. This observation confirms the importance of thermodynamic descriptions for these materials.

Surface energies calculated from the θ_a with the component approaches indicated relatively high polar component contributions on facet (201), (001) and (011). The polar component on facet (110) was lower, indicating that specific interactions of probe liquids with the surface were limited. Surface energy of the cleaved facet (010) confirms that the surface is hydrophobic and may not possess any potential for hydrogen bond formations.

The surface energies of form II paracetamol were evaluated with the Owens-Wendt approach and are shown in Table 9.5. γ_S^d for the weakest attachment energy plane, facet (001) was also found to be higher than the other facets. For the case of form I paracetamol crystals, the facet (010) was an internal facet not available in the native crystal. One may suggest that the lower values of γ_S^d for form I external facets were due to contamination. However, the same trend was observed for form II, thus it is suggested that this is a real intrinsic property of the material. It is further suggested

that a higher density of methyl groups is responsible for this behaviour, but this analysis requires further work to confirm this viewpoint.

Table 9.5: Results of Surface Energy for Form II Paracetamol by the Owens-Wendt Approach

Facet	γ_{sv}^{d}	γ_{sv}^{p}	γ_{sv}	$\gamma_{sv}^{p}/\gamma_{sv}$
(110)	33.4	38.5	71.9	0.54
(010)	32.2	38.9	71.1	0.55
(001)	42.3	9.5	51.8	0.18

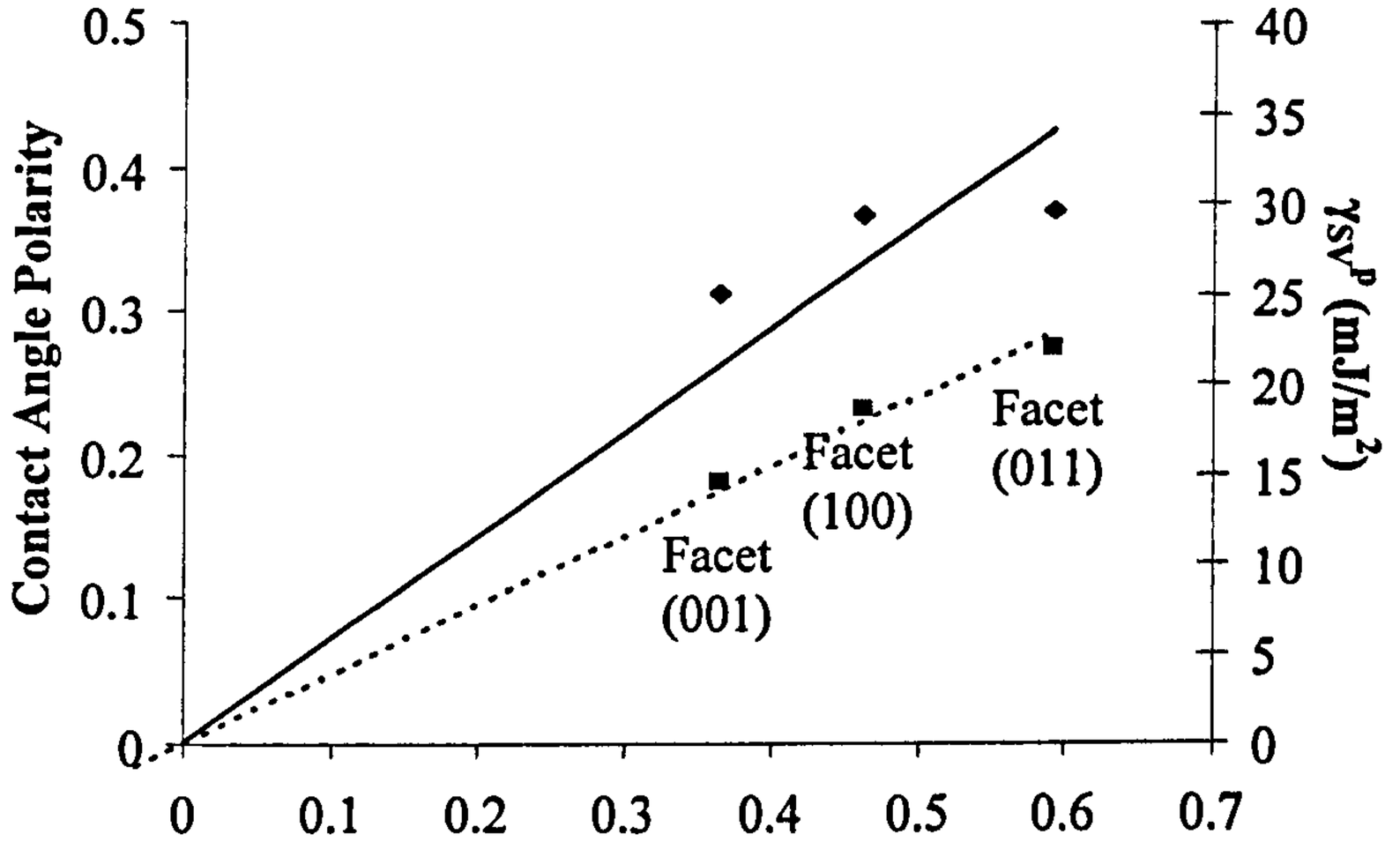
9.1.2 Aspirin

The surface energy of various facets of aspirin single crystals has been calculated by the components approach and the results are shown in Table 9.6. The γ_S^{d} was found to vary slightly with varying facets, while the polar contribution to the surface energy, γ_S^{p} on facet (001) is just under 50% that of facet (011). Differences in polar energy components were reflective of the crystalline surface chemistry, indicative of the contributions from various functional groups. The polarity based on surface energies were found to be in good agreement with those determined by XPS (Chapter 8) and is shown in Figure 9.3.

Table 9.6: Results of Surface Energy for Aspirin by the Owens- Wendt Approach

Facet	γ_{sv}^{d}	γ_{sv}^{p}	γ_{sv}	$\gamma_{sv}^{p}/\gamma_{sv}$
(001)	32.4	13.8	46.2	0.2987
(100)	32.5	18.6	51.1	0.3640
(011)	37.2	22.7	59.9	0.3790

Figure 9.3: Surface polarity of aspirin facets based on surface energies and XPS analysis.



The scales proposed by both van Oss et al. and Della Volpe and Siboni gave a similar trend with facet (011) being less basic than both facets (001) and (100) (Table 9.7and Table 9.8), although (011) was found to be the most polar facet. The ratio of $\gamma^+:\gamma^-$ is indicative of the acidity and basicity of a surface, and is commonly used for such comparisons.

Table 9.7: Results of Surface Energy for Aspirin by the van Oss et al. Acid-Base Approach

Facet	γsv^{LW}	γsv^{+}	γsv^{-}	γsv^{AB}	γsv
(001)	36.1	0.0	25.1	1.9	38.0
(100)	36.3	0.1	32.8	3.4	39.7
(011)	40.1	0.6	35.0	9.0	49.1

Table 9.8: Results of Surface Energy for Aspirin by the Della Volpe Acid-Base Approach

Facet	γsv^{LW}	γsv^{+}	γsv^{-}	γsv^{AB}	γsv
(001)	35.6	1.14	8.1	6.1	41.7
(100)	35.4	1.9	10.6	9.0	44.4
(011)	39.1	3.3	12.2	12.6	51.7

Facet (011) was found to be more acidic than both facets (001) and (100) due to a surface preferentially exposing the carboxylic acid functionality. The –OH of the carboxylic group is a reliable hydrogen bond donor while the C=O is a reliable hydrogen bond acceptor and the ether portion of the ester group is an occasional hydrogen bond acceptor [18]. Only on facet (011) is the hydroxyl group present as a potential donor, thus giving rise to the acidity of the facet. Facets (001) and (100) do not possess any hydrogen bond donors and as such are relatively more basic than facet (011). The potential of donating or accepting hydrogen bonds on various facets is dissimilar and is reflected by the differences in surface acidity and basicity. The hydrophobicity of facet (001) reflects the reduced accessibility of surface acid, ester and hydroxyl groups and concomitant exposure of the aromatic aspirin backbone.

9.1.3 Ibuprofen and S-(+)-Ibuprofen

The calculated surface energy by the classical Owens-Wendt analysis is shown in Table 9.9 for racemic ibuprofen crystals. Facets (100) and (001) possessed almost identical polar surface energy, albeit facet (100) marginally less. On the other hand, facet (011) is about twice as polar, confirming the presence and contribution of the carboxylic functionality at the specific surface. These values will be compared to the values calculated for S-(+)-ibuprofen reported in the following section.

Table 9.9: Results of Surface Energy for Racemic Ibuprofen Analysis Using the Classical Owens-Wendt Approach

Facet	γ_{sv}^{d}	γ_{sv}^{p}	γ_{sv}	$\gamma_{sv}^{p}/\gamma_{sv}$
(100)	36.7	5.1	41.8	0.122
(001)	41.1	7.7	48.8	0.157
(011)	42.0	18.9	60.9	0.310

The calculated surface energy for S-(+)-ibuprofen is shown in Table 9.10. The total surface energies of both facets (100) and (001) also appear to be almost identical, as in the case of racemic ibuprofen, with only small differences in both the dispersive and polar components. Facet (100) is only slightly (0.5 mJ/m^2) more energetic than facet (001), well within experimental errors. Nevertheless, if either of the facets were found to be the weakest attachment energy, this again supports the notion that this face will be the most hydrophobic facet. Interestingly, facet (110) is also about twice as polar, confirming the presence and contribution of the carboxylic functionality to the specific properties.

Table 9.10: Results of Surface Energy for S-(+)-Ibuprofen Analysis Using the Classical Owens-Wendt Approach

Facet	γsv^d	γsv^p	γsv	$\gamma sv^p/\gamma sv$
(100)	43.7	6.0	49.7	0.121
(001)	40.4	9.8	50.2	0.196
(110)	39.8	19.0	58.8	0.322

Although the surface energetics for racemic ibuprofen and S-(+)-ibuprofen are very similar, the biggest difference is found in θ_a for diiodomethane. If a comparison is made between the facets (100) for both forms, a difference of about 15 ° is noted with S-(+)-ibuprofen possessing higher dispersive energies. However, θ_a of diiodomethane for facets (100) and (011) for the racemic form and facets (100) and (110) for the S-(+)-ibuprofen all agree within the experimental errors. This result is in good agreement with computed crystal lattice energies of both these ibuprofen forms. The force fields of Mayo and Gavezzotti [324] were indicative that the van der Waals term contributes more in the packing energy of S-(+)-ibuprofen crystal compared to the racemic form. Although the results of the computational methods correlate well

with experimental contact angle measurements (for that of the weakest attachment energy facet), it may be premature to conclude that the crystal lattice energies may be directly applicable to predict wetting behaviours. This has been demonstrated earlier that the γ_s is not only reflective of whether a functional group is present, but also if this functional group can participate in intermolecular interactions. Gavezzoti and Filippini [368] have presented a critical analysis for the use of computer simulation for the study of organic crystal energetics which includes solid-solid, solid-liquid and solid-vapour equilibrium conditions.

On the contrary, it appears that both racemic and S-(+)-ibuprofens have relatively similar wetting behaviour. θ_a of diiodomethane and water and hence hydrophobicity/hydrophilicity appears to be in a similar trend on similarly indexed facets. Similarly indexed facets on racemic ibuprofen are just as hydrophobic or hydrophilic as the facet on S-(+)-ibuprofen. This contradicts an earlier conclusion (for paracetamol polymorphs) which cautions that the wetting behaviour of similarly indexed facets may not be the same. In actual fact, they were directly in contrast for the case of form I and form II paracetamol. If one looks carefully at the crystal lattice of these materials, the justification will be obvious.

In the case of the paracetamol polymorphs, the hydrogen bonding network was very different. In the monoclinic form, hydrogen bonds were formed between the hydroxyl group of a molecule with the amine and carbonyl of an adjacent molecule, resulting in a corrugated ac-sheet along the b axis. In the orthorhombic form, the hydrogen bonds were formed between the same functional groups, but between three different molecules resulting in a very different structure. This resulted in a planar ab-sheet along the c axis. Furthermore, the two forms assumed different crystal lattice systems, of which $\beta = 115.9^{\circ}$ for the monoclinic system while the orthorhombic

system has $\beta = 90.0$ °. The unit length and space groups of both systems are also very different (see Chapter 4). However, for the racemates of ibuprofen, they crystallise in the same crystal lattice, and the unit lengths and β were found to be relatively similar (also see Chapter 4). Furthermore, the two forms of ibuprofen also have the same hydrogen bonding between the carboxylic groups forming dimers.

This illustrates the importance of surface chemistry, the availabilities of functional groups and the orientation of these molecules in determining the wetting behaviour of organic solids.

9.2 Crystal Habit

9.2.1 Influence of Solvent on Crystal Habit of Aspirin

The growth of crystalline materials resulting in a characteristic shape has puzzled many researchers for centuries. Gibbs [320] suggested that crystals grow to a particular habit, by wanting to minimise the total free energy of the surface. A high energy surface will therefore be of low morphological importance. Wulff proposed that the distance of the facet from its centre was proportionate to their surface energies. Bravais, Freidle Donnay and Harker later introduced what is known as the BFDH theory, postulating that facet growth rate was inversely proportionate to the interplanar spacing, d_{hkl}. Intermolecular forces rather than geometric considerations were taken into account by Hartman and Perdok [369-371], proposing that growth rates were proportional to the attachment energies of crystalline facets. Various computational methods and packages such as MORANG, HABIT and Cerius have been used to aid the prediction of the habit of crystalline solids [372]. These models however do not take into account the environmental effects or process conditions influence on the crystal growth and as such may fail to predict experimentally observed habits especially from organic crystal growth from solution. For growth

from solution, it is necessary to take into account the crystal surface – solution interface [373].

Crystal growth from solution is controlled by volume diffusion through the boundary layer and surface diffusion. The surface diffusion step includes desolvation of solvent-solute and incorporation of solute from surface to crystal lattice. The role of the solvent is thought to be an important factor in crystal growth as it may determine the limiting step. Solvents can inhibit the growth of a facet by adsorption on crystal facet or enhance growth by reduction of the solid-liquid interfacial energy. Crystallisation from different solvents can often result in crystalline solids of the same polymorph but of different habits, as reported for succinic acid [374] and ibuprofen [328]. Other factors which may influence the formation of a particular crystal habit include dominant growth mechanism, degree of solvent supersaturation, temperature, agitation rates and a range of other processing conditions. Liu et al. [375] and Winn and Doherty [376, 377] recently proposed models taking into account the effects of the solvent. Crystalline properties including their growth mechanisms are discussed in Chapter 3.

Crystallisation of aspirin from different solvents has resulted in various crystal habits. Needles were produced from hexane due to optimum growth rate of facet (100) while planar shaped crystals (Figure 4.5) were obtained for growth from ethanol solution due to optimum growth of facet (001) [135]. Based on our wetting studies and crystallographic information, it is recognized that facet (001) is hydrophobic while facet (100) is slightly more polar with presence of carbonyl end groups. The surface chemistry of both facets (001) and (100) and polarity of crystallisation solvent is seen to relate directly with their growth rates. For growth in a polar ethanol solvent,

one might expect that the solvent molecules adsorb on the polar (100) face and hence optimum growth of facet (001) occurs resulting in the plate habit.

In the case for growth of aspirin crystals from acetone solution, the most apparent difference is the increased morphological importance of facet (011). From a surface chemistry approach, this could be attributed to the hydrophilicity and presence of carboxylic acid groups on facet (011) as determined by contact angle and XPS measurements. We postulate that acetone molecules may have adsorbed on the crystal facet and therefore inhibited the growth of this acidic (011) facet. However, it is harder to predict the disappearance of facet (110) and the relative growth rates of facets (001) and (100) with respect to facet (011). However, as a note of caution, the role of surface chemistry may be very much a zeroth order approximation for crystal habit determination as crystal growth is very much influenced by various other kinetic factors. This work however illustrates the importance of a comprehensive knowledge of facet specific surface properties may play in habit determination.

9.2.2 Influence of Solvent on Crystal Habit of Ibuprofen

Crystallisation of ibuprofen from ethanol and acetone also resulted in different crystal habits. As in the case of aspirin crystals, it appears that the morphological importance of facet (011) for racemic ibuprofen increases when grown in ethanol as compared to an acetone solution. Changes in the morphology of ibuprofen due to variations in crystallisation solvent have been reported elsewhere, with a lower aspect ratio crystal, as polarity of the crystallising solvent increases. Based on these wetting studies, it is argued that due to the polarity of facet (011), adsorption of the solvent molecules is expected which will lead to an inhibition to growth on this facet. Slow growing surfaces will result in the facet being dominant or in possession of higher morphological importance. However, as noted in this chapter, the direct link between

surface chemistry and crystal growth rates may not be conclusively established solely from γ_s as numerous other kinetic factors are involved in crystal growth mechanisms. It may however, give us a first order insight into this phenomenon.

9.3 Conclusions

The surface energetics calculated, for all crystalline solid systems investigated in this research, reveals a direct correlation between localised surface chemistry and their wetting behaviour. An excellent agreement was also observed for surface polarities determined by contact angle analysis and XPS measurements. This correlation also agreed very well with the predicted surface hydroxyl group density based on crystallographic data. Of great interest is the differences observed for polymorphic and racemic materials. This serves to illustrate the importance of surface chemistry, as emphasized in this thesis. The results of this work vindicate Fowkes' component approach, while casting doubts on Neumann's equation of state models.

CHAPTER 10 CONCLUSIONS

10.1 Introduction

In this section, the thesis is summarised and some major points, findings and challenges are highlighted. The aim of this research was to establish the role of surface chemistry in the wetting behaviour of liquids on crystalline pharmaceutical solids. A range of model drugs were investigated, employing a systematic and detailed approach. The crystalline solids included both polymorphs of paracetamol (thermodynamically stable monoclinic and the metastable orthorhombic forms), aspirin, racemic ibuprofen and S-(+)-ibuprofen. To characterise these solids, contact angle measurements, gas adsorption and X-ray photoelectron spectroscopy (XPS) techniques were employed. The suitability and applicability of these techniques were evaluated, and computed surface energies were correlated to crystallographic structure of the materials. An evaluation of the various semi-empirical approaches for surface energy evaluation from contact angle data was also reported.

10.2 Overall Summary

The investigation of the wettability of complex organic crystalline solids started with the evaluation of conventional wetting methods; sessile drop contact angle measurements and capillary rise techniques, both on powder beds. Tablets were prepared by compaction under various pressures for contact angle measurements. For paracetamol, no equilibrium contact angle was experimentally obtained for compacts prepared under 10 – 40 kN. On ibuprofen (racemic) compacts, a correlation between the computed γ_{SV}^{d} and γ_{SV}^{p} with the compaction force was obtained. However, in

view of the complications introduced by compaction, often resulting in porous and deformed surfaces, the technique offers a limited or otherwise poor representation and evaluation of the solid surface chemistry.

It is well-known that the sessile drop contact angle measurement is the most surface sensitive technique available, probing the first ten Å of the surface. Typical samples are relatively large surface areas substrates such as tablets and films which may be examined with either large or small liquid droplets. For very small liquid droplets, line tension effects cannot be neglected and furthermore, the vapour pressure of droplets increases exponentially with decreasing drop size. Evaporation may also affect the apparent contact angle which is an issue if advancing angles are required. This renders the direct sessile measurement of contact angles on crystalline particles, typically < 100 μm as impractical.

The alternative, as proposed in this thesis, is to obtain large surface area samples for direct liquid contact angle measurement. These large surfaces were obtained by slow solvent evaporation from saturated solutions over a period of 3-4 weeks. This resulted in macroscopic crystals with well defined habits and surfaces of > 1 cm^2 (Chapter 4). This enabled direct contact angle measurements of probe liquids on the specific crystalline facets. The first major finding, reported for the first time, in this thesis was the anisotropic surface energetics for complex crystalline organic solids. This implied that the wettability of crystalline solids was dissimilar for different crystal faces of the same material. It was postulated that chemical groups exposed on each crystal facet were dissimilar as various crystalline planes slice through the crystal lattice at different planes and angles. This anisotropic wetting behaviour was true for all pharmaceutical solid systems investigated (Chapter 6). It is therefore concluded that this is a general behaviour for all organic crystalline solids.

The second major finding was on the wetting behaviour of polymorphs and enantiomeric compounds. Polymorphs are crystalline solids of the same molecule, packed in a different crystal lattice, while enantiomers are molecules that do not super-impose or are mirror images. Due to their different molecular arrangements and conformations within the respective crystal lattice, the wetting behaviour though anisotropic, was also dissimilar. For example on paracetamol, facet (001) of the monoclinic form was the most hydrophilic (θ_a for water = 15.9 °) surface but was found to be the most hydrophobic (θ_a for water = 64.5 °) surface on the orthorhombic form. For the enantiomeric compounds, racemic ibuprofen and S-(+)-ibuprofen exhibited small differences in wetting behaviour. These observations implied that the wetting behaviour of pharmaceutical solids was dependent on the local surface chemistry; the availabilities of chemical functionalities and their densities. Therefore, a knowledge of the surface chemistry of one polymorphic form or one optical isomer, provides limited, possibly no, insight into the behaviour of other materials from that same family.

Another key point was the observation that the facet with the weakest attachment energy facet was also found to exhibit the most hydrophobic properties. Assuming that crystalline solids will preferentially fracture along this plane during milling, and thus exposing the weakest attachment energy facet, this finding has a potentially important impact on the manufacturing of pharmaceutical solids. The customary route in manufacturing of drug solids involves crystallisation, milling, wet granulation and then tabletting, in that order. The effect of milling thus entails the exposure of a hydrophobic surface, which may undermine the liquid wetting phase of a wet granulation process.

At this point, it is worth reflecting how the anisotropic wetting behaviour results we obtain from single crystal characterisation compare to the conventional powder based techniques using liquid probes as reported in Chapter 5. This thesis will conclude that the characterisation of complex organic solid powders by these conventional methods may not sufficiently reveal the solid's detailed surface chemistry. The conventional characterisation techniques were found to be complicated both from an experimental and theoretical perspective. The use of a large single crystal and their analysis by sessile drops provides a comprehensive and detailed methodology for studying their surface chemistry. Such a strategy may not however, suit all classes of materials. This method revealed a rich level of detailed surface chemistry for crystalline pharmaceutical solids not previously highlighted in any literature reported in the past 30 years.

A number of experiments were undertaken to confirm that the anistropic wetting observed was not due to surface roughness or surface dissolution effects. The use of paracetamol saturated water revealed the same anisotropic wetting behaviour. In addition, the contact angles of water and diiodomethane on a range of gold coated paracetamol facets were equal within experimental error, eliminating a suggested view that the anisotropic behaviour was due to roughness. In the design of superhydrophobic surfaces, it is generally accepted that the effect roughness of < 100 nm is negligible. In the case where surface chemistry may play a major role, it is not known at what scales one can neglect the effects of surface roughness.

To further support the hypothesis of variable chemical functional group presence, X-ray photoelectron spectroscopy (XPS) was performed at the specific crystalline facets (Chapter 7). The XPS technique is presently the most surface sensitive technique to evaluate the functional groups present at the surface. XP spectra

revealed significant differences, with the fraction of polar functional groups in excellent agreement with surface energy polarity computed from contact angle data. This supports the argument that the anisotropic wetting behaviour is a direct implication of the localised surface chemistry which is in turn directly related to the molecular crystal structure.

Chapter 8 reports an evaluation of the effects of milling on crystalline solids' surface properties. This work was undertaken by IGC where the retention behaviour of vapour probes by solids is employed to characterise the particulate samples. It is the commonly accepted view that upon milling, crystalline solids will fracture and expose predominantly the weakest attachment energy facet. In the case of paracetamol, the weakest attachment energy is an internal face (010) which is not present on the native external facets. The surface properties of milled samples were found to be representative of the weakest attachment energy facet, with increasing dominance as particle size is reduced. The surface energy was found to depend clearly on particle size. For unmilled single particulate crystals, the surface energies were representative of the native external facets and were independent of particle size. The IGC technique was found to be sensitive to such small variations in surface properties.

The current wetting theories are made up of two opposing thoughts. The observations and conclusions reached in this research suggest that the surface chemistry does indeed influence the wetting behaviour of solids, and is supportive of the approach put forward by Fowkes.

The results presented in this thesis, provide an insight into one reason, of the possibly many, of why manufacturing of these classes of materials is highly complicated and problematic.

10.3 Future Work

Future work should centre around three main issues; the implication of the anisotropic wetting behaviour on the current wetting theories, the investigation of the suitability of the IGC for heterogeneity studies and the implications of the anisotropic behaviour in industrial solids processing.

Water is probably the most commonly used liquid for contact angle and surface energy evaluation. Water molecules are held together by four hydrogen bonds, contributing to the complexity in predicting and rationalising the specific interactions between liquids and solid surfaces. The synthesis of new novel and simple functional liquids for determination of functional groups present at surfaces would certainly be a step forward. This can be coupled with studies by ionisable functional groups and contact angle titration will lead to an enhanced understanding of solid state surface chemistry.

The effect of milling of pharmaceutical solids was determined by infinite dilution IGC and described in chapter 8. In view of the sensitivity of the technique to determine small differences in surface properties, developing an approach to study heterogeneity of solids is proposed. This essentially involves injection of an accurate amount of probe, such that a BET monolayer of vapour is adsorbed on the surface, and thus the total contribution of the solid energies can be evaluated. The challenge will be to quantify competitive attraction and the partitioning of interactions to specific crystal facets. Another possibility for heterogeneity studies is via rapid temperature molecular desorption experiments, where desorption time variation could be related to the differences in heat of adsorption for high and low energy surface sites.

The theoretical models associated with crystal growth and for predicting their resulting habits often neglect the effects of local chemical environment resulting in poor predictive ability, especially so for solvent mediated crystal growth. An area to explore with the now available anisotropic data is to fully understand the mechanisms and thermodynamics involved in crystal growth. This may aid solvent selection or crystallisation conditions for the engineering of such materials.

The anisotropic wetting behaviour will also have implications on manufacturing processes such as wet granulation. An investigation on the impact of the surface properties on the granulation process and its resulting granule properties will be a useful insight to an inadequately understood process. Of specific interest would be the binder spreading phenomenon, and establishing if this too would be anisotropic.

10.4 Final Remarks

Growth of macroscopic single crystals enabled the direct measurement of liquid contact angles on individual facets of organic crystalline solids. This work has successfully exemplified the importance and role of surface chemistry in the wetting behaviour of pharmaceutical solids, which is anisotropic. The hypothesis that this anisotropic wetting behaviour is due to the variation in localised surface chemistry was further confirmed by XPS. This complete description of the wetting behaviour resulted in a successful prediction of the effects of milling on crystalline solids. Furthermore, this work may illustrate that the Fowkes' approach for surface energy determination fits very well with experimental observation. It is certainly worthwhile to apply this new understanding to the engineering of such classes of materials.

REFERENCES

1. Young, T., *An essay on the cohesion of fluids.* Philosphical Transactions of The Royal Society of London, 1805. **95**: p. 65-87.
2. Dupre, A., *Theorie Mechanique de la Chaleur.* 1869, Paris: Gauthier-Villars.
3. Washburn, E.W., *The Dynamics of Capillary Flow.* Physical Review, 1921. **17**: p. 273-283.
4. Butt, H.-J. and R. Raiteri, *Measurement of the Surface Tension and Surface Stress of Solids*, in *Surface Characterisation Methods*, A.J. Milling, Editor. 1999, Marcel Dekker, Inc.: New York.
5. Ellison, A.H. and W.A. Zisman, *Wettability studies on nylon, polyethylene terephthalate and polystyrene.* Journal of Physical Chemistry, 1954. **58**: p. 503-506.
6. Ellison, A.H. and W.A. Zisman, *Wettability of Halogenated Organic Solid Surfaces.* Journal of Physical Chemistry, 1954. **58**: p. 260-265.
7. Fowkes, F.M., *Additivity of intermolecular forces at interface. 1. Determination of the contribution to surface and interfacial tensions of dispersion forces in various liquids.* Journal of Physical Chemistry, 1963. **67**: p. 2538 - 2541.
8. Fowkes, F.M., *Determination of interfacial tensions, contact angles, and dispersion forces in surface by assuming additivity of intermolecular interactions in surfaces.* Journal of Physical Chemistry, 1962. **66**: p. 382.
9. Neumann, A.W., R.J. Good, C.J. Hope, and M. Sejpal, *An equation-of-state approach to determine surface tensions of low-energy solids from contact angles.* Journal of Colloid and Interface Science, 1974. **49**: p. 291-304.
10. Neumann, A.W., *Contact Angles And Their Temperature Dependence:Thermodynamic Status, Measurement, Interpretation And Application.* Advances in Colloid and Interface Science, 1974. **4**: p. 105-191.
11. Israelachvili, J.N., *Intermolecular and Surface Forces*. 1992, London: Academic Press.
12. Pak, C., H.M. Lee, J.C. Kim, D. Kim, and K.S. Kim, *Theoretical investigation of normal to strong hydrogen bonds.* Structural Chemistry, 2005. **16**: p. 187-202.
13. Etter, M.C., *Encoding and decoding hydrogen-bond patterns of organic compounds.* Accounts of Chemical Research, 1990. **23**: p. 120-126.
14. Desiraju, G.R., *The C-H¨O hydrogen bond in crystals - What is it?* Accounts of Chemical Research, 1991. **24**: p. 290-296.
15. Aakeröy, C.B. and K.R. Seddon, *The hydrogen bond and crystal engineering.* Chemical Society Reviews, 1993. **22**: p. 397-407.
16. Kollman, P.A. and L.C. Allen, *Theory of the hydrogen bond.* Chemical Reviews, 1972. **72**: p. 283-303.
17. Steiner, T., *The hydrogen bond in the solid state.* Angewandte Chemie - International Edition, 2002. **41**: p. 48-76.
18. Byrn, S.R., R.R. Pfeiffer, and J.G. Stowell, *Solid-State Chemistry of Drugs.* 2nd ed. 1999, Indiana: SSCI Inc.
19. Tabor, D., *Surface forces and surface interactions.* Journal of Colloid and Interface Science, 1977. **58**: p. 2-13.
20. Berthelot, D., Comptes Rendus, 1898. **126**: p. 1857.

21. Fowkes, F.M., *Attractive forces at interfaces.* Industrial and Engineering Chemistry, 1964. **56**: p. 40-52.
22. Aveyard, R. and S.M. Saleem, *Interfacial tensions at alkane aqueous electrolyte interfaces.* Journal of the Chemical Society, Faraday Transactions 1, 1976. **72**: p. 1609-1617.
23. Shuttleworth, R., *The surface tension of solids.* Proceedings of the Physical Society A, 1950. **63**: p. 444-457.
24. Galvin, K.P., *A conceptually simple derivation of the Kelvin equation.* Chemical Engineering Science, 2005. **60**: p. 4659-4660.
25. Adamson, A.W. and A.P. Gast, *Physical Chemistry of Surfaces*. 6th ed. 1997, New York: Wiley-Interscience.
26. Langmuir, I., *The adsorption of gases on plane surfaces of glass, mica and platinum.* Journal of the American Chemical Society, 1918. **40**: p. 1361-1403.
27. Langmuir, I., *Vapor pressures, evaporation, condensation and adsorption.* Journal of the American Chemical Society, 1932. **54**: p. 2798-2832.
28. Brunauer, S., P.H. Emmett, and E. Teller, *Adsorption of gases in multimolecular layers.* Journal of the American Chemical Society, 1938. **60**: p. 309-319.
29. Barrett, E.P., L.G. Joyner, and W.P. Halenda, *The determination of pore volume and area distributions in porous substances. I. Computations from nitrogen isotherms.* Journal of the American Chemical Society, 1951. **73**: p. 373-380.
30. Liu, X., X. Lu, Q. Hou, Z. Lu, K. Yang, R. Wang, and S. Xu, *A new integrated method for characterizing surface energy heterogeneity from a single adsorption isotherm.* Journal of Physical Chemistry B, 2005. **109**: p. 15828-15834.
31. Lombardo, S.J. and A.T. Bell, *A review of theoretical models of adsorption, diffusion, desorption and reaction of gases on metal surfaces.* Surface Science Reports, 1991. **13**: p. 1-72.
32. Dabrowski, A., *Adsorption - from theory to practice.* Advances in Colloid and Interface Science, 2001. **93**: p. 135-224.
33. Law, B.M., *Wetting, adsorption and surface critical phenomena.* Progress in Surface Science, 2001. **66**: p. 159-216.
34. Talu, O., *Needs, status, techniques and problems with binary gas adsorption experiments.* Advances in Colloid and Interface Science, 1998. **76-77**: p. 227-269.
35. Hertz, H., *Miscellaneous Papers*. 1896, London: Macmillan.
36. Johnson, K.L., K. Kendall, and A.D. Roberts, *Surface energy and the contact of elastic solids.* Proceedings of the Royal Society of London A, 1971. **324**: p. 301-313.
37. Derjaguin, B.V., V.M. Muller, and Y.P. Toporov, *Effect of contact deformations on the adhesion of particles.* Journal of Colloid and Interface Science, 1975. **53**: p. 314-326.
38. Shi, X. and Y.-P. Zhao, *Comparison of various adhesion contact theories and the influence of dimensionless load parameter.* Journal of Adhesion Science and Technology, 2004. **18**: p. 55-68.
39. Muller, V.M., V.S. Yushchenko, and B.V. Derjaguin, *On the influence of molecular forces on the deformation of an elastic sphere and its sticking to a rigid plane.* Journal of Colloid and Interface Science, 1980. **77**: p. 91-101.

40. Maugis, D., *Adhesion of spheres: The JKR-DMT transition using a Dugdale model.* Journal of Colloid and Interface Science, 1992. **150**: p. 243-269.
41. Greenford, J.A., *Adhesion of elastic spheres.* Proceedings of the Royal Society of London A, 1997. **453**: p. 1277-1297.
42. Schwarz, U.D., *A generalized analytical model for the elastic deformation of an adhesive contact between a sphere and a flat surface.* Journal of Colloid and Interface Science, 2003. **261**: p. 99-106.
43. Clint, J.H. and A.C. Wicks, *Adhesion under water: surface energy considerations.* International Journal of Adhesion & Adhesives, 2001. **21**: p. 267-273.
44. Clint, J.H., *Adhesion and components of solid surface energies.* Current Opinion in Colloid & Interface Science, 2001. **6**: p. 28-33.
45. Good, R.J., *Contact angles and the surface free energy of solids*, in *Surface and Colloid Science*, R.J. Good and R.R. Stromberg, Editors. 1979, Plenum Press: New York. p. 1-29.
46. Adamson, A.W., *Physical Chemistry of Surfaces*. 5th ed. 1990, New York: John Wiley & Sons.
47. Girifalco, L.A. and R.J. Good, *A Theory for the Estimation of Surface and Interfacial Energies. I. Derivation and Application to Interfacial Tension.* Journal of Physical Chemistry, 1957. **61**: p. 904-909.
48. Good, R.J. and L.A. Girifalco, *A theory for estimation of surface and interfacial energies. III. Estimation of of surface energies of solids from contact angle data.* Journal of Physical Chemistry, 1960. **64**: p. 561-565.
49. Owens, D.K. and R.C. Wendt, *Estimation of the surface free energy of polymers.* Journal of Applied Polymer Science, 1969. **13**: p. 1741-1747.
50. vanOss, C.J., R.J. Good, and M.K. Chaudhury, *Additive and nonadditive surface tension components and the interpretation of contact angles.* Langmuir, 1988. **4**: p. 884-891.
51. Gindl, M., G. Sinn, W. Gindl, A. Reiterer, and S. Tschegg, *A comparison of different methods to calculate the surface free energy of wood using contact angle measurements.* Colloids and Surfaces A: Physicochemical and Engineering Aspects, 2001. **181**: p. 279-287.
52. Kloubek, J., *Development of methods for surface free energy determination using contact angles of liquids on solids.* Advances in Colloid and Interface Science, 1992. **38**: p. 99-142.
53. Fowkes, F.M. and M.A. Mostafa, *Acid-base interactions in polymer adsorption.* Industrial & Engineering Chemistry Product Research and Development, 1978. **17**: p. 3-7.
54. vanOss, C.J., *Acid—base interfacial interactions in aqueous media.* Colloids and Surfaces A, 1993. **78**: p. 1-49.
55. vanOss, C.J., *Interfacial Forces in Aqueous Media*. 1994, New York: Marcel Dekker Inc.
56. Good, R.J., *Contact angle, wetting and adhesion: A critical review*, in *Contact Angle, Wettability and Adhesion*, K.L. Mittal, Editor. 1993, VSP: Utrecht, The Netherlands. p. 3-36.
57. van-Oss, C.J., *Interfacial Forces in Aqueous Media*. 1994, New York: Marcel Dekker Inc.
58. Volpe, C.D. and S. Siboni, *Some Reflections on Acid–Base Solid Surface Free Energy Theories.* Journal of Colloid and Interface Science, 1997. **195**: p. 121-136.

59. Clint, J.H. and T.S. Dunstan, *Acid-base components of solid surfaces and the triboelectric series.* Europhysics Letters, 2001. **54**(3): p. 320-322.
60. Chen, F. and W.V. Chang, *Applicability study of a new acid base interaction model in polypeptides and polyamides.* Langmuir, 1991. **7**: p. 2401-2404.
61. Drago, R.S., G.C. Vogel, and T.E. Needham, *Four-parameter equation for predicting enthalpies of adduct formation.* Journal of the American Chemical Society, 1971. **93**: p. 6014-6026.
62. Gutmann, V., *Coordination chemistry of certain transition-metal ions. The role of solvent.* Coordination Chemistry Reviews, 1966. **2**: p. 239-256.
63. Mulliken, R.S., *Lewis acids and bases and molecular complexes.* The Journal of Chemical Physics, 1951. **19**: p. 514-515.
64. Drago, R.S., N. Wong, C. Bilgrien, and G.C. Vogel, *E and C parameters from Hammett substituent constants and use of E and C to understand cobalt-carbon bond energies.* Inorganic Chemistry, 1987. **26**: p. 9-14.
65. Kroeger, M.K. and R.S. Drago, *Quantitative prediction and analysis of enthalpies for the interaction of gas-phase ion-ion, gas-phase ion-molecule, and molecule-molecule Lewis acid-base system.* Journal of the American Chemical Society, 1981. **103**: p. 3250-3262.
66. Riddle, F.L. and F.M. Fowkes, *Spectral shifts in acid-base chemistry. 1. van der Waals contribution to acceptor numbers.* Journal of the American Chemical Society, 1990. **112**: p. 3259-3264.
67. Sun, C. and J.C. Berg, *A review of the different techniques for solid surface acid-base characterization.* Advances in Colloid and Interface Science, 2003. **105**: p. 151-175.
68. Fredenslund, A., R.L. Jones, and J.M. Prausnitz, *Group-contribution estimation of activity coefficients in nonideal liquid mixtures.* AIChE Journal, 1975. **21**: p. 1086-1899.
69. Hansen, H.K., P. Rasmussen, A. Fredenslund, M. Schiller, and J. Gmehling, *Vapor-liquid equilibria by UNIFAC group contribution. 5. Revision and extension.* Industrial & Engineering Chemistry Research, 1991. **30**: p. 2352-2355.
70. Banerjee, S. and F.M. Etzler, *An algorithm for estimating contact angles.* Langmuir, 1995. **11**: p. 4141-4142.
71. Li, D. and A.W. Neumann, *Equation of state for interfacial tensions of solid-liquid systems.* Advances in Colloid and Interface Science, 1992. **39**: p. 299-345.
72. Kwok, D.Y.H., *Contact Angles and Surface Energetics.* **1998**, Ph.D Thesis, University of Toronto: Canada.
73. Volpe, C.D., D. Maniglio, M. Brugnara, S. Siboni, and M. Morra, *The solid surface free energy calculation: I. In defense of the multicomponent approach.* Journal of Colloid and Interface Science, 2004. **271**: p. 434-453.
74. Siboni, S., C.D. Volpe, D. Maniglio, and M. Brugnara, *The solid surface free energy calculation: II. The limits of the Zisman and of the "equation-of-state".* Journal of Colloid and Interface Science, 2004. **271**: p. 454-472.
75. Kwok, D.Y. and A.W. Neumann, *Contact angle measurement and contact angle interpretation.* Advances in Colloid and Interface Science, 1999. **81**: p. 167-249.
76. Graf, K. and H. Riegler, *Is there a general equation of state approach for interfacial tensions?* Langmuir, 2000. **16**: p. 5187-5191.

77. Krasovitski, B. and A. Marmur, *Drops down the hill: Theoretical study of limiting contact angles and the hysteresis range on a tilted plate.* Langmuir, 2005. **21**: p. 3881-3885.
78. Li, D. and A.W. Neumann, Colloids & Polymer Science, 1992. **270**: p. 498.
79. Wenzel, R.N., *Resistance of solid surfaces to wetting by water.* Industrial and Engineering Chemistry, 1936. **28**: p. 988-994.
80. Cassie, A.B.D., *Contact angles.* Discussions of the Faraday Society, 1948. **3**: p. 11-16.
81. Cassie, A.B.D. and S. Baxter, *Wettability of porous surfaces.* Transactions of the Faraday Society, 1944. **40**: p. 546-550.
82. Fowkes, F.M. and W.D. Harkins, *The state of monolayers adsorbed at the interface solid-aqueous solution.* Journal of the American Chemical Society, 1940. **62**: p. 3377-3386.
83. Eick, J.D., R.J. Good, and A.W. Neumann, *Thermodynamics of contact angles. II. Rough solid surfaces.* Journal of Colloid and Interface Science, 1975. **53**: p. 235-238.
84. Gennes, P.G.d., *Wetting: statics and dynamics.* Reviews of Modern Physics, 1985. **57**: p. 827-863.
85. Schwartz, L.W. and S. Garoff, *Contact Angle Hysteresis on Heterogeneous Surfaces.* Langmuir, 1985. **1**: p. 219-230.
86. Pomeau, Y. and J. Vannimenus, *Contact angle on heterogeneous surfaces: Weak heterogeneities.* Journal of Colloid and Interface Science, 1985. **104**: p. 477-488.
87. Shanahan, M.E.R., *Meniscus shape and contact angle of a slightly deformed axisymmetric drop.* Journal of Physics D: Applied Physics, 1989. **22**: p. 1128-1135.
88. Good, R.J., *A thermodynamic derivation of Wenzel's modification of Young's equation for contact angles; Together with a theory of hysteresis.* Journal of the American Chemical Society, 1952. **74**: p. 5041-5042.
89. Shuttleworth, R. and G.L.J. Bailey, *The spreading of a liquid over a rough solid.* Discussions of the Faraday Society, 1948. **3**: p. 16-22.
90. Wolansky, G. and A. Marmur, *Apparent contact angles on rough surfaces: the Wenzel equation revisited.* Colloids and Surfaces A: Physicochemical and Engineering Aspects, 1999. **156**: p. 381-388.
91. Brandon, S., N. Haimovich, E. Yeger, and A. Marmur, *Partial wetting of chemically patterned surfaces: The effect of drop size.* Journal of Colloid and Interface Science, 2003. **263**: p. 237-243.
92. Marmur, A., *Wetting on hydrophobic rough surfaces: To be heterogeneous or not to be?* Langmuir, 2003. **19**: p. 8343-8348.
93. Bikerman, J.J., *Surface roughness and contact angle.* Journal of Physical Chemistry, 1950. **54**: p. 653-658.
94. Wenzel, R.N., *Surface roughness and contact angle.* Journal of Physical Chemistry, 1949. **53**: p. 1466-1467.
95. Bartell, F.E. and J.W. Shepard, *Surface roughness as related to hysteresis of contact angles. i. The system paraffin - water - air.* Journal of Physical Chemistry, 1953. **57**: p. 211-215.
96. Bartell, F.E. and J.W. Shepard, *Surface roughness as related to hysteresis of contact angles. ii. The systems paraffin-3 molar calcium chloride solution-air and paraffin-glycerol-air.* Journal of Physical Chemistry, 1953. **57**: p. 455-458.

97. Shepard, J.W. and F.E. Bartell, *Surface roughness as related to hysteresis of contact angles. iii. The systems paraffin-ethylene glycol-air, paraffin-methyl cellosolve-air and paraffin-methanol-air.* Journal of Physical Chemistry, 1953. **57**(458-463).
98. Kamusewitz, H. and W. Possart, *Wetting and scanning force microscopy on rough polymer surfaces: Wenzel's roughness factor and the thermodynamic contact angles.* Applied Physics A, 2003. **76**: p. 899-902.
99. Adam, N.K. and G. Jessop, *CCL.—Angles of contact and polarity of solid surfaces.* Journal of the Chemical Society, Transactions, 1925. **127**: p. 1863-1868.
100. Berim, G.O. and E. Ruckenstein, *Microscopic interpretation of the dependence of the contact angle on roughness.* Langmuir, 2005. **21**: p. 7743-7751.
101. Onda, T., S. Shibuichi, N. Satoh, and K. Tsujii, *Super-Water-Repellent Fractal Surfaces.* Langmuir, 1996. **12**: p. 2125-2127.
102. Shibuichi, S., T. Onda, N. Satoh, and K. Tsujii, *Super water-repellent surfaces resulting from fractal structure.* Journal of Physical Chemistry, 1996. **100**: p. 19512-19517.
103. Carbone, G. and L. Mangialardi, *Hydrophobic properties of a wavy rough substrate.* The European Physical Journal E, 2005. **16**: p. 67-76.
104. Extrand, C.W., *Model for contact angles and hysteresis on rough ultrahydrophobic surfaces.* Langmuir, 2002. **18**: p. 7991-7999.
105. Extrand, C.W., *Criteria for ultrlyophobic surfaces.* Langmuir, 2004. **20**: p. 5013-5018.
106. Extrand, C.W., *Contact angles and their hysteresis as a measure of liquid-solid adhesion.* Langmuir, 2004. **20**: p. 4017-4021.
107. Extrand, C.W., *Contact angles and hysteresis on surfaces with chemically heterogeneous islands.* Langmuir, 2003. **19**: p. 3793-3796.
108. Jopp, J., H. Grull, and R. Yerushalmi-Rozen, *Wetting behaviour of water droplets on hydrophobic microtextures of comparable size.* Langmuir, 2004. **20**: p. 10015-10019.
109. Abdelsalam, M.E., P.N. Bartlett, T. Kelf, and J. Baumberg, *Wetting of regularly structured gold surfaces.* Langmuir, 2005. **21**: p. 1753-1757.
110. Shirtcliffe, N.J., G. McHale, M.I. Newton, and C.C. Perry, *Wetting and wetting transitions of copper-based super-hydrophobic surfaces.* Langmuir, 2005. **21**: p. 937-943.
111. Ramos, S.M.M., E. Charlaix, and A. Benyagoub, *Contact angle hysteresis on nano-structured surfaces.* Surface Science, 2003. **540**: p. 355-362.
112. Morita, M., T. Koga, H. Otsuka, and A. Takahara, *Macroscopic-wetting anisotropy on the line-patterned surface of fluoroalkylsilane monolayers.* Langmuir, 2005. **21**: p. 911-918.
113. Drelich, J., J.L. Wilbur, J.D. Miller, and G.M. Whitesides, *Contact angles for liquid drops at a model heterogeneous surface consisting of alternating and parallel hydrophobic/hydrophilic strips.* Langmuir, 1996. **12**: p. 1913-1922.
114. Neumann, A.W. and R.J. Good, *Thermodynamics of contact angles. I. Heterogeneous solid surfaces.* Journal of Colloid and Interface Science, 1972. **38**: p. 341-358.
115. Meiron, T.S., A. Marmur, and I.S. Saguy, *Contact angle measurements on rough surfaces.* Journal of Colloid and Interface Science, 2004. **274**: p. 637-644.

116. Noblin, X., A. Buguin, and F. Brochard-Wyart, *Vibrated sessile drops: Transition between pinned and mobile contact line oscillations.* The European Physical Journal E, 2004. **14**: p. 395-404.
117. Long, J., M.N. Hyder, R.Y.M. Huang, and P. Chen, *Thermodynamic modeling of contact angles on rough, heterogeneous surfaces.* Advances in Colloid and Interface Science, 2005. **118**: p. 173-190.
118. Chibowski, E., *Surface free energy of a solid from contact angle hysteresis.* Advances in Colloid and Interface Science, 2003. **103**: p. 149-172.
119. Gupta, P., A. Ulman, S. Fanfan, A. Korniakov, and K. Loos, *Mixed self-assembled monolayers of alkanethiols on ultrasmooth gold do not exhibit contact-angle hysteresis.* Journal of the American Chemical Society, 2005. **127**: p. 4-5.
120. Radelczuk, H., L. Holysz, and E. Chibowski, *Comparison of the Lifshitz-van der Waals/acid-base and contact angle hysteresis approaches for determination of solid surface free energy.* Journal of Adhesion Science and Technology, 2002. **16**: p. 1547-1568.
121. Chibowski, E.J., *Surface free energy and wettability of silyl layers on silicon determined from contact angle hysteresis.* Advances in Colloid and Interface Science, 2005. **113**: p. 121-131.
122. Bangham, D.H. and R.I. Razouk, *Adsorption and the wettability of solid surfaces.* Transactions of the Faraday Society, 1937. **33**: p. 1459-1463.
123. Adamson, A.W., *An adsorption model for contact angle and spreading.* Journal of Colloid and Interface Science, 1968. **27**(2): p. 180-187.
124. Tadros, M.E., P. Hu, and A.W. Adamson, *Adsorption and Contact Angle Studies I. Water on Smooth Carbon, Linear Polyethylene, and Stearic Acid-Coated Copper.* Journal of Colloid and Interface Science, 1974. **49**(2): p. 184-195.
125. Busscher, H.J., G.A.M. Kip, A.v. Silfhout, and J. Arends, *Spreading pressures of water and n-propanol on polymer surfaces.* Journal of Colloid and Interface Science, 1986. **114**: p. 307-313.
126. Fowkes, F.M., D.C. McCarthy, and M.A. Mostafa, *Contact angles and the equilibrium spreading pressures of liquids on hydrophobic solids.* Journal of Colloid and Interface Science, 1980. **78**: p. 200-206.
127. vanOss, C.J., R.F. Giese, Z. Li, K. Murphy, J. Norris, M.K. Chaudhury, and R.J. Good, *Determination of contact angles and pore sixes of porous media by column and thin layer wicking.* Journal of Adhesion Science and Technology, 1992. **6**: p. 413-428.
128. Schrader, M.E., *Negative Gas-Solid Adsorption and Its Influence on Wettability.* Journal of Physical Chemistry B, 2000. **104**: p. 731-733.
129. Mullin, J.W., *Crystallization*. 3rd ed. 1993, Oxford: Butterworth-Heinemann Ltd.
130. Vippagunta, S.R., H.G. Brittain, and D.J.W. Grant, *Crystalline solids.* Advanced Drug Delivery Reviews, 2001. **48**: p. 3-26.
131. Kossel, W., *Zur energetik von oberflachenvorgangen.* Annalen der Physik, 1934. **21**: p. 457-480.
132. O'Hara, M. and R.C. Reid, *Modelling Crystal Growth Rates from Solution.* 1973, Englewood Cliffs: Prentice-Hall.
133. Eerden, J.P.v.d., P. Bennema, and T.A. Cherepanova, *Survey of Monte Carlo simulations of crystal surfaces and crystal growth.* Progress in Crystal Growth and Characterization, 1978. **1**: p. 219-254.

134. Burton, W.K., N. Cabrera, and F.C. Frank, *The growth of crystals and the equilibrium structure of their surfaces.* Philosophical Transactions of the Royal Society of London, 1951. **A243**: p. 299-358.
135. Danesh, A., M.C. Davies, S.J. Hinder, C.J. Roberts, S.J.B. Tendler, P.M. Williams, and M.J. Wilkins, *Surface characterization of aspirin crystal planes by dynamic chemical force microscopy.* Analytical Chemistry, 2000. **72**: p. 3419-3422.
136. Hanawalt, J.D., H.W. Rinn, L.K. Frevel, and I.E.C.A. Ed., *Chemical analysis by X-ray diffraction.* Industrial and Engineering Chemistry Analytical Edition, 1938. **10**: p. 457-512.
137. Suryanarayanan, R., *Determination of the relative amounts of anhydrous carbamazepine ($C_{15}H_{12}N_2O$) and carbamazepine dihydrate ($C_{15}H_{12}N_2O \cdot 2H_2O$) in a mixture by powder X-ray diffractometry.* Pharmaceutical Research, 1989. **6**: p. 1017 - 1024.
138. Suryanarayanan, R., *Determination of the relative amounts of alpha-carbamazepine and beta- carbamazepine in a mixture by powder X-Ray.* Powder Diffraction, 1990. **5**: p. 155-159.
139. Barham, A.S. and B.K. Hodnett, *In situ X-ray diffraction study of the crystallization of spray-dried lactose.* Crystal Growth & Design, 2005. **5**: p. 1965-1970.
140. Li, Z.G., R.L. Harlow, C.M. Foris, H. Li, R.D. Vickery, M.B. Maurin, and B.H. Toby, *New applications of electron diffraction in the pharmaceutical industry: Polymorph determination by using a combination of electron diffraction and synchrotron X-ray powder diffraction techniques.* Microscopy and Microanalysis, 2002. **8**: p. 134-138.
141. Nunes, C., A. Mahendrasingam, and R. Suryanarayanan, *Quantification of crystallinity in substantially amorphous materials by synchrotron X-ray powder diffractometry.* Pharmaceutical Research, 2005. **22**: p. 1942-1953.
142. Reich, G., *Near-infrared spectroscopy and imaging: Basic principles and pharmaceutical applications.* Advanced Drug Delivery Reviews, 2005. **57**: p. 1109-1143.
143. Kawai, K., T. Hagiwara, R. Takai, and T. Suzuki, *Comparative investigation by two analytical approaches of enthalpy relaxation for glassy glucose, sucrose, maltose, and trehalose.* Pharmaceutical Research, 2005. **22**: p. 490-495.
144. Wartewig, S. and R.H.H. Neubert, *Pharmaceutical applications of Mid-IR and Raman spectroscopy.* Advanced Drug Delivery Reviews, 2005. **57**: p. 1144-1170.
145. Willson, R.J. and A.E. Beezer, *The determination of equilibrium constants, dG, dH and dS for vapour interaction with a pharmaceutical drug, using gravimetric vapour sorption.* International Journal of Pharmaceutics, 2003. **258**: p. 77-83.
146. Richardson, J.C., R.W. Bowtell, K. Mader, and C.D. Melia, *Pharmaceutical applications of magnetic resonance imaging (MRI).* Advanced Drug Delivery Reviews, 2005. **57**: p. 1191-1209.
147. Rodriguez-Spong, B., C.P. Price, A. Jayasankar, A.J. Matzger, and N. Rodriguez-Hornedo, *General principles of pharmaceutical solid polymorphism:A supramolecular perspective.* Advanced Drug Delivery Reviews, 2004. **56**: p. 241-274.

148. Bugay, D.E., *Characterization of the solid-state: spectroscopic techniques.* Advanced Drug Delivery Reviews, 2001. **48**: p. 43-65.
149. Stephenson, G.A., R.A. Forbes, and S.M. Reutzel-Edens, *Characterization of the solid state: quantitative issues.* Advanced Drug Delivery Reviews, 2001. **48**: p. 67-90.
150. Brittain, H.G., S.J. Bogdanowich, D.E. Bugay, J. DeVincentis, G. Lewen, and A.W. Newman, *Physical characterization of pharmaceutical solids.* Pharmaceutical Research, 1991. **8**: p. 963-973.
151. Markovich, R. and C. Pidgeon, *Introduction to Fourier transform infrared spectroscopy and application in the pharmaceutical sciences.* Pharmaceutical Research, 1991. **8**: p. 663-675.
152. Price, S.L., *The computational prediction of pharmaceutical crystal structures and polymorphism.* Advanced Drug Delivery Reviews, 2004. **56**: p. 301-319.
153. Hammond, C., *Introduction to Crystallography*. 1992, Oxford: Oxford University Press.
154. Nichols, G. and C.S. Frampton, *Physicochemical characterization of the orthorhombic polymorph paracetamol crystallized from solution.* Journal of Pharmaceutical Sciences, 1998. **87**(6): p. 684-693.
155. Espeau, P., R. Ceolin, J.-L. Tamarit, M.-A. Perrin, J.-P. Gauchi, and F. Leveiller, *Polymorphism of paracetamol: relative stabilities of the monoclinic and orthorhombic phases inferred from topological pressure-temperature and temperature-volume phase diagrams.* Journal of Pharmaceutical Sciences, 2005. **94**: p. 524-539.
156. Ivanova, B.B., *Monoclinic and orthorhombic polymorphs of paracetamol—solid state linear dichroic infrared spectral analysis.* Journal of Molecular Structure, 2005. **738**: p. 233-238.
157. DiMartino, P., A.-M. Guyot-Hermann, P. Conflant, M. Drache, and J.-C. Guyot, *A new pure paracetamol for direct compression: The orthorhombic form.* International Journal of Pharmaceutics, 1996. **128**: p. 1-8.
158. Epple, M., H.K. Cammenga, S.M. Sarge, R. Diedrich, and V. Balek, *The phase transformation of caffeine: Investigation by dynamic X-ray diffraction and emanation thermal analysis.* Thermochimica Acta, 1995. **250**: p. 29-39.
159. Sacchetti, M., *Thermodynamic analysis of DSC data for acetaminophen polymorphs.* Journal of Thermal Analysis and Calorimetry, 2001. **63**: p. 345-350.
160. Griesser, U.J. and A. Burger, *The effect of water vapor pressure on desolvation kinetics of caffeine 4/5-hydrate.* International Journal of Pharmaceutics, 1995. **120**: p. 83-93.
161. Khankari, R.K. and D.J.W. Grant, *Pharmaceutical hydrates.* Thermochimica Acta, 1995. **248**: p. 61-79.
162. Giron, D., *Thermal analysis and calorimetric methods in the characterisation of polymorphs and solvates.* Thermochimica Acta, 1995. **248**: p. 1-59.
163. Brittain, H.G., *Spectral Methods for the Characterization of Polymorphs and Solvates.* Journal of Pharmaceutical Sciences, 1997. **86**: p. 405-412.
164. Fachaux, J.-M., A.-M. Guyot-Hermann, J.-C. Guyot, P. Conflant, M. Drache, S. Veesler, and R. Boistelle, *Pure paracetamol for direct compression Part I. Development of sintered-like crystals of Paracetamol.* Powder Technology, 1995. **82**: p. 123-128.

165. McGregor, P.A., D.R. Allan, S. Parsons, and C.R. Pulham, *Preparation and crystal structure of a trihydrate of paracetamol.* Journal of Pharmaceutical Sciences, 2002. **91**: p. 1308-1311.
166. Chidavaenzi, O.C., G. Buckton, F. Koosha, and R. Pathak, *The use of thermal techniques to assess the impact of feed concentration on the amorphous content and polymorphic forms present in spray dried lactose.* International Journal of Pharmaceutics, 1997. **159**: p. 67-74.
167. Ahlneck, C. and G. Zografi, *The molecular basis of moisture effects on the physical and chemical stability of drugs in the solid state.* International Journal of Pharmaceutics, 1990. **62**: p. 87-95.
168. Roos, Y.H., *Phase Transition in Foods*. 1995, London: Academic Press.
169. Crowley, K.J. and G. Zografi, *The effect of low concentrations of molecularly dispersed poly(Vinylpyrrolidone) on indomethacin crystallization from the amorphous state.* Pharmaceutical Research, 2003. **20**: p. 1417-1422.
170. Tong, P., L.S. Taylor, and G. Zografi, *Influence of alkali metal counterions on the glass transition temperature of amorphous indomethacin salts.* Pharmaceutical Research, 2002. **19**: p. 649-654.
171. Buckton, G. and P. Darcy, *Assessment of disorder in crystalline powders—a review of analytical techniques and their application.* International Journal of Pharmaceutics, 1999. **179**: p. 141-158.
172. Ahmed, H., G. Buckton, and D.A. Rawlins, *The use of isothermal microcalorimetry in the study of small degrees of amorphous content of a hydrophobic powder.* International Journal of Pharmaceutics, 1996. **130**: p. 195-201.
173. Buckton, G. and P. Darcy, *The use of gravimetric studies to assess the degree of crystallinity of predominantly crystalline powders.* International Journal of Pharmaceutics, 1995. **123**(2): p. 265-271.
174. Yu, L., *Amorphous pharmaceutical solids: preparation, characterization and stabilization.* Advanced Drug Delivery Reviews, 2001. **48**: p. 27-42.
175. Sekizaki, H., K. Danjo, H. Eguchi, Y. Yonezawa, H. Sunada, and A. Otsuka, *Solid-state interaction of ibuprofen with poly(vinylpyrrolidone).* Chemical and Pharmaceutical Bulletin, 1995. **42**: p. 988-993.
176. Politov, A.A., V.G. Kostrovskii, and V.V. Boldyrev, *Conditions of Preparation and Crystallization of Amorphous Paracetamol.* Russian Journal of Physical Chemistry, 2001. **75**: p. 1903-1911.
177. Ristic, R.I., S. Finnie, D.B. Sheen, and J.N. Sherwood, *Macro- and micromorphology of monoclinic paracetamol grown from pure aqueous solution.* Journal of Physical Chemistry B, 2001. **105**: p. 9057-9066.
178. Duncan-Hewitt, W.C., D.L. Mount, and A. Yu, *Hardness anisotropy of acetaminophen crystals.* Pharmaceutical Research, 1994. **11**: p. 616-623.
179. Prasad, K.V.R., D.B. Sheen, and J.N. Sherwood, *Fracture Property Studies of Paracetamol Single Crystals Using Microindentation Techniques.* Pharmaceutical Research, 2001. **18**: p. 867 - 872.
180. Yesook, K., M. Matsumoto, and K. Machida, *Specific surface energies and dissolution behaviour of aspirin crystal.* Chemical and Pharmaceutical Bulletin, 1985. **33**: p. 4125-4131.
181. Mao, G., D. Chen, H. Handa, W. Dong, D. Kurth, and H. Mohwald, *Deposition and aggregation of aspirin molecules on a phospholipid bilayer pattern.* Langmuir, 2005. **21**: p. 578-585.

182. Rasenack, N. and B.W. Muller, *Crystal habit and tableting behavior.* International Journal of Pharmaceutics, 2002. **244**: p. 45-57.
183. Nichols, G. and C.S. Frampton, *Physicochemical characterization of the orthorhombic polymorph of paracetamol crystallized from solution.* Journal of Pharmaceutical Sciences, 1998. **87**(6): p. 684-692.
184. Mikhailenko, M.A., *Growth of large single crystals of the orthorhombic paracetamol.* Journal of Crystal Growth, 2004. **265**: p. 616-618.
185. Fletcher, D.A., R.F. McMeeking, and D. Parkin, *The United Kingdom Chemical Database Service.* Journal of Chemical Information & Computer Sciences, 1996. **36**: p. 746-749.
186. Haisa, M., S. Kashino, R. Kawai, and H. Maeda, *The monoclinic form of p-Hydroxyacetanilide.* Acta Crystallography, 1976. **B32**: p. 1283-1285.
187. Haisa, M., S. Kashino, and H. Maeda, *The orthorhombic form of p-Hydroxyacetanilide.* Acta Crystallography, 1974. **B30**: p. 2510-2512.
188. Shankland, N., C.C. Wilson, A.J. Florence, and P.J. Cox, *Refinement of ibuprofen at 100 K by single-crystal pulsed neutron diffraction.* Acta Crystallographica, 1997. **C53**: p. 951-954.
189. Cuppen, H.M., G.M. Day, P. Verwer, and H. Meekes, *Sensitivity of morphology prediction to the force field: Paracetamol as an example.* Crystal Growth & Design, 2004. **4**: p. 1341-1349.
190. Beyer, T., G.M. Day, and S.L. Price, *The prediction, morphology, and mechanical properties of the polymorphs of paracetamol.* Journal of American Chemical Society, 2001. **123**: p. 5086-5094.
191. Umeyama, H., S. Nakagawa, and I. Moriguchi, *Molecular orbital study of the cleavage of Aspirin crystals.* Journal of Physical Chemistry, 1979. **83**: p. 2048-2052.
192. Winn, D. and M.F. Doherty, *Modeling crystal shapes of organic materials grown from solution.* AIChE Journal, 2000. **46**: p. 1348-1367.
193. Williams, D., *Inverse Gas Chromatography*, in *Characterisation of Composite Materials*, H. Ishida, Editor. 1994, Butterworth-Heinemann: London. p. 80-104.
194. Thielmann, F., *Introduction into the characterisation of porous materials by inverse gas chromatography.* Journal of Chromatography A, 2004. **1037**: p. 115-123.
195. Roselman, I.C. and D. Tabor, *The friction of carbon fibres.* Journal of Physics D: Applied Physics, 1976. **9**: p. 2517-2532.
196. Roselman, I.C. and D. Tabor, *Friction and wear of individual carbon-fibers.* Journal of Physics D: Applied Physics, 1977. **10**: p. 1181-1194.
197. Adams, M.J., B.J. Briscoe, J.Y.C. Law, P.F. Luckham, and D.R. Williams, *Influence of vapor condensation on the adhesion and friction of carbon-carbon nanocontacts.* Langmuir, 2001. **17**: p. 6953-6963.
198. Buckton, G., *Contact angle, adsorption and wettability - a review with respect to powders.* Powder Technology, 1990. **61**: p. 237-249.
199. Buckton, G., *Assessment of the wettability of pharmaceutical powders*, in *Contact Angle, Wettability and Adhesion*, K.L. Mittal, Editor. 1993, VSP: Ultrecht, The Netherlands. p. 437-451.
200. Buckton, G., *Characterisation of small changes in the physical properties of powders of significance for dry powder inhaler formulations.* Advanced Drug Delivery Reviews, 1997. **26**: p. 17-27.

201. Buckton, G. and J.M. Newton, *Assessment of the wettability of powders by use of compressed powder discs.* Powder Technology, 1986. **46**: p. 201-208.
202. Dove, J.W., G. Buckton, and C. Doherty, *A comparison of two contact angle measurement methods and inverse gas chromatography to assess the surface energies of theophylline and caffeine.* International Journal of Pharmaceutics, 1996. **138**: p. 199-206.
203. Grimsey, I.M., J.C. Feeley, and P. York, *Analysis of the Surface Energy of Pharmaceutical Powders by Inverse Gas Chromatography.* Journal of Pharmaceutical Sciences, 2002. **91**(2): p. 571-583.
204. Grimsey, I.M., J.C. Osborn, S.W. Doughty, P. York, and R.C. Rowe, *The application of molecular modelling to the interpretation of inverse gas chromatography data.* Journal of Chromatography A, 2002. **969**: p. 49-57.
205. Iveson, S.M., S. Holt, and S. Biggs, *Contact angle measurements of iron ore powders.* Colloids and Surfaces A: Physicochemical and Engineering Aspects, 2000. **166**: p. 203-214.
206. Pepin, X., S. Blanchon, and G. Couarraze, *A new approach for determination of powder wettability.* International Journal of Pharmaceutics, 1997. **152**: p. 1-5.
207. Prestidge, C.A. and J. Ralston, *Contact angle studies of ethyl xanthate coated galena particles.* Journal of Colloid and Interface Science, 1996. **184**: p. 512-518.
208. Prestidge, C.A. and J. Ralston, *Contact Angle Studies of Particulate Sulphide Particles.* Minerals Engineering, 1996. **9**: p. 85-102.
209. Prestidge, C.A. and G. Tsatouhas, *Wettability studies of morphine sulfate powders.* International Journal of Pharmaceutics, 2000. **198**: p. 201-212.
210. Prestige, C.A. and J. Ralston, *Contact Angle Studies on Galena Particles.* Journal of Colloid and Interface Science, 1995. **172**: p. 302-310.
211. Vargha-Butler, E.I., E. Moy, and A.W. Neumann, *Sedimentation behaviour of low surface energy powders in different non-polar liquid systems.* Colloids and Surfaces, 1987. **24**: p. 315-324.
212. Frank, B.P. and G. Belfort, *Atomic Force Microscopy for Low-Adhesion Surfaces: Thermodynamic Criteria, Critical Surface Tension, and Intermolecular Forces.* Langmuir, 2001. **17**: p. 1905-1912.
213. Relini, A., S. Sottini, S. Zuccotti, M. Bolognesi, A. Gliozzi, and R. Rolandi, *Measurement of the Surface Free Energy of Streptavidin Crystals by Atomic Force Microscopy.* Langmuir, 2003. **19**: p. 2908-2912.
214. Kwok, D.Y. and A.W. Neumann, *Contact angle techniques and measurements*, in *Surface Characterization Methods: Principles, Techniques and Applications*, A.J. Milling, Editor. 1999, Marcel Dekker Inc.: New York.
215. Lam, C.N.C., R.Wu, D. Li, M.L. Hair, and A.W. Neumann, *Study of the advancing and receding contact angles: liquid sorption as a cause of contact angle hysteresis.* Advances in Colloid and Interface Science, 2002. **96**: p. 169-191.
216. Lam, C.N.C., N. Kim, D. Hui, D.Y. Kwok, M.L. Hair, and A.W. Neumann, *The effect of liquid properties to contact angle hysteresis.* Colloids and Surfaces A: Physicochemical and Engineering Aspects, 2001. **189**: p. 265-278.
217. Extrand, C.W. and Y. Kumagai, *An experimental study of contact angle hysteresis.* Journal of Colloid and Interface Science, 1997. **191**: p. 378-383.
218. Nakae, H., R. Inui, Y. Hirata, and H. Saito, *Effects of surface roughness on wettability.* Acta Materialia, 1998. **46**(7): p. 2313-2318.

219. Hazlett, R.D., *On surface roughness effects in wetting phenomena*, in *Contact Angle, Wettability and Adhesion*, K.T. Mittal, Editor. 1993, VSP. p. 173-181.
220. Duncan-Hewitt, W. and R. Nisman, *Investigation of the surface free energy of pharmaceutical materials from contact angle, sedimentation, and adhesion measurements*, in *Contact Angle, Wettability and Adhesion*, K.L. Mittal, Editor. 1993, VSP: Utrecht, The Netherlands. p. 791-811.
221. Muster, T.H. and C.A. Prestidge, *Application of time-dependent sessile drop contact angles on compacts to characterise the surface energetics of sulfathiazole crystals.* International Journal of Pharmaceutics, 2002. **234**: p. 43-54.
222. Bartell, F.E. and H.J. Osterhof, *Determination of the Wettability of a Solid by a Liquid.* Industrial and Engineering Chemistry, 1927. **19**: p. 1277-1280.
223. Labajos-Broncano, L., M.L. Gonzalez-Martyn, J.M. Bruque, C.M. Gonzalez-Garcya, and B. Janczuk, *On the Use of Washburn's Equation in the Analysis of Weight–Time Measurements Obtained from Imbibition Experiments.* Journal of Colloid and Interface Science, 1999. **219**: p. 275-281.
224. Crawford, R., L.K. Koopal, and J. Ralston, *Contact angles on particles and plates.* Colloids and Surfaces, 1987. **27**: p. 57-64.
225. Gu, Y., D. Li, and P. Cheng, *A novel contact angle measurement technique by analysis of capillary rise profile around a cylinder (ACRPAC).* Colloids and Surfaces A: Physicochemical and Engineering Aspects, 1997. **122**: p. 135-149.
226. Heertjes, P.M. and N.W.F. Kossen, *Measuring contact angles of powder-liquid systems.* Powder Technology, 1967. **1**: p. 33-42.
227. Brakel, J.V. and P.M. Heertjes, *Capillary rise in porous media. Part I: A problem.* Powder Technology, 1977. **16**: p. 75-81.
228. Brakel, J.V. and P.M. Heertjes, *Capillary rise in porous media. Part II: Secondary phenomena.* Powder Technology, 1977. **16**: p. 83-90.
229. Brakel, J.V. and P.M. Heertjes, *Capillary rise in porous media. Part III: Role of the contact angle.* Powder Technology, 1977. **16**: p. 91-96.
230. Shi, S.Q. and D.J. Gardner, *A new model to determine contact angles on swelling polymer particles by the column wicking method.* Journal of Adhesion Science and Technology, 2000. **14(2)**: p. 301-314.
231. Lockington, D.A. and J.-Y. Parlange, *A new equation for macroscopic description of capillary rise in porous media.* Journal of Colloid and Interface Science, 2004. **278**: p. 404-409.
232. Martic, G., J.D. Coninck, and T.D. Blake, *Influence of the dynamic contact angle on the characterization of porous media.* Journal of Colloid and Interface Science, 2003. **263**: p. 213-216.
233. Wilhelmy, L., *Ueber die abhangigkeit der capillaritats - constanten des alkohols von substanz und gestalt des benetzten festen korpers.* Annalen Der Physik Und Chimie, 1863. **119**: p. 179-217.
234. Heertjes, P.M., *The determination of interfacial tensions with the Wilhelmy plate method.* Chemical Engineering Science, 1971. **26**: p. 1479-1480.
235. Cassie, A.B.D., Discussions Faraday Society, 1948. **3**: p. 11-16.
236. Pepin, X., S. Blanchon, and G. Couarraze, *Powder dynamic contact angle measurements: Young contact angles and effective wet perimeters.* Powder Technology, 1998. **99**: p. 264-271.
237. Chawla, A., G. Buckton, K.M.G. Taylor, J.M. Newton, and M.C.R. Johnson, *Wilhelmy plate contact angle data on powder compacts: considerations of*

plate perimeter. European Journal of Pharmaceutical Sciences, 1994. **2**: p. 253-258.
238. Muster, T.H., *Dynamic contact angle measurement on materials with an unknown wet perimeter.* International Journal of Pharmaceutics, 2004. **282**: p. 189-191.
239. Conder, J.R. and C.L. Young, *Physicochemical Measurement by Gas Chromatography*. 1979, Chichester: Wiley.
240. Kiselev, A.V. and Y.I. Yashin, *Gas-Adsorption Chromatography*. 1969, London: Plenum Press.
241. Papirer, E. and H. Balard, *Interfacial Phenomena in Chromatography*, E. Pefferkorn, Editor. 1999, Marcel Dekker Inc.: New York.
242. Newell, H.E., G. Buckton, D.A. Butler, F. Thielmann, and D.R. Williams, *The use of inverse phase gas chromatography to study the change of surface energy of amorphous lactose as a function of relative humidity and the processes of collapse and crystallisation.* International Journal of Pharmaceutics, 2001. **217**: p. 45-56.
243. Newell, H.E., G. Buckton, D.A. Butler, F. Thielmann, and D.R. Williams, *The use of inverse gas chromatography to measure the surface energy of crystalline, amorphous and recently milled lactose.* Pharmaceutical Research, 2001. **18**: p. 662-666.
244. Ticehurst, M.D., R.C. Rowe, and P. York, *Determination of the surface properties of two batches of salbutamol sulphate by inverse gas chromatography.* International Journal of Pharmaceutics, 1994. **111**: p. 241-249.
245. York, P., M.D. Ticehurst, J.C. Osborn, R.J. Roberts, and R.C. Rowe, *Characterisation of the surface energetics of milled dl-propranolol hydrochloride using inverse gas chromatography and molecular modelling.* International Journal of Pharmaceutics, 1998. **174**: p. 179-186.
246. Levoguer, C.L. and D.R. Williams, *Measurement of the surface energies of pharmaceutical powders using a novel vapour adsorption method.* Surface Measurement Systems Application Note 17.
247. Yan, N., Y. Maham, J.H. Masliyah, M.R. Gray, and A.E. Mather, *Measurement of contact angles for fumed silica nanospheres using enthalpy of immersion data.* Journal of Colloid and Interface Science, 2000. **228**: p. 1-6.
248. Chessick, J.H., F.H. Healey, and A.C. Zettlemoyer, *Adsorption and heat of wetting studies of teflon.* Journal of Physical Chemistry, 1956. **60**: p. 1345-1347.
249. Spagnolo, D.A., Y. Maham, and K.T. Chuang, *Calculation of contact angle for hydrophobic powders using heat of immersion data.* Journal of Physical Chemistry, 1996. **100**: p. 6626-6630.
250. Buckton, G. and A.E. Beezer, *The applications of microcalorimetry in the field of physical pharmacy.* International Journal of Pharmaceutics, 1991. **72**: p. 181-191.
251. Watts, J.F. and J. Wolstenholme, *An Introduction to Surface Analysis by XPS and AES*. 2003, Chichester: John Wiley & Sons Ltd.
252. McGuire, G.E., J. Fuchs, P. Han, J.G. Kushmerick, P.S. Weiss, S.J. Simko, R.J. Nemanich, and D.R. Chopra, *Surface characterization.* Analytical Chemistry, 1999. **71**: p. 373R-388R.

253. Turner, N.H. and J.A. Schreifels, *Surface analysis: X-ray Photoelectron Spectroscopy and Auger Electron Spectroscopy.* Analytical Chemistry, 2000. **72**: p. 99-110.
254. Binnig, G., C.F. Quate, and C. Gerber, *Atomic force microscope.* Physical Review Letters, 1986. **56**: p. 930-933.
255. Hansma, H.G. and L. Pietrasanta, *Atomic force microscopy and other scanning probe microscopies.* Current Opinion in Chemical Biology, 1998. **2**: p. 579-584.
256. Cappella, B. and G. Dietler, *Force-distance curves by atomic force microscopy.* Surface Science Reports, 1999. **34**: p. 1-104.
257. Green, N.H., S. Allen, M.C. Davies, C.J. Roberts, S.J.B. Tendler, and P.M. Williams, *Force sensing and mapping by atomic force microscopy.* Trends in Analytical Chemistry, 2002. **21**: p. 64-73.
258. Jalili, N. and K. Laxminarayana, *A review of atomic force microscopy imaging systems: application to molecular metrology and biological sciences.* Mechatronics, 2004. **14**: p. 907-945.
259. Meurk, A., P.F. Luckham, and L. Bergstrom, *Direct measurement of repulsive and attractive van der Waals forces between inorganic materials.* Langmuir, 1997. **13**: p. 3896-3899.
260. Edwardson, J.M. and R.M. Henderson, *Atomic force microscopy and drug discovery.* Drug Discovery Today, 2004. **9**: p. 64-71.
261. Garg, A. and E. Kokkoli, *Characterizing particulate drug-delivery carriers with atomic force microscopy.* IEEE Engineering in Medicine and Biology Magazine, 2005. **Jan/Feb**: p. 87-95.
262. Pereira, R.d.S., *Atomic force microscopy as a novel pharmacological tool.* Biochemical Pharmacology, 2001. **62**: p. 975-983.
263. Yamada, H. and K. Nakayama, *Imaging of organic molecules by atomic force microscopy.* Japanese Journal of Applied Physics, 1993. **32**: p. 2958-2961.
264. Seitavuopio, P., J. Rantanen, and J. Yliruusi, *Tablet surface characterisation by various imaging techniques.* International Journal of Pharmaceutics, 2003. **254**: p. 281-286.
265. Li, T. and K. Park, *Fractal analysis of pharmaceutical particles by atomic force microscopy.* Pharmaceutical Research, 1998. **15**: p. 1222-1232.
266. Shi, H.G., L. Farber, J.N. Michaels, A. Dickey, K.C. Thompson, S.D. Shelukar, P.N. Hurter, S.D. Reynolds, and M.J. Kaufman, *Characterization of crystalline drug nanoparticles using atomic force microscopy and complementary techniques.* Pharmaceutical Research, 2003. **20**: p. 479-484.
267. Sangwal, K., J. Torrent-Burgues, F. Sanz, and P. Gorostiza, *Atomic force microscopic study of step bunching and macrostep formation during the growth of L-arginine phosphate monohydrate single crystals.* Journal of Crystal Growth, 1997. **172**: p. 209-218.
268. Ogawa, K., L.A. Guzman, and K. Shimizu, *Surface topography of growing L-alanine crystals in magnetic field.* Journal of Chemical Engineering of Japan, 2004. **37**: p. 791-795.
269. Lechuga-Ballesteros, D. and N. Rodriguez-Hornedo, *The influence of additives on the growth kinetics and mechanism of L-alanine crystals.* International Journal of Pharmaceutics, 1995. **115**: p. 139-149.
270. Thompson, C., M.C. Davies, C.J. Roberts, S.J.B. Tendler, and M.J. Wilkinson, *The effects of additives on the growth and morphology of paracetamol*

(acetaminophen) crystals. International Journal of Pharmaceutics, 2004. **280**: p. 137-150.
271. Keel, T.R., C. Thompson, M.C. Davies, S.J.B. Tendler, and C.J. Roberts, *AFM studies of the crystallization and habit modification of an excipient material, adipic acid.* International Journal of Pharmaceutics, 2004. **280**: p. 185-198.
272. Cleaver, J.A.S. and P. Wong, *Humidity-induced surface modification of boric acid.* Surface and Interface Analysis, 2004. **36**: p. 1592-1599.
273. Li, B.S., G.P. Li, C. Wang, M. Wang, D.C. Wang, and C. Bai, *Structure-governed growth phenomenon of a trichosanthin crystal.* Langmuir, 2002. **18**: p. 6723-6726.
274. Danesh, A., S.D. Connell, M.C. Davies, C.J. Roberts, S.J.B. Tendler, P.M. Williams, and M.J. Wilkins, *An in situ dissolution study of aspirin crystal planes (100) and (001) by atomic force microscopy.* Pharmaceutical Research, 2001. **18**: p. 299-303.
275. Li, T., K.R. Morris, and K. Park, *Influence of solvent and crystalline supramolecular structure on the formation of etching patterns on acetaminophen single crystals: A study with atomic force microscopy and computer simulation.* Journal of Physical Chemistry B, 2000. **104**: p. 2019-2032.
276. Li, T., K.R. Morris, and K. Park, *Influence of tailor-made additives on etching patterns of acetaminophen single crystals.* Pharmaceutical Research, 2001. **18**: p. 398-402.
277. Wen, H., T. Li, K.R. Morris, and K. Park, *How solvents affect acetaminophen etching pattern formation: Interaction between solvent and acetaminophen at the solid/liquid interface.* Journal of Physical Chemistry B, 2004. **108**: p. 2270-2278.
278. Ashayer, R., P.F. Luckham, S. Manimaaran, and P. Rogueda, *Investigation of the molecular interactions in a pMDI formulation by atomic force microscopy.* European Journal of Pharmaceutical Sciences, 2004. **21**: p. 533-543.
279. Louey, M.D., P. Mulvaney, and P.J. Stewart, *Characterisation of adhesional properties of lactose carriers using atomic force microscopy.* Journal of Pharmaceutical and Biomedical Analysis, 2001. **25**: p. 559-567.
280. Sindel, U. and I. Zimmermann, *Measurement of interaction forces between individual powder particles using an atomic force microscope.* Powder Technology, 2001. **117**: p. 247-254.
281. Beach, E.R., G.W. Tormoen, J. Drelich, and R. Han, *Pull-off force measurements between rough surfaces by atomic force microscopy.* Journal of Colloid and Interface Science, 2002. **247**: p. 84-99.
282. Islam, N., P. Stewart, I. Larson, and P. Hartley, *Surface roughness contribution to the adhesion force distribution of salmeterol xinafoate on lactose carriers by atomic force microscopy.* Journal of Pharmaceutical Sciences, 2005. **94**: p. 1500-1511.
283. Hooton, J.C., C.S. German, S. Allen, M.C. Davies, C.J. Roberts, S.J.B. Tendler, and P.M. Williams, *Characterization of particle-interactions by atomic force microscopy: Effect of contact area.* Pharmaceutical Research, 2003. **20**: p. 508-514.
284. Hooton, J.C., C.S. German, S. Allen, M.C. Davies, C.J. Roberts, S.J.B. Tendler, and P.M. Williams, *An atomic force microscopy study of the effect of nanoscale contact geometry and surface chemistry on the adhesion of pharmaceutical particles.* Pharmaceutical Research, 2004. **21**: p. 953-961.

285. Davies, M., A. Brindley, X. Chen, M. Marlow, S.W. Doughty, I. Shrubb, and C.J. Roberts, *Characterization of drug particle surface energetics and Young's modulus by atomic force microscopy and inverse gas chromatography.* Pharmaceutical Research, 2005. **22**: p. 1158-1166.
286. Danesh, A., X. Chen, M.C. Davies, C.J. Roberts, G.H.W. Sanders, S.J.B. Tendler, P.M. Williams, and M.J. Wilkins, *Polymorphic discrimination using atomic force microscopy: Distinguishing between two polymorphs of the drug cimetidine.* Langmuir, 2000. **16**: p. 866-870.
287. Danesh, A., X. Chen, M.C. Davies, C.J. Roberts, G.H.W. Sanders, S.J.B. Tendler, P.M. Williams, and M.J. Wilkins, *The discrimination of drug polymorphic forms from single crystals using atomic force microscopy.* Pharmaceutical Research, 2000. **17**: p. 887-890.
288. Cao, X., C. Sun, and T.J. Thamann, *A study of sulfamerazine single crystals using atomic force microscopy, transmission light microscopy, and Raman spectroscopy.* Journal of Pharmaceutical Sciences, 2005. **94**: p. 1881-1892.
289. Heng, J.Y.Y., A. Bismarck, A.F. Lee, K. Wilson, and D.R. Williams, *Anisotropic wettability of macroscopic form I paracetamol crystals.* Langmuir (Accepted), 2006.
290. Zhang, D., J.H. Flory, S. Panmai, U. Batra, and M.J. Kaufman, *Wettability of pharmaceutical solids: its measurement and influence on wet granulation.* Colloids and Surfaces A: Physicochemical and Engineering Aspects, 2002. **206**: p. 547-554.
291. Ahfat, N.M., G. Buckton, R. Burrows, and M.D. Ticehurst, *Predicting mixing performance using surface energy measurements.* International Journal of Pharmaceutics, 1997. **156**: p. 89-95.
292. Aranberri-Askargorta, I., T. Lampke, and A. Bismarck, *Wetting behavior of flax fibers as reinforcement for polypropylene.* Journal of Colloid and Interface Science, 2003. **263**: p. 580-589.
293. Schultz, J., L. Lavielle, and C. Martin, *The role of the interface in carbon fibre-spoxy composites.* Journal of Adhesion, 1987. **23**: p. 45-60.
294. Eiliazadeh, B., K. Pitt, and B. Briscoe, *Effects of punch geometry on powder movement during pharmaceutical tabletting processes.* International Journal of Solids and Structures, 2004. **41**: p. 5967-5977.
295. Clarke, A., T.D. Blake, K. Carruthers, and A. Woodward, *Spreading and imbibition of liquid droplets on porous surfaces.* Langmuir, 2002. **18**: p. 2980-2984.
296. Binks, B.P. and J.H. Clint, *Solid wettability from surface energy components: Relevance to pickering emulsions.* Langmuir, 2002. **18**(4): p. 1270-1273.
297. Etzler, F.M., *Characterization of surface free energies and surface chemistry of solids*, in *Contact Angle, Wettability and Adhesion*, K.L. Mittal, Editor. 2003, VSP: Ultrecht, The Netherlands. p. 1-46.
298. Carstensen, J.T., *Pharmaceutical Principles of Solid Dosage Forms*. 1993, Pennsylvania: Technomic Publishing Company.
299. Fujii, H. and H. Nakae, *Equilibrium contact angle in the magnesium oxide/aluminium system.* Acta Materialia, 1996. **44**: p. 3567-3573.
300. Grigogrenko, N., V. Zhuravlev, V. Poluyanskaya, Y.V. Naidich, N. Eustathopoulos, J.F. Silvain, and J.C. Bihr. *Wettability of α-Al_2O_3 single crystals by Ni-Al melts*. in *Proceedings of Internation Conference of High Temperature Capillarity*. 1997. Cracow, Poland.

301. Nogi, K., M. Nishikawa, H. Fujii, and S. Hara, *Wettability of Diamond by Liquid Pure Tin.* Acta Materialia, 1998. **46**(7): p. 2305-2311.
302. Shen, P., H. Fujii, T. Matsumoto, and K. Nogi, *Wetting of (0001) α-Al_2O_3 single crystals by molten Al.* Scripta Materialia, 2003. **48**: p. 779-784.
303. Suzuki, T., G. Hirose, and S. Oishi, *Contact angle of water droplet on apatite single crystals.* Materials Research Bulletin, 2003. **XXX**: p. XXX-XXX.
304. Nogi, K., M. Tsujimoto, K. Ogino, and N. Iwamoto, *Wettability of MgO single crystal by liquid pure Pb, Sn and Bi.* Acta Metallurgica et Materialia, 1992. **40**: p. 1045-1050.
305. Muster, T.H. and C.A. Prestidge, *Face Specific Surface Properties of Pharmaceutical Crystals.* Journal of Pharmaceutical Sciences, 2002. **91**: p. 1432-1444.
306. DiMartino, P., P. Conflant, M. Drache, J.-P. Huvenne, and A.-M. Guyot-Hermann, *Preparation and physical characterization of forms II and III of paracetamol.* J. Therm. Anal. Calorim., 1997. **48**: p. 447-458.
307. Moynihan, H.A. and I.P. O'Hare, *Spectroscopic characterisation of the monoclinic and orthorhombic forms of paracetamol.* International Journal of Pharmaceutics, 2002. **247**: p. 179-185.
308. Ebril, H.Y., *Surface Tension of Polymers*, in *Surface and Colloid Chemistry*, K.S. Birdi, Editor. 1997, CRC Press: New York. p. 265-312.
309. Morra, M., E. Occhiello, and F. Garbassi, *Knowledge About Polymer Surfaces From Contact Angle Measurements.* Advances in Colloid and Interface Science, 1990. **32**: p. 79-116.
310. Granberg, R.A. and A.C. Rasmuson, *Solubility of paracetamol in pure solvents.* Journal of Chemical and Engineering Data, 1999. **44**(6): p. 1391-1395.
311. Heng, J.Y.Y., F. Thielmann, and D.R. Williams, *The effects of milling on the surface properties of form I paracetamol crystals.* Pharmaceutical Research (submitted), 2005.
312. Mikhailenko, M.A., T.N. Drebushchak, T.P. Shakhtsneider, and V.V. Boldyrev, *Etching patterns on the monoclinic and orthorhombic paracetamol.* Arkivoc, 2004. **xii**: p. 156-169.
313. Kim, Y., K. Machida, T. Taga, and K. Osaki, *Structure redetermination and packing analysis of aspirin crystal.* Chemical and Pharmaceutical Bulletin, 1985. **33**: p. 2641-2647.
314. Payne, R.S., R.C. Rowe, R.J. Roberts, M.H. Charlton, and R. Docherty, *Potential polymorphs of aspirin.* Journal of Computational Chemistry, 1999. **20**: p. 262-273.
315. Glaser, R., *Aspirin. An ab initio quantum-mechanical study of conformational preferences and of neighboring group interactions.* Journal of Organic Chemistry, 2001. **66**: p. 771-779.
316. Binev, I.G., B.A. Stamboliyska, and Y.I. Binev, *The infrared spectra and structure of acetylsalicylic acid (aspirin) and its oxyanion: an ab initio force field treatment.* Journal of Molecular Structure, 1996. **378**: p. 189-197.
317. Tawashi, R., *Aspirin: Dissolution rates of two polymorphic forms.* Science, 1968. **160**: p. 76.
318. Wen, H., T. Li, K.R. Morris, and K. Park, *Dissolution study on Aspirin and α-Glycine crystals.* Journal of Physical Chemistry B, 2004. **108**: p. 11219-11227.

319. McLoughlin, C.M., W.A.M. McMinn, and T.R.A. Magee, *Physical and dielectric properties of pharmaceutical powders.* Powder Technology, 2003. **134**: p. 40-51.
320. Gibbs, J.W., *The collected works of J. Willard Gibbs*. 1928, New Haven: Yale University Press.
321. Lommerse, J.P.M., S.L. Price, and R. Taylor, *Hydrogen Bonding of Carbonyl, Ether, and Ester Oxygen Atoms with Alkanol Hydroxyl Groups.* Journal of Computational Chemistry, 1997. **18**: p. 757-774.
322. Li, T. and Z. Wang, *Analysis of the anisotropic wettability of aspirin single crystals with the ab initio calculation.* AAPS PharmSci, 2003. **5(4)**: p. Abstract W4286.
323. Li, T., S. Liu, S. Feng, and C.E. Aubrey, *Face-integrated Fukui function: Understanding wettability anisotropy of molecular crystals from density functional theory.* Journal of the American Chemical Society, 2005. **127**: p. 1364-1365.
324. Perlovich, G.L., S.V. Kurkov, L. Kr.Hansen, and A. Bauer-Brandl, *Thermodynamics of sublimation, crystal lattice energies, and crystal structures of racemates and enantiomers: (+)- and (+-)-ibuprofen.* Journal of Pharmaceutical Sciences, 2004. **93**: p. 654-666.
325. Martino, P.D., M. Beccerica, E. Joiris, G.F. Palmieri, A. Gayot, and S. Martelli, *Infuence of crystal habit on the compression and densification mechanism of ibuprofen.* Journal of Crystal Growth, 2002. **243**: p. 345-355.
326. Garekani, H.A., F. Sadeghi, A. Badiee, S.A. Mostafa, and A.R. Rajabi-Siahboomi, *Crystal habit modifications of ibuprofen and their physicomechanical characteristics.* Drug Development and Industrial Pharmacy, 2001. **27**: p. 803-809.
327. Rasenack, N. and B.W. Muller, *Properties of ibuprofen crystallized under various conditions: A comparative study.* Drug Development and Industrial Pharmacy, 2002. **28**: p. 1077-1089.
328. Cano, H., N. Gabas, and J.P. Canselier, *Experimental study on the ibuprofen crystal growth morphology in solution.* Journal of Crystal Growth, 2001. **224**: p. 335-341.
329. Rasenack, N. and B.W. Muller, *Ibuprofen crystals with optimized properties.* International Journal of Pharmaceutics, 2002. **245**: p. 9-24.
330. Chen, Y., L. Chen, H. Nie, E.T. Kang, and R.H. Vora, *Fluorinated polyimides grafted with poly(ethylene glycol) side chains by the RAFT-mediated process and their membranes.* Materials Chemistry and Physics, 2005. **94**: p. 195-201.
331. Bismarck, A., A.F. Lee, A.S. Saraç, E. Schulz, and K. Wilson, *Electrocoating of carbon fibres: A route for interface control in carbon fibre reinforced poly methylmethacrylate?* Composites Science and Technology, 2005. **65**: p. 1564-1573.
332. Cantrell, D.G., L.J. Gillie, A.F. Lee, and K. Wilson, *Structure-reactivity correlations in MgAl hydrotalcite catalysts for biodiesel synthesis.* Applied Catalysis A, 2005. **287**: p. 183-190.
333. Ramirez-Cabrera, E., A. Atkinson, and D. Chadwick, *Reactivity of ceria, Gd- and Nb-doped ceria to methane.* Applied Catalysis B, 2002. **36**: p. 193-206.
334. Jonat, S., S. Hasenzahl, M. Drechsler, P. Albers, K.G. Wagner, and P.C. Schmidt, *Investigation of compacted hydrophilic and hydrophobic colloidal silicon dioxides as glidants for pharmaceutical excipients.* Powder Technology, 2004. **141**: p. 31-43.

335. Mu, L., M.M. Teo, H.Z. Ning, C.S. Tan, and S.S. Feng, *Novel powder formulations for controlled delivery of poorly soluble anticancer drug: Application and investigation of TPGS and PEG in spray-dried particulate system.* Journal of Controlled Release, 2005. **103**: p. 565-575.
336. Fitzpatrick, M.F., J.S.G. Ling, and J.F. Watts, *Failure mechanism of phosphated adhesively bonded hot-dipped galvanized steel: a small-area XPS study.* Surface and Interface Analysis, 2000. **29**: p. 131-138.
337. Davis, S.J. and J.F. Watts, *Interfacial chemistry of adhesive joint failure: an investigation by small area XPS, imaging XPS and TOF-SIMS.* Journal of Materials Science, 1996. **6**: p. 479-493.
338. Mori, Y., M. Tanemura, and S. Tanemura, *Surface morphological influence on charging at metal-insulator interface in XPS depth profiling.* Applied Surface Science, 2004. **228**: p. 292-296.
339. Oswald, S. and W. Bruckner, *XPS depth profile analysis of non-stoichiometric NiO films.* Surface and Interface Analysis, 2004. **36**: p. 17-22.
340. Kaciulis, S., L. Pandolfi, and R. White, *Depth profiling of thin films of binary metal oxides.* Surface and Interface Analysis, 2004. **36**: p. 845-848.
341. Conder, J.R., G.J. Rees, and S. McHale, *Evaluation of methods of measuring gas liquid chromatographic retention on skewed peaks.* Journal of Chromatography A, 1983. **258**: p. 1-10.
342. Dorris, G.M. and D.G. Gray, *Adsorption of n-alkanes at zero surface coverage on cellulose paper and wood fibers.* Journal of Colloid and Interface Science, 1980. **77**: p. 353-362.
343. Panzer, U. and H.P. Schreiber, *On the evaluation of surface interactions by inverse gas chromatography.* Macromolecules, 1992. **25**: p. 3633-3631.
344. Emmett, P.H. and S. Brunauer, *The use of low temperature van der Waals adsorption isotherms in determining the surface area of iron synthetic ammonia catalysts.* Journal of the American Chemical Society, 1937. **59**: p. 1553-1564.
345. Planinsek, O., J. Zadnik, S. Rozman, M. Kunaver, R. Dreu, and S. Srcic, *Influence of inverse gas chromatography measurement conditions on surface energy parameters of lactose monohydrate.* International Journal of Pharmaceutics, 2003. **256**: p. 17-23.
346. Planinsek, O. and G. Buckton, *Inverse gas chromatography: Considerations about appropriate use for amorphous and crystalline powders.* Journal of Pharmaceutical Sciences, 2003. **92**: p. 1286-1294.
347. Sunkersett, M.R., I.M. Grimsey, S.W. Doughty, J.C. Osborn, P. York, and R.C. Rowe, *The changes in surface energetics with relative humidity of carbamazepine and paracetamol as measured by inverse gas chromatography.* European Journal of Pharmaceutical Sciences, 2001. **13**: p. 219-225.
348. Ohta, M. and G. Buckton, *A study of the differences between two amorphous spray-dried samples of cefditoren pivoxil which exhibited different physical stabilities.* International Journal of Pharmaceutics, 2005. **289**: p. 31-38.
349. Tong, H.H.Y., O.Y. Shekunov, P. York, and A.H.L. Chow, *Surface characterization of saimeterol xinafoate powders by inverse gas chromatography at finite coverage.* Journal of Pharmaceutical Sciences, 2005. **94**: p. 695-700.
350. Grimsey, I.M., M. Sunkersett, J.C. Osborn, P. York, and R.C. Rowe, *Interpretation of the differences in the surface energetics of two optical forms*

of mannitol by inverse gas chromatography and molecular modelling. International Journal of Pharmaceutics, 1999. **191**: p. 43-50.
351. Alessi, P., I. Kikic, and A. Cortesi, *Characterization of tocopherols by inverse chromatographic data.* Industrial & Engineering Chemistry Research, 2002. **41**: p. 4873-4878.
352. Granberg, R.A., D.G. Bloch, and A.C. Rasmuson, *Crystallization of paracetamol in acetone-water mixtures.* Journal of Crystal Growth, 1999. **198/199**: p. 1287-1293.
353. Boerrigter, S.X.M., H.M. Cuppen, R.I. Ristic, J.N. Sherwood, P. Bennema, and H. Meekes, *Explanation for the supersaturation-dependent morphology of monoclinic paracetamol.* Crystal Growth & Design, 2002. **2**: p. 357-361.
354. Storey, R.A., P. York, and C. Doherty, *The effects of the crystallisation environment on the surface properties of ibuprofen.* (Unpublished).
355. Newell, H.E., G. Buckton, D.A. Butler, F. Thielmann, and D.R. Williams, *The use of inverse phase gas chromatography to measure the surface energy of crystalline, amorphous, and recently milled lactose.* Pharmaceutical Research, 2001. **18**: p. 662-666.
356. Feeley, J.C., P. York, B.S. Sumby, and H. Dicks, *Determination of surface properties and how characteristics of salbutamol sulphate, before and after micronisation.* International Journal of Pharmaceutics, 1998. **172**: p. 89-96.
357. York, P., M.D. Ticehurst, J.C. Osborn, R.J. Roberts, and R.C. Rowe, *Characterisation of the surface energetics of milled dl-propranolol hydrochloride using inverse gas chromatography and molecular modellin.* International Journal of Pharmaceutics, 1998. **174**: p. 179-186.
358. Feeley, J.C., P. York, B.S. Sumby, and H. Dicks, *Processing effects on the surface properties of alpha-lactose monohydrate assessed by inverse gas chromatography (IGC).* Journal of Materials Science, 2002. **37**: p. 217-222.
359. Ohta, M. and G. Buckton, *Determination of the changes in surface energetics of cefditoren pivoxil as a consequence of processing induced disorder and equilibration to different relative humidities.* International Journal of Pharmaceutics, 2004. **269**: p. 81-88.
360. Rousset, P., P. Sellappan, and P. Daoud, *Effect of emulsifiers on surface properties of sucrose by inverse gas chromatography.* Journal of Chromatography A, 2002. **969**: p. 97-101.
361. Surana, R., L. Randall, A. Pyne, N.M. Vemuri, and R. Suryanarayanan, *Determination of glass transition temperature and in situ study of the plasticizing effect of water by inverse gas chromatography.* Pharmaceutical Research, 2003. **20**: p. 1647-1654.
362. Buckton, G., A. Ambarkhane, and K. Pincott, *The use of inverse phase gas chromatography to study the glass transition temperature of a powder surface.* Pharmaceutical Research, 2004. **21**: p. 1554-1557.
363. Thielmann, F. and D. Williams, *Determination of the glass transition temperature of maltose and its dependence on relative humidity by inverse gas chromatography.* Deutsche Lebensmittel-Rundschau, 2000. **96**: p. 255.
364. Ticehurst, M.D., R.C. Rowe, and P. York, *Determination of the surface properties of 2 batches of salbutamol sulfate by inverse gas chromatography.* International Journal of Pharmaceutics, 1994. **111**: p. 241-249.
365. Ticehurst, M.D., P. York, R.C. Rowe, and S.K. Dwivedi, *Characterisation of the surface properties of alpha-lactose monohydrate with inverse gas*

chromatography, used to detect batch variation. International Journal of Pharmaceutics, 1996. **141**: p. 93-99.
366. Ålander, E.M., M.S. Uusi-Penttila, and Å.C. Rasmuson, *Agglomeration of paracetamol during crystallization in pure and mixed solvents.* Industrial and Engineering Chemistry Research, 2004. **43**: p. 629-637.
367. Prasad, K.V.R., R.I. Ristic, D.B. Sheen, and J.N. Sheerwood, *Dissolution kinetics of paracetamol single crystals.* International Journal of Pharmaceutics, 2002. **238**: p. 29-41.
368. Gavezzotti, A. and G. Filippini, *Energetic aspects of crystal packing: Experimental and computer simulations*, in *Theoretical Aspects and Computer Modeling of the Molecular Solid State*, A. Gavezzotti, Editor. 1997, John Wiley & Sons: New York.
369. Hartman, P. and W.G. Perdok, *On the relations between structure and morphology of crystals. III.* Acta Cryst., 1955. **8**: p. 525-529.
370. Hartman, P. and W.G. Perdok, *On the relations between structure and morphology of crystals. II.* Acta Cryst., 1955. **8**: p. 521-524.
371. Hartman, P. and W.G. Perdok, *On the relations between structure and morphology of crystals. I.* Acta Cryst., 1955. **8**: p. 49-52.
372. Brunsteiner, M. and S.L. Price, *Morphologies of organic crystals: Sensitivity of attachment energy predictions to the model intermolecular potential.* Crystal Growth & Design, 2001. **1**: p. 447-453.
373. Berkovitch-Yellin, Z., *Toward an ab initio derivation of crystal morphology.* Journal of the American Chemical Society, 1985. **107**: p. 8239-8253.
374. Davey, R.J., J.W. Mullin, and M.J.L. Whiting, *Habit modification of succinic acid crystals grown from different solvents.* Journal of Crystal Growth, 1982. **58**: p. 304-312.
375. Liu, X.Y., E.S. Boek, W.J. Briels, and P. Bennema, *Prediction of crystal-growth morphology based on structural-analysis of the solid-fluid interface.* Nature, 1995. **374**: p. 342-345.
376. Winn, D. and M.F. Doherty, *Predicting the shape of organic crystals grown from polar solvents.* Chemical Engineering Science, 2002. **57**: p. 1805-1813.
377. Winn, D. and M.F. Doherty, *A new technique for predicting the shape of solution-grown organic crystals.* AIChE Journal, 1998. **44**: p. 2501-2514.

BIBL. LOND. UNIV